Modeling Implicit Quadrics and Free-Form Surfaces With Trimmed Rational Quadratic Bézier Patches

Seth J. Teller
Carlo H. Séquin

June 26, 1990

This work was supported in part by an equipment grant from Silicon Graphics, Inc., and in part by the consortium for Microelectronics Innovation and Computer Research Opportunies (MICRO), funded by industrial sponsors and the State of California.

Abstract

Designers require familiar, well-behaved surfaces for solid modeling tasks. Implementers desire modeling primitives that can be specified compactly, computed efficiently, and rendered quickly. Implicit surface representations are cumbersome in these contexts.

We present a method for constructing a rational quadratic Bézier patch that interpolates a portion of a quadric surface, and clarify the geometric and parametric degrees of freedom inherent in any such construction. The surface to be interpolated is specified implicitly, along with a (possibly empty) set of halfspaces in $\Re^3$ whose intersection bounds the desired region of the surface.

We demonstrate a novel equivalence between familar stereographic maps in two dimensions and rational quadratic Bézier curves, and extend this equivalence in three dimensions to an important subset of Bézier surfaces– namely, those that interpolate quadrics. This equivalence can be exploited to produce trivially invertible parametric curves and surfaces, with no loss of representational power. We describe a new method of altering control weights that, given a triangular or quadrilateral subpatch of a quadric, produces the entire quadric.

These techniques are demonstrated for a collection of common modeling situations, and frequently occurring surface fragments, such as hyperbolic and toroidal fillets, cylindrical joins, and rounded corners. We argue that current heterogeneous representations of implicit quadrics can be replaced with a single *trimmed* surface representation based on the stereographic map correspondence. Finally, we discuss the prospects for integration of these new representational techniques into existing modeling environments.

Contents

List of Figures

Chapter 1

Introduction

1.1 Research Into Compact, Efficient Surface Representations

This work describes an investigation into the suitability of rational quadratic parametric patches as primitives for free-form modeling and design systems. This formulation is considered as an alternative to the current use of more complex surface representations. In an important set of realistic design situations, the quadratic formulation is shown to be appropriate and useful.

Surface and solid modeling design systems often employ *interpolating surface patches* as primitives for object representation, rendering, and automated machining. However, patch representations in current use do not provide convenient, exact interpolation of desired surfaces. Two common patch types, the bicubic polynomial Bézier and B-Spline patches, are unable to exactly interpolate an important surface class, the *quadric* surfaces. These include, among other things, cones, spheres, cylinders, and other second-order rotationally symmetric objects. The quartic surface class of *toroids*, surfaces swept by the revolution of closed planar curves, is also unrealizable with this surface formulation.

A non-polynomial patch construct, the *rational quadratic triangular* patch, is the lowest-order parametric formulation able to exactly interpolate, or *cover*, quadric surfaces. In this respect, the rational quadratic formulation is more powerful than any polynomial formulation, regardless of order. The slightly more complex *rational biquadratic* or *tensor-product* patch, in turn, can exactly represent tori. Both quadratic and biquadratic patches [1] may interpolate surfaces more complex than implicit quadrics. The lower order of the patch provides more efficient evaluation, rendering, and storage than equivalent operations using higher-order (e.g., cubic) constructs.

These alternative patch representations have not been employed to their full advantage in today's design systems. Higher-order primitives are and will continue to be necessary for the design of very complex surfaces. However, with the new techniques described here, rational quadratic patches are shown to be a sufficient primitive for two important classes of modeling situations.

[1] Henceforth, this report will use the term *quadratic Bézier patch* to mean *rational quadratic triangular Bézier patch*, and the term *biquadratic Bézier patch* to mean *rational quadratic tensor-product Bézier patch*, unless otherwise stated.

1.2 Parametric Representation of Quadric Surfaces

Many methods have been proposed for exactly representing implicit quadrics with parametric formulations. Some have needlessly resorted to higher-order parametric patches ([6],[25]), while others have not satisfactorily addressed the issue of full control over patch parametrization and boundaries ([32], [40]). Typically, these important degrees of freedom are not explicitly specifiable but rather arise as artifacts of the patch construction.

The rational quadratic triangular Bézier patch is the lowest-order parametric formulation able to cover quadrics. In the following work, we propose this patch type as a necessary and sufficient parametric representation for quadric surfaces.

First, the problem is considered in two dimensions for the class of *conic* curves (planar curves having quadratic implicit equations). We show that quadratic Bézier curves are equivalent to planar stereographic maps of conics, and give intuitive geometric algorithms for obtaining each representation from its counterpart. The result is a novel method for constructing Bézier curves that are trivially *invertible* onto their domain pre-images. We reduce to a simple sequence of geometric operations the task of constructing a parametric Bézier segment that sweeps any desired portion of a conic segment.

In three dimensions, we show an analogous result: quadratic triangular Bézier surfaces that interpolate quadrics are equivalent to stereographic maps of quadrics. Straightforward, coordinate-independent algorithms are presented for transforming each representation into its counterpart. The fruit of this correspondence is a new method for generating trivially invertible parametric surfaces that interpolate quadrics. The correspondence also yields a clarification of the number and types of degrees of freedom inherent in any construction of such interpolating quadratic patches.

We show that surfaces constructed with our methods inherit advantageous properties from both the Bézier and stereographic map formulations. We demonstrate that it is easy to construct a Bézier patch and trimmed domain ([31], [34]) that together cover any desired portion of a quadric surface. Our construction takes as input a specification of a quadric surface in implicit form and a set of bounding halfspaces that are to enclose the desired portion of the surface. Our notion of containment within the intersection of bounding halfspaces is similar to intersection in the *constructive solid geometry* paradigm ([27],[28]).

1.3 Parametric Representation of Higher-Order Surfaces and Tori

The main body of this work involves using quadratic patches to cover implicit quadrics. We use the term *restricted patch* for such patches, since in general the surface swept by a rational quadratic triangular Bézier patch has a *quartic*, rather than quadratic, implicit equation (however, not all quartic implicit surfaces are representable as quadric patches [36]). Therefore, we may represent some quartic implicit surfaces with unrestricted quadratic patches. Finally, toroidal surfaces are not achievable with quadratic triangular patches; rather, we must employ tensor-product, or *biquadratic*, patches for these shapes. In general, such patches cover implicit surfaces of degree eight [10].

We extend the notion of quadratic curve complementation ([30], [18]) to quadratic triangular

patches and biquadratic quadrilateral patches. We show that complementing a triangular patch allows the "tiling" of complete quadric and quartic surfaces with a small number of patches. Similarly, we show that complementing biquadratic patches yields a useful tiling of toroids.

1.4 Organization of the Report

This report extends and applies previous results concerning quadratic patches that interpolate implicit quadric surfaces ([38]), and is arranged into five major sections. The first section is comprised of this introduction and the motivation for our investigations, followed by a a review of relevant coordinate systems and operations. The second section reviews the Bézier curve representation for conics and introduces the equivalence between Bézier curves and stereographic maps of conics. The third section generalizes these results to three spatial dimensions. Bézier surfaces are briefly reviewed. The number and types of degrees of freedom inherent in construction of Bézier patches that cover quadric surfaces are clarified, and a straightforward construction of such patches is demonstrated. Bézier patches that cover quadrics are shown to be equivalent to stereographic maps of quadrics. The use of Bézier patches as representations for quadric surfaces is discussed. This section also includes some minor results relevant to covering complete quadric surfaces; that is, those that have empty constraint sets. The fourth section reviews quadratic tensor-product Bézier patches, and extends the notion of patch complementation to this patch formulation. We demonstrate that complementation yields a simple method of tiling tori. The fifth section summarizes our results and demonstrates the application of the techniques presented here to real-world modeling situations. Finally, we discuss some limitations of the techniques, and the prospects for integrating quadratic patches into existing systems that employ higher-order parametric primitives, both triangular and tensor-product.

Chapter 2

Motivation

Quadrics and Toroids as Useful Surface Classes

Cones, spheres, ellipsoids, paraboloids, and hyperboloids are indispensable to the design of many objects, including: machine parts, such as bearings, crankshafts, and gears; surface "joins," such as cylindrical fillets and rounded corners; smooth objects such as spherical caps and cylindrical posts. These objects may have point or line symmetries. More generally, they may be represented as *piecewise-polynomial* collections of portions of quadric surfaces.

A more complex class of objects is comprised of those surfaces generated by revolution of space curves with respect to a line, or translation of space curves along a curvilinear path. These *toroids* and *generalized cylinders*, respectively, are not in general representable with quadrics since the composition operations necessary to create them may produce surfaces of high implicit order. Such high-order surfaces are outside the scope of this study. However, there are a few important and often-used surfaces that result under restriction of the degree of both the swept curve and the sweep path. Foremost of these are the circular and elliptical tori.

Criteria for Assessing Representational Utility

We sought the simplest method of *exactly* representating both exact quadrics, and a useful subset of more complex, composite, surfaces. The criteria for the evaluation of the utility and appropriateness of candidate surface representations included:

- the ability to exactly interpolate desired surface classes;
- the computational efficiency of patch creation and evaluation;
- the computational efficiency of patch inversion;
- the intuitive geometrical appeal of the formulation; and
- the compactness of the representation.

Quadratic Patches as a Superset of Quadrics

Rational quadratic patches have utility beyond the representation of second-order implicit (quadric) surfaces. In fact, an implicit description of the surface swept by a quadratic triangular patch may require a *quartic* implicit equation. For quadrilateral patches, the implicit order required may rise to eight. This suggests that quadratic patches may be useful in free-form modeling applications beyond those requiring only quadratic implicit surfaces; for instance, as blending or fillet surfaces.

Consider quadratic space curves swept along quadratically-described space paths. The resulting surfaces are clearly not, in general, quadrics. However, they will have a quartic implicit equation and, as such, are representable with quadratic tensor-product patches. A torus, for example, may be described as a circle swept along a circle (or, equivalently, revolved about a line). Tori are not quadrics. A torus, however, may be modeled as a collection of rational biquadratic patches, as will be demonstrated later in this work.

We investigated the extent to which rational quadratic patches, both triangular and quadrilateral, are useful in general modeling environments.

Current Surface Representations Have Drawbacks

Historically, quadric objects have been represented either with spatial approximation schemes (e.g., octrees [23]), implicit surface descriptions ([19], [16]), or as collections of cubic or higher-order B-spline and Bézier surface patches ([24], [25], [40]). Each of these representations presents problems to implementers desiring to model exact quadrics. Spatial subdivision schemes (i.e., octrees) cannot exactly interpolate quadrics, or any continuous implicit surface. Polynomial patches cannot exactly interpolate quadric surfaces.

Arbitrarily small error bounds can be achieved with both representations, by decreasing the granularity of the approximation (e.g., generating more octree cells, or more polynomial patches). However, tolerable error bounds may force a prohibitive penalty in storage and computation on an increasingly large data set.

Both implicit surface representations and quadratic (and higher-order) rational parametric descriptions, in contrast, can exactly represent quadrics. Implicit surface representations have utility in situations that require the "inside" and "outside" of a surface to be distinguished. Rendering implicit representations, however, is a cumbersome process loosely equivalent to converting the surface into parametric form [19], scan-converting it directly [22], converting it into a form suitable for scan-conversion using silhouettes [16], or employing ray-tracing or other non-interactive techniques. This suggests that a parametric formulation might be a sensible choice for representing quadrics in systems that require interactive rendering rates.

Finally, cubic or higher-order rational parametric surface formulations can also model quadrics exactly. Increasing parametric degree, however, demands more computational resources, and introduces degrees of representational freedom that can be non-intuitive for the designer and troublesome for the implementer ([21], [35], [33]). By limiting the order of the rational patch to quadratic, both difficulties are greatly ameliorated; quadratic patches are the simplest parametric representation applicable.

Quadratic Patches Are Attractive to Implementers

The *quadric surface* is a useful primitive for designers. The *quadratic rational Bézier patch*, we shall argue here, is a particularly simple and well-behaved object from the implementer's point of view. Rational quadratic patches are compact surface representations. Only moderate computational resources are required to evaluate and render (and, we shall show, invert) these surfaces. The Bézier patch formulation *interpolates* the corners of its data set, and provides a C^∞ surface everywhere in the interior of the patch. Two different rational quadratic patches may be matched along boundaries with C^1 or G^1 continuity. The conditions for achieving such continuity are simpler for quadratic patches than for higher-order parametric representations such as non-uniform rational B-Splines, or NURBS [2].

Thus, for implementers, quadratic rational patches combine representational flexibility with computational simplicity. Since, as will be shown later, quadratic rational patches are actually a superset of the quadrics, these patches have representational power "to spare."

Of course, rational cubic patches are more flexible in that they can model a superset of those surfaces achievable quadratically. The boundaries of cubic patches are cubic space curves, which may be an advantage in modeling situations requiring non-planar patch boundaries. We consider the extent to which these advantages are balanced or even outweighed by considerations of simplicity. We list some of these considerations here:

- Quadratic patch boundaries and isoparametric curves are planar.
- Quadratic patches may be constructed and rendered more efficiently than cubics.
- Conditions for G^1 continuity of quadratic patches are simpler than those for cubics.

Furthermore, as we shall show:

- The degrees of freedom in restricted quadratic patch construction are well understood.
- Arbitrarily bounded quadric surfaces may be easily modeled with quadratic patches.
- Quadratic patches may be *complemented* to tile quadric or quartic surfaces.
- A trivial inversion algorithm exists for quadratic patches that interpolate quadrics.

Chapter 3

Preliminaries

We review homogeneous notation for points, lines, and planes, and operations that combine them. Readers unfamiliar with homogeneous coordinates should refer to [3] or [29] for a more thorough treatment.

3.1 Points and Lines in Homogeneous $\Re^2$

We denote an arbitrary two-dimensional homogeneous point as $\mathbf{p} = (x, y, w)^T$, where the superscripted T signifies that the point should be treated as a column vector in matrix operations. When $w = 0$, $\mathbf{p}$ represents the *direction vector* $\pm(x, y)$.

Infinitely many homogeneous points $\mathbf{p}$ produce the point $\text{Proj}(\mathbf{p}) = (\frac{x}{w}, \frac{y}{w})$ under projection. That is, for any non-zero α,

$$\alpha\mathbf{p} = (\alpha x, \alpha y, \alpha w).$$

Dividing each of the first two coordinates of $\mathbf{p}$ by its last coordinate (i.e., αw), we find that

$$\text{Proj}(\alpha\mathbf{p}) = (\frac{\alpha x}{\alpha w}, \frac{\alpha y}{\alpha w}) = (\frac{x}{w}, \frac{y}{w}) = \text{Proj}(\mathbf{p}),$$

as expected.

Line equations are particularly simple in homogeneous coordinates. A line $\mathbf{L} = (L_x, L_y, L_w)$ may be specified as the set of points $\mathbf{P} = (x, y, w)$ such that

$$\mathbf{L}\mathbf{P}^T = \begin{pmatrix} L_x & L_y & L_w \end{pmatrix} \begin{pmatrix} x \\ y \\ w \end{pmatrix} = 0.$$

Lines are written as row vectors and points as column vectors; the composition operation is the familiar inner product.

Expressing coordinates in this way avoids many annoying problems that arise in representing, and computing, geometric data. For example, computing the intersection of two lines in Cartesian coordinates generates tiny divisors for near-parallel lines. By contrast, the intersection of two homogeneous lines (a, b, c) and (r, s, t), is simply [37]:

$$(bt - cs, cr - at, as - br). \tag{3.1}$$

This is just the familiar cross product of two 3-vectors. The representation has a powerful dual quality: if the triads (a, b, c) and (r, s, t) are interpreted as points, Equation 3.1 yields the line containing them.

3.2 Points and Planes in Homogeneous $\Re^3$

Three-dimensional homogeneous coordinates are directly analogous to those of two dimensions. Specifically, a general homogeneous point of $\Re^3$ is written $\mathbf{p} = (x, y, z, w)^T$, and corresponds to the point $\text{Proj}(\mathbf{p}) = (\frac{x}{w}, \frac{y}{w}, \frac{z}{w})$ under projection. When $w = 0$, $\mathbf{p}$ represents the *direction vector* $\pm(x, y, z)$.

Plane equations are straightforwardly expressed in homogeneous coordinates of $\Re^3$. A plane $\mathbf{E} = (E_x, E_y, E_z, E_w)$ can be written as the set of points $\mathbf{P} = (x, y, z, w)$ such that

$$\mathbf{E}\mathbf{P}^T = \begin{pmatrix} E_x & E_y & E_z & E_w \end{pmatrix} \begin{pmatrix} x \\ y \\ z \\ w \end{pmatrix} = 0. \tag{3.2}$$

As in the two-dimensional case, planes are written as row vectors, points as column vectors, and the inner product is taken.

Two planes intersect in a line, although this is not easy to represent directly in homogeneous coordinates of $\Re^3$ [30]. Instead, the line can be represented parametrically in $\Re^3$ (e.g., as an origin and a direction vector), or as a linear constraint on a generally positioned and coordinatized plane.

A common operation in three dimensions is finding the coincident point of three planes. Given three distinct planes $\mathbf{P}_i = (a_i, b_i, c_i, d_i)$, their point of intersection $\mathbf{T}$ is [30]:

$$\mathbf{T} = \left(\begin{vmatrix} d_1 & b_1 & c_1 \\ d_2 & b_2 & c_2 \\ d_3 & b_3 & c_3 \end{vmatrix}, \begin{vmatrix} a_1 & d_1 & c_1 \\ a_2 & d_2 & c_2 \\ a_3 & d_3 & c_3 \end{vmatrix}, \begin{vmatrix} a_1 & b_1 & d_1 \\ a_2 & b_2 & d_2 \\ a_3 & b_3 & d_3 \end{vmatrix}, \begin{vmatrix} a_1 & c_1 & b_1 \\ a_2 & c_2 & b_2 \\ a_3 & c_3 & b_3 \end{vmatrix} \right). \tag{3.3}$$

Equation 3.3 has a dual quality as well. Since $\mathbf{T} \cdot \mathbf{P}_i = 0$, interpreting the $\mathbf{P}_i$ as points yields the plane $\mathbf{T}$ containing them.

Chapter 4

Formulating Implicit Conics as Quadratic Bézier Curves

This chapter briefly reviews the mechanics of Bézier curve generation, and methods for the generation of parametric *conic curves*; i.e., planar curves arising from the intersection of circular or elliptic cones with generally positioned planes. This exposition is based principally on [18] and [26].

4.1 Rational Quadratic Bézier Curves

This section reviews the machinery for quadratic Bézier segments in the plane, and discusses the behavior of rational quadratic Bézier segments.

4.1.1 Univariate Bernstein-Bézier Polynomials

The univariate *Bernstein-Bézier polynomials* [1] of degree n can be written as

$$B_i^n(t) = \frac{n!}{i!(n-i)!} t^i (1-t)^{n-i}, \qquad 0 \le i \le n. \tag{4.1}$$

For given n, there are $n+1$ such linearly independent polynomials $B_0^n \ldots B_n^n$. These *sum to one* for all values of t, and are *non-negative* for $0 \le t \le 1$. The B_i^n form a basis for all univariate polynomials of degree n; that is, all such polynomials may be expressed as a linear combination of the $B_i^n(t)$.

Since we are concerned primarily with quadratic curves, the degree-2 Bernstein-Bézier polynomials are given here explicitly (Figure 4.1):

$$\begin{aligned} B_0^2(t) &= B_0(t) &&= (1-t)^2 \\ B_1^2(t) &= B_1(t) &&= 2t(1-t) \\ B_2^2(t) &= B_2(t) &&= t^2. \end{aligned} \tag{4.2}$$

The superscripts have been suppressed, as the basis functions are understood to be quadratic.

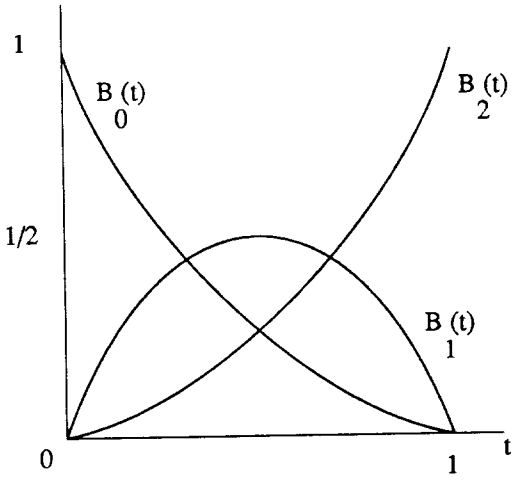

Figure 4.1: The Quadratic Bernstein-Bézier Polynomials $B_k(t)$.

Rational Quadratic Bézier Curves

A rational quadratic (degree 2) Bézier curve is defined as

$$\mathbf{P}(t) = \frac{\sum_{k=0}^{2} w_k \mathbf{p}_k B_k(t)}{\sum_{k=0}^{2} w_k B_k(t)}, \qquad 0 \le t \le 1. \tag{4.3}$$

The $\mathbf{p}_k$ are called *control points*, and are in general vector-valued. The sum in Equation 4.3 must be performed once for each component of the $\mathbf{p}_k$. The discussion of this chapter is restricted to two dimensions[1]; thus the $\mathbf{p}_k$ are of the form (x_k, y_k, w_k) and the curve expression $\mathbf{P}(t)$ has two components, $P_x(t)$ and $P_y(t)$, after division by $w = P_w(t)$. Restricting our attention to the two-dimensional case does not sacrifice the generality of the quadratic Bézier representation, since (as we show) all quadratic Bézier curves are planar. Figure 4.2 depicts a typical Bézier curve $\mathbf{P}(t)$.

The expression $\mathbf{P}(t)$ is a map from the real line into $\Re^2$. Following [18], we call the image of [0..1] under $\mathbf{P}(t)$ the "standard segment". Allowing the parameter t to range outside this interval has meaning that will become apparent later. The weights w_k are generally positive, but need not be so.

Equation 4.3 can be rewritten as

$$\mathbf{P}(t) = \sum \left\{ \frac{w_k B_k(t)}{\sum w_k B_k(t)} \right\} \mathbf{p}_k. \tag{4.4}$$

The denominator serves to normalize the coefficients of the $\mathbf{p}_k$ [the bracketed terms of (4.4)] so

[1] For clarity in the remainder of this chapter, the symbol $\sum$ should be read as $\sum_{k=0}^{2}$. Since only the quadratic basis functions $B_k^2(t)$ are employed, these shall henceforth be written as $B_k(t)$.

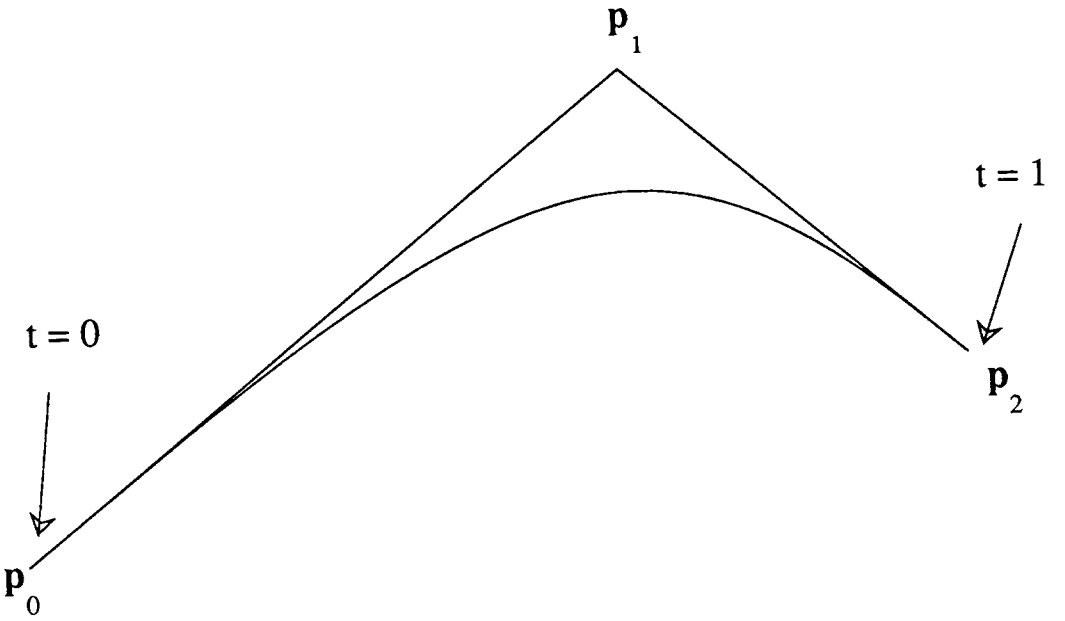

Figure 4.2: A Rational Quadratic Bézier Curve $\mathbf{P}(t)$, $0 \leq t \leq 1$.

that they sum to one for any weights w_k. The coefficients must sum to one since

$$\sum \left\{ \frac{w_k B_k(t)}{\sum w_k B_k(t)} \right\} = \frac{\sum w_k B_k(t)}{\sum w_k B_k(t)} = 1.$$

Thus, $\mathbf{P}(t)$ is a planar curve, since for all values of t, $\mathbf{P}(t)$ lies in the plane of $\mathbf{p}_0$, $\mathbf{p}_1$, and $\mathbf{p}_2$. When $0 \leq t \leq 1$, each bracketed term of Equation 4.4 is positive and less than or equal to one. Since the terms also sum to one, $\mathbf{P}(t)$ lies inside the *convex hull* $\Delta \mathbf{p}_0 \mathbf{p}_1 \mathbf{p}_2$ of the $\mathbf{p}_k$.

Rational quadratic Bézier curves have other notable properties. Substituting $t = 0$ and $t = 1$ into Equation 4.3 shows that $\mathbf{p}_0$ and $\mathbf{p}_2$ are the *endpoints* of the standard segment $\mathbf{P}(t)$:

$$\mathbf{P}(0) = \mathbf{p}_0 \qquad \text{and} \qquad \mathbf{P}(1) = \mathbf{p}_2. \tag{4.5}$$

Differentiating Equation 4.3 with respect to t and evaluating at $t = 0$ and $t = 1$ yields

$$\mathbf{P}'(0) = \frac{2w_1}{w_0}(\mathbf{p}_1 - \mathbf{p}_0) \qquad \text{and} \qquad \mathbf{P}'(1) = \frac{2w_1}{w_2}(\mathbf{p}_2 - \mathbf{p}_1). \tag{4.6}$$

Thus $\mathbf{P}(t)$ is tangent to its control hull at $\mathbf{p}_0$ and $\mathbf{p}_2$. The extended tangents $\mathbf{P}'(0)$ and $\mathbf{P}'(1)$ intersect at $\mathbf{p}_1$.

The weights w_k play no role in the interpolatory behavior of $\mathbf{P}(t)$. Nor do they affect the *directions* of the tangents $\mathbf{P}'(0)$ and $\mathbf{P}'(1)$; these are determined solely by the vectors $\overline{\mathbf{p}_0\mathbf{p}_1}$ and $\overline{\mathbf{p}_1\mathbf{p}_2}$.

The weights w_k do, however, affect the *shape* of the curve $\mathbf{P}(t)$, due to the dependence of the magnitudes of $\mathbf{P}'(0)$ and $\mathbf{P}'(1)$ on the ratios $\frac{w_1}{w_0}$ and $\frac{w_1}{w_2}$, respectively. If the end weights w_0 and w_2 are held fixed, Equation 4.6 shows that the magnitudes of $\mathbf{P}'(0)$ and $\mathbf{P}'(1)$ scale linearly with the middle weight w_1.

As w_1 increases, the curve is "pulled" toward the control point $\mathbf{p}_1$, as the term $w_1\,\mathbf{p}_1$ increases its contribution to $\mathbf{P}(t)$ in Equation 4.3. Conversely, as w_1 vanishes, every point on $\mathbf{P}(t)$ approaches

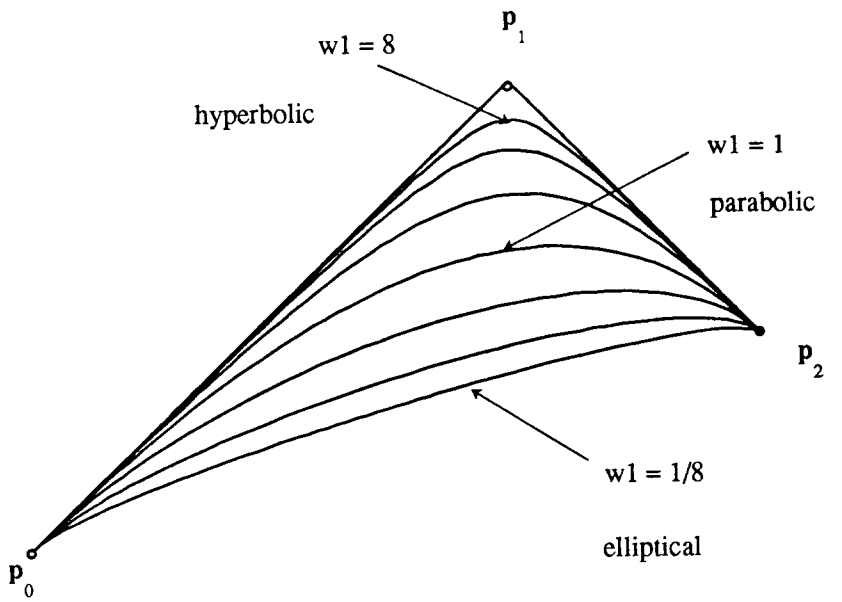

Figure 4.3: Rational Quadratic Bézier Curves with Varying w_1.

the segment $\overline{\mathbf{p}_0\mathbf{p}_2}$. Examples of the behavior of the curve $\mathbf{P}(t)$ for various values of w_1 are shown in Figure 4.3, with all other quantities held fixed. Here, the w_k are non-negative; we discuss later the implications of relaxing this condition.

4.2 Conics as Implicit Functions in $\Re^2$

A *conic* may be defined as the set of points in $\Re^2$ satisfying a *quadratic implicit* equation in the plane variables x and y:

$$\xi(x,y) = Ax^2 + 2Bxy + 2Cx + Dy^2 + 2Ey + F = 0. \tag{4.7}$$

This can be written in homogeneous matrix form [4] as

$$\begin{pmatrix} x & y & w \end{pmatrix} \begin{pmatrix} A & B & C \\ B & D & E \\ C & E & F \end{pmatrix} \begin{pmatrix} x \\ y \\ w \end{pmatrix} = 0. \tag{4.8}$$

Since we may multiply both sides of Equation 4.7 by any non-zero scale factor, any of the six coefficients A, B, C, D, E, or F may be scaled to unity. Thus there are exactly *five* degrees of freedom available in the specification of a conic with six coefficients. Geometrically this implies that through any five distinct points in $\Re^2$ there lies a unique conic [14].

For five distinct points $\mathbf{P}$, $\mathbf{Q}$, $\mathbf{R}$, $\mathbf{S}$, and $\mathbf{T}$ in $\Re^2$, the implicit equation for the unique conic ξ containing these five points is given by the expansion of the determinant [26]:

$$\xi(x,y) = \begin{vmatrix} x^2 & xy & y^2 & x & y & 1 \\ x_p^2 & x_p y_p & y_p^2 & x_p & y_p & 1 \\ x_q^2 & x_q y_q & y_q^2 & x_q & y_q & 1 \\ x_r^2 & x_r y_r & y_r^2 & x_r & y_r & 1 \\ x_s^2 & x_s y_s & y_s^2 & x_s & y_s & 1 \\ x_t^2 & x_t y_t & y_t^2 & x_t & y_t & 1 \end{vmatrix} = 0. \tag{4.9}$$

Expanding Equation 4.9 produces a quadratic implicit equation in the plane variables x and y. Substituting any of **P**, **Q**, **R**, **S**, or **T** for (x, y) yields two identical rows in the matrix and a zero determinant, as expected. Comparison of Equations 4.7 and 4.9 shows that each of the six coefficients $A \ldots F$ corresponds to a 5×5 sub-determinant.

Determinant computations like these are inefficient and may attain ill-conditioned intermediate states even for reasonable data. Superior methods exist in practice. Liming has exhibited a well-conditioned algorithm that, given a sufficient number of incidence and/or tangency conditions, constructs the implicit equation of the conic satisfying these conditions [12]. This algorithm avoids determinant computations such as Equation 4.9. Instead, it generates implicit conic equations as combinations of linear equations derived from incidence or tangency data.

There are many classical geometric methods for deducing conic behavior using only discrete data. For example, given five or more points on a conic, it is possible to generate with only a straightedge the intersection of the conic with any line containing a known point. Tangents at known points can be constructed in a similar fashion [41]. These constructions are algorithmic in nature and may easily be encoded into any reasonable computer language.

Equation 4.8 describes a *zero-set* of points; those points whose quadratic form with ξ is the scalar 0. Equation 4.8 also provides an inside-outside test[2] for points with respect to the surface ξ.

The conics are *circles*, *ellipses*, *parabolae*, *hyperbolae*, *single lines*, and *double lines*. The last two are degenerate, in that their equations are respectively linear (i.e., A, B, and D are zero) or factorable into a product of two linear terms. Figure 4.4 depicts some representative conics.

4.3 Conic Degrees of Freedom

It is worthwhile to consider further the notion of how many *degrees of freedom*, or independent adjustable scalar parameters, are necessary to specify a unique conic. We saw above that the six arbitrarily scalable coefficients $A \ldots F$ in the implicit conic equation (4.7) implied five scalar degrees of freedom in conic specification.

Differentiating Equation 4.7 with respect to $A \ldots F$ (while holding x and y fixed) produces six quantities that are not, in general, zero. Thus, an infinitesimal change in any one of the $A \ldots F$ must force some point (say, **Q**) off of the conic $\xi(x, y) = 0$.

Thus five scalars suffice to determine a conic. However, it is also true that five *points* of $\Re^2$ are necessary and sufficient for this purpose. Since each point is of the form (x, y), this seems to allow *ten* degrees of scalar freedom, not five. There is no discrepancy, for the following reason: unlike

[2]Consistent inside-outside tests require a convention for the determinant of the conic matrix, since negating all of the conics' coefficients reverses its inside-outside sense without affecting its satisfying point locus [4].

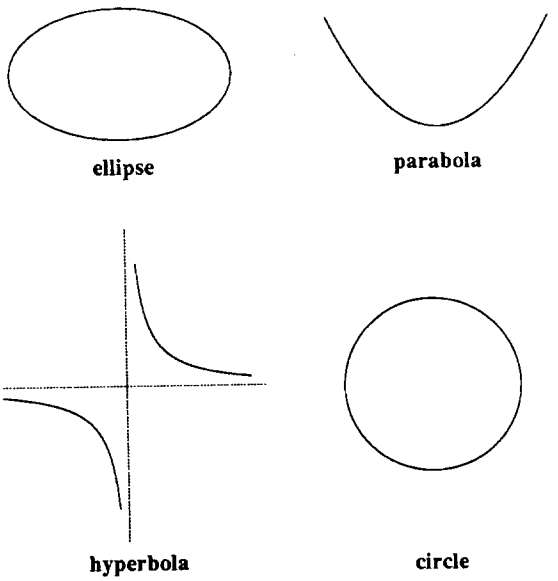

Figure 4.4: The Non-Degenerate Conics.

the scalar coefficients $A \ldots F$, each of the five points can always be moved, independently of the other four, in a direction such that the conic through it and its four companions is unchanged. This direction is, of course, along the conic itself. Imagining each point as a "bead" free to slide along the conic "wire," it is easy to see that each of the five points is free to slide along what is essentially an unconstrained curvilinear coordinate: position on the conic. Each of the five points encodes a redundant coordinate, and we are left with the expected $10 - 5 = 5$ degrees of freedom.

There are other methods of degree of freedom "counting" applicable to conics. For example, one might wish to specify that the conic have a particular *normal* (or, equivalently, *tangent*) at a given position. A specification of this type implies that the conic pass through the point at which the normal is specified. This is tantamount to the consumption of *two* scalar degrees of freedom: one that pins the conic to a given point, and one that specifies its normal at that point. The following list, though not exhaustive, contains several methods of conic specification:

- five scalars;
- five distinct points;
- one point, a normal at that point, and three other points $(2 + 3)$;
- two points, a normal at each point, and a third point $(2 + 2 + 1)$.

4.4 Implicit Conics as Parametric Bézier Curves

It is desirable to replace the implicit conic description of Equation 4.7 with an equivalent *parametric* description. We shall say that a Bézier curve $\mathbf{P}(t)$ *covers* the conic $\xi(x, y) = 0$ if the implicit equation $\xi(P_x(t), P_y(t)) = 0$ is satisfied[3]; that is, $\mathbf{P}(t)$ lies on the conic ξ for all values of t.

[3]Here, the control points $\mathbf{p}_k$ are two-dimensional.

We can rewrite the definition of a rational quadratic Bézier curve (Equation 4.3) as

$$\mathbf{P}(t) = \frac{w_0\mathbf{p}_0B_0(t) + w_1\mathbf{p}_1B_1(t) + w_2\mathbf{p}_2B_2(t)}{w(t)}, \tag{4.10}$$

where

$$w(t) = \sum w_kB_k(t);$$

that is, the denominator $w(t)$ is a polynomial Bézier combination of the weights w_k.

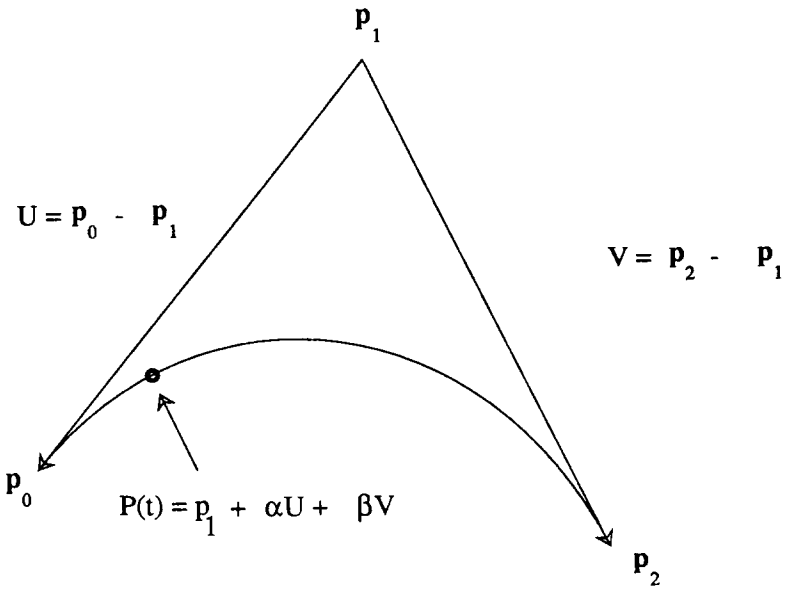

Figure 4.5: The Oblique $\mathbf{U}, \mathbf{V}$ Coordinate System with Origin $\mathbf{p}_1$.

As in [18], we express the curve $\mathbf{P}(t)$ in an *oblique* coordinate system (Figure 4.5) with origin $\mathbf{p}_1$ and spanning basis $\mathbf{U} \equiv (\mathbf{p}_0 - \mathbf{p}_1)$ and $\mathbf{V} \equiv (\mathbf{p}_2 - \mathbf{p}_1)$. Since $\mathbf{P}(t)$ lies in the plane $\mathbf{p}_0\mathbf{p}_1\mathbf{p}_2$, any point on the curve must be expressible as the origin $\mathbf{p}_1$ plus some scalar multiples (say, α and β) of $\mathbf{U}$ and $\mathbf{V}$:

$$\mathbf{P}(t) = \mathbf{p}_1 + \alpha(t)\mathbf{U} + \beta(t)\mathbf{V}. \tag{4.11}$$

Here α and β are some functions of t. Comparison with Equation 4.10 gives

$$\alpha(t) = \frac{w_0B_0(t)}{w(t)}, \text{ and} \qquad \beta(t) = \frac{w_2B_2(t)}{w(t)}.$$

Taking their product yields

$$\alpha(t)\beta(t) = \frac{w_0w_2}{4w_1^2}(B_1(t))^2, \tag{4.12}$$

where we have used the identity that $B_0(t)B_2(t) = \frac{(B_1(t))^2}{4}$. Since the basis functions $B_k(t)$ sum to one, we can write

$$\alpha\beta = k(1 - \alpha - \beta)^2 \qquad k \equiv \frac{w_0w_2}{4w_1^2}, \tag{4.13}$$

where $\alpha(t)$ and $\beta(t)$ are now written merely as α and β since the relation holds for all t. The scalar k is defined as a function only of the weights w_k.

Equation 4.13 is a quadratic *implicit* equation in the oblique basis variables α and β (and, via a simple affine transformation, quadratic in the usual Cartesian variables x and y). Since each point of $\mathbf{P}(t)$ satisfies this implicit equation, $\mathbf{P}(t)$ covers a conic.

4.5 Degrees of Freedom: Identifying the Class of Parametric Conic

Suppose the $\mathbf{p}_k$ (but not the weights w_k) of a Bézier curve have been fixed so that $\mathbf{p}_0$ and $\mathbf{p}_2$ lie on some implicit conic ξ, and $\mathbf{p}_1$ is placed at the intersections of the tangents to the conic at $\mathbf{p}_0$ and $\mathbf{p}_2$ (cf. Figure 4.3). The parametric curve $\mathbf{P}(t)$ will have the same interpolatory and derivative behavior as the implicit conic $\xi(x, y) = 0$ at $\mathbf{p}_0$ and $\mathbf{p}_2$. Recall from §4.3 the list of necessary and sufficient methods for implicit conic specification. Choosing the $\mathbf{p}_k$ as we have is tantamount to specifying four degrees of freedom: two points, and a tangent at each endpoint. Of these five conic degrees of freedom, one remains. Thus there exists an infinite *family* of conics, each of which interpolates $\mathbf{p}_0$ and $\mathbf{p}_2$, and has tangents there respectively parallel to $\overline{\mathbf{p}_0\mathbf{p}_1}$ and $\overline{\mathbf{p}_1\mathbf{p}_2}$. This family must be indexed by the single remaining degree of freedom.

Lee shows in [2] that the scalar parameter k, a function only of the w_k, can be related to the class of conic produced as:

$4k < 1$: $\mathbf{P}(t)$ is a hyperbola, and is unbounded;
$4k = 1$: $\mathbf{P}(t)$ is a parabola, the boundary case;
$4k > 1$: $\mathbf{P}(t)$ is an ellipse, and is bounded.

Specifying an additional point $\mathbf{p}_s$ on the conic is necessary and sufficient to fix the *shape*, but not the *parametrization*, of the conic segment [18]. That is, although only a single *implicit* conic satisfies five general interpolatory and tangent conditions, there is still a family of Bézier curves $\mathbf{P}(t)$ that do so, differing only in their parametrizations. Fixing the scalar k (a ratio of weights) determines $\mathbf{p}_s$, and vice-versa. Unique determination of the w_k requires that we choose a parameter value t_s and require that the parametric curve interpolate $\mathbf{p}_s$ at this value. That is, we demand that $\mathbf{P}(t_s) = \mathbf{p}_s$. The interpolated point $\mathbf{p}_s$ is called a "shoulder point." Although the parameter value t_s may be taken as any value (other than 0 or 1), we can fully exploit the parametric freedom with any fixed t_s. The choice $t_s = \frac{1}{2}$ proves convenient, as it produces useful symmetries in the ensuing geometric and algebraic operations.

Lee demonstrates a geometric connection between the choice of shoulder point $\mathbf{p}_s$ and the parameter value t_s. Connect $\mathbf{p}_s$ to each of $\mathbf{p}_0$, $\mathbf{p}_1$, and $\mathbf{p}_2$, to form opposing triangles of area a_0, a_1, and a_2 (Figure 4.6). The a_k are the barycentric coordinates of the shoulder point in the oblique coordinate system of the three $\mathbf{p}_k$. Requiring that $\mathbf{P}(t_s) = \mathbf{p}_s$ implies that [18]

$$\frac{w_0}{a_0/B_0(t_s)} = \frac{w_1}{a_1/B_1(t_s)} = \frac{w_2}{a_2/B_2(t_s)}, \tag{4.14}$$

where the $B_k(t)$ are the univariate Bernstein-Bézier polynomials of §4.1. For the particular parameter value $t_s = \frac{1}{2}$, Equation 4.14 reduces to

$$\frac{w_0}{a_0} = \frac{2w_1}{a_1} = \frac{w_2}{a_2}. \tag{4.15}$$

Since the three weights w_k can always be scaled by a non-zero constant, we may choose one of them (say, w_0) to be unity. Thus the w_k encapsulate two degrees of freedom. But these must be exactly the two degrees of *parametric* conic freedom implied previously; the first being the shape parameter k, and the second a parametrization convention that dictates the actual values of the w_k, but has no effect on the shape of the generated Bézier segment.

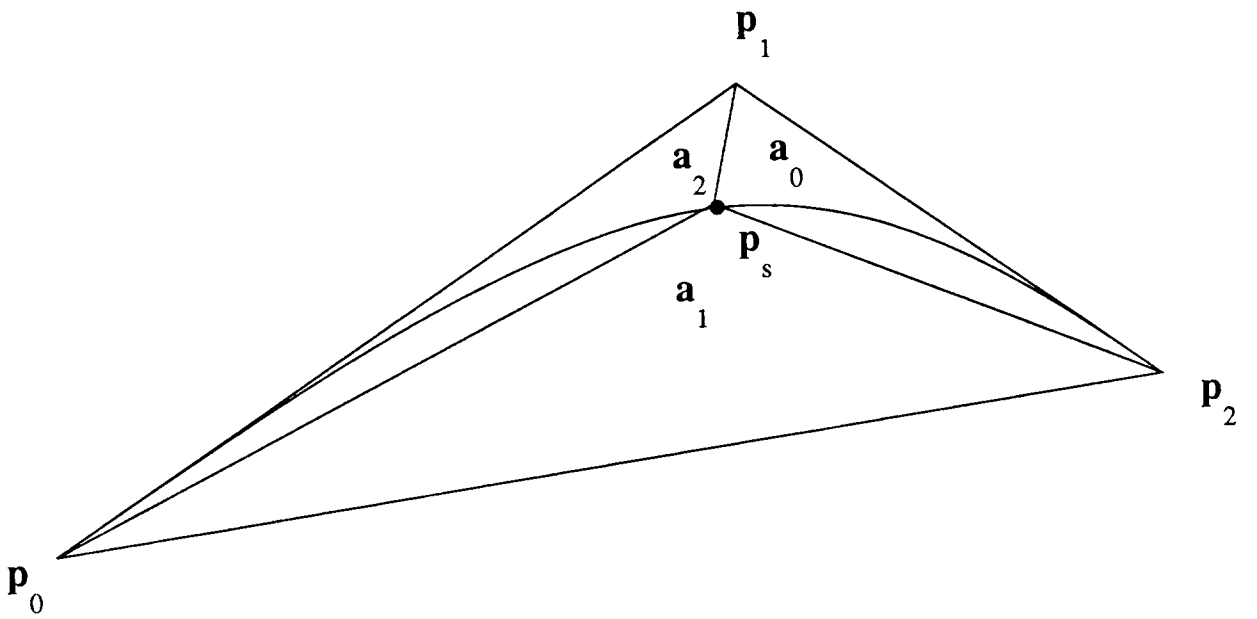

Figure 4.6: The Areas Implied by the Shoulder Point $\mathbf{p}_s$.

There are many parametrization conventions. Two of the next three sections discuss conventions of particular interest. The *rho-conic* convention [18] depends only on the standard Bézier segment $\mathbf{P}(t), t \in [0..1]$, and its *local* behavior; that is, its behavior inside the convex hull of the $\mathbf{p}_k$ (for nonnegative w_k). We also present a novel method that we call the *pole*-conic parametrization convention. This method fixes the w_k according to the *non-local* behavior of the Bézier segment $\mathbf{P}(t)$.

4.5.1 The Rho-Conic Parametrization Convention

Choose $t_s = \frac{1}{2}$, and the shoulder point $\mathbf{p}_s$ as the intersection of the conic with the line segment from $\mathbf{p}_1$ to the midpoint of $\mathbf{p}_0$ and $\mathbf{p}_2$ (Figure 4.7, after [18]). Forrest defines the conic shape factor ρ in [13] as

$$\rho = \frac{\mathbf{p}_s - \mathbf{p}_m}{\mathbf{p}_1 - \mathbf{p}_m}, \qquad \mathbf{p}_m \equiv \frac{\mathbf{p}_0 + \mathbf{p}_2}{2}. \tag{4.16}$$

This choice yields a symmetric ratio relationship among the weights w_k, namely that

$$w_0 : w_1 : w_2 \quad = \quad (1-\rho) : \rho : (1-\rho) \quad = \quad 1 : \frac{\rho}{1-\rho} : 1, \qquad \rho \neq 1. \tag{4.17}$$

The shape factor k is a simple function of the w_k. We can express it in terms of ρ as

$$k = \frac{w_0 w_2}{4w_1^2} = \frac{(1-\rho)^2}{4\rho^2}. \tag{4.18}$$

This is a quadratic polynomial in ρ [18], yielding the two ρ values

$$\rho_1 = \frac{1}{1+2\sqrt{k}}, \qquad \rho_2 = \frac{1}{1-2\sqrt{k}}. \tag{4.19}$$

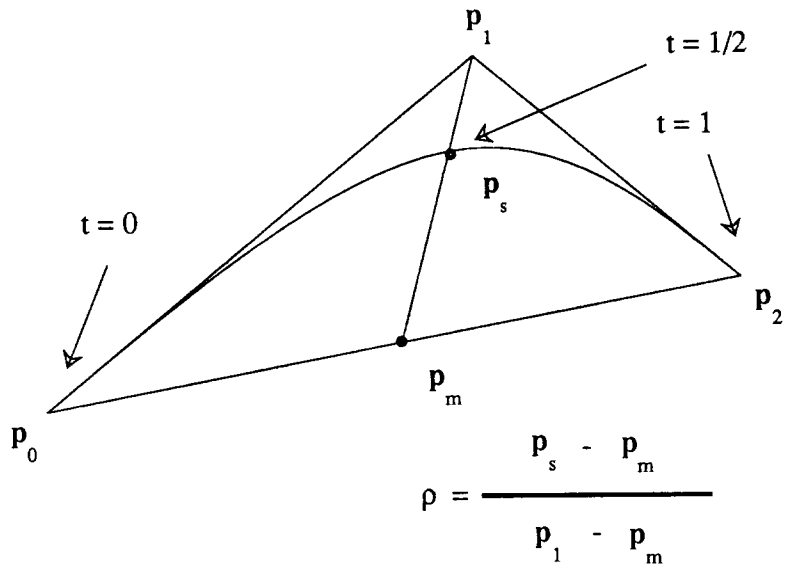

Figure 4.7: The Rho-Conic Parametrization Convention.

Since, for positive w_0 and w_2, k is strictly positive, ρ_1 is bounded by 0 and 1. These values of ρ correspond to choices of the shoulder point $\mathbf{p}_s$ inside $\Delta\mathbf{p}_0\mathbf{p}_1\mathbf{p}_2$. Choosing $\mathbf{p}_s$ outside the convex hull of the control points leads to a ρ_2 that is either negative (if $\mathbf{p}_s$ and $\mathbf{p}_1$ are on opposite sides of $\overline{\mathbf{p}_0\mathbf{p}_2}$), or greater than one (if they are on the same side). Choosing $\mathbf{p}_s$ as the midpoint of $\mathbf{p}_m$ and $\mathbf{p}_1$ yields the special value $\rho_1 = \frac{1}{2}$ (so that $\rho_2 = \infty$) and weights $w_0 = w_1 = w_2$; that is, the familiar (parabolic) polynomial Bézier segment. Figure 4.8 depicts some typical Bézier curves, with the implicit conics that they cover rendered as dotted lines.

The rho-conic parametrization convention yields a formulation of parametric conics that hass exactly five degrees of freedom (cf. Figure 4.7). Choosing the three control points $\mathbf{p}_k$ consumes four degrees of freedom, since together they imply two interpolatory and two tangent conditions. The fifth and final freedom is consumed by the specification of the shoulder point $\mathbf{p}_s$ on the conic, and the requirement that it lie at the "halfway" point $t_s = \frac{1}{2}$ of the corresponding Bézier segment. This conforms to the analysis of implicit conics in §4.2, in which exactly five scalar degrees of freedom were shown to be necessary for unique specification of an implicit conic.

There is no perturbation of the position of any of the four points $\mathbf{p}_0$, $\mathbf{p}_1$, $\mathbf{p}_2$, $\mathbf{p}_s$, in Figure 4.7 that leaves the shape of the resulting conic unchanged. For instance, $\mathbf{p}_1$ is pinned because any motion would remove it from at least one of the extended tangents. Similarly, motion of the shoulder point $\mathbf{p}_s$ would affect $\mathbf{p}_m$, which in turn would perturb $\mathbf{p}_0$ and $\mathbf{p}_2$. Thus there are no redundant degrees of freedom encoded in the choice of these four points.

Figure 4.9 depicts the use of the rho-conic parametrization convention in the construction of an elliptical segment. The construction takes as input an implicit equation for some conic ξ and two points $\mathbf{p}_0$ and $\mathbf{p}_2$ on ξ. Its output consists of the weighted control points $\mathbf{p}_k$ of a Bézier segment $\mathbf{P}(t)$, such that $\mathbf{P}$ has endpoints $\mathbf{p}_0$ and $\mathbf{p}_2$ and covers the conic ξ from $\mathbf{p}_0$ to $\mathbf{p}_2$.

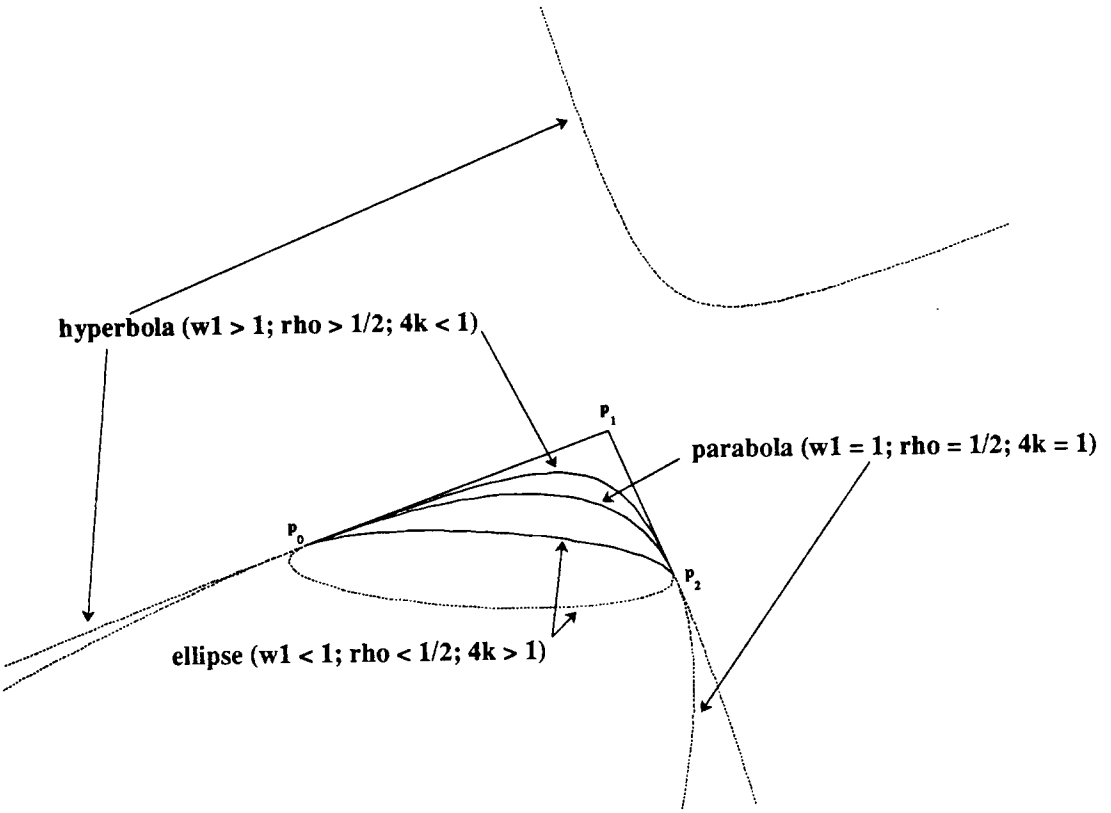

Figure 4.8: Three Classes of Conic, and the Scalars w_1, k, and ρ.

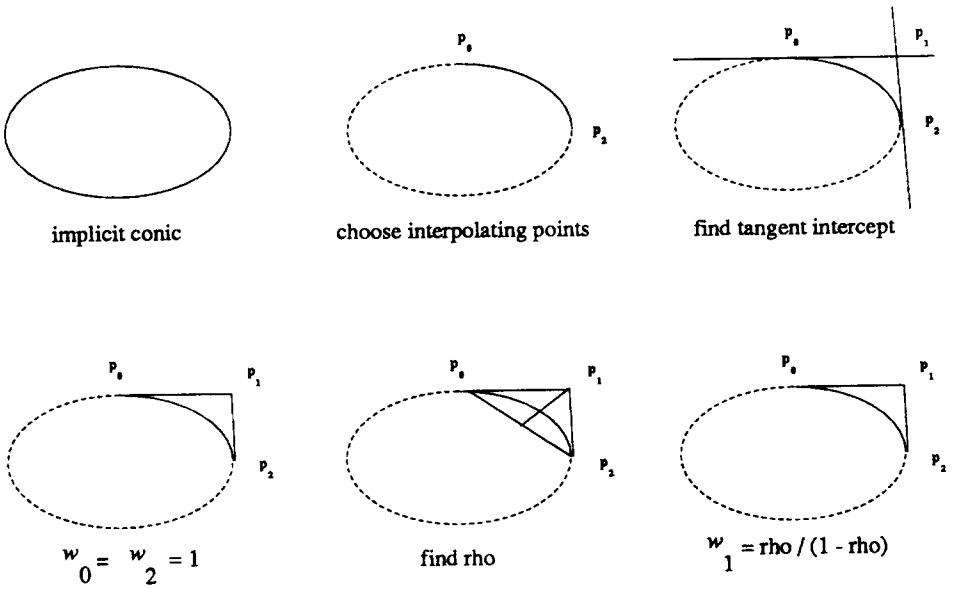

Figure 4.9: Constructing a Rho-Parametrized Conic From an Implicit Description.

4.5.2 The Standard and Extended Bézier Segments

Three examples of curves $\mathbf{P}(t)$ with end weights equal to unity, and various values of k (and ρ), are shown in Figure 4.10 (compare to Figure 4.8). The standard segment swept by $0 \leq t \leq 1$ is rendered as a solid line. The remainder of the implicit conic, the portion not between $\mathbf{p}_0$ and $\mathbf{p}_2$, is rendered as a broken line.

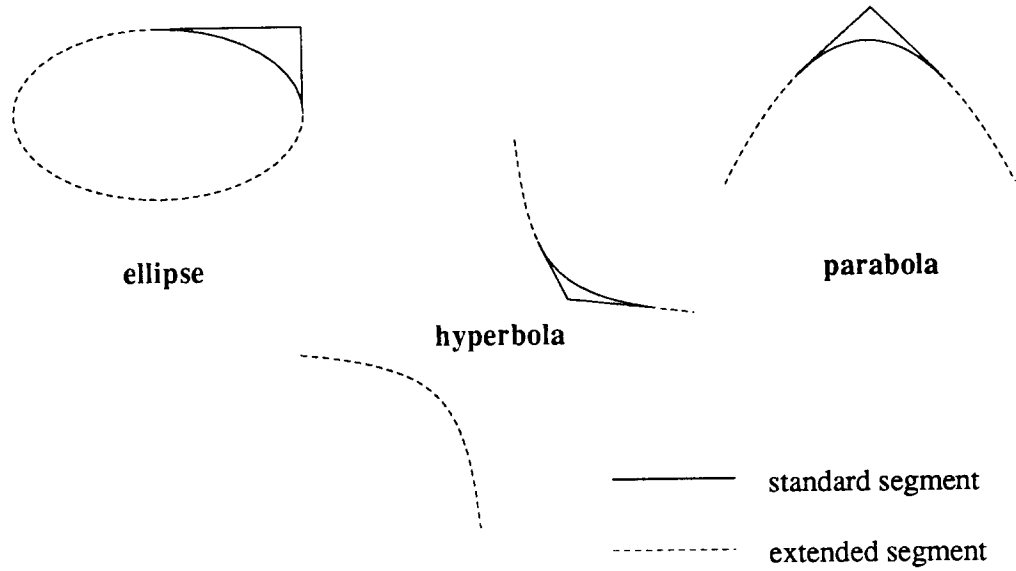

Figure 4.10: Portions of an Ellipse, Hyperbola, and Parabola as Bézier Segments.

Since, for $0 \leq t \leq 1$, $\mathbf{P}(t)$ satisfies an implicit conic equation, points $\mathbf{P}(t)$ for t outside this interval must also satisfy this equation. This is true simply because the implicit equation for the conic in oblique coordinates, Equation 4.13, nowhere depends on t. Referring again to Figure 4.10, the broken-line portions of the diagram are exactly the curves $\mathbf{P}(t)$ swept as t is allowed to range outside of the interval $0 \leq t \leq 1$. We call the two curve segments generated by $-\infty \leq t \leq 0$ and $1 \leq t \leq \infty$, collectively, the "extended segment" of $\mathbf{P}(t)$. As t is allowed to range over all the reals, the entire conic is swept; first by the negative extended segment, then by the standard segment, and finally by the positive extended segment.

In practice, there are computational difficulties inherent in allowing t to attain infinite values in order to cover the entire implicit conic. In the next section we discuss an alternative method of generating the portion of the conic that is not reached by the standard segment.

4.5.3 The Complementary Segment $\tilde{\mathbf{P}}(t)$

Changing the *sign* of the weight w_1 of a parametric conic, while leaving all other control points and weights fixed, produces a useful new Bézier segment ([18], [30]). This segment is called the *complementary segment* of the standard Bézier curve $\mathbf{P}(t)$, and denoted $\tilde{\mathbf{P}}(t)$.

We examine the effects of negating the weight w_1 on the definition of $\mathbf{P}(t)$, Equation 4.3.

Negating w_1 and expanding, the complementary segment is

$$\tilde{\mathbf{P}}(t) = \frac{w_0\mathbf{p}_0 B_0(t) - w_1\mathbf{p}_1 B_1(t) + w_2\mathbf{p}_2 B_2(t)}{\tilde{w}(t)}. \tag{4.20}$$

Here $\tilde{w}(t)$ is the denominator of the standard curve equation with w_1 negated:

$$\tilde{w}(t) = w_0 B_0(t) - w_1 B_1(t) + w_2 B_2(t). \tag{4.21}$$

Thus $\tilde{\mathbf{P}}(t)$ interpolates $\mathbf{p}_0$ and $\mathbf{p}_2$ at $t = 0$ and $t = 1$, as does the standard segment $\mathbf{P}(t)$:

$$\tilde{\mathbf{P}}(0) = \mathbf{p}_0 \qquad \text{and} \qquad \tilde{\mathbf{P}}(1) = \mathbf{p}_2. \tag{4.22}$$

Evaluating the derivatives of $\tilde{\mathbf{P}}(t)$ at its endpoints, we find that

$$\tilde{\mathbf{P}}'(0) = \frac{2w_1}{w_0}(\mathbf{p}_0 - \mathbf{p}_1) \qquad \text{and} \qquad \tilde{\mathbf{P}}'(1) = \frac{2w_1}{w_2}(\mathbf{p}_1 - \mathbf{p}_2). \tag{4.23}$$

Comparison with Equation 4.6 shows that the derivatives of the complementary segment are *antiparallel* to those of the standard segment at the endpoints.

Finally, since the weight w_1 appears only as a squared term in the derivation of the oblique implicit equation (4.11), its sign is irrelevant; all points on the complementary segment $\tilde{\mathbf{P}}(t)$ satisfy the same implicit conic equation as those of $\mathbf{P}(t)$. The two curves, evaluated over the interval $0 \le t \le 1$, share only their endpoints; thus the term "complementary segment" for $\tilde{\mathbf{P}}(t)$. The antiparallelism of the derivatives of the endpoints implies that the curves $\mathbf{P}(t)$ and $\tilde{\mathbf{P}}(t)$ traverse the conic in an opposed sense (Figure 4.11). In general $\tilde{\mathbf{P}}(t)$ will not lie inside the convex hull of its control points.

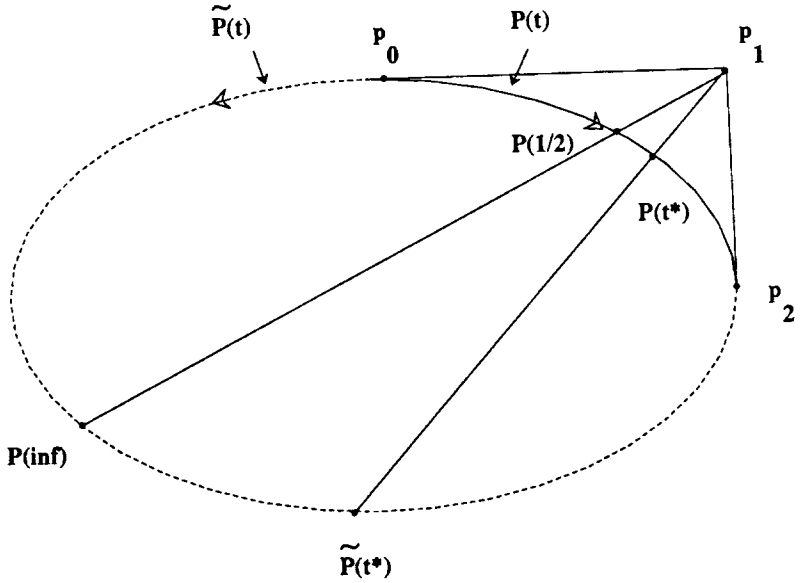

Figure 4.11: The Complementary Segment $\tilde{\mathbf{P}}(t)$.
The points $\mathbf{p}_1$, $\mathbf{P}(t^*)$ and $\tilde{\mathbf{P}}(t^*)$ are collinear for any t^*.

There are several useful identities relating $\mathbf{P}(t)$ and its complementary segment $\tilde{\mathbf{P}}(t)$. First, direct substitution into the standard or complementary curve definitions (Equations 4.3 and 4.20)

yields

$$\tilde{\mathbf{P}}(t) = \mathbf{P}(\frac{t}{2t-1}). \tag{4.24}$$

This equation is symmetric in $\mathbf{P}$ and $\tilde{\mathbf{P}}$. It is a rather remarkable identity, true for all w_k and $\mathbf{p}_k$. Evaluating either curve at $t = \frac{1}{2}$ is equivalent to evaluating its complementary curve at $t = \infty$.

Recall the oblique **UV** basis with $\mathbf{p}_1$ as origin (cf. Figure 4.5). Again using the definitions of the standard and complementary curve, some manipulation yields

$$\mathbf{p}_0 = \frac{\tilde{w}(t)}{\tilde{w}(t) - w(t)}\tilde{\mathbf{P}}(t) + \frac{-w(t)}{\tilde{w}(t) - w(t)}\mathbf{P}(t). \tag{4.25}$$

Since the coefficients of $\mathbf{P}(t)$ and $\tilde{\mathbf{P}}(t)$ sum to one, the three points $\mathbf{p}_1$, $\mathbf{P}(t)$, and $\tilde{\mathbf{P}}(t)$ are collinear for all t (Figure 4.11). We deduce from Equation 4.24 that, for any Bézier segment $\mathbf{P}(t)$,

$$\mathbf{p}_1,\ \mathbf{P}(\frac{1}{2}),\ \text{and}\ \mathbf{P}(\infty)\ \text{are collinear, regardless of parametrization.} \tag{4.26}$$

Analysis of the complementary segment yields insight about the non-local behavior of the standard segment, and vice-versa. We exploit this with a novel parametrization convention that fixes the parametrization of a Bézier segment according to the behavior of its complement. We call this method the *pole*-conic parametrization convention.

4.5.4 The Pole-Conic Parametrization Convention

We define the *pole* $\mathbf{P}$ of a Bézier segment as the point reached by $\mathbf{P}(t)$ in the limit $t \to \pm\infty$. The pole-conic convention fixes the parametrization of $\mathbf{P}(t)$ according to the position of this point.

Equations 4.24 and 4.25 together implied, for any Bézier segment, collinearity of three points: $\mathbf{P}(\frac{1}{2})$, $\mathbf{P}(\infty)$, and the control point $\mathbf{p}_1$. This relation holds regardless of the weights w_k. Suppose we choose a point $\mathbf{P}$ on the implicit conic, but not on the standard segment, and require that it be the pole $\mathbf{P}(\infty)$. By the collinearity relation, this is equivalent to choosing $t_s = \frac{1}{2}$, and the shoulder point $\mathbf{p}_s$ as the intersection of the line connecting $\mathbf{P}$ and the control point $\mathbf{p}_1$ (Figure 4.12). This shoulder point can be used directly as input to the rho-conic convention.

The pole-conic convention is no more or less general than the rho-conic method. Choosing the pole of the Bézier segment directly, however, affords us explicit control over the segment's behavior at infinite parameter values. This control will prove useful in later constructions.

Choosing a pole off the standard segment implies a shoulder point inside the convex hull of the $\mathbf{p}_k$. The areas a_k are easily found (cf. Figure 4.6), yielding the weight ratio $w_0{:}w_1{:}w_2$, $w_k \geq 0$. Figure 4.13 shows rho-conic and pole-conic parametrizations of a portion of a parabola and a quarter circle. In the parabolic case the methods yield identical weight ratios for $\mathbf{P}$ at infinity.

If the role of pole and shoulder point are interchanged (for example, by choosing the pole $\mathbf{P}$ inside the convex hull of the $\mathbf{p}_i$), a negative weight w_1 will result. This occurrence is easy to detect, either at the start or finish of the construction.

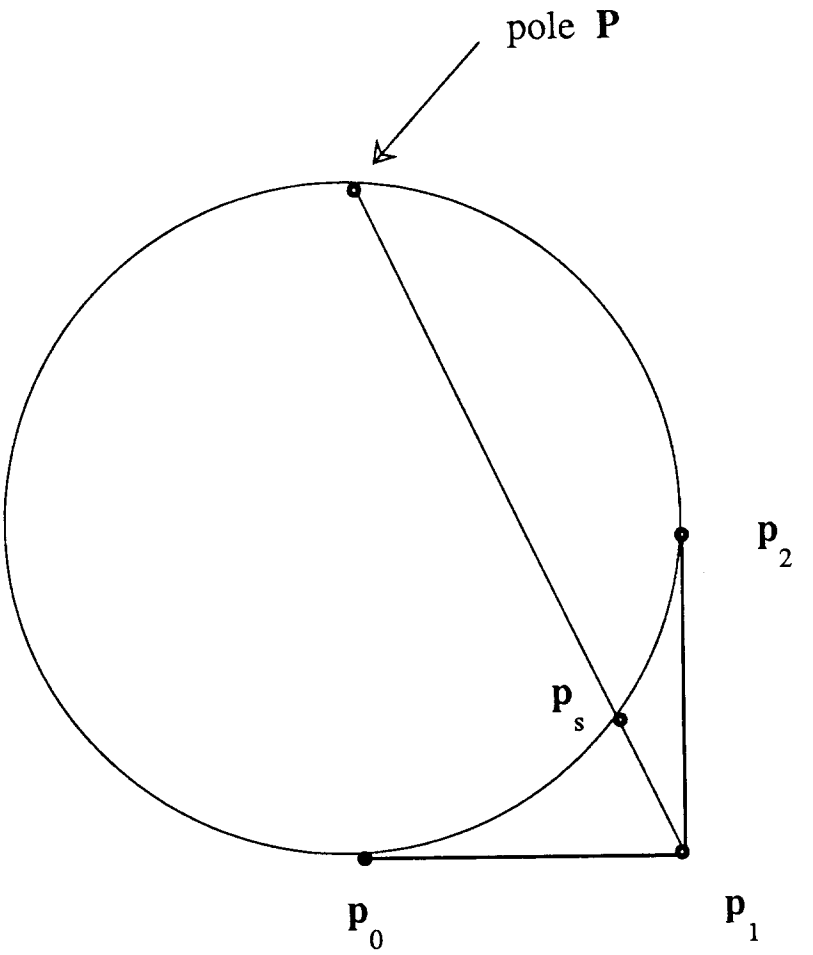

Figure 4.12: The Pole-Conic Parametrization Convention.
The position of the pole $\mathbf{P} = \mathbf{P}(\infty)$ implies
the position of the shoulder point $\mathbf{p}_s = \mathbf{P}(\frac{1}{2})$.

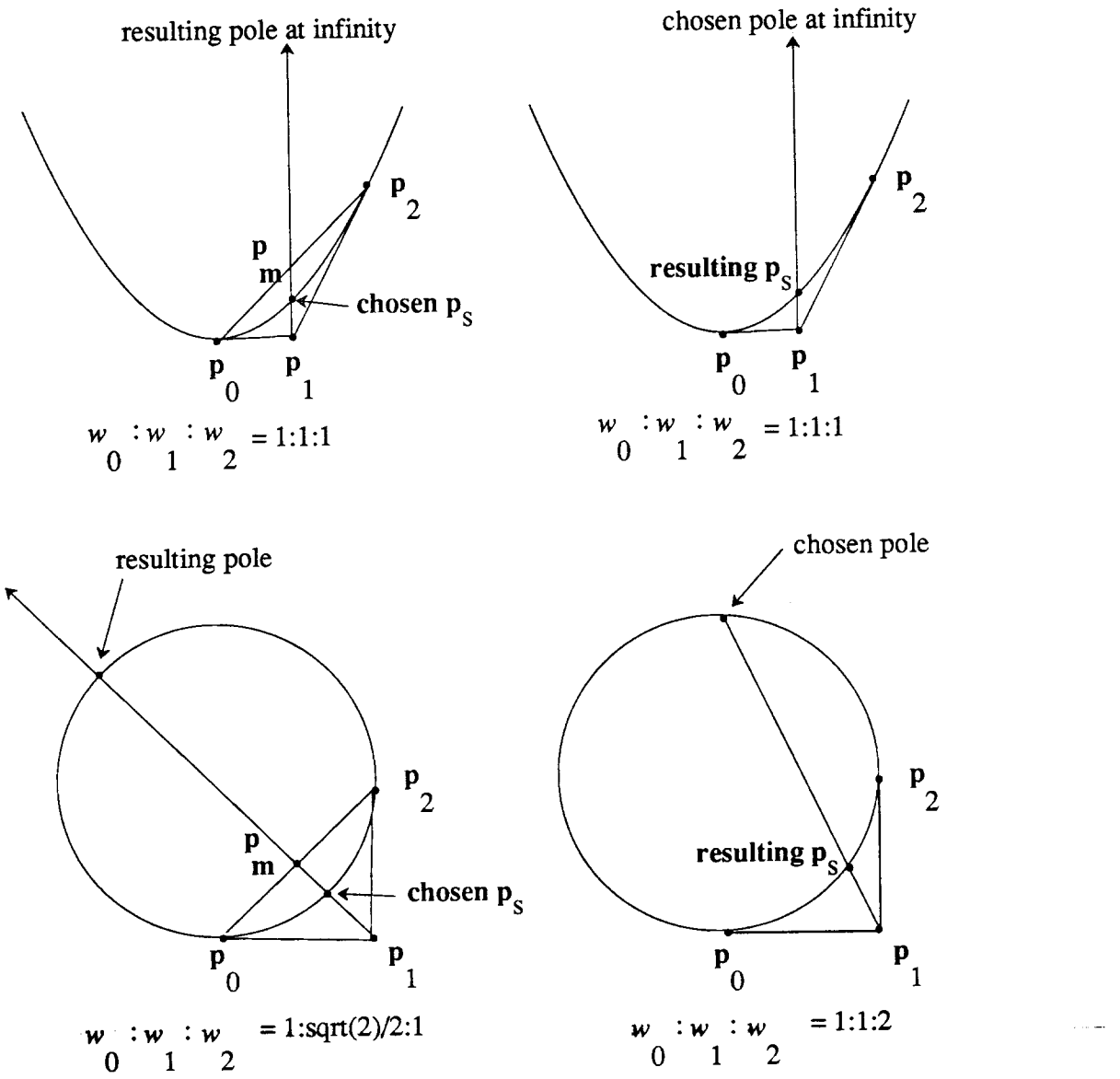

Figure 4.13: The Rho-Conic (Left) and Pole-Conic (Right) Parametrization Conventions.

Chapter 5

Quadratic Bézier Segments as Stereographic Maps of the Line

This chapter unifies the notions of rational quadratic Bézier curves and stereographic maps from the line onto implicit conics, with a novel demonstration that each formulation may be generated by a straightforward transformation of its counterpart. The transformation is intuitive, purely constructive, and coordinate independent. This unification yields an intuitive geometric framework in which to specify Bézier segments, and generally understand their behavior. For some important operations (e.g., inversion), computation on the unified representation is shown to be more efficient than on either formulation alone.

The correspondence is a novel result of this research. We show in Chapter 8 that it extends to three dimensions, and rational quadratic Bézier patches that interpolate quadrics.

5.1 Stereographic Maps Onto Conics

A *stereographic map* onto a conic, in the context of this work, is a continuous, constructive map of points on the real line onto points of a given conic (Figure 5.1). Such a map can be constructed for any conic ξ by choosing a point $\mathbf{Z}$ on the conic as a *center of projection*, and some *baseline* $\mathbf{L}$ not containing $\mathbf{Z}$. Identify each point $\mathbf{p}$ on $\mathbf{L}$ with a point $\mathbf{M}(\mathbf{p})$ on ξ, such that $\mathbf{M}(\mathbf{p})$ is the intersection (apart from $\mathbf{Z}$) of the given conic with the line through $\mathbf{Z}$ and $\mathbf{p}$. We call this identification the stereographic map of $\mathbf{L}$ *through* $\mathbf{Z}$ and *onto* the conic ξ.

Points at infinite distance in either direction on $\mathbf{L}$ are sent by $\mathbf{M}$ to a single point that ~~we call~~ the *pole* $\mathbf{P}$ of the stereographic map[1]. This pole is $\mathbf{Z}$ itself if and only if the baseline $\mathbf{L}$ is parallel to the conic's tangent at $\mathbf{Z}$. We say that maps with this property are in *standard form*.

The notion of stereographic maps above is purely geometric, in the sense that no particular coordinates have been imposed, for example, on the conic ξ or the baseline $\mathbf{L}$. A coordinate system is required if such maps are to be useful in a constructive sense. Imposing one on an arbitrary stereographic map is easily accomplished. We replace $\mathbf{L}$ with an origin $\mathbf{O}$ and a unit vector $\hat{\mathbf{L}}$.

[1] We use *pole* here analogously to the manner in which we call the point $\mathbf{P}(\infty)$ reached by a Bézier segment $\mathbf{P}(t)$, in the limit $t \to \infty$, the *pole* of the segment. This initially confusing terminology is deliberate, for reasons to be explained.

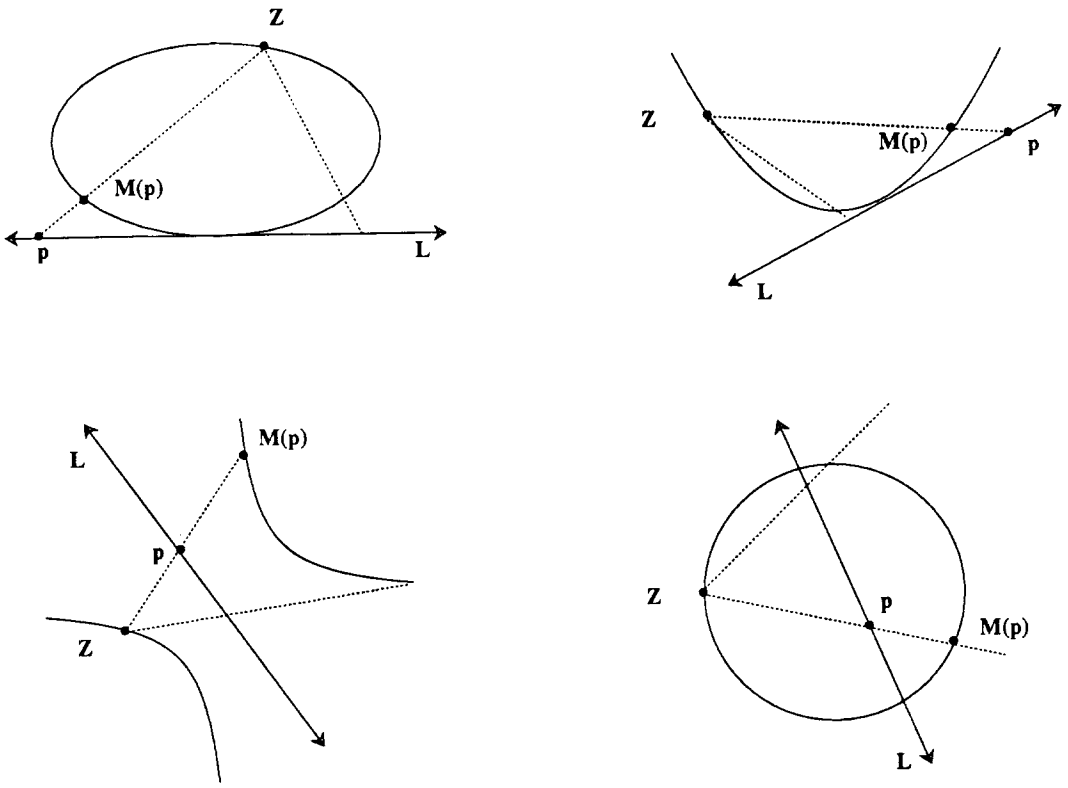

Figure 5.1: Geometric Stereographic Maps of Conics.

Together, these define $\mathbf{L}$'s direction and coordinate metric. Any point $\mathbf{p}$ on $\mathbf{L}$ may then be written

$$\mathbf{p} = \mathbf{p}(t) = \mathbf{O} + t\hat{\mathbf{L}}, \qquad t \text{ some scalar.} \tag{5.1}$$

In this manner, we define point-valued functions $\mathbf{p}(t)$ and $\mathbf{M}(t)$, that yield, respectively, points $\mathbf{p}(t)$ on $\mathbf{L}$ and their images $\mathbf{M}(t)$ under the stereographic map of $\mathbf{L}$ through $\mathbf{Z}$. We shall refer to a geometric stereographic map augmented with coordinates in this manner as a *coordinatized stereographic map* or simply *coordinatized map.*

Coordinatized stereographic maps of conics have a trivial *inversion procedure.* That is, for any point $\mathbf{M}(t)$ on the conic, it is easy to find the scalar t such that $\mathbf{M}(t) = \mathbf{p}$. To do so, simply intersect the line through $\mathbf{Z}$ and $\mathbf{p}$ with the baseline $\mathbf{L}$ of the map (Figure 5.2). By construction, the resulting baseline point has position t such that $\mathbf{M}(t) = \mathbf{p}$.

We call two coordinatized maps $\mathbf{A}$ and $\mathbf{B}$ *equivalent* if the following conditions hold (Figure 5.3):

$\mathbf{Z_A} = \mathbf{Z_B}$ (i.e., the centers are coincident at some point $\mathbf{Z}$);
$\hat{\mathbf{L}}_\mathbf{A}$ is parallel to $\hat{\mathbf{L}}_\mathbf{B}$;
$\mathbf{Z}$ is collinear with $\mathbf{O_A}$ and $\mathbf{O_B}$; and
$\mathbf{Z}$ is collinear with $\mathbf{O_A} + \hat{\mathbf{L}}_\mathbf{A}$ and $\mathbf{O_B} + \hat{\mathbf{L}}_\mathbf{B}$.

This serves to eliminate redundant stereographic maps from consideration. This elimination is justified by the simple observation that the baselines of two equivalent maps are, in a strong sense,

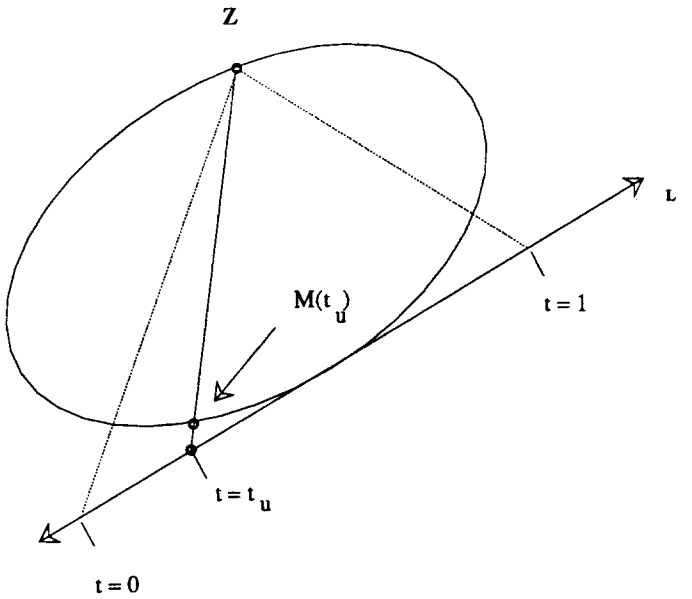

Figure 5.2: Inverting a Coordinatized Stereographic Map $\mathbf{M}(t)$.

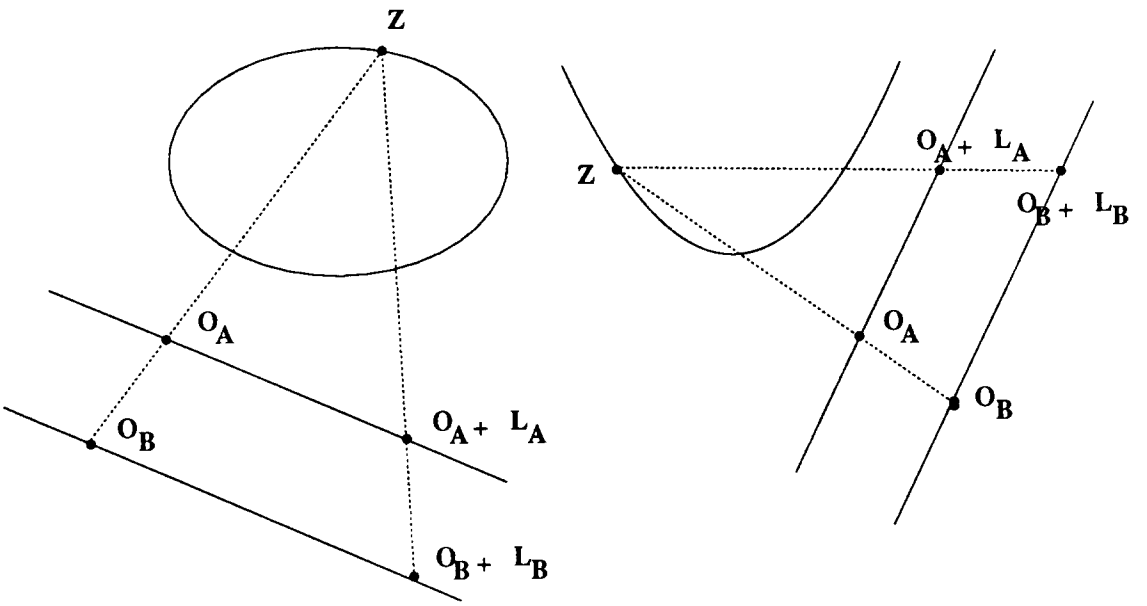

Figure 5.3: Equivalent Stereographic Maps of Two Conics.

indistinguishable when "viewed" from the maps' common center. That is, the baseline interval $\overline{t_1 t_2}$ produces an identical conic segment when sent through either map. Stereographic maps that are not equivalent we call *distinct*.

We demonstrate the construction and coordinatizion of a typical stereographic map. Consider the simple case of a unit circle tangent at its "South pole" to a horizontal line. Place the center of projection **Z** at the circle's "North pole" (Figure 5.4). The stereographic map through **Z** arises from the identification of each point **p** on **L** with the intersection, apart from **Z**, of the circle and the line through **p** and **Z**. This description could be considered purely geometric, apart from orientation. To *coordinatize* the map, we minimally require some origin **O**, basis vector $\hat{\mathbf{L}}$, and center **Z** on the circle but not on **L**. Here we might place **O** at the circle's South pole, **Z** at the North pole, **L** on the x-axis, and choose $\hat{\mathbf{L}}$ as the vector (1,0).

A line drawn from **Z**, the point $(0,2)$, to the point $\mathbf{p}(t) = (t,0)$ on **L** intersects the unit circle with center $(0,1)$ at the point

$$\mathbf{M}(t) = (\frac{4t}{4+t^2}, \frac{2t^2}{4+t^2}). \tag{5.2}$$

Thus, a homogeneous expression for the point $\mathbf{M}(t)$ is

$$\begin{aligned} M_x(t) &= 4t \\ M_y(t) &= 2t^2 \\ M_w(t) &= 4+t^2. \end{aligned} \tag{5.3}$$

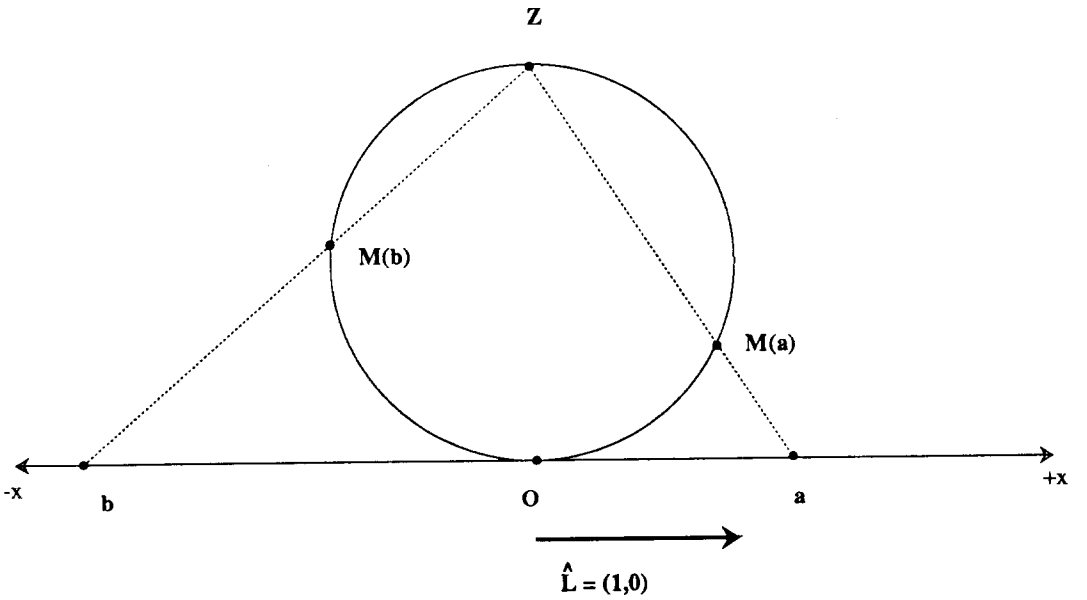

Figure 5.4: A Coordinatized Stereographic Map of a Circle Through its North Pole.

Equations 5.3 are quadratic polynomials. Indeed, following this procedure for *any* conic, with **Z** chosen on the conic, yields a rational quadratic expression for the generated point [17]. This expression may be represented as a linear combination of the quadratic Bézier basis functions (cf. §4.1). In the case of the circle map, for example, we can construct coefficients x_k, y_k, and w_k such that

$$\sum_k x_k B_k(t) \quad = M_x(t) \quad = 4t$$

$$\begin{aligned} \sum_k y_k B_k(t) &= M_y(t) &= 2t^2 \\ \sum_k w_k B_k(t) &= M_w(t) &= 4 + t^2. \end{aligned} \tag{5.4}$$

Interpreting the (x_k, y_k, w_k) as control points $\mathbf{p}_k$ produces a Bézier segment $\mathbf{P}(t)$, each point of which lies on the given unit circle.

This method of directly converting of a stereographic map to parametric form, though appealing in its geometric simplicity, is deficient in several ways. First, it will not, in general, yield a unique parametric representation. There are many sets of coefficients (x_k, y_k, w_k) that produce the homogeneous expressions of Equations 5.4. This squanders several important and appealing features of Bézier curves: their intuitive interpolatory and derivative behavior, and their convex hull property. Second, the conversion as outlined above makes no reference to the parametrization of the curve. That is, although we have established a Bézier curve $\mathbf{P}(t_p)$ and a coordinatized stereographic map $\mathbf{M}(t_m)$ that cover the same *geometric* point locus, there is no unique *a priori* relationship between the parameters t_p and t_m. As noted in §4.5, control over the parametrization of a Bézier curve is an important and useful degree of freedom.

Nevertheless, there is such a striking resemblance of form between stereographic maps (Equation 5.2), and rational quadratic Bézier curves (Equation 4.3), that it is natural to wonder if they are equivalent in some sense. Indeed, a novel result of this research is that *coordinatized stereographic maps of conics are equivalent to rational quadratic Bézier curves.* For each such Bézier curve there corresponds a unique coordinatized stereographic map, and vice versa. The remainder of this chapter is devoted to proving and demonstrating this result. In a subsequent chapter, we extend this work to the third spatial dimension and show an analogous relationship between stereographic maps of quadrics, and rational quadratic triangular Bézier patches that interpolate quadrics.

As we shall show, we can deduce from this equivalence that all stereographic maps of conics have a canonical, equivalent standard form. Moreover, this standard form is easily obtainable from any stereographic map.

5.2 A Theorem About Conics

We digress to prove a property of conics required for our demonstration of the equivalence of coordinatized stereographic maps and Bézier segments.

Proposition 1 *Consider any conic, three distinct points* $\mathbf{P}$, $\mathbf{A}$, *and* $\mathbf{C}$ *on the conic, and three lines* $\mathbf{p}$, $\mathbf{a}$, *and* $\mathbf{c}$ *respectively tangent to the conic at these points (Figure 5.5). Compute* $\mathbf{B}$, *the intersection of* $\mathbf{a}$ *and* $\mathbf{c}$. *Compute the line* $\mathbf{b}$ *through* $\mathbf{B}$ *parallel to* $\mathbf{p}$. *Compute the lines* $\mathbf{PA}$ *and* $\mathbf{PC}$ *through* $\mathbf{P}$ *and each of* $\mathbf{A}$ *and* $\mathbf{C}$, *respectively. Call the intersections of* $\mathbf{b}$ *with these lines* $\mathbf{A}'$ *and* $\mathbf{C}'$, *respectively. Then* $\mathbf{B}$ *is the midpoint of segment* $\overline{\mathbf{A}'\mathbf{C}'}$.

Proof 1 *We review two elements of computational machinery before proceeding. First, given a symmetric* 3×3 *conic matrix* ξ, *the* tangent *to the conic at a point* $\mathbf{P} = (x, y, w)$ *is simply*

$$\mathbf{p} = \xi \mathbf{P}^T \tag{5.5}$$

Proposition:

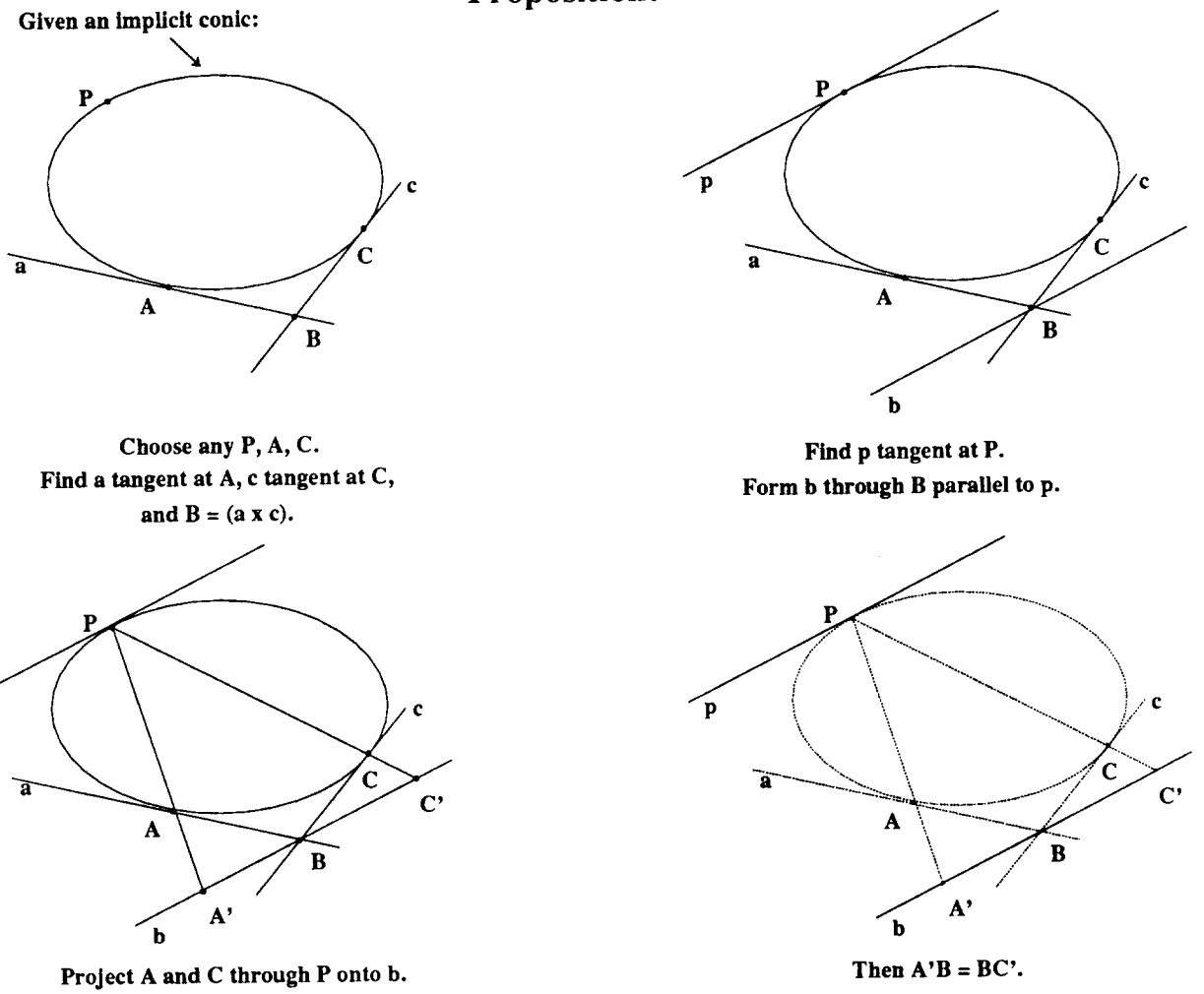

Figure 5.5: An Illustration of Proposition 1.

where lowercase $\mathbf{p}$ *denotes the line tangent to* ξ *at* $\mathbf{P}$. *The superscripted* T *signifies that* $\mathbf{P}$ *is transposed into a column vector.*

We use Equation 3.1, the statement that the intersection of two lines (a,b,c) *and* (r,s,t) *in homogeneous coordinates is their cross product:*

$$(bt - cs, cr - at, as - br).$$

This expression also describes the line through the points (a,b,c) *and* (r,s,t).

We work in a perspective coordinate space, and are free to choose a reference frame *of four points (Figure 5.6) and label them in a convenient manner [20]. Here, we choose* $\mathbf{P}$ *as the point* $(1,0,0)$; $\mathbf{A}$ *as* $(0,1,0)$; $\mathbf{C}$ *as* $(0,0,1)$; *and* $\mathbf{B}$ *as* $(1,1,1)$. *The line at infinity in this coordinate system does not have the usual equation* $(0,0,1)^T$. *Rather, it is transformed to some other line that we leave unspecified and write as* $\mathbf{m} = (m_0, m_1, m_2)^T$.

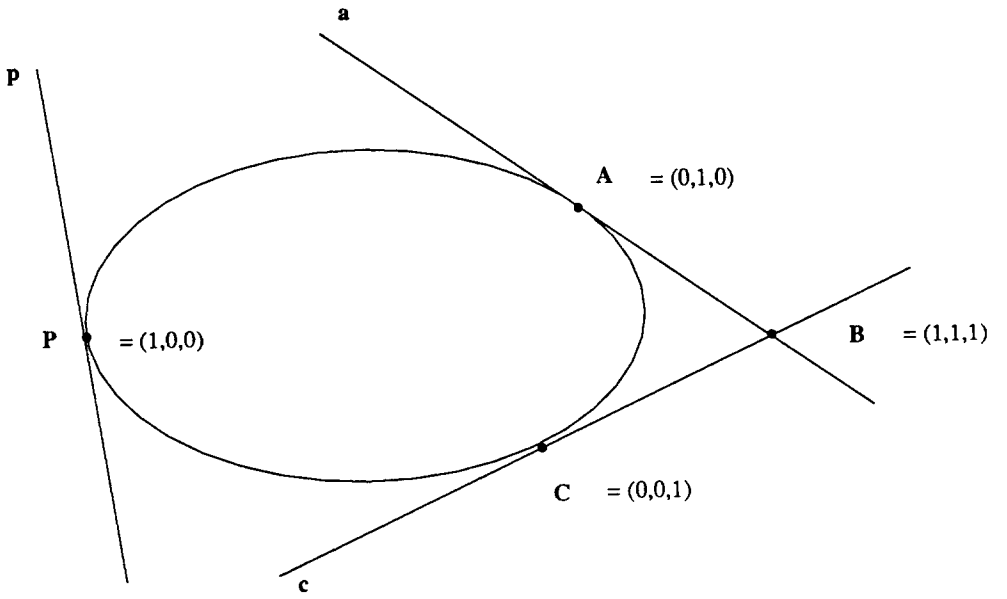

Figure 5.6: The Reference Frame of Proposition 1.

The goal of the proof is to show that the point $\mathbf{B}$ *lies on both diagonals of a parallelogram having* $\mathbf{A}'$ *and* $\mathbf{C}'$ *as opposing vertices (Figure 5.7). Since parallelogram diagonals bisect eachother,* $\mathbf{B}$ *will have been established as the midpoint of* $\mathbf{A}'$ *and* $\mathbf{C}'$.

The conic matrix ξ *is symmetric, and may be written*

$$\xi = \begin{pmatrix} 0 & a_2 & a_1 \\ a_2 & 0 & a_0 \\ a_1 & a_0 & 0 \end{pmatrix}.$$

We derive the entries of the matrix in the chosen reference frame. The tangent lines $\mathbf{a}$ *and* $\mathbf{c}$ *may be written both in terms of the conic matrix* ξ *and as lines through two points. The line* $\mathbf{a}$ *can be computed as*

$$\mathbf{a} = \xi \mathbf{A}^T = \xi \begin{pmatrix} 0 \\ 1 \\ 0 \end{pmatrix} = \begin{pmatrix} a_2 \\ 0 \\ a_0 \end{pmatrix} = \mathbf{A} \times \mathbf{B} = \begin{pmatrix} 1 \\ 0 \\ -1 \end{pmatrix},$$

and the line $\mathbf{c}$ *as*

$$\mathbf{c} = \xi \mathbf{C}^T = \xi \begin{pmatrix} 0 \\ 0 \\ 1 \end{pmatrix} = \begin{pmatrix} a_1 \\ a_0 \\ 0 \end{pmatrix} = \mathbf{B} \times \mathbf{C} = \begin{pmatrix} 1 \\ -1 \\ 0 \end{pmatrix}.$$

Thus $a_1 = a_2 = -a_0$, *determining the* a_i *to within an unimportant scale factor. Set* $a_0 = -1$; *then* $a_1 = a_2 = 1$, *completely specifying* ξ. *Computing the tangent* $\mathbf{p}$, *and rewriting* $\mathbf{a}$ *and* $\mathbf{c}$ *yields*

$$\mathbf{p} = \begin{pmatrix} 0 \\ 1 \\ 1 \end{pmatrix}; \qquad \mathbf{a} = \begin{pmatrix} 1 \\ 0 \\ -1 \end{pmatrix}; \qquad \mathbf{c} = \begin{pmatrix} 1 \\ -1 \\ 0 \end{pmatrix}.$$

Observe that $\mathbf{B} = \mathbf{a} \times \mathbf{c}$. *Thus* $\mathbf{B}$ *lies on the tangents* $\mathbf{a}$ *and* $\mathbf{c}$ *as expected.*

Next, construct the line $\mathbf{b}$ *through* $\mathbf{B}$ *and parallel to* $\mathbf{p}$. *Since* $\mathbf{b}$ *and* $\mathbf{p}$ *meet on* $\mathbf{m}$, *the line at infinity,* $\mathbf{b}$ *must be the line containing* $\mathbf{B}$ *and* $\mathbf{p}$*'s intersection with* $\mathbf{m}$. *That is,*

$$\begin{aligned} \mathbf{b} &= (\mathbf{p} \times \mathbf{m}) \times \mathbf{B} \\ &= (m_1 - m_2, -m_0, m_0) \times (1,1,1) \\ &= (2m_0, -m_0 + m_1 - m_2, -m_0 - m_1 + m_2). \end{aligned}$$

Compute $\mathbf{A}'$ *and* $\mathbf{C}'$ *by intersecting* $\mathbf{PA}$ *and* $\mathbf{PC}$, *respectively, with* $\mathbf{b}$:

$$\begin{aligned} \mathbf{A}' &= (\mathbf{P} \times \mathbf{A}) \times \mathbf{b} = (m_0 - m_1 + m_2, 2m_0, 0), \text{ and} \\ \mathbf{C}' &= (\mathbf{P} \times \mathbf{C}) \times \mathbf{b} = (m_0 + m_1 - m_2, 0, 2m_0). \end{aligned}$$

Finally, construct a parallelogram that has $\mathbf{A}'\mathbf{C}'$ *as one diagonal (Figure 5.7). Two of its sides are* $\mathbf{PA}'$ *and* $\mathbf{PC}'$. *The third and fourth sides meet in an auxiliary point* $\mathbf{Q}$, *the intersection of two lines: one through* $\mathbf{A}'$ *and parallel to* $\mathbf{PC}'$, *the second through* $\mathbf{C}'$ *and parallel to* $\mathbf{PA}'$.

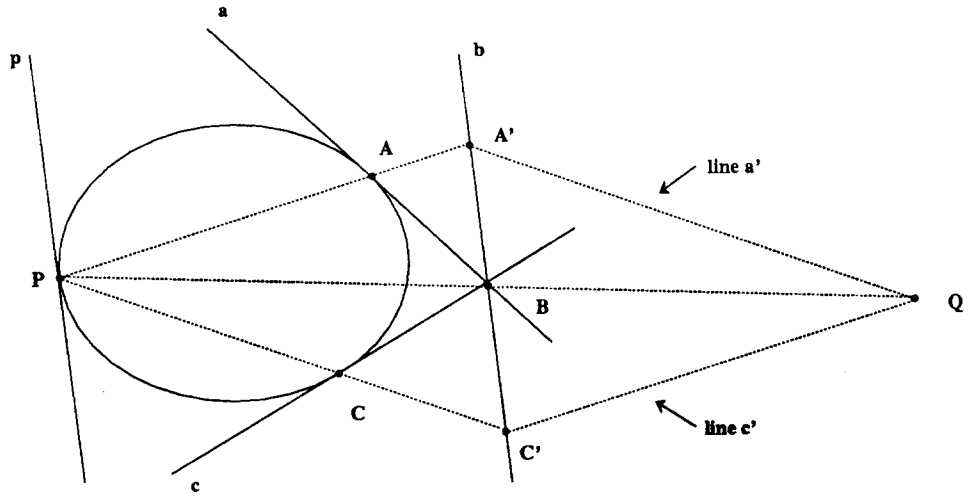

Figure 5.7: The Parallelogram $\mathbf{PA'QC'}$.

$\mathbf{Q}$ *is easily computed. Again employing* $\mathbf{m}$, *the line at infinity, we find the line* $\mathbf{a}'$ *through* $\mathbf{A}'$ *and parallel to* $\mathbf{PC}'$:

$$\begin{aligned} \mathbf{a}' &= ((\mathbf{p} \times \mathbf{A}') \times \mathbf{m}) \times \mathbf{C}' \\ &= (2m_0^2, -m_0(m_0 - m_1 + m_2), 2m_0 m_2) \\ &= (2m_0, -m_0 + m_1 - m_2, 2m_2), \end{aligned}$$

where we have divided through by m_0 in the last line. Similarly, $\mathbf{c}'$ may be found:

$$\begin{aligned}\mathbf{c}' &= ((\mathbf{p} \times \mathbf{C}') \times \mathbf{m}) \times \mathbf{A}' \\ &= (2m_0, 2m_1, -m_0 - m_1 + m_2).\end{aligned}$$

The auxiliary point $\mathbf{Q}$ is the intersection of $\mathbf{a}'$ and $\mathbf{c}'$:

$$\mathbf{Q} = \mathbf{a}' \times \mathbf{c}' = (-m_0^2 + (m_1 + m_2)^2, -2m_0(m_0 + m_1 + m_2), -2m_0(m_0 + m_1 + m_2)).$$

For $\mathbf{B}$ to lie on the line $\mathbf{PQ}$, the inner product of $\mathbf{PQ}$'s line equation with $\mathbf{B}$ must be zero:

$$\begin{aligned}(\mathbf{P} \times \mathbf{Q}) \cdot \mathbf{B} &= ((0, 2(m_0 + m_1 + m_2), -2(m_0 + m_1 + m_2)) \times (1,1,1)) \cdot (1,1,1) \\ &= (0, 2(m_0 + m_1 + m_2), -2(m_0 + m_1 + m_2)) \cdot (1,1,1) \\ &= 0.\end{aligned}$$

The diagonals of the parallelogram $\mathbf{PA'QC'}$ are $\mathbf{A'C'}$ and $\mathbf{PQ}$. The point $\mathbf{B}$ lies on diagonal $\mathbf{A'C'}$ by construction. We have shown $\mathbf{B}$ to lie on the second diagonal $\mathbf{PQ}$. Since diagonals of a parallelogram intersect at their midpoints, $\mathbf{B}$ is the midpoint of segment $\mathbf{A'C'}$. □

5.3 Constructing a Coordinatized Stereographic Map $\mathbf{M}(t)$ From a Rational Quadratic Bézier Segment $\mathbf{P}(t)$

With the proposition of segment congruence established, we may demonstrate the first direction of the postulated equivalence: that for every rational quadratic Bézier curve $\mathbf{P}(t)$, there exists a unique geometric stereographic map of conic ξ with center of projection $\mathbf{Z}$ and baseline $\mathbf{L}$, and a unique coordinatized stereographic map $\mathbf{M}(t)$, such that

$$\mathbf{P}(t) = \mathbf{M}(t) \qquad \text{for all } t. \tag{5.6}$$

Moreover, we show that for any Bézier segment $\mathbf{P}(t)$ an equivalent coordinatized map $\mathbf{M}(t)$ is trivially obtainable.

Consider any three Bézier control points $\mathbf{p}_k = (x_k, y_k, w_k)$. They comprise a rational quadratic Bézier segment $\mathbf{P}(t)$ that covers some conic ξ. Four values of t are of particular interest: $\mathbf{P}(0) = \mathbf{p}_0$; $\mathbf{P}(\frac{1}{2}) = \mathbf{p}_s$; $\mathbf{P}(1) = \mathbf{p}_2$; and $\mathbf{P}(\infty)$, which we earlier labeled as $\mathbf{P}$, the pole (cf. §5.1). Recall from §4.5.3, Equation 4.26, that $\mathbf{p}_s$ and $\mathbf{P}$ are collinear with the middle control point $\mathbf{p}_1$ (cf. Figure 4.12). Thus we may extend the line $\overline{\mathbf{p}_1\mathbf{p}_s}$ to find that it intersects ξ at the pole $\mathbf{P}$.

Figure 5.8 depicts the construction. As in the proof of Proposition 1, we construct the line $\mathbf{p}$ tangent to ξ at $\mathbf{P}$, and the line $\mathbf{b}$ through $\mathbf{p}_1$ and parallel to $\mathbf{p}$. Project $\mathbf{p}_0$ and $\mathbf{p}_2$ through $\mathbf{P}$ onto $\mathbf{b}$, labeling the projected points $\mathbf{A}'$ and $\mathbf{C}'$. Choose the map center of projection $\mathbf{Z}$ coincident with the Bézier curve pole $\mathbf{P}$. Together, the conic ξ, the line $\mathbf{b}$ and the point $\mathbf{Z}$ (not on $\mathbf{b}$) comprise a geometric stereographic map. Note that the constructed map is in standard form, since its pole and center are coincident (or, equivalently, since the baseline $\mathbf{L}$ is parallel to the conic's tangent at $\mathbf{Z}$).

We seek a coordinatization of this geometric map that will produce a map $\mathbf{M}(t)$ equivalent to the Bézier curve $\mathbf{P}(t)$. We can achieve such a coordinatization easily. Choose the baseline origin $\mathbf{O}$

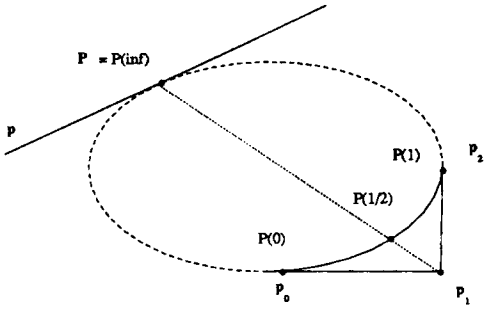

Given any Bezier control points, comprising a curve P(t):

Find P, the point at P(infinity), and p, the tangent at P.

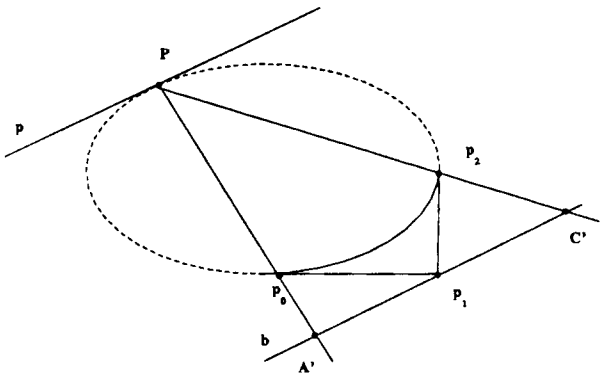

Form b through B parallel to p.

Project control points through P onto baseline b.

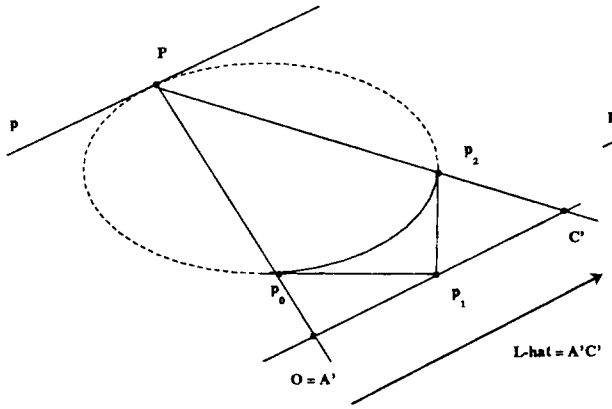

Coordinatize the map. Choose O = A', L-hat = vector from A' to C'.

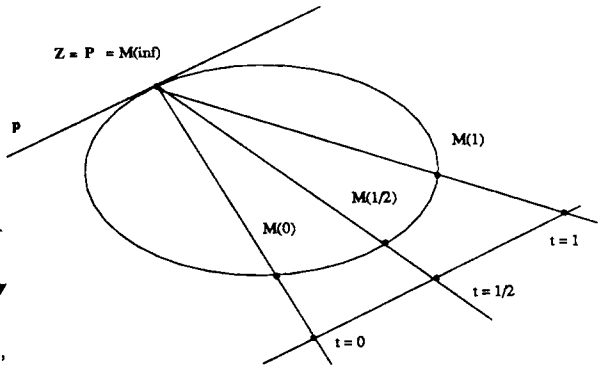

The map M(t) is equivalent to the Bezier curve P(t).

Figure 5.8: Constructing a Coordinatized Stereographic Map $\mathbf{M}(t)$ From a Bézier Segment $\mathbf{P}(t)$.

as $\mathbf{A}'$, and the unit vector $\hat{\mathbf{L}}$ as the directed line segment $\overline{\mathbf{A}'\mathbf{C}'}$. That is, coordinatize the line $\mathbf{b}$ as the t-axis, labeling $\mathbf{A}'$ as $t = 0$, and $\mathbf{C}'$ as $t = 1$.

By construction, the coordinatized map $\mathbf{M}(t)$ agrees with $\mathbf{P}(t)$ for $t = 0$, since it sends the point $\mathbf{O} + 0\hat{\mathbf{L}} = \mathbf{A}'$ to $\mathbf{p}_0$, the Bézier point $\mathbf{P}(t = 0)$. Similarly, the maps agree at $t = 1$, since $\mathbf{O} + 1\hat{\mathbf{L}} = \mathbf{C}'$ is sent to $\mathbf{p}_2$, or $\mathbf{P}(t = 1)$. Moreover, $\mathbf{M}(t)$ agrees with $\mathbf{P}(t)$ at infinity, since by construction $\mathbf{M}(\infty) = \mathbf{P} = \mathbf{P}(\infty)$, the pole of the Bézier segment.

Finally, consider either map evaluated at $t_s = \frac{1}{2}$. The Bézier curve point $\mathbf{P}(\frac{1}{2})$ is simply $\mathbf{p}_s$, the intersection of the line $\overline{\mathbf{p}_1\mathbf{P}}$ with the conic ξ (by Equation 4.26, §4.5.3). Consider the baseline point $t = \frac{1}{2}$. This is $\mathbf{O} + \frac{1}{2}\hat{\mathbf{L}}$, or halfway from the origin $\mathbf{A}'$ to the point $\mathbf{C}'$. By Proposition 1, this midpoint is exactly $\mathbf{B}$, the middle control point of the Bézier segment. The stereographic map must send this point to $\mathbf{p}_s$, the point on ξ collinear with $\mathbf{P}$ and $\mathbf{B}$ (where $\mathbf{B} = \mathbf{p}_1$). Thus $\mathbf{P}(\frac{1}{2}) = \mathbf{M}(\frac{1}{2})$; that is, the maps $\mathbf{P}(t)$ and $\mathbf{M}(t)$ produce the same point for $t = \frac{1}{2}$.

We have shown that the two formulations $\mathbf{P}(t)$ and $\mathbf{M}(t)$ agree at four distinct parameter values: $t = 0, \frac{1}{2}, 1$, and ∞. A brief argument shows that they must therefore agree for all values of t.

Consider two three-valued rational quadratic expressions $\mathbf{P}(t) = [P_x(t), P_y(t), P_w(t)]$ and $\mathbf{M}(t) = [M_x(t), M_y(t), M_w(t)]$. The expressions agree, after division by w, for four distinct values of t. Expand $\mathbf{P}(t)$ and $\mathbf{M}(t)$, writing them explicitly as rational quadratic polynomials in t:

$$\mathbf{P}(t) = \left(\frac{P_x(t)}{P_w(t)}, \frac{P_y(t)}{P_w(t)}\right) = \left(\frac{at^2 + bt + c}{gt^2 + ht + i}, \frac{dt^2 + et + f}{gt^2 + ht + i}\right), \text{ and}$$

$$\mathbf{M}(t) = \left(\frac{M_x(t)}{M_w(t)}, \frac{M_y(t)}{M_w(t)}\right) = \left(\frac{a't^2 + b't + c'}{g't^2 + h't + i'}, \frac{d't^2 + e't + f'}{g't^2 + h't + i'}\right).$$

Both $\mathbf{P}(t)$ and $\mathbf{M}(t)$ have nine coefficients, and eight scalar degrees of freedom. Each value of t input to these expressions yields, after division by w, a two-vector (x, y). Matching the expressions at four distinct values of t provides eight knowns, fully determining the eight unknown scalar coefficients. Thus any $\mathbf{P}(t)$ and $\mathbf{M}(t)$ that match for four distinct values of t are *identical expressions*, and must therefore represent *identical curves*. That is, they cover the same point locus, and reach every point of this locus at identical parameter values.

We have arranged by construction that the parametric representations $\mathbf{P}(t)$ and $\mathbf{M}(t)$ are *geometrically* and *parametrically* equivalent. The construction unifies two *interpretations* of the single expression $\mathbf{P}(t)$ or $\mathbf{M}(t)$: as a Bézier curve segment, or weighted sum of vector-valued control points; and as a stereographic map, an identification of points on some coordinatized baseline with their images under projection on some implicit conic.

With this dual interpretation come advantages of both the Bézier and stereographic representations. From the Bézier formulation we obtain a host of familar, useful properties, including interpolation, derivatives, convex hull, and efficient subdivision. Constructing the equivalent coordinatized stereographic map yields, foremost, an extra measure of geometric intuition into the nature of the Bézier formulation and its deep connection to stereographic maps. Moreover, since stereographic maps are trivially invertible, their equivalence to Bézier curves yields a *trivial inversion procedure* for Bézier curves onto their preimages (cf. Figure 5.2). Compare this to the difficulty of inverting a general Bézier curve expression (for example, Equations 4.3, §4.1.1) to find t for some given $(x, y) = \mathbf{P}(t)$.

We have demonstrated a simple construction that, for any Bézier curve $\mathbf{P}(t)$ specified in terms of

its homogeneous control points, produces a unique, coordinatized map $\mathbf{M}(t)$ identical to $\mathbf{P}(t)$. However, this is only one direction of the curve-map correspondence. We next demonstrate a construction that, given a coordinatized stereographic map $\mathbf{M}(t)$, produces a unique set of Bézier control points $\mathbf{p}_k$ comprising a curve segment $\mathbf{P}(t)$ equivalent to $\mathbf{M}(t)$.

We could not achieve such a construction by, for example taking a simple time reversal or dual of the construction in this section. In constructing stereographic maps from Bézier segments, we choose the map baseline $\mathbf{L}$ always parallel to $\mathbf{p}$, the tangent to the conic at $\mathbf{Z}$ (and at $\mathbf{P}$). Thus, the map constructed is in standard form. However, stereographic maps may in general have any line as baseline, provided that it does not contain $\mathbf{Z}$. Thus the space of all maps *output* by the curve→map construction of this section is a proper subset of the space of all maps that may be *input* to its map→curve counterpart. A more general approach is required.

5.4 Another Theorem About Conics

Again, we must digress to prove a property of conics.

Proposition 2 *Consider any conic, and four distinct points* $\mathbf{E}$, $\mathbf{F}$, $\mathbf{A}$, *and* $\mathbf{C}$ *on the conic (Figure 5.9). Find the lines* $\mathbf{a}$ *and* $\mathbf{c}$ *tangent to the conic at* $\mathbf{A}$ *and* $\mathbf{C}$, *respectively. Compute* $\mathbf{B}$, *the intersection of* $\mathbf{a}$ *and* $\mathbf{c}$. *Compute the line* $\mathbf{b}$ *through* $\mathbf{B}$ *parallel to the line through* $\mathbf{E}$ *and* $\mathbf{F}$. *Project points* $\mathbf{A}$ *and* $\mathbf{C}$ *through* $\mathbf{E}$ *onto* $\mathbf{b}$, *creating the points* $\mathbf{A}'$ *and* $\mathbf{C}'$, *respectively. Find* $\mathbf{D}$, *the conic's intersection apart from* $\mathbf{F}$ *with the line through* $\mathbf{B}$ *and* $\mathbf{F}$. *Project* $\mathbf{D}$ *through* $\mathbf{E}$ *onto* $\mathbf{b}$, *creating* $\mathbf{D}'$. *Then* $\mathbf{D}'$ *is the midpoint of the segment* $\overline{\mathbf{A}'\mathbf{C}'}$.

Proof 2 *We choose a* reference frame *of four points (Figure 5.10) and label them in a convenient manner [20]. Here, we choose* $\mathbf{E}$ *as the point* $(1,0,0)$; $\mathbf{F}$ *as* $(0,1,0)$; $\mathbf{A}$ *as* $(0,0,1)$; *and* $\mathbf{C}$ *as* $(1,1,1)$. *The line at infinity is left unspecified and will be denoted simply as* $\mathbf{m} = (m_0, m_1, m_2)^T$.

The goal of the proof will be to show that the point $\mathbf{D}'$ *lies on both diagonals of parallelogram having* $\mathbf{A}'$ *and* $\mathbf{C}'$ *as opposing vertices. Thus* $\mathbf{D}'$ *will have been established as the midpoint of* $\mathbf{A}'$ *and* $\mathbf{C}'$.

The conic matrix ξ *is symmetric, and may be written as*

$$\xi = \begin{pmatrix} 0 & a_2 & a_1 \\ a_2 & 0 & a_0 \\ a_1 & a_0 & 0 \end{pmatrix}.$$

Although we cannot completely specify the entries of the matrix in the transformed coordinate system, we can deduce one constraint on the a_k *from the fact that the point* $\mathbf{C}$ *lies on* ξ:

$$\begin{aligned} \mathbf{C} \cdot \xi \cdot \mathbf{C}^T &= (1,1,1) \cdot \begin{pmatrix} 0 & a_2 & a_1 \\ a_2 & 0 & a_0 \\ a_1 & a_0 & 0 \end{pmatrix} \cdot \begin{pmatrix} 1 \\ 1 \\ 1 \end{pmatrix} \\ &= 2(a_0 + a_1 + a_2) \\ &= 0. \end{aligned}$$

Proposition:

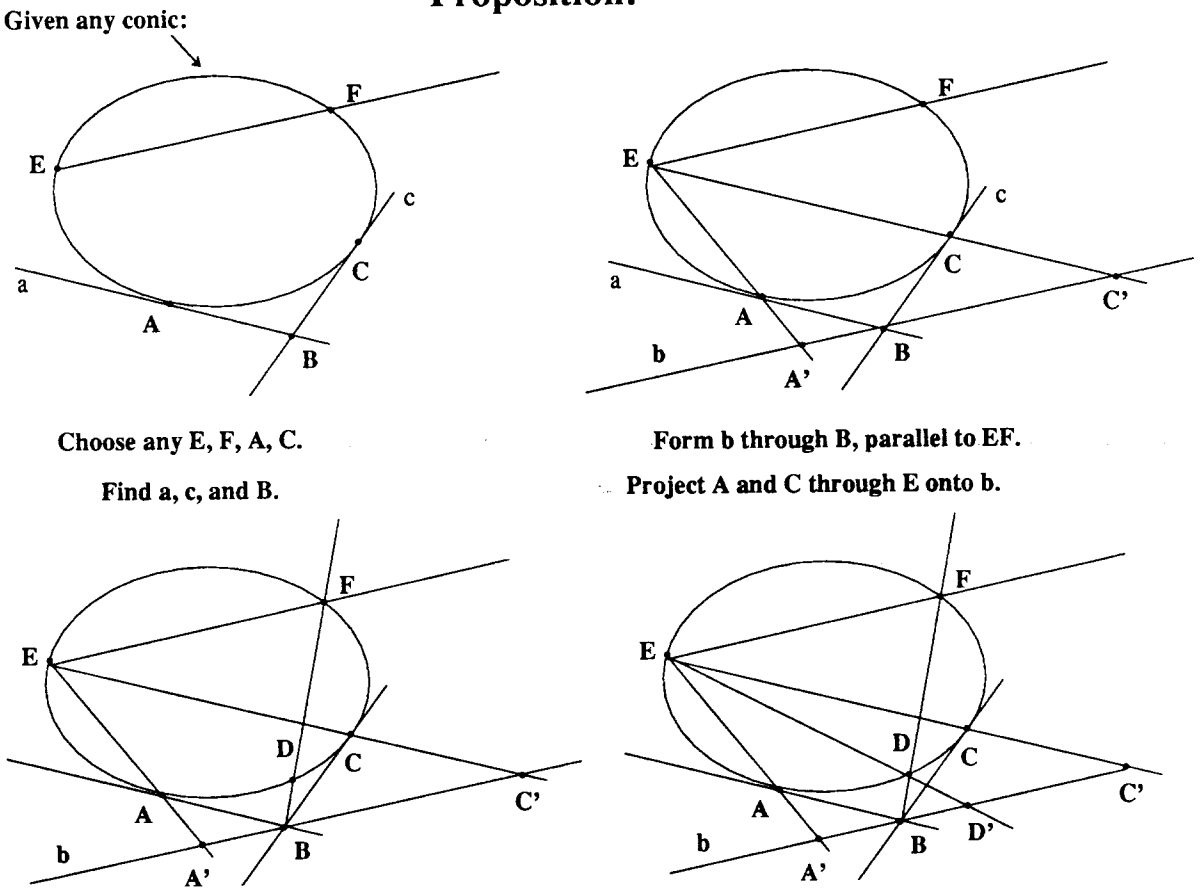

Then A'D' = D'C'.

Figure 5.9: An Illustration of Proposition 2.

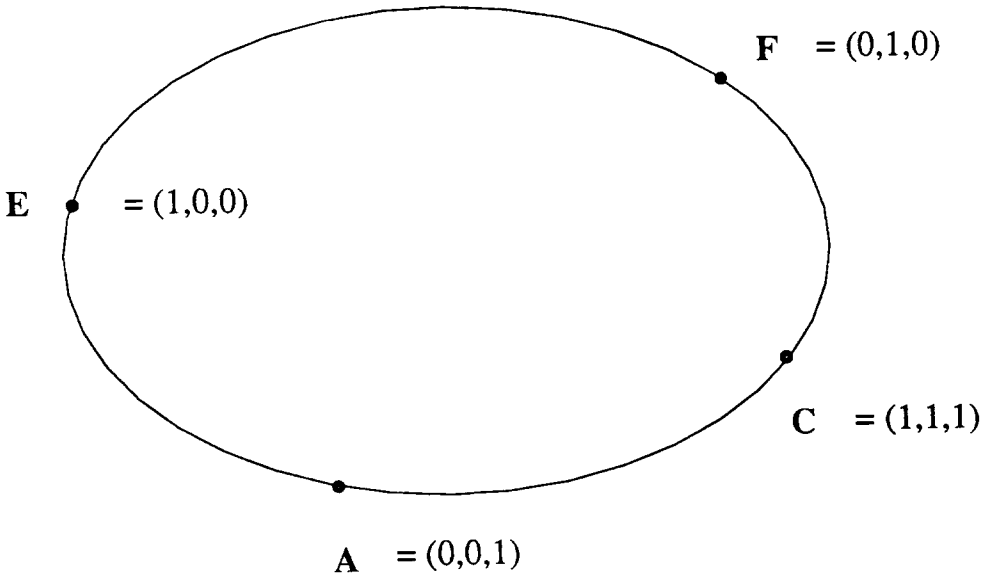

Figure 5.10: The Reference Frame of Proposition 2.

Thus we have one equation and three unknowns, and may eliminate one of the a_k. *Solving for* a_2 *gives*

$$a_2 = -a_0 - a_1.$$

Henceforth, a_2 *will be replaced wherever it appears by* $(-a_0 - a_1)$.

The tangent line $\mathbf{a}$ *may be written in terms of* $\mathbf{A}$ *and* ξ *as*

$$\mathbf{a} = \xi \mathbf{A}^T = \xi \begin{pmatrix} 0 \\ 0 \\ 1 \end{pmatrix} = \begin{pmatrix} a_1 \\ a_0 \\ 0 \end{pmatrix},$$

and the line $\mathbf{c}$ *in terms of* $\mathbf{C}$ *and* ξ *as*

$$\mathbf{c} = \xi \mathbf{C}^T = \xi \begin{pmatrix} 1 \\ 1 \\ 1 \end{pmatrix} = \begin{pmatrix} -a_0 \\ -a_1 \\ a_0 + a_1 \end{pmatrix}.$$

Compute $\mathbf{B}$, *the tangent intercept of* $\mathbf{a}$ *and* $\mathbf{c}$:

$$\mathbf{B} = \mathbf{a} \times \mathbf{c} = (a_0, -a_1, a_0 - a_1).$$

Construct the line $\mathbf{b}$ *through* $\mathbf{B}$ *and parallel to* $\mathbf{EF}$:

$$\mathbf{b} = ((\mathbf{E} \times \mathbf{F}) \times \mathbf{m}) \times \mathbf{B} = \begin{pmatrix} m_0(a_1 - a_0) \\ m_1(a_1 - a_0) \\ a_0 m_0 - a_1 m_1 \end{pmatrix}.$$

Project $\mathbf{A}$ *and* $\mathbf{C}$ *through* $\mathbf{P}$ *onto* $\mathbf{b}$, *by intersecting the lines* $\mathbf{EA}$ *and* $\mathbf{EC}$ *with* $\mathbf{b}$:[2]

$$\begin{aligned} \mathbf{A}' &= (\mathbf{E} \times \mathbf{A}) \times \mathbf{b} = (a_1 m_1 - a_0 m_0, 0, m_0(a_1 - a_0)), \text{ and} \\ \mathbf{C}' &= (\mathbf{E} \times \mathbf{C}) \times \mathbf{b} = (a_0 m_1 - a_0 m_0, m_0(a_1 - a_0), m_0(a_1 - a_0)). \end{aligned}$$

[2]The equations for $\mathbf{A}'$ and $\mathbf{C}'$ are not symmetric with respect to the a_k or m_k. This is due to the choice of projective reference frame.

Find the intersection of the line $\mathbf{BF}$ *with the conic* ξ. *There are two such points of intersection;* $\mathbf{F}$ *and some point (say,* $\mathbf{D}$*) on segment* $\mathbf{BF}$. *Every linear combination of* $\mathbf{E}$ *and* $\mathbf{F}$ *lies on the line* $\mathbf{EF}$*; one combination lying on* ξ *is*

$$\begin{aligned}\mathbf{D} &= \frac{2}{2+(a_0+a_1)^2}\mathbf{B} + \frac{(a_0+a_1)^2}{2+(a_0+a_1)^2}\mathbf{F} \\ &= (2a_0, a_0-a_1, 2(a_0-a_1)).\end{aligned}$$

As with $\mathbf{A}$ *and* $\mathbf{C}$, *project* $\mathbf{D}$ *through* $\mathbf{E}$ *onto* $\mathbf{b}$:

$$\begin{aligned}\mathbf{D}' &= (\mathbf{E}\times\mathbf{D})\times\mathbf{b} \\ &= (2a_0m_0 - a_0m_1 - a_1m_1, m_0(a_0-a_1), 2m_0(a_0-a_1)).\end{aligned}$$

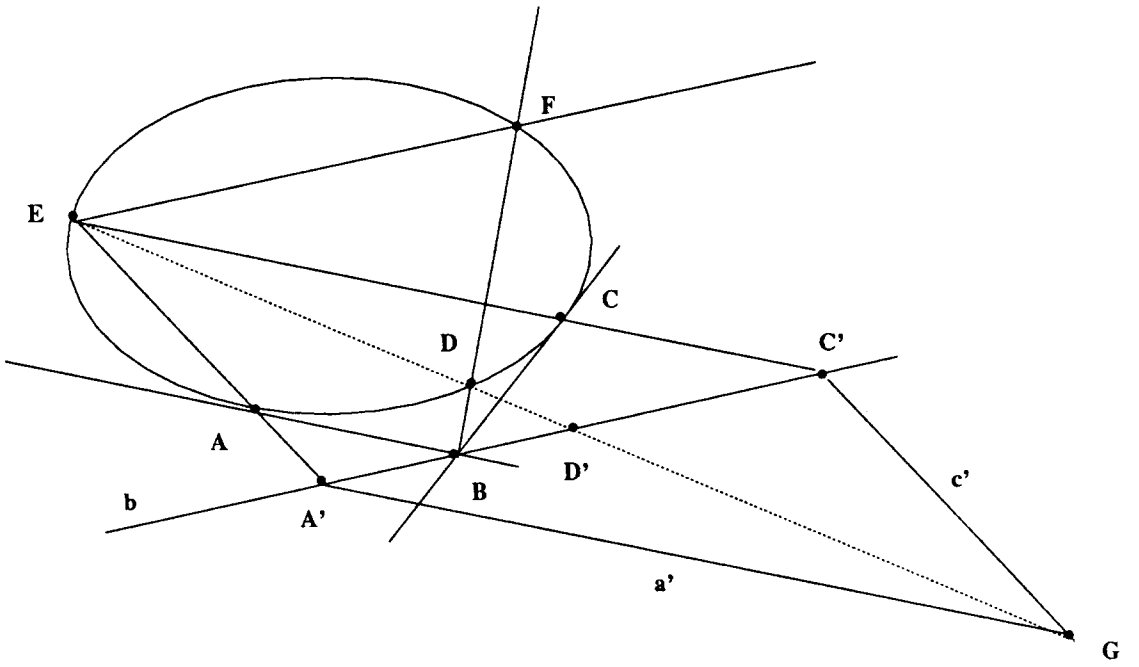

Figure 5.11: The Parallelogram $\mathbf{EA'GC'}$.

The final step of the proof is the construction of a parallelogram with $\mathbf{EA'}$ *and* $\mathbf{EC'}$ *as two sides, and* $\mathbf{A'C'}$ *as one diagonal (Figure 5.11). The parallelogram has two more sides; one through* $\mathbf{A'}$ *and parallel to* $\mathbf{EC'}$, *the second through* $\mathbf{C'}$ *and parallel to* $\mathbf{EA'}$. *Employing* $\mathbf{m}$, *the line at infinity, find the line* $\mathbf{a'}$ *parallel to* $\mathbf{EC'}$ *and through* $\mathbf{A'}$:

$$\begin{aligned}\mathbf{a}' &= ((\mathbf{E}\times\mathbf{C}')\times\mathbf{m})\times\mathbf{A}' \\ &= (m_0(a_1-a_0), a_1(2m_1+m_2) - a_0(m_0+m_1+m_2), a_0m_0 - a_1m_1).\end{aligned}$$

Similarly, $\mathbf{c'}$ *may be found:*

$$\begin{aligned}\mathbf{c}' &= ((\mathbf{E}\times\mathbf{A}')\times\mathbf{m})\times\mathbf{C}' \\ &= (m_0(a_0-a_1), a_1m_2 - a_0(m_0-m_1+m_2), m_2(a_0-a_1)).\end{aligned}$$

The intersection $\mathbf{G}$ *of these two sides may then be computed:*

$$\begin{aligned}\mathbf{G} &= \mathbf{a}' \times \mathbf{c}' \\ &= ((a_0 m_0 - a_0 m_1 - a_0 m_2 + a_1 m_2), \\ &\quad m_0(a_0 - a_1), \\ &\quad 2m_0(a_0 - a_1)).\end{aligned}$$

For $\mathbf{D}'$ *to lie on the line* $\mathbf{EG}$*, the inner product of* $\mathbf{D}'$ *with* $\mathbf{EG}$*'s line equation must be zero. Some manipulation indeed shows that*

$$(\mathbf{E} \times \mathbf{G}) \cdot \mathbf{D}' = 0. \tag{5.7}$$

The diagonals of the parallelogram $\mathbf{EA'GC'}$ *are* $\mathbf{A'C'}$ *and* $\mathbf{EG}$*.* $\mathbf{D}'$ *lies on the diagonal* $\mathbf{A'C'}$ *by construction. We have shown* $\mathbf{D}'$ *to lie on the second diagonal* $\mathbf{EG}$*. Since diagonals of a parallelogram bisect eachother,* $\mathbf{D}'$ *is the midpoint of segment* $\mathbf{A'C'}$*.* □

Proposition 1, derived in §5.2, emerges as a special case of Proposition 2 when $\mathbf{E} = \mathbf{F}$.

5.5 Constructing a Bézier Segment From a Coordinatized Stereographic Map

Our goal before digressing was to exhibit a construction that, given any coordinatized stereographic map $\mathbf{M}(t)$ of a conic ξ, produces the control points $\mathbf{p}_k$ of a rational quadratic Bézier segment $\mathbf{P}(t)$ such that $\mathbf{P}(t) = \mathbf{M}(t)$ for all t. The construction requires as input some coordinatized stereographic map: that is, a center $\mathbf{Z}$, a baseline $\mathbf{L}$ encoded as an origin $\mathbf{O}$ and unit vector $\hat{\mathbf{L}}$; and a rational quadratic expression $\mathbf{M}(t)$ such that $\mathbf{M}(t)$ lies on ξ, and $\mathbf{Z}$, $\mathbf{M}(t)$, and $\mathbf{O} + t\hat{\mathbf{L}}$ are collinear, for all t (Figure 5.12). The construction does *not* require as input, or employ at any time, the conic ξ in implicit form.

Mark the points $t = 0$, $t = \frac{1}{2}$, and $t = 1$ on $\mathbf{L}$, labeling them (respectively) $\mathbf{A}'$, $\mathbf{D}'$, and $\mathbf{C}'$. Intersect the lines $\mathbf{ZA}'$ and $\mathbf{ZC}'$ with the conic ξ to produce points $\mathbf{A}$ and $\mathbf{C}$ (distinct from $\mathbf{Z}$). Form the tangent intercept $\mathbf{B}$ of the lines $\xi\mathbf{A}^T = \mathbf{M}'(0)$ and $\xi\mathbf{C}^T = \mathbf{M}'(1)$ tangent to the conic (respectively) at $\mathbf{A}$ and $\mathbf{C}$.

Construct the Bézier control points (ignoring weights for the moment):

$$\begin{aligned}\mathbf{p}_0 &= \mathbf{A} \\ \mathbf{p}_1 &= \mathbf{B} \\ \mathbf{p}_2 &= \mathbf{C}.\end{aligned}$$

Form the line $\mathbf{p}$ through $\mathbf{Z}$ parallel to the baseline $\mathbf{b}$, and intersect $\mathbf{p}$ with ξ, labeling the resulting point $\mathbf{P}$. (Clearly $\mathbf{Z}$ and $\mathbf{P}$ are coincident if and only if line $\mathbf{p}$ is tangent to ξ at $\mathbf{Z}$.) The point $\mathbf{P}$ is the point reached by $\mathbf{M}(t)$ for infinite t; thus the construction must assure that $\mathbf{P}$ is the Bézier pole $\mathbf{P}(\infty)$ as well. This is accomplished with the pole-conic convention of §4.5.4. Here, the shoulder point implied by pole $\mathbf{P}$ is the intersection of segment $\mathbf{BP}$ with ξ; that is, the point labeled $\mathbf{D}$ in Figures 5.11 and 5.12.

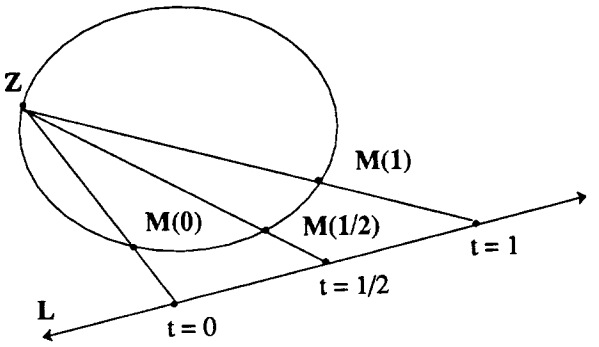

Given any coordinatized stereographic map:

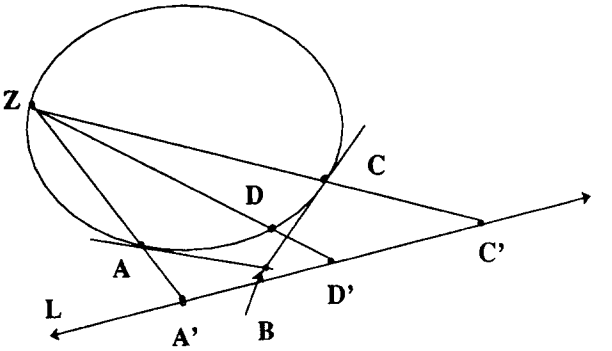

Project A' and C' through Z onto A and C.
Form B, the tangent intercept of A and C.

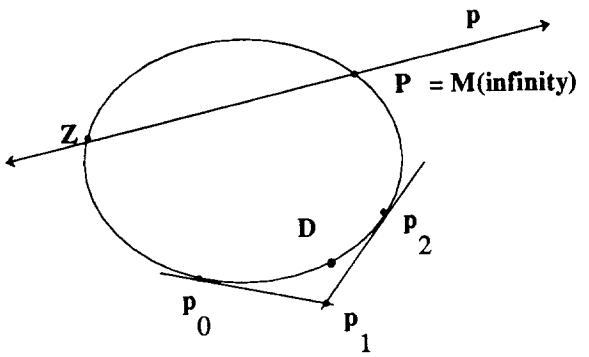

Construct p through Z parallel to baseline L.
Label as P the conic's intersection with p.
Relabel A, B, C as p_0, p_1, p_2

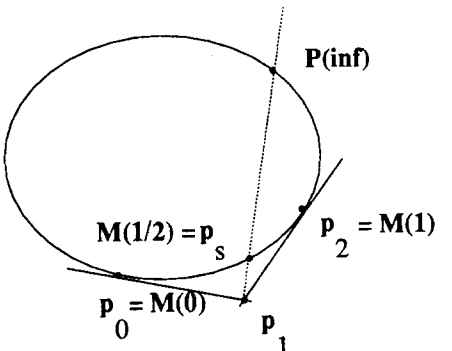

Relabel D, P as p_s, P(inf).
Pole-conic parameterization convention yields
weight ratios $w_0 : w_1 : w_2$.

Figure 5.12: Constructing a Bézier Segment $\mathbf{P}(t)$ from a Coordinatized Stereographic Map $\mathbf{M}(t)$.

The result is a Bézier curve $\mathbf{P}(t)$ identical to $\mathbf{M}(t)$ for all t. By construction, $\mathbf{P}(0) = \mathbf{M}(0)$ and $\mathbf{P}(1) = \mathbf{M}(1)$. By Proposition 2, point $\mathbf{D}$ is collinear with $t = \frac{1}{2}$ under the coordinatized stereographic map $\mathbf{M}(t)$. Thus $\mathbf{D} = \mathbf{M}(\frac{1}{2})$. But $\mathbf{D}$ is also collinear with points $\mathbf{B}$ and $\mathbf{P}$. All Bézier segments have $\mathbf{p}_1$, $\mathbf{P}(1/2)$, and $\mathbf{P}(\infty)$ collinear. Thus we can always arrange through the pole-conic parameterization convention that the $\mathbf{p}_k$ are weighted so that $\mathbf{P}(\frac{1}{2}) = \mathbf{D} = \mathbf{p}_s$, and $\mathbf{P}(\infty) = \mathbf{P}$. The result is a Bézier segment $\mathbf{P}(t)$ that agrees with $\mathbf{M}(t)$ for four values of t, and is thus identical to $\mathbf{M}(t)$.

This construction has a notable property: it is *symmetric* with respect to the order of operations. That is, rather than taking a coordinatized map as input, and proceeding in Figure 5.12 from upper left to lower right, we can take a Bézier segment as input, and proceed from lower right to upper left. A striking aspect of this reversal is that, in moving from step 4 (lower right) to step 3 (lower left), we may choose *any* point on the implicit conic (apart from $\mathbf{p}_0$ or $\mathbf{p}_2$) as the center of projection $\mathbf{Z}$. This follows directly from Proposition 2, applied to the four points $\mathbf{Z}$, $\mathbf{P}$, $\mathbf{A}$, and $\mathbf{C}$. We exploit this property in Chapter 8, when we generalize the correspondence introduced here to three dimensions.

We remarked earlier that the input space (i.e., the space of all stereographic maps of conics) of this construction is a proper superset of the output space of the analogous procedure transforming Bézier curves to maps. If stereographic maps are restricted so that the baseline $\mathbf{L}$ is parallel to the conic tangent at the center of projection $\mathbf{Z}$, then the two constructions are simple reversals of each other.

Chapter 6

A Unified Representation for Parametric Conics

The constructions exhibited in the previous chapter illustrate the advantages of combining the Bézier and stereographic map formulations. The stereographic map is simplicity itself; a synthetic method for generating the conic is encoded in a point, line, and implicit conic (in the geometric map), or in a single rational quadratic polynomial expression (in the coordinatized map). We noted earlier the appealing result that such maps are trivially invertible. But stereographic maps encode no *direct* information about, for example, the convex hull of a segment swept by a particular parameter range, or the derivative of the swept curve at fixed parametric endpoints. These quantities are available through computation on the map, although the effort extended might be considerable. The Bézier formulation, by contrast, provides this information for the cost of a small, constant-time computation. Moreover, the Bézier formulation submits to highly efficient evaluation and rendering via de Casteljau subdivision and its rational generalization ([7], [11]).

The conic matrix ξ defines the implicit form of any particular conic, and plays an important role in the formulation and proof of Propositions 1 and 2. It may seem that the constructions exhibited here also require the conic to be represented in implicit form, perhaps at some intermediate step in the computation. Certainly if this were so, the constructions would be less valuable, since any curve representation scheme employing them would be forced to retain the notion of, and machinery for, implicit representations.

We reemphasize that both constructions *operate directly on two types of parametric representation: coordinatized stereographic maps and rational quadratic Bézier curves.* At no time is the curve represented as, or required to be represented as, a zero set of an implicit function. To show this, we briefly revisit the constructions.

The first construction took as input three control points of a rational quadratic Bézier curve, and produced an equivalent coordinatized map. One step was to find the pole, and tangent at the pole, of the Bézier curve $\mathbf{P}(t)$. This step can easily be done within the parametric formulation, simply by evaluating the limit of the patch expression $\mathbf{P}(t)$ and its derivative as $t \to \infty$ (or, equivalently, evaluating the complementary patch expression $\tilde{\mathbf{P}}(t)$ and its derivative at $t = \frac{1}{2}$). The remainder of the construction is purely geometric and has no dependence on the particular form of ξ.

In turn, the second construction takes as input a coordinatized map $\mathbf{M}(t)$, and produces an equivalent rational quadratic Bézier curve $\mathbf{P}(t)$. Here, conic tangents are required at $t = 0$ and

$t = 1$. These may be obtained directly by differentiating $\mathbf{M}(t)$. In the construction, point $\mathbf{P}$ (Figure 5.12) is identified as the intersection of a line in general position with the conic ξ. But $\mathbf{P}$ is simply the pole of the map $\mathbf{M}(t)$; that is, the point $\mathbf{M}(\infty)$. Thus $\mathbf{P}$ is obtainable directly from the map expression $\mathbf{M}(t)$.

A coordinatized stereographic map $\mathbf{M}(t)$ is a rational polynomial in t, interpreted as a map of a line onto some desired conic. A rational quadratic Bézier curve is a rational polynomial in t, interpreted as a weighted parametric sum of discrete points. The constructions exhibited guarantee *equivalence* of $\mathbf{M}(t)$ and $\mathbf{P}(t)$ for all t. Indeed, the two expressions are identical polynomials. For this reason, the constructions provide a method of exchanging one's *interpretation* of a given curve representation for its counterpart, while leaving the concomitant analytic expression unchanged. The constructions provide a computational advantage as well: knowledge of the correspondence simplifies both the construction and inversion of the parametric curve. These benefits accrue even though the implicit form of the curve is never required.[1]

We note an interesting side effect of the correspondence. Using the constructions here, general Bézier curves produce equivalent stereographic maps in standard form. Thus, the center of projection and pole of the generated stereographic map are coincident. Yet we have exhibited a construction that takes *general* stereographic maps to *general* Bézier curves. Thus we may easily convert a general stereographic map $\mathbf{M}(t)$, with center $\mathbf{Z}$ and baseline $\mathbf{L}$, to standard form. To do so, we need only use the constructions of the previous chapter to convert it to Bézier form, then from Bézier form back to stereographic form. This produces a new center of projection $\mathbf{Z}'$, and coordinatized baseline $\mathbf{L}'$, such that the (fixed) expression $\mathbf{M}(t)$ may be reinterpreted as a standard-form stereographic map that covers the same conic, for identical parameter values, as did $\mathbf{M}(t)$, $\mathbf{Z}$, and $\mathbf{L}$.

The two-dimensional constructions we have introduced ensure the linear coordinatization of the baseline. This is particularly important since, as we show in Chapter 8, this linearity allows a straightforward generalization of the correspondence to three dimensions.

[1] The implicit form may be necessary, however, for initial specification or construction of the Bézier curve or stereographic map, depending on the form of input accepted by the modeling system.

Chapter 7

Formulating Implicit Quadrics as Quadratic Bézier Patches

This chapter briefly reviews the mechanics of rational triangular Bézier patches, and presents a simple method for constructing quadratic patches that interpolate portions of desired quadric surfaces. These patches we call *restricted patches*, since their implicit equations have been constrained to ensure quadric interpolation. Patches with unconstrained implicit equations we call *unrestricted patches*. We enumerate and clarify the degrees of geometric and parametric freedom inherent in the construction of restricted patches over portions of quadric surfaces.

We conclude by generalizing the notion of complementary Bézier curves to *complementary Bézier patches*. These allow us to cover entire quadric surfaces over finite parametric domains.

7.1 The Patch Domain Δ, and Basis Functions Over Δ

7.1.1 Barycentric Coordinates

Consider a triangle Δ in general position in $\Re^3$, with vertices $\mathbf{S}$, $\mathbf{T}$, and $\mathbf{U}$. Any point $\mathbf{P}$ in the plane of the triangle may be uniquely represented as:

$$\mathbf{P} = s\mathbf{S} + t\mathbf{T} + u\mathbf{U}, \qquad \text{where } s + t + u = 1. \tag{7.1}$$

The s, t and u are called *barycentric coordinates* and form a partition of unity (Figure 7.1). If s, t and u are restricted to *non-negative* values, $\mathbf{P}(s, t, u)$ is constrained to lie inside Δ.

7.1.2 Bivariate Bernstein-Bézier Polynomials

The *bivariate Bernstein-Bézier polynomials of degree n* are analogous to the univariate polynomials of §4.1. They may be written as quadratic functions of the barycentric coordinates s, t, and u:

$$B^n_{ijk}(s, t, u) = \frac{n!}{i!j!k!} s^i t^j u^k, \qquad i + j + k = n; \quad i, j, k \geq 0. \tag{7.2}$$

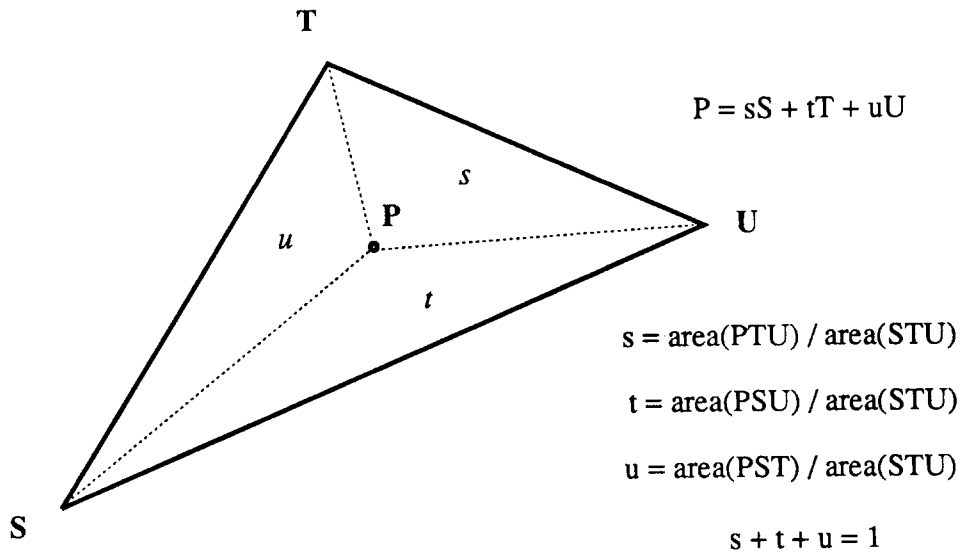

Figure 7.1: The Barycentric Coordinates s, t, and u over Δ.

These polynomials are actually functions of only two independent variables s and t, since $u = 1 - s - t$ (and $k = n - i - j$). Thus we may eliminate u and rewrite the B^n_{ijk} as

$$B^n_{ij}(s,t) = \frac{n!}{i!j!(n-i-j)!} s^i t^j (1-s-t)^{n-i-j}, \qquad i+j \leq n; \quad i,j \geq 0, \tag{7.3}$$

where we have suppressed the redundant third subscript.

For non-negative s and t such that $s + t \leq 1$, the Bernstein-Bézier polynomials are themselves non-negative. For any s and t, they form a *partition of unity* (that is, sum to one). Formally,

$$\sum_{\substack{i+j \leq n \\ i,j \geq 0}} B^n_{ij}(s,t) = 1.$$

The Bernstein-Bézier polynomials form a basis for all bivariate polynomials of degree n. They will be referred to here simply as *Bézier basis functions.*

This work primarily involves the quadratic Bézier basis functions $B^2_{ij}(s,t)$:

$$\begin{aligned}
B^2_{002}(s,t,u) &= B^2_{00}(s,t) = B_{00}(s,t) &&= u^2 = (1-s-t)^2 \\
B^2_{101}(s,t,u) &= B^2_{10}(s,t) = B_{10}(s,t) &&= 2su = 2s(1-s-t) \\
B^2_{011}(s,t,u) &= B^2_{11}(s,t) = B_{11}(s,t) &&= 2tu = 2t(1-s-t) \\
B^2_{200}(s,t,u) &= B^2_{20}(s,t) = B_{20}(s,t) &&= s^2 \\
B^2_{110}(s,t,u) &= B^2_{21}(s,t) = B_{21}(s,t) &&= 2st \\
B^2_{020}(s,t,u) &= B^2_{22}(s,t) = B_{22}(s,t) &&= t^2.
\end{aligned} \tag{7.4}$$

The single superscript and final subscript are redundant and have been eliminated.

7.2 The Rational Triangular Bézier Patch Over Domain Δ

A *rational triangular Bézier patch* of degree 2 is defined as[1]:

$$\mathbf{P}(s,t) = (P_x(s,t), P_y(s,t), P_z(s,t)) = \frac{\sum w_{ij}\mathbf{p}_{ij}B_{ij}(s,t)}{\sum w_{ij}B_{ij}(s,t)}. \tag{7.5}$$

The $\mathbf{p}_{ij}$ are called *control points* and are, in general, vector-valued. Figure 7.2 depicts a typical triangular Bézier patch. We can rewrite the patch equation (7.5) as:

$$\mathbf{P}(s,t) = \sum \left\{ \frac{w_{ij}B_{ij}(s,t)}{\sum w_{ij}B_{ij}(s,t)} \right\} \mathbf{p}_{ij}. \tag{7.6}$$

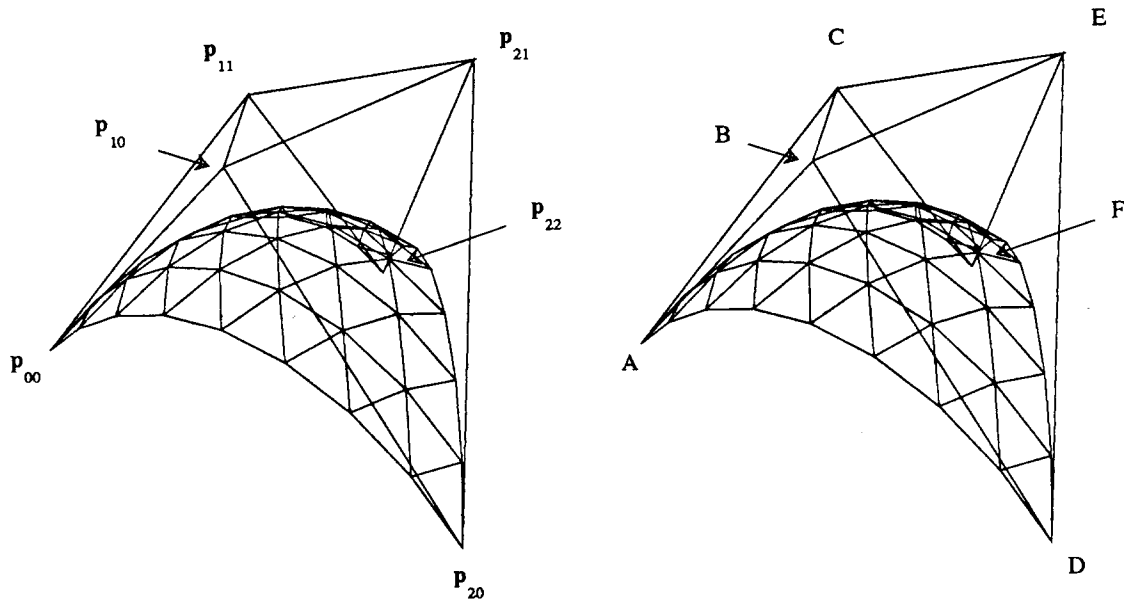

Figure 7.2: A Rational Quadratic Triangular Bézier Patch $\mathbf{P}(s,t)$.
Two control hull labelings are shown.

Each of the coefficients of the $\mathbf{p}_{ij}$ (the bracketed terms above) is nonnegative over the domain Δ, due to the nonnegativity of the w_{ij} and the $B_{ij}(s,t)$. Summing the coefficients of the $\mathbf{p}_{ij}$ yields

$$\sum \left\{ \frac{w_{ij}B_{ij}(s,t)}{\sum w_{ij}B_{ij}(s,t)} \right\} = \frac{\sum w_{ij}B_{ij}(s,t)}{\sum w_{ij}B_{ij}(s,t)} = 1.$$

Thus, the coefficients are non-negative and sum to unity, and the patch equation (7.5) constitutes a *convex combination* of the control points $\mathbf{p}_{ij}$ for all $0 \le s,t \le 1$, $s+t \le 1$. Extending the terminology of the previous chapter, we call this domain the "standard domain," and the patch swept over it a "standard triangular patch."

[1] As in Chapter 4, we employ solely quadratic basis functions. Accordingly, except where explicitly noted, the unadorned symbol $\sum$ should be read as a sum over positive i,j such that $i+j \le 2$; that is, as $\sum_{i,j \ge 0}^{i+j \le 2}$. The sum is evaluated *four* times; once for each of the x, y, z and w components of the $\mathbf{p}_{ij}$.

Later discussion of the tangent and boundary properties of this patch will refer to specific control points. Since the w_{ij} labeling can be somewhat clumsy, an alternate alphabetic labeling of the control hull is given for future reference. The control points $\mathbf{p}_{ij}$ need not contribute equally to the swept patch, since they are, in general, differentially weighted by the w_{ij}. Recall the univariate Bézier curve, for which varying the middle weight w_1 generated a continuous one-index[2] family of Bézier curves. For bivariate Bézier surfaces, there are *three* "middle" or "edge" weights (that is, w_{10}, w_{11}, and w_{21}) that together generate a continuous three-index family of Bézier patches.

The term w_{ij} multiplying each $\mathbf{p}_{ij}$ is called a *rational weight*; it lessens or increases the contribution of the control point $\mathbf{p}_{ij}$ to the surface $\mathbf{P}(s,t)$ for all s and t. The special case of unity weights (i.e., $w_{ij} = 1$ for all i, j) forces the denominator of the patch definition to be identically one, whereupon $\mathbf{P}(s,t)$ reduces to a polynomial Bézier patch. For general positive w_{ij}, the denominator Equation 7.5 serves to normalize the generated point $\mathbf{P}(s,t)$ so that it lies in the convex hull of the $\mathbf{p}_{ij}$.

Bézier patches have interpolatory behavior analogous to that of Bézier curves. For example, direct substitution into Equation 7.6 yields the three *corner points* of the patch:

$$\mathbf{P}(0,0) = \mathbf{P}_{00} = \mathbf{A}; \qquad \mathbf{P}(1,0) = \mathbf{P}_{20} = \mathbf{D}; \text{ and} \qquad \mathbf{P}(0,1) = \mathbf{P}_{22} = \mathbf{F}.$$

7.3 The Boundary Curves of the Standard Patch

Figure 7.3 shows the standard domain of the triangular patch formulation. The three corner points of the domain triangle (labeled **S**, **T**, and **U** in Figure 7.1) are respectively (1,0), (0,1) and (0,0). The edges of this domain are of particular interest; their images under the patch equation $\mathbf{P}(s,t)$ are the boundaries of the standard patch. Equivalently, we say that these segments in domain space are the *preimages* of the patch boundaries. A single point on the Bézier surface may have more than one preimage (that is, the surface may be self-intersecting).

In terms of the scalar barycentric coordinates s and t, the three edges of the triangular domain shown in Figure 7.3 are the s and t axes (along which $t = 0$ and $s = 0$, respectively), and the line $s + t = 1$ (that is, the line segment along which $u = 0$). Recall the definitions of the quadratic Bézier basis functions (Equation 7.4). Substituting $s = 0$ into the definitions of the basis functions obliterates B_{10}, B_{20}, and B_{21}, and all terms in s in the remaining functions. We are left with expressions for the bivariate basis functions evaluated along the $s = 0$ edge of the standard domain:

$$\begin{aligned} B_{00}(s=0,t) &= B_0(t) \\ B_{01}(s=0,t) &= B_1(t) \\ B_{02}(s=0,t) &= B_2(t). \end{aligned} \tag{7.7}$$

The bivariate basis functions, evaluated on this domain line, are exactly the univariate basis functions of the previous chapter. Analogous identities hold for the $t = 0$ and $u = 0$ patch boundaries.

Direct substitution into the patch definition (Equation 7.5) yields

$$\mathbf{P}(s=0,t) = \frac{\sum_k w_{kk}\mathbf{p}_{kk}B_k(t)}{\sum_k w_{kk}B_k(t)}$$

[2]Usually, this type of object is referred to as a one-*parameter* family. However, this word is so overused in geometric modeling that introducing it here in yet another context would only create confusion.

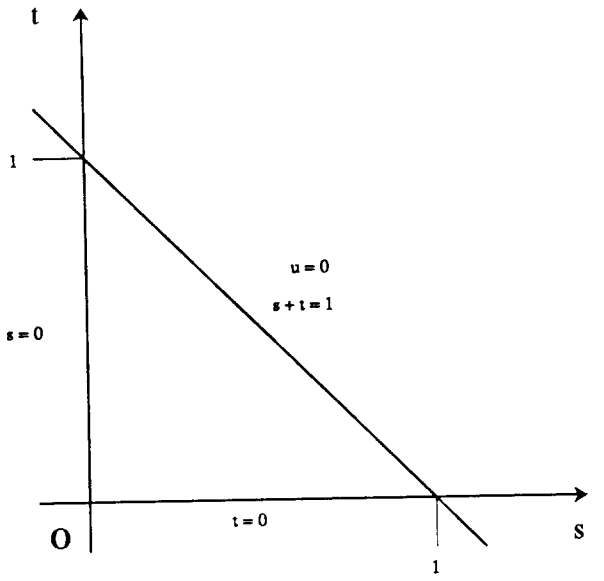

Figure 7.3: The Edges of the Standard Domain $s, t \geq 0$; $s + t \leq 1$.

$$\begin{aligned} \mathbf{P}(s, t = 0) &= \frac{\sum_k w_{k0} \mathbf{p}_{k0} B_k(s)}{\sum_k w_{k0} B_k(s)} \\ \mathbf{P}(s, t = 1 - s) &= \frac{\sum_k w_{2k} \mathbf{p}_{2k} B_k(t)}{\sum_k w_{2k} B_k(t)}. \end{aligned} \tag{7.8}$$

Thus each boundary curve of the patch is an ordinary rational quadratic Bézier curve, involving only three control points of the original patch (Figure 7.4). More generally, *every* line segment in the domain space of the patch maps to an ordinary rational quadratic Bézier curve in $\Re^3$. This curve has three defining Bézier control points $\mathbf{p}_i$, whose locations and weights are simple linear combinations of the patch control points $\mathbf{p}_{ij}$. Since all such curves are planar, and equivalent to some implicit conic (cf. Chapter 4), lines in the domain space of the patch must have complete conics as their images. As such, they are encodable both as Bézier segments and as stereographic maps of the line, using the constructions of the previous two chapters.

Lastly, we remark that the plane tangent to the patch at a given corner point is simply the plane spanned by the derivatives of the two boundary curves originating at the corner. If the derivatives are linearly dependent, the tangent plane is undefined.

7.4 Quadrics as Implicit Functions in $\Re^3$

Analogously to conic curves in $\Re^2$, a *quadric surface* in $\Re^3$ may be defined as the set of points in $\Re^3$ satisfying a *quadratic implicit* equation in the space variables x, y, and z. We can express the satisfying constraint as the zero set of a polynomial in x, y, and z:

$$Ax^2 + 2Bxy + 2Cxz + 2Dx + Ey^2 + 2Fyz + 2Gy + Hz^2 + 2Iz + J = 0. \tag{7.9}$$

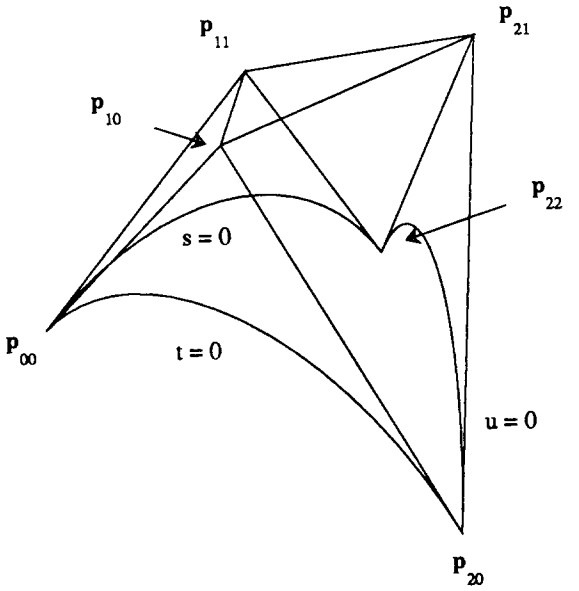

Figure 7.4: The Three Boundary Curves of the Standard Patch $\mathbf{P}(s,t)$.

In homogeneous matrix form [4], this becomes

$$\begin{pmatrix} x & y & z & w \end{pmatrix} \begin{pmatrix} A & B & C & D \\ B & E & F & G \\ C & F & H & I \\ D & G & I & J \end{pmatrix} \begin{pmatrix} x \\ y \\ z \\ w \end{pmatrix} = 0. \tag{7.10}$$

Since we are free to multiply both sides of Equation 7.9 by any non-zero scale factor, any of the ten coefficients $A \ldots J$ may be scaled to unity. Thus there are exactly *nine* scalar degrees of freedom available in the specification of a quadric with ten coefficients. This has an immediate geometric implication: through any nine non-degenerate points in $\Re^3$ there lies a unique quadric [14]. In this context, the nine points are non-degenerate if no two are coincident, no four are collinear, no six lie on one conic, and no seven are coplanar [36].

Planes, lines, and points have constant or linear implicit equations and are thus doubly or triply *degenerate* quadrics. *Cones* and *cylinders* are singly degenerate quadrics. The non-degenerate quadrics are: *ellipsoids* (including, of course, *spheres*); *hyperboloids* of one and two sheets; *paraboloids*; and *hyperbolic paraboloids*. Figures 7.5 through 7.10 exhibit some of these.

The matrix formulation (Equation 7.10) is particularly convenient for expressing planes tangent to the quadric and coordinate transformations involving the quadric. The plane $\mathbf{T}$ tangent to quadric χ at point $\mathbf{P}$ is [30]:

$$\mathbf{T} = \chi \mathbf{P}^T. \tag{7.11}$$

Given a coordinate transformation $\mathbf{M}$ that takes points $\mathbf{P}$ to points $\mathbf{P}' = \mathbf{PM}$, the matrix χ' of the quadric in the transformed system is [4]:

$$\chi' = \mathbf{M}^A \chi \mathbf{M}^{A^T}. \tag{7.12}$$

The superscript A denotes the *adjoint*, or generalized inverse, of the matrix $\mathbf{M}$:

$$\mathbf{M}^A = |\mathbf{M}| \ \mathbf{M}^{-1}, \tag{7.13}$$

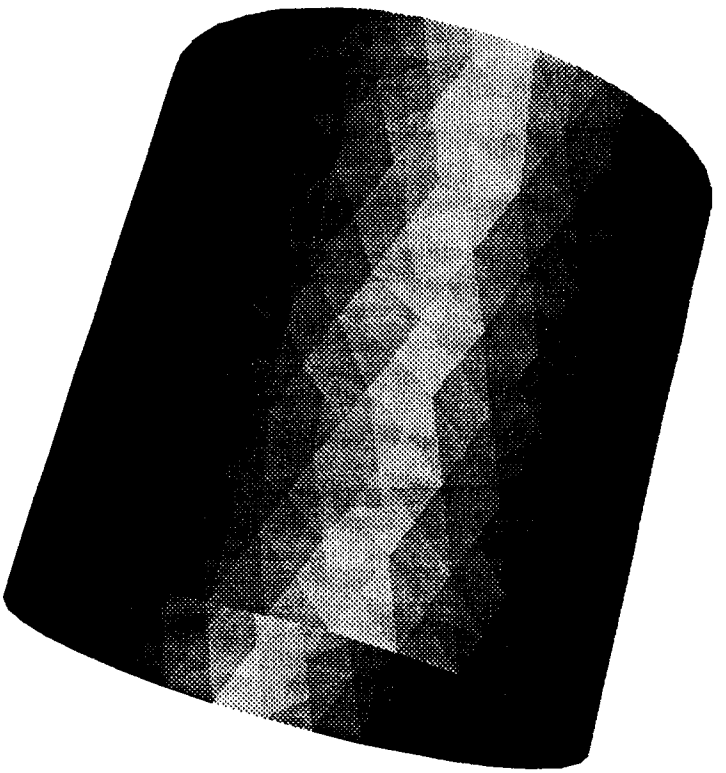

Figure 7.5: A Cylinder

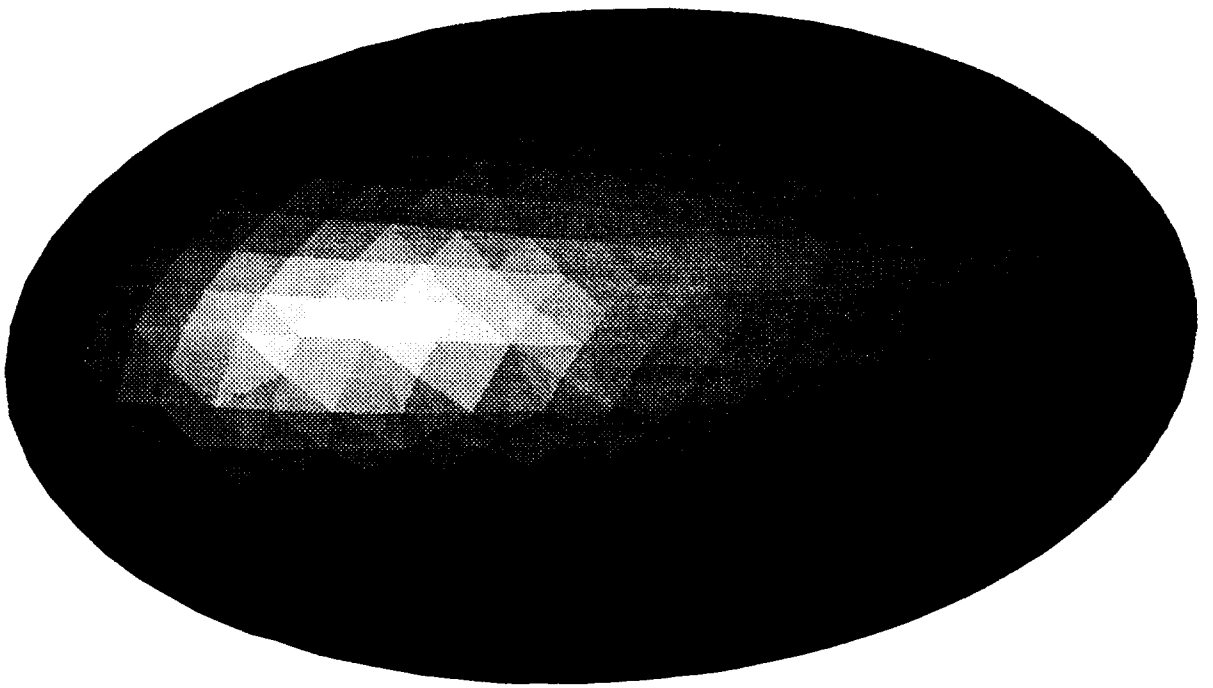

Figure 7.6: An Ellipsoid

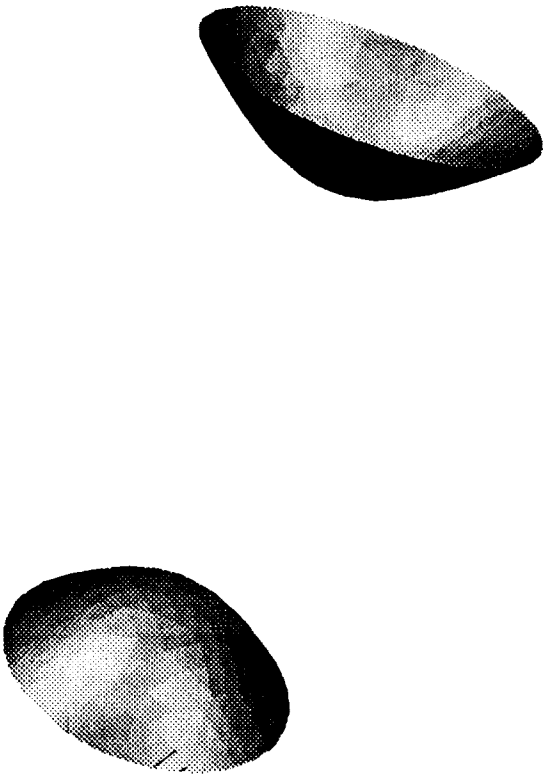

Figure 7.7: A Hyperboloid of Two Sheets

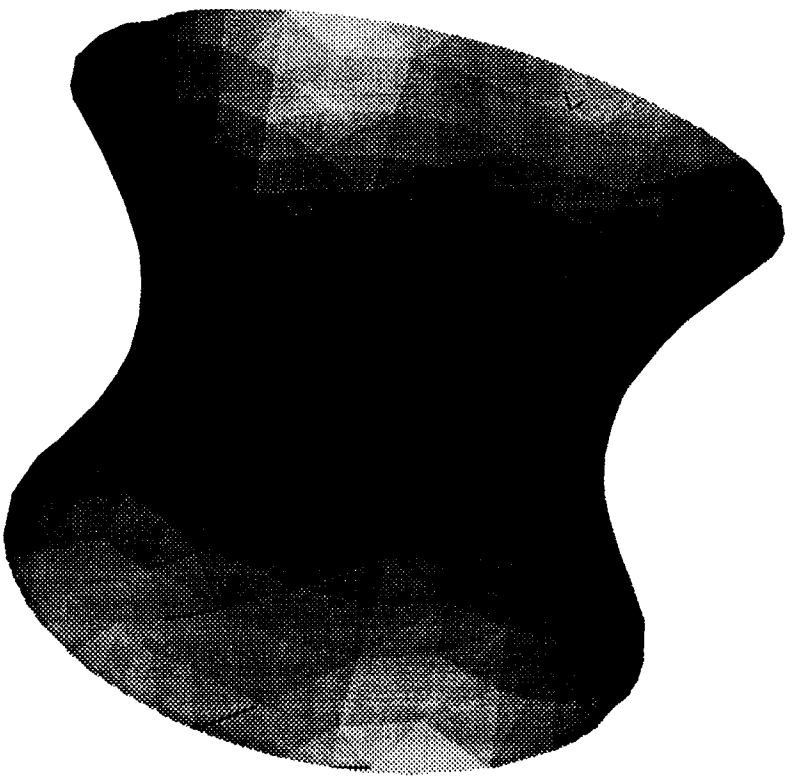

Figure 7.8: A Hyperboloid of One Sheet

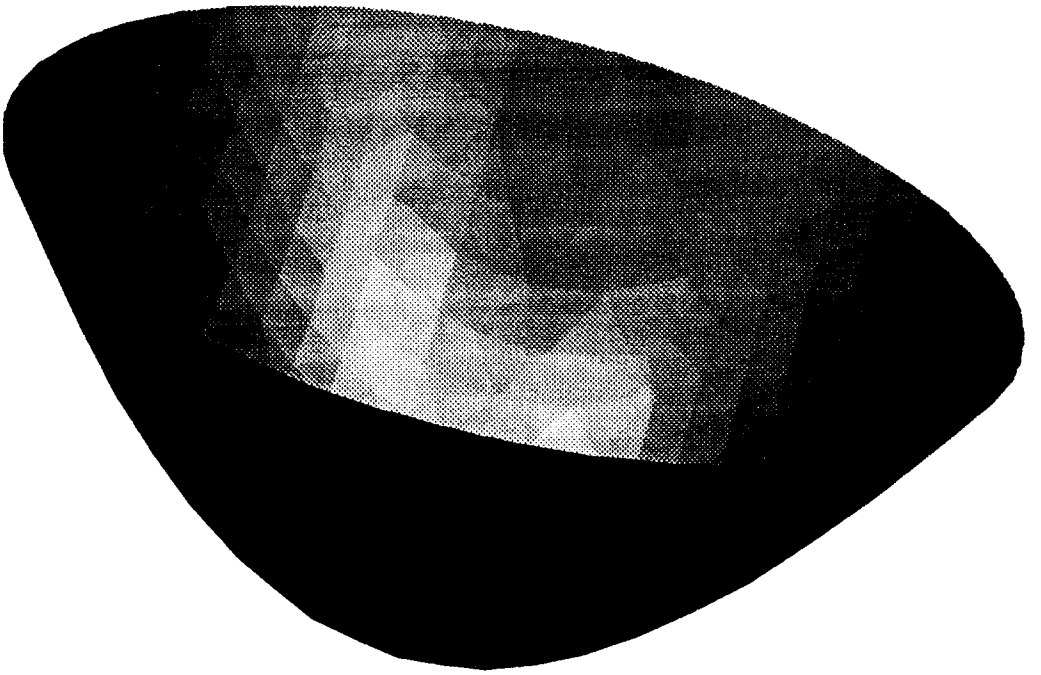

Figure 7.9: A Paraboloid

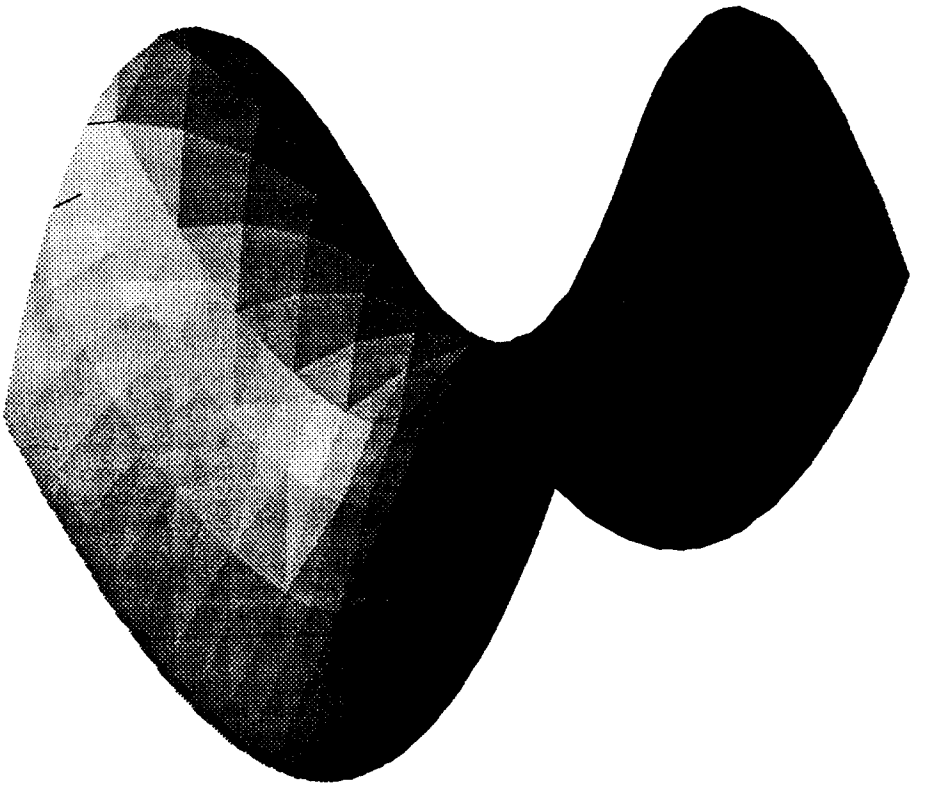

Figure 7.10: A Hyperbolic Paraboloid

that is, its determinant times its inverse.

A quadric may in principle be described as the determinant of a 10×10 matrix with entries derived from nine points $\mathbf{K} \ldots \mathbf{T}$ on the quadric. By analogy with Equation 4.9 we write:

$$\chi(x,y) = \begin{vmatrix} x^2 & xy & y^2 & yz & z^2 & xz & x & y & z & 1 \\ x_k^2 & x_k y_k & y_k^2 & y_k z_k & z_k^2 & x_k z_k & x_k & y_k & z_k & 1 \\ x_l^2 & x_l y_l & y_l^2 & y_l z_l & z_l^2 & x_l z_l & x_l & y_l & z_l & 1 \\ x_m^2 & x_m y_m & y_m^2 & y_m z_m & z_m^2 & x_m z_m & x_m & y_m & z_m & 1 \\ x_n^2 & x_n y_n & y_n^2 & y_n z_n & z_n^2 & x_n z_n & x_n & y_n & z_n & 1 \\ x_p^2 & x_p y_p & y_p^2 & y_p z_p & z_p^2 & x_p z_p & x_p & y_p & z_p & 1 \\ x_q^2 & x_q y_q & y_q^2 & y_q z_q & z_q^2 & x_q z_q & x_q & y_q & z_q & 1 \\ x_r^2 & x_r y_r & y_r^2 & y_r z_r & z_r^2 & x_r z_r & x_r & y_r & z_r & 1 \\ x_s^2 & x_s y_s & y_s^2 & y_s z_s & z_s^2 & x_s z_s & x_s & y_s & z_s & 1 \\ x_t^2 & x_t y_t & y_t^2 & y_t z_t & z_t^2 & x_t z_t & x_t & y_t & z_t & 1 \end{vmatrix} = 0. \qquad (7.14)$$

As in the conic case, each scalar coefficient $A \ldots J$ of Equation 7.9 corresponds to a 9×9 sub-determinant of (7.14). In practice, such computations are cumbersome and numerically unstable. Fortunately, constructing quadrics from nine general points is an uncommon operation in modeling. More probably, the general class (e.g., ellipsoid, saddle surface, cone, cylinder) of the quadric is known, along with a few interpolatory or tangent conditions. Foreknowledge of the surface class simplifies the derivation of the appropriate quadric matrix. A set of "canonical" quadric matrices (e.g., unit-radius spheres, cylinders, and single-sheet hyperboloids; right cones and paraboloids) can be kept by the modeling system [16]. The standard modeling operations of translation, rotation, and anisotropic scaling are applied to the canonical quadrics via the adjoint multiplication of their associated matrices (cf. Equation 7.12). Similar matrix manipulations are used in rendering systems to derive the silhouettes, or outlines, of the quadrics as seen from varying viewpoints ([4], [16]).

7.5 Quadric Degrees of Freedom

It is worthwhile to consider the number and type of degrees of freedom that are necessary and sufficient for the unambiguous specification of a quadric surface. It is clear from the implicit and determinant equations above that nine (scalar) coefficients and nine (vector-valued) points constitute equivalent means of quadric specification. But this can only be true if each point, a three-tuple, encodes two redundant values. This is analogous to the situation of the previous chapter and two dimensions. There, each two-dimensional coordinate was free to slide along a conic that amounted to a one-dimensional curvilinear coordinate system. Each interpolated point therefore pinned exactly one scalar degree of freedom. In the three-dimensional case, each interpolated point may move on a locally two-dimensional, curvilinear coordinate mesh (the quadric itself) and must therefore pin at most one of the quadric's nine scalar degrees of freedom.

7.5.1 Specifying a Quadric With Planar Cuts

The intersection of a quadric and a plane is a conic. Thus, in principle, we can specify quadrics via the auxiliary specification of a set of conics, along with the demand that each specified conic be the intersection of its embedding plane with the desired quadric.

For example, consider the specification of two *disjoint* conics lying in planes in general position in $\Re^3$. Specifying each conic consumes five points in $\Re^3$, for a total of ten points. However, these are not sufficient for the specification of a unique quadric. Figure 7.11 depicts two situations in which two disjoint conics are required to lie on the same quadric. In the first case, the only quadric containing both conics is a plane pair. The second case is ambiguous; the quadric containing both given conics might be a plane pair, a sphere, an ellipsoid, or a cone. Deciding among these alternatives requires some other point on the quadric but not on either conic.

Next consider a pair of conics that intersect in exactly *one* point $\mathbf{P}$. A quadric exists that contains these two conics as planar cuts if and only if the two embedding planes intersect in a line tangent to the quadric at $\mathbf{P}$. The conics are coincident and have identical tangents at $\mathbf{P}$, and in this sense share a double root, or *two* points of intersection. For example, consider a sphere of unit radius and a cube of side $\frac{\sqrt{2}}{2}$, both centered at the origin (Figure 7.12). Any two faces of the cube intersect the sphere in circles that meet in a single point $\mathbf{P}$. The line embedding the cube edge shared by the two faces lies in the plane tangent to the sphere at $\mathbf{P}$. Again, another point is necessary to rule out the possibilities that the satisfying quadric is an elliptical cylinder or plane pair.

Finally, consider a pair of conics that intersect in exactly *two* distinct points. Specifying the conics requires eight points; five for the first (of which two are shared), and three for the second. These eight points *underspecify* a quadric surface; that is, an infinite number of quadrics have the given conics as planar cuts [36]. Figure 7.13 depicts two ellipses that share two points. The quadric embedding both ellipses might be a plane pair, ellipsoid, or (circular) cylinder. Disambiguating this situation requires a ninth point, off of the given conics, but perhaps in the plane of one or both.

We can generalize to situations involving three or more conics. Imagine an initially empty set into which conics are incrementally inserted. Upon each insertion we demand that *some* quadric contain the resulting set of conics; otherwise we reject the insertion, as it would produce the null quadric (a quadric with no satisfying real-valued points). If plane pairs, cylinders, and cones are disallowed, two conic cuts will be sufficient for unambiguous specification of quadrics. This is a rather severe restriction; instead, one might accept three conics as specification. The first two conics underspecify the quadric; inserting the third conic either specifies the quadric exactly or overspecifies it. In the latter case, the conic should be rejected. We show in §7.6 that specification of three portions of conics is both an appropriate and useful method for the construction of triangular Bézier patches that interpolate quadric).

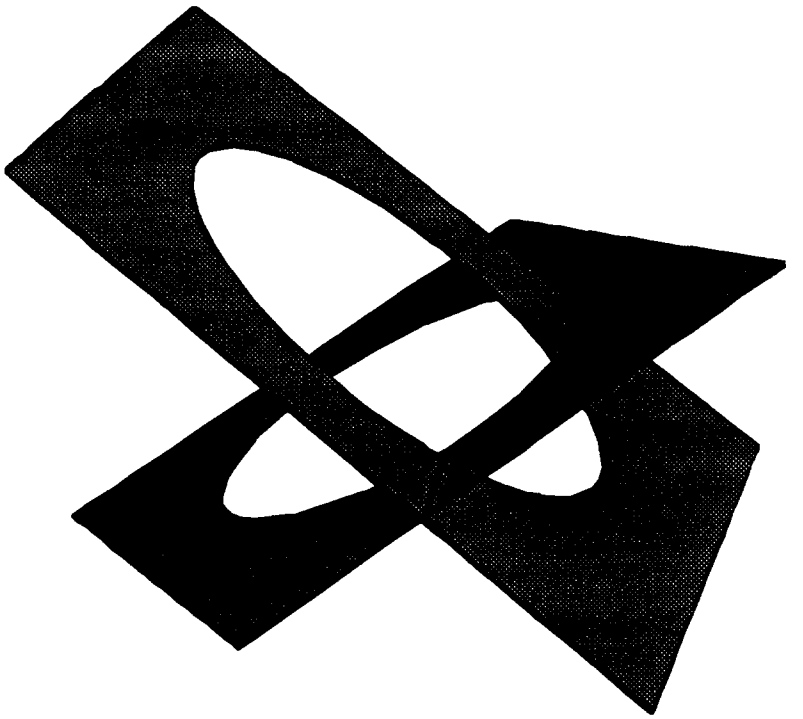

The Only Quadric Embedding These Two Conic Cuts is a Plane Pair.

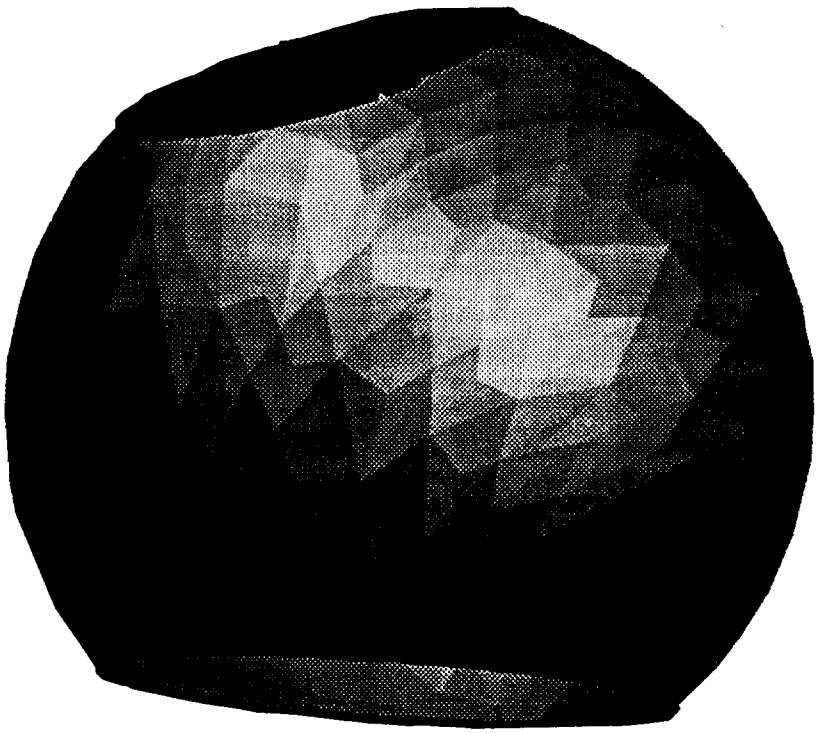

A Sphere Embeds These Disjoint Conic Cuts.

Figure 7.11: Two Disjoint Conics May Imply a (Degenerate) Plane Pair or a General Quadric.

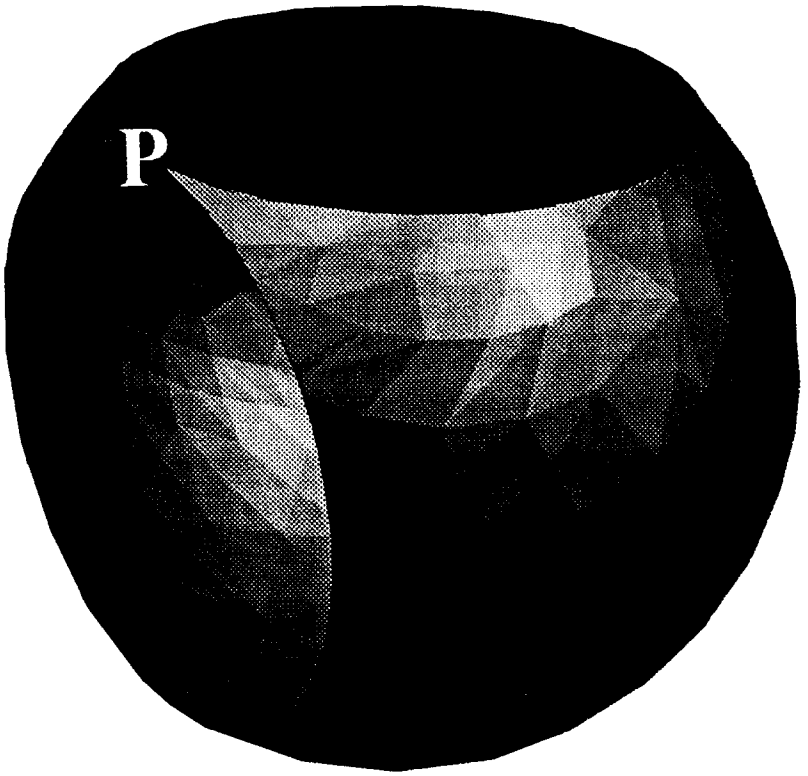

Figure 7.12: A Sphere of Unit Radius, and Cube of Side $\frac{\sqrt{2}}{2}$ Centered at The Origin. Any two faces of the cube cut the sphere in circles; any two of these circles intersect in a double root at the single point **P**. The edge shared by the faces lies in the plane tangent to the sphere at **P**.

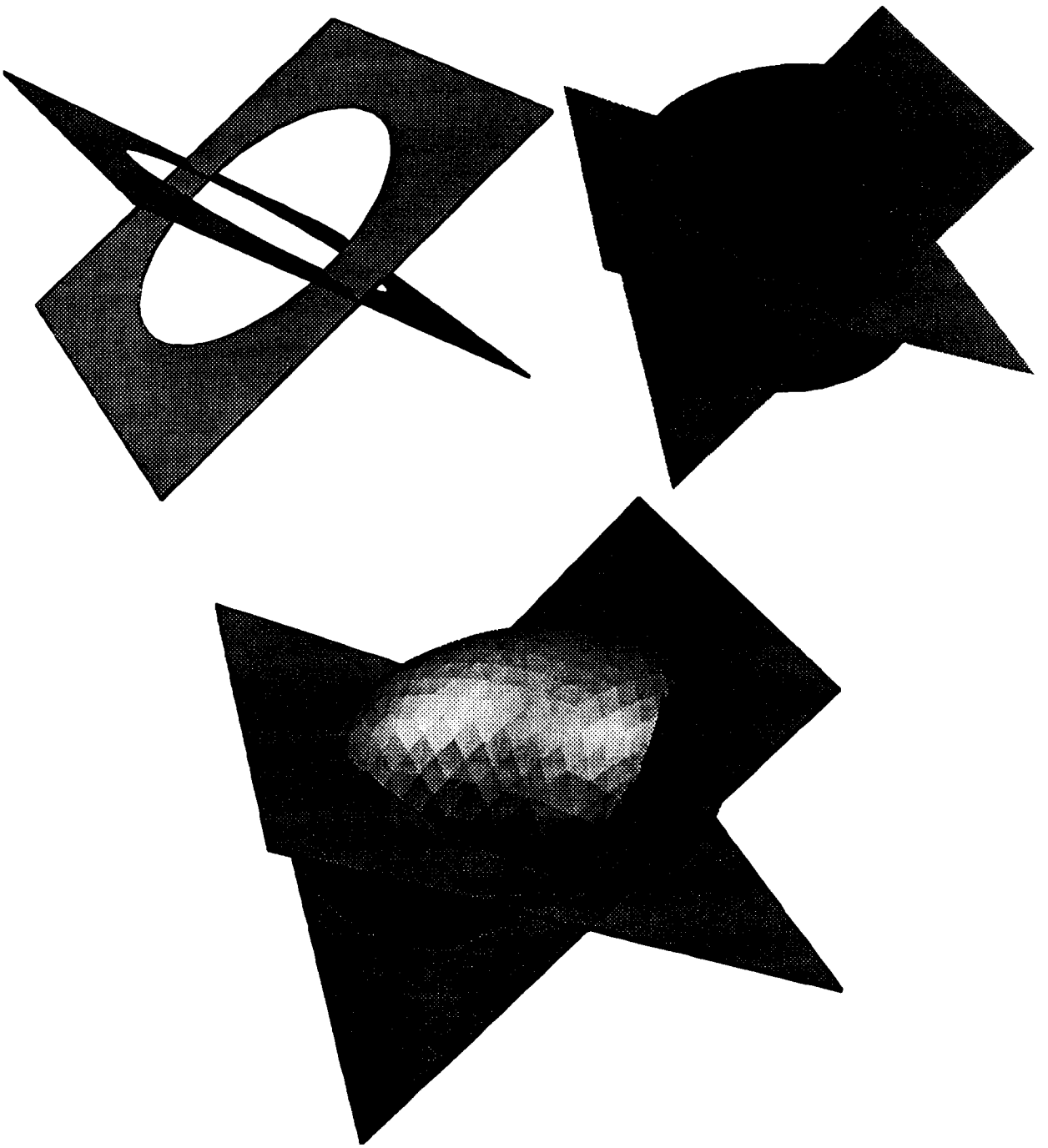

Figure 7.13: Two Conics Sharing Two Points Ambiguously Specify a Quadric Surface. The satisfying quadric might be a plane pair, cylinder, or ellipsoid.

7.5.2 Joining Implicit Quadrics With G^1, or First-Derivative, Continuity

Given two quadric surfaces cut by a single plane, one may ask: under what conditions will the two surfaces "fit together" smoothly? More precisely, we ask when two quadrics meet, along a shared planar cut or *seam*, with G^1 or *tangent plane* continuity [8].

In addressing this question, it is helpful to review the notions of ***polar points*** and *polar planes.* Given a quadric and some cut plane **C** that intersects the quadric, the point *polar(***C***)* is the single point contained in all of the planes tangent to the quadric along the planar seam generated by **C** (Figure 7.14). Analogously, for any point **P** outside the quadric one may consider the family of planes tangent to the quadric and containing **P**. The locus of the planes' points of tangency is planar; the plane embedding this locus is *polar(***P***)*. All points, regardless of their location, have associated polar planes. Points outside the quadric have polar planes that intersect the quadric; points on the quadric are contained in their own polar plane, tangent to the quadric; and points inside the quadric have polar planes disjoint from the quadric [4]. Polar points need not be local. With respect to a sphere, for example, the polar plane of any point at infinity would embed some great circle of the sphere. Conversely, *polar(***C***)* is an ideal point for any plane **C** containing the sphere's center (Figure 7.15).

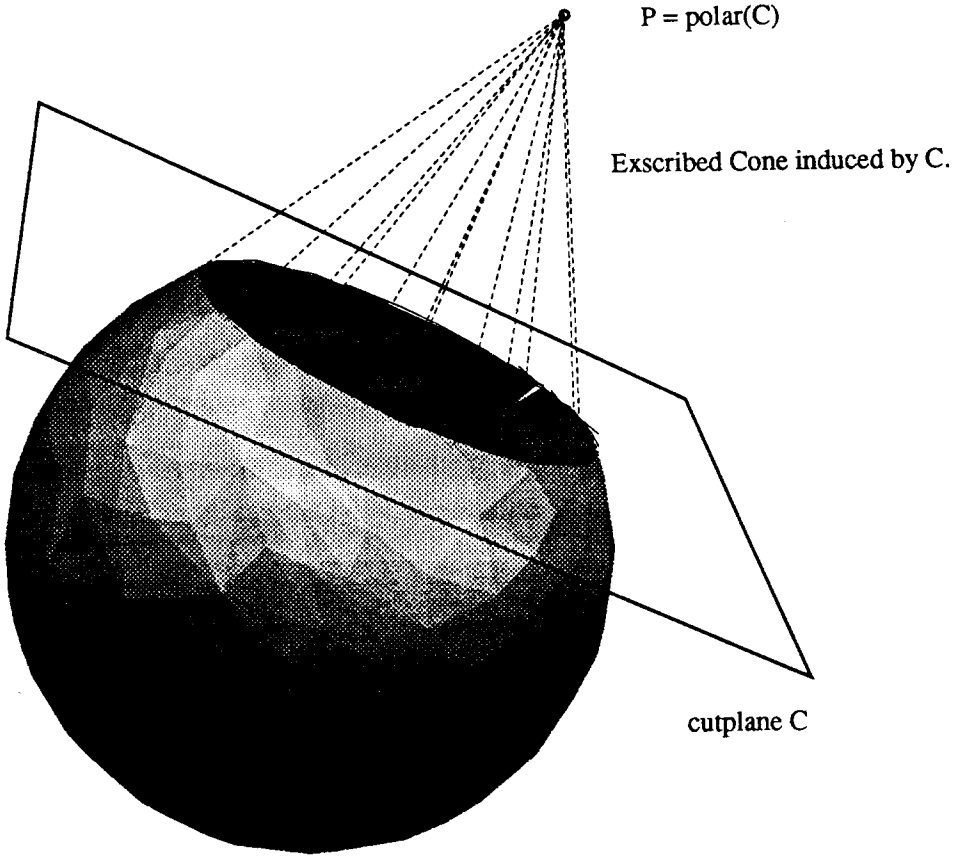

Figure 7.14: A Sphere, Cut by a Plane **C** That Does Not Contain Its Center. The induced plane cut is not a great circle. Polar(**C**) is a finite point, and **C** induces an exscribed *cone* that intersects the sphere only along **C**.

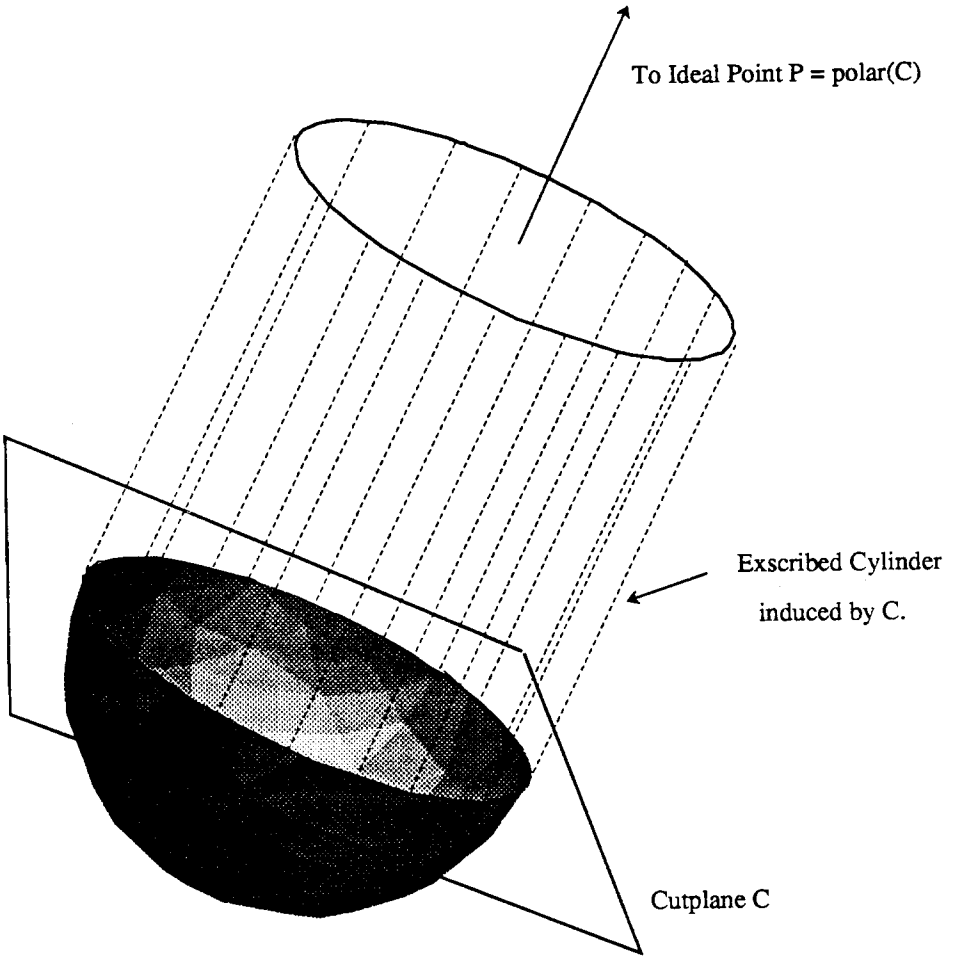

Figure 7.15: A Sphere, Cut by a Plane C That Contains Its Center.
The induced plane cut is a great circle. Polar(C) is an ideal point, and C induces an exscribed *cylinder* that intersects the sphere only along C.

Relating polar points and planes is a straightforward procedure with the matrix notation of §7.4. The polar plane of a homogeneous point $\mathbf{P} = (x, y, z, w)$ with respect to a quadric χ is simply

$$\text{polar}(\mathbf{P}) = \chi\mathbf{P}^T = \begin{pmatrix} A & B & C & D \\ B & E & F & G \\ C & F & H & I \\ D & G & I & J \end{pmatrix} \begin{pmatrix} x \\ y \\ z \\ w \end{pmatrix} = \begin{pmatrix} a \\ b \\ c \\ d \end{pmatrix}. \tag{7.15}$$

The column vector on the right is a homogeneous plane equation (cf. Equation 3.2, §3.2).

There are alternative methods of computing polar points and planes that do not involve the implicit equation of the quadric. If the quadric is represented in a form that allows computation of tangent planes, the polar point of any plane may be found by choosing three distinct points on the plane's intersection with the quadric, and computing the intersection of the three tangent planes induced there.

The notion of polarity associates a cone (or cylinder, in the case of ideal polar points) with every point outside the quadric. Consider such a point, and all planes that both contain the point and are tangent to the quadric. The intersection of the halfspaces bounded by the planes is the interior of a cone; its boundary is unique and a function solely of the quadric and the choice of polar point. We call the cone so formed for a given quadric $\mathbf{Q}$ and point $\mathbf{P}$ the *exscribed cone* (*cylinder*) of $\mathbf{Q}$ from $\mathbf{P}$. The exscribed cone (cylinder) can also be defined for a quadric $\mathbf{Q}$ and cut plane $\mathbf{C}$ by forming $\mathbf{P} = \textit{polar}(\mathbf{C})$.

With the machinery of polar points, polar lines, and exscribed cones and cylinders, the question of necessary and sufficient conditions for G^1 continuity of two quadrics along a shared planar seam is easily answered. For two quadrics $\mathbf{Q}_1$ and $\mathbf{Q}_2$ and a cut plane $\mathbf{C}$ defining their shared seam, the quadrics are G^1 continuous everywhere along $\mathbf{C}$ if and only if

$$\text{exscribed}(\mathbf{Q}_1, \mathbf{C}) = \text{exscribed}(\mathbf{Q}_2, \mathbf{C}). \tag{7.16}$$

That is, the quadrics meet with G^1 continuity along a shared seam if and only if, with respect to the seam, the quadrics have identical exscribed cones (cylinders).

Imagine sliding along the shared (G^0) seam. Looking "left" (say, towards $\mathbf{Q}_1$), the horizon is simply the vanishing line of the plane tangent to $\mathbf{Q}_1$. Similarly, the "right" horizon is determined by the plane tangent to $\mathbf{Q}_2$. If the two planes become distinct, a cusp, or first-derivative geometric discontinuity, would appear on the seam. By definition, replacing $\mathbf{Q}_1$ and $\mathbf{Q}_2$ with their exscribed cones cannot change the tangent planes at any point on the seam. Thus, to ensure G^1 continuity, the cones must have identical zeroth and first derivatives at every point on the seam. Since cones are singly-degenerate quadratic implicit functions, two cones having identical zeroth and first derivatives everywhere must be identical.

7.6 Constructing a Restricted Bézier Patch: A Rational Quadratic Bézier Patch That Interpolates an Implicit Quadric

Several authors ([6], [24], [25], [32], [40]) have presented methods for constructing particular quadrics, or classes of quadrics, using the Bézier formulation. However, these methods have not

satisfactorily addressed the issue of general control over the *parametrization* or *boundaries* of these patches. Typically, these important degrees of freedom are determined as artifacts of the construction, or depend implicitly on the availability of an inversion equation for the constructed patch.

This section reviews the necessary and sufficient conditions for a quadratic triangular patch to interpolate an implicit quadric. Since not all patches interpolate quadrics, we call those that do *restricted* Bézier patches. We demonstrate the construction of Bézier patches that interpolate general quadrics. In the following chapter, we generalize the construction by showing how the constructed patch may be made to have any desired (possible) boundary curves, while still interpolating the given implicit quadric.

Sederberg, in [32], has shown that in order for a rational quadratic triangular Bézier patch to interpolate a quadric surface, a *necessary* condition is that the planes containing the three boundary curves of the patch must meet in a point lying on the quadric. A *sufficient* condition for the patch to interpolate a quadric is that the boundary curves, when extended or complemented, must also contain this point [40].

Figure 7.16 depicts three cut planes that meet in a point **Z** at the top of an ellipsoid. The three planes cut the ellipsoid in ellipses, each passing through **Z**. (However, the patch boundary curves, considered as independently parametrized planar curves, need not pass through the point at the same parameter value.) We call this special point **Z** the *center of projection* of the patch; the next chapter's discussion of three-dimensional stereographic maps justifies this terminology.

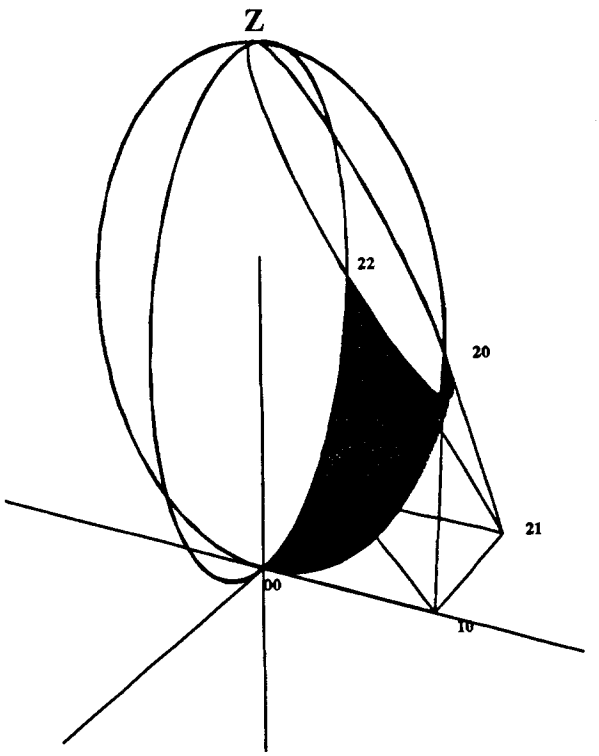

Figure 7.16: The Three Boundary Curves of a Patch That Interpolates an Ellipsoid.

Given a quadric surface in implicit form, a center of projection, and three points on the quadric, we can construct a triangular patch interpolating the quadric. The three specified points will serve

as the patch corner control points. The three patch boundary planes will be the planes through the center of projection **Z** and each of the three pairs of corner points.

The construction first finds the *positions* of of six control points such that the Bézier patch swept by the points has the desired interpolatory and tangent behavior at the patch corners. Control *weights* are then assigned so that the patch boundary curves and interior also interpolate the desired quadric (Figure 7.17).

First check that the given center of projection **Z** and three corner points (call them **A**, **D**, and **F**; cf. Figure 7.2) lie on the implicit quadric. If not the input is erroneous and may be rejected.

Points **A** and **D** will serve respectively as the $(0,0)$ and $(1,0)$ corner points of the patch. We must find the position of the edge control point **B** that, together with **A** and **D**, will correctly determine the patch's $t = 0$ boundary curve. **B** must lie in three planes. The first of these is the plane **ZAD**, since the plane **ABD** of the patch boundary curve must contain the center of projection. **B** must also lie in the planes **a** and **d** tangent to the quadric at **A** and **D**, respectively, since **B** is simply the tangent intercept of the (conic) boundary curve **ABD**, considered as a plane cut of the quadric.

Thus the position of **B** is easily, and uniquely, found as the common point of the planes **ZAD**, **a**, and **d**. Similarly, the input point **F** will serve as the $(0,1)$ corner point of the patch. Thus **C** and **E** (in planes **ZAF** and **ZDF**, respectively) are easily computed.

The remainder of the construction involves deriving *weights* for the constructed control points **A**...**F** so that the patch over these control points interpolates the implicit quadric. By the sufficient condition given above, we can assure that the patch interpolates the given quadric by arranging that each extended boundary curve contains the center of projection, and covers the conic induced by the appropriate plane cut of the implicit quadric.

Since weight ratios are to be developed, we need some fixed weight upon which the values of the other five weights in the patch can be based. Without loss of generality, choose $A_w = 1$.

Every planar cut of a quadric is a conic. In particular, the planes **ZAD**, **ZDF**, and **ZBF** imply conics that interpolate (respectively) **A** and **D**, **D** and **F**, and **B** and **F**. Thus we may treat each boundary curve of the patch separately and compute its weights with the methods of Chapter 4.

In this way, the $t = 0$ curve **ABD** is constructed, as are the weights A_w, B_w, and D_w (with $A_w = 1$). Similarly, we construct the weights C_w and F_w (and thus the $s = 0$ boundary curve) using the conic intersection of plane **ACF** with the quadric. Only one scalar quantity remains unspecified; the edge weight E_w of the $u = 0$ (or $s + t = 1$) boundary curve. We have somewhat less freedom in determining this weight, since at this stage of the construction both end weights (i.e., D_w and F_w) have been completely determined by the shapes and parametrizations of the s and t boundary curves. Although we may still specify the *shape* of the $u = 0$ boundary curve, we are unable to control its parametrization.

Formally, suppose all weights but E_w have been defined. From §4.5.1, we know that ρ, Forrest's conic shape factor, may be written in terms of Lee's shape factor k as

$$k = \frac{D_w F_w}{4{E_w}^2} = \frac{(1-\rho)^2}{4\rho^2}. \tag{7.17}$$

We exploit the fact that the ratio k is constant, for a conic of fixed shape. Equation 7.17 has one

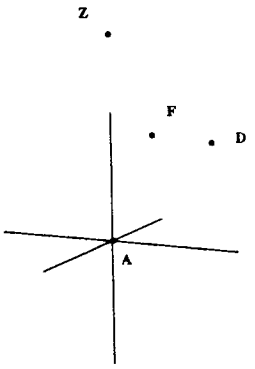

Given: Implicit Quadric,
Z on Quadric, and
Corner Points A, D, and F.

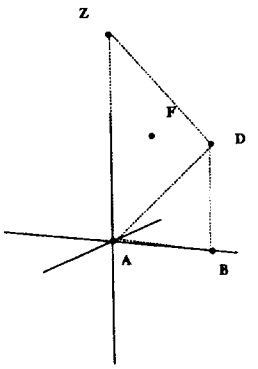

Find B: intersection of
plane (Z, A, D), tangent
at A, and tangent at D.

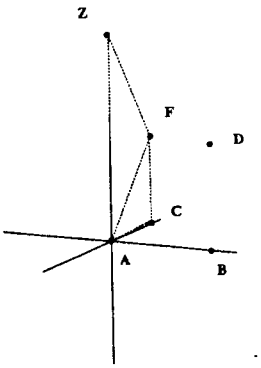

Find C: intersection of
plane (Z, A, F), tangent
at A, and tangent at F.

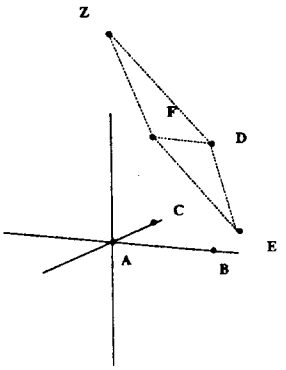

Find E: intersection of
plane ZDF, tangent at D,
and tangent at F.

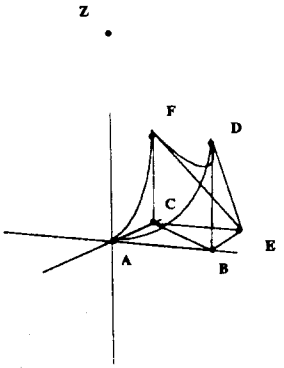

Fix Aw = 1. Find
remaining control weights
with pole-conic convention
and center of projection Z.

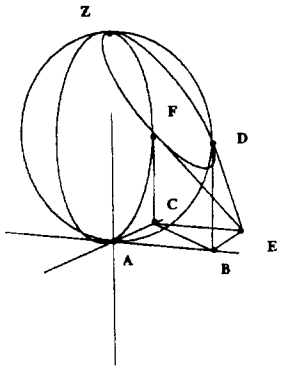

Each boundary curve,
when extended or
complemented, contains
the center of projection.

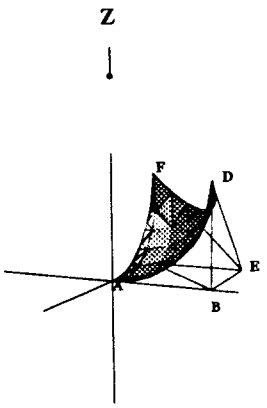

The resulting patch has three
boundary planes that intersect in Z,
as do its three boundary curves.
The triangular patch, whether standard,
extended, or complemented, interpolates
the given implicit quadric for all s and t.

Figure 7.17: Constructing a Bézier Patch That Interpolates a Quadric, Given An Implicit Equation, A Center of Projection, and Three Corner Points.

unknown: E_w. From Equations 4.17 and 4.18, §4.5.1, some manipulation yields that

$$E_w = \sqrt{\frac{D_w F_w \rho^2}{(1-\rho)^2}}. \tag{7.18}$$

Thus, although the two end weights are fixed, we have just enough freedom in fixing E_w to ensure the correctness of the *shape* of the $u = 0$ boundary curve.

By construction, the resulting standard patch interpolates the implicit quadric, has the corner points given as input, and is bounded by the three cut planes implied by the corner points and center of projection. We show later that this patch, when extended or complemented in the manner of Sections 4.5.2 and 4.5.3, continues to interpolate the quadric.

7.6.1 Example: Constructing a Portion of The Unit Sphere as a Rational Quadratic Triangular Bézier Patch

We demonstrate the construction of the previous section for a sphere of unit radius, tangent to the xy-plane at the origin (Figure 7.17). We place the center of projection $\mathbf{Z}$ at the North pole $(0,0,2)$ of the sphere. The three corner points $\mathbf{A}$, $\mathbf{D}$, and $\mathbf{F}$ will be $(0,0,0)$, $(1,0,1)$, and $(0,1,1)$ respectively.

The tangent planes induced are either vertical or horizontal. By symmetry, the positions of $\mathbf{B}$, $\mathbf{C}$, $\mathbf{E}$ are easily found as $(1,0,0)$, $(0,1,0)$, and $(1,1,0)$. The pole-conic convention yields weight ratios $A_w : B_w : D_w = 1:1:2$ for the s boundary curve, and $A_w : C_w : F_w = 1:1:2$ for the t boundary curve. Finally, Equation 7.18 yields the weight ratio $D_w : E_w : F_w$ as $2:1:2$ for the $u = 0$ boundary curve. Summarizing, the construction has generated the control points

$$\begin{aligned}
\mathbf{P}_{00} &= \mathbf{A} = (0,0,0,1) \\
\mathbf{P}_{10} &= \mathbf{B} = (1,0,0,1) \\
\mathbf{P}_{11} &= \mathbf{C} = (0,1,0,1) \\
\mathbf{P}_{20} &= \mathbf{D} = (1,0,1,2) = (2,0,2,2) \\
\mathbf{P}_{21} &= \mathbf{E} = (1,1,0,1) \\
\mathbf{P}_{22} &= \mathbf{F} = (0,1,1,2) = (0,2,2,2),
\end{aligned} \tag{7.19}$$

where $\mathbf{D}$ and $\mathbf{F}$, the two points with $w \neq 1$, have been written as they appear both before and after multiplication through by w.

We verify analytically that the triangular patch $\mathbf{P}(s,t)$ swept over these six control points interpolates the implicit sphere. Write the non-homogeneous equation for a sphere of unit radius, tangent to the plane $z = 0$, with center on the z-axis:

$$x^2 + y^2 + (z-1)^2 = 0. \tag{7.20}$$

In homogeneous coordinates this is simply[3]

$$\begin{pmatrix} x & y & z & w \end{pmatrix} \begin{pmatrix} 1 & 0 & 0 & 0 \\ 0 & 1 & 0 & 0 \\ 0 & 0 & 1 & -1 \\ 0 & 0 & -1 & 0 \end{pmatrix} \begin{pmatrix} x \\ y \\ z \\ w \end{pmatrix} = x^2 + y^2 + z^2 - 2zw = 0. \tag{7.21}$$

[3]The non-homogeneous quadratic equation in x, y, and z may be converted into homogeneous form simply by substituting $\frac{x}{w}$, $\frac{y}{w}$, and $\frac{z}{w}$, respectively, and clearing w from the denominators.

The definition of a rational triangular patch (Equation 7.5), applied to the control points (7.19), yields an expression for each homogeneous coordinate as a function of s and t:

$$\begin{aligned} P_x(s,t) &= 2s \\ P_y(s,t) &= 2t \\ P_z(s,t) &= 2(s^2+t^2) \\ P_w(s,t) &= 1+s^2+t^2. \end{aligned}$$

Direct substitution into Equation 7.21 yields zero, as expected. Identity (7.21) holds for all parameter values (s,t); thus $\mathbf{P}(s,t)$ interpolates the sphere regardless of (s,t). Given any rational triangular map and implicit conic χ, the control points may be decomposed and substituted symbolically (or numerically) in this manner to verify that the implicit equation is satisfied.

For a *standard* patch, one that is the image of the canonical triangular domain Δ, requiring that the three patch boundaries meet at a point on the quadric is a severe constraint. In the spherical construction above, for example, we are prevented from modeling an octant of the sphere with a standard quadratic patch (three planes bounding any sphere octant must intersect at the center of the sphere, not on its surface). Although two of the boundary curves may be chosen as portions of great circles, the third curve, when extended, must meet the first two in one of their two points of intersection: in this example, the North or South pole of the sphere. If the former is chosen, the resulting patch appears at the top of Figure 7.18.

7.6.2 Extended Bézier Patches

For conics, the standard Bézier segment parametrized by $0 \leq t \leq 1$ covers only a portion of its associated implicit conic. In this case, the parametric curve is an image of the real line, and there are two ways to map the remainder of the conic. First, we can relax the condition that the parameter t lie in the interval [0..1]. This produces two extended segments that cover the remainder of the implicit conic. Unfortunately, t must attain infinite values if the swept curve is to cover every point on the implicit conic (even for bounded curves such as ellipses and circles). Second, we can complement the curve by negating the edge control weight. This produces a complementary segment that interpolates the implicit conic and shares only its endpoints with the standard segment. Both procedures have analogues in the the three-dimensional, quadric case.

For any standard patch $\mathbf{P}(s,t)$, an *extended patch* can be produced by allowing the values of s and t to become unbounded. This extended patch covers the entire quadric. Extended patches over the domains s,t in [0..1] and s,t in [−1..1] are depicted in Figure 7.18.

Unfortunately, extending the patch domain of a Bézier surface suffers from the same limitation as did extending the domain of Bézier curves: in order to cover every point on the quadric, the domain variables s and t must attain infinite values. This presents computational difficulties in practice.

In our investigations, we addressed these difficulties by obviating them. In analogy to Lee's complementation of Bézier curves, we have developed a procedure for complementing Bézier patches. The next section demonstrates the method, which involves negating selected patch *control weights* in order to cover unbounded surfaces over finite domains.

DeRose, in concurrent investigations [9], has approached the problem differently. Rather than

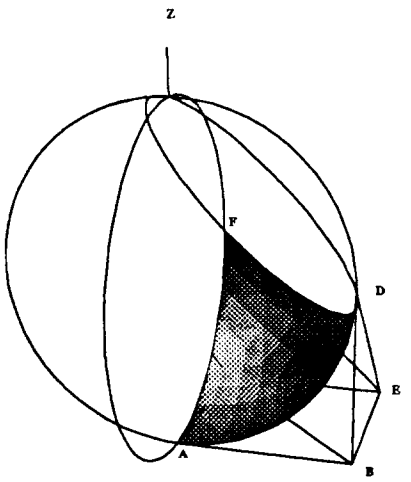

The Standard Patch.

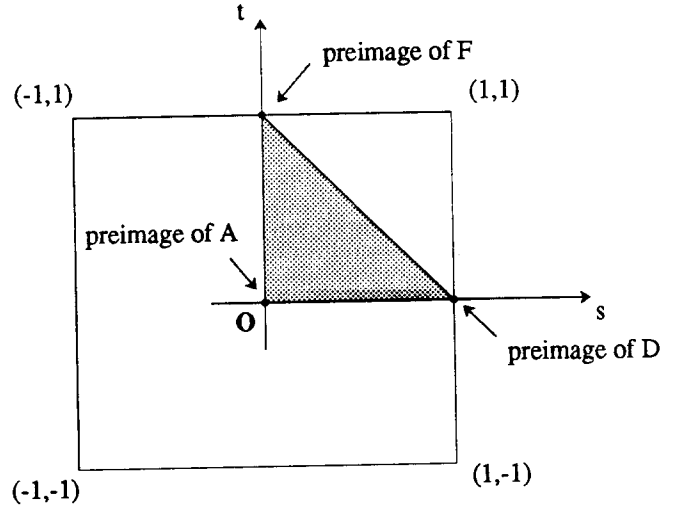

The Domain Δ: $s, t \geq 0, s + t \leq 1$.

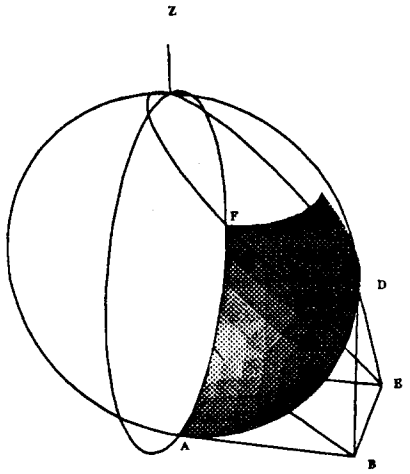

The Patch Over $s, t \in [0..1]$.

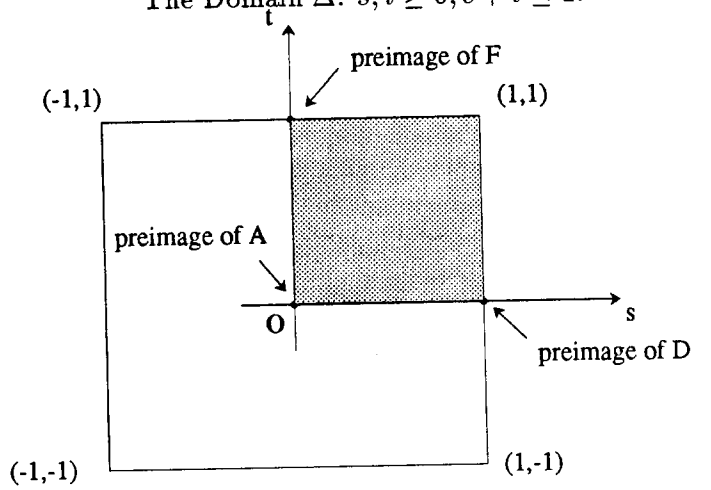

The Domain $s, t \in [0..1]$.

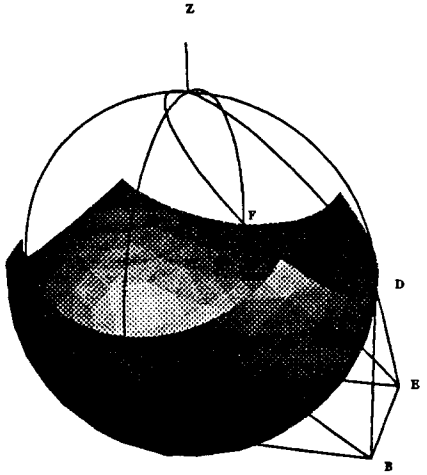

The Patch Over $s, t \in [-1..1]$.

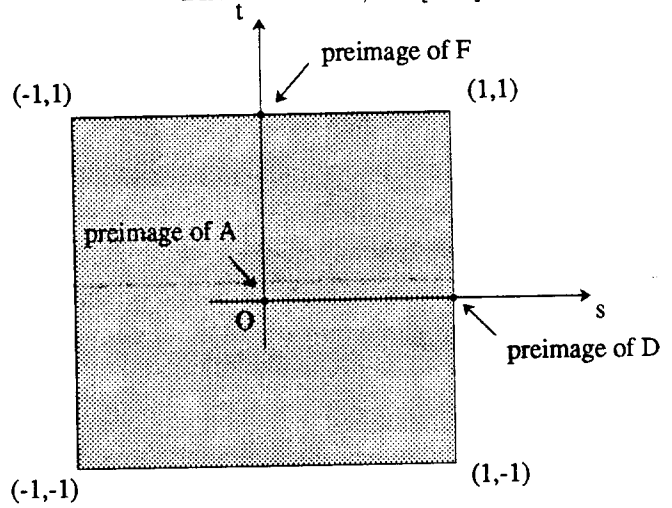

The Domain $s, t \in [-1..1]$.

Figure 7.18: A Standard Triangular Bézier Patch $\mathbf{P}(s, t)$, and Two Extended Patches.

modifying the patch control weights, he redefines the patch domain to be *projective* in nature. Treating s and t projectively effectively allows them to become unbounded; thus the entire extended surface can be swept, at the cost of some extra computational complexity in both the specification and evaluation of the patch. We briefly recount DeRose's method in §7.6.4.

The two approaches appear quite distinct, geometrically and intuitively. We demonstrate, perhaps suprisingly, that they are functionally, although not computationally, equivalent. That is, they cover identical surfaces, but in different fashions. After presenting both methods, we contrast their computational advantages and disadvantages.

7.6.3 Complementary Bézier Patches

Negating the edge weight of any Bézier curve $\mathbf{P}(t)$ produces a complementary curve $\tilde{\mathbf{P}}(t)$, as shown in §4.5.3. We have discovered that the procedure extends to three dimensions and the case of triangular Bézier surfaces. Rather than *one* complementary curve that shares its endpoints with its counterpart, our procedure generates *three* complementary patches, each of which shares one point and one boundary curve with the standard patch.

To see this, we must briefly digress to consider the images, under $\mathbf{P}(s,t)$, of lines in the standard domain. We call these objects *isoparametric lines*, or simply *isolines*, since they may be generated by holding one barycentric coordinate fixed and varying the other two. The images of the lines are curves on the swept Bézier patch, called *isoparametric curves* or *isocurves*.

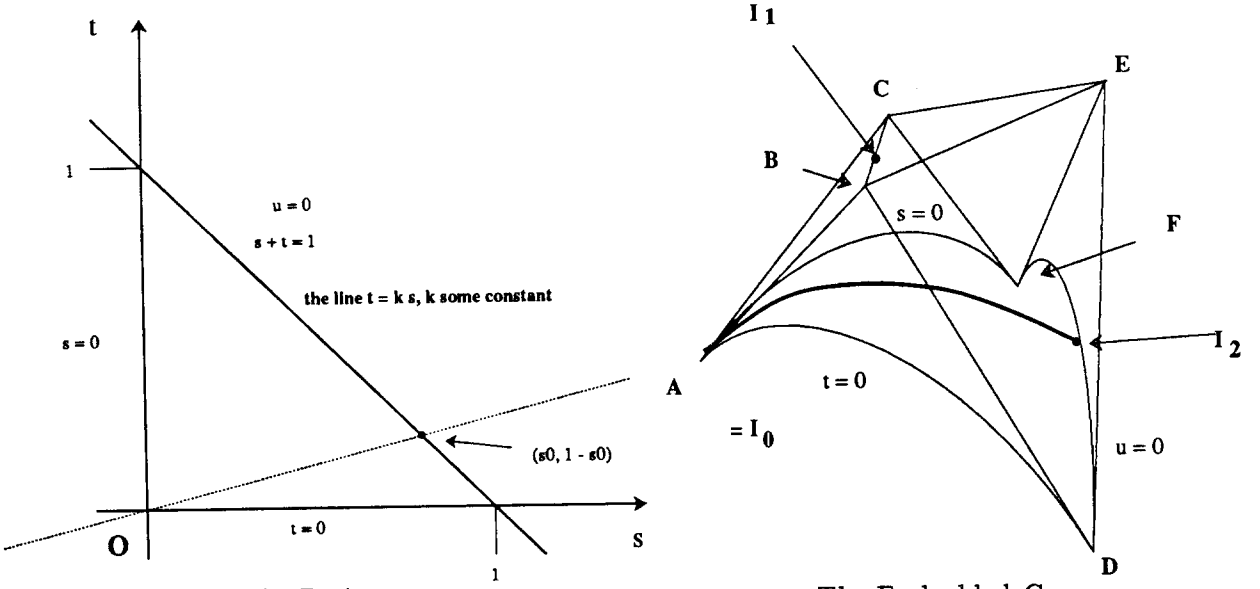

The Preimage. The Embedded Curve.

Figure 7.19: An Isoline of the Form $t = ks$, k Constant, in Domain Space, and its Associated Isocurve Embedded in the Patch $\mathbf{P}(s,t)$.

We examine a particular class of isoline; one that contains the domain space origin $(s,t) = (0,0)$. However, the following argument may be generalized to any isoline. Choose some fixed value s_0. The point on the $u = 0$ line in domain space with this s value (recall that $u = 1 - s - t$) must be $(s,t) = (s_0, 1 - s_0)$. Now form the isoline connecting the origin and this point *in domain space*; it

must have equation[4] $t = \frac{1-s_0}{s_0}s$ (Figure 7.19). The image under $\mathbf{P}$ of this domain line is a planar curve on the patch. As such, the image is expressible as a standard Bézier combination of three control points (say, $\mathbf{I}_k$). These points must be linear combinations of the patch control points. We can deduce two of these three points (say, $\mathbf{I}_0$ and $\mathbf{I}_2$) by inspection (Figure 7.19). Plainly,

$$\begin{aligned} \mathbf{I}_0 &= \mathbf{A}, \text{ and} \\ \mathbf{I}_2 &= \mathbf{P}(s_0, 1-s_0) = {s_0}^2\mathbf{D} + 2s_0(1-s_0)\mathbf{E} + (1-s_0)^2\mathbf{F}. \end{aligned} \tag{7.22}$$

The middle control point $\mathbf{I}_1$ can be found by subtracting an appropriate Bézier combination of $\mathbf{I}_0$ and $\mathbf{I}_2$ from the patch equation $\mathbf{P}(s,t)$, evaluated along the line $t = \frac{1-s_0}{s_0}s$. Some algebra yields[5]:

$$\mathbf{I}_1 = s_0\mathbf{B} + (1-s_0)\mathbf{C}. \tag{7.23}$$

The image of the domain space line $t = \frac{1-s_0}{s_0}s$ is just a planar Bézier curve with control points $\mathbf{I}_k$. Relabeling the corners of the standard domain triangle yields analogous expressions for lines incident on the $(0,1)$ and $(1,0)$ corners of the domain.

These isocurves have two important features. First, we can in principle choose any corner of the domain (say, the origin), and consider the standard Bézier patch to be composed of a family of isocurves (actually, isosegments) anchored at that corner. Second, we have shown that the middle control point for any corner-anchored isocurve is a function only of the two boundary curves originating at that corner. In fact, it is a function only of the *middle control points* of these curves (Equation 7.23). This suggests a natural extension, to surfaces, of the weight-negation procedure for Bézier curves.

We define the complementary patch $\tilde{\mathbf{P}}_u(s,t)$ by negating the weights of control points $\mathbf{B}$ and $\mathbf{C}$ (Figure 7.20). Consider the effect of this negation on the $\mathbf{I}_k$ constructed above. $\mathbf{I}_0$ and $\mathbf{I}_2$ are unaffected. But $\mathbf{I}_1$'s weight is negated, since it is a linear combination of two negated quantities. Thus the modified patch $\tilde{\mathbf{P}}_u(s,t)$ must be swept by the *complements* of the family of isocurves $\mathbf{I}_k$.

Each of these complementary curves shares its endpoints with its counterpart on the standard patch. $\mathbf{P}(s,t)$ and $\tilde{\mathbf{P}}_u(s,t)$ thus share the point $\mathbf{A}$ and the $u = 0$ boundary curve (since the control points $\mathbf{D}$, $\mathbf{E}$, and $\mathbf{F}$ are unmodified).

As before, a superscripted tilde denotes complementation. Since we can complement with respect to each corner of the standard domain, there are three ways to complement the patch, rather than one as in the curve case. For a standard patch $\mathbf{P}(s,t)$, we define the complementary patches $\tilde{\mathbf{P}}_u(s,t)$, $\tilde{\mathbf{P}}_s(s,t)$, and $\tilde{\mathbf{P}}_t(s,t)$, that result respectively from complementation of the isocurves anchored at the $u = 1$, $s = 1$, and $t = 1$ corners of the standard domain.

We note some useful properties of the complementary patches. First, they are mutually *disjoint*, except along their boundary curves and at the center of projection. We deduce this from our earlier observation that any patch is swept by a family of isocurves. The standard patch is bounded by three planes, each of which contains the center of projection $\mathbf{Z}$. The complement patches must lie "outside" of the halfspaces that are excluded by the complementation of their generating isocurves. (The patches might become coincident with the halfspaces, depending on whether the (s,t) domain is defined as an open or closed region.) For example, in Figure 7.20, the standard patch is bounded by planes **ZAD**, **ZAF**, and **ZDF**. Complementing it with respect to $u = 1$ generates a family of

[4]Here we assume s_0 is not 0; if it were, we could use t as the independent variable.

[5]Strictly speaking, we must reparametrize the curve so that $t \in [0..1]$, but that is irrelevant here.

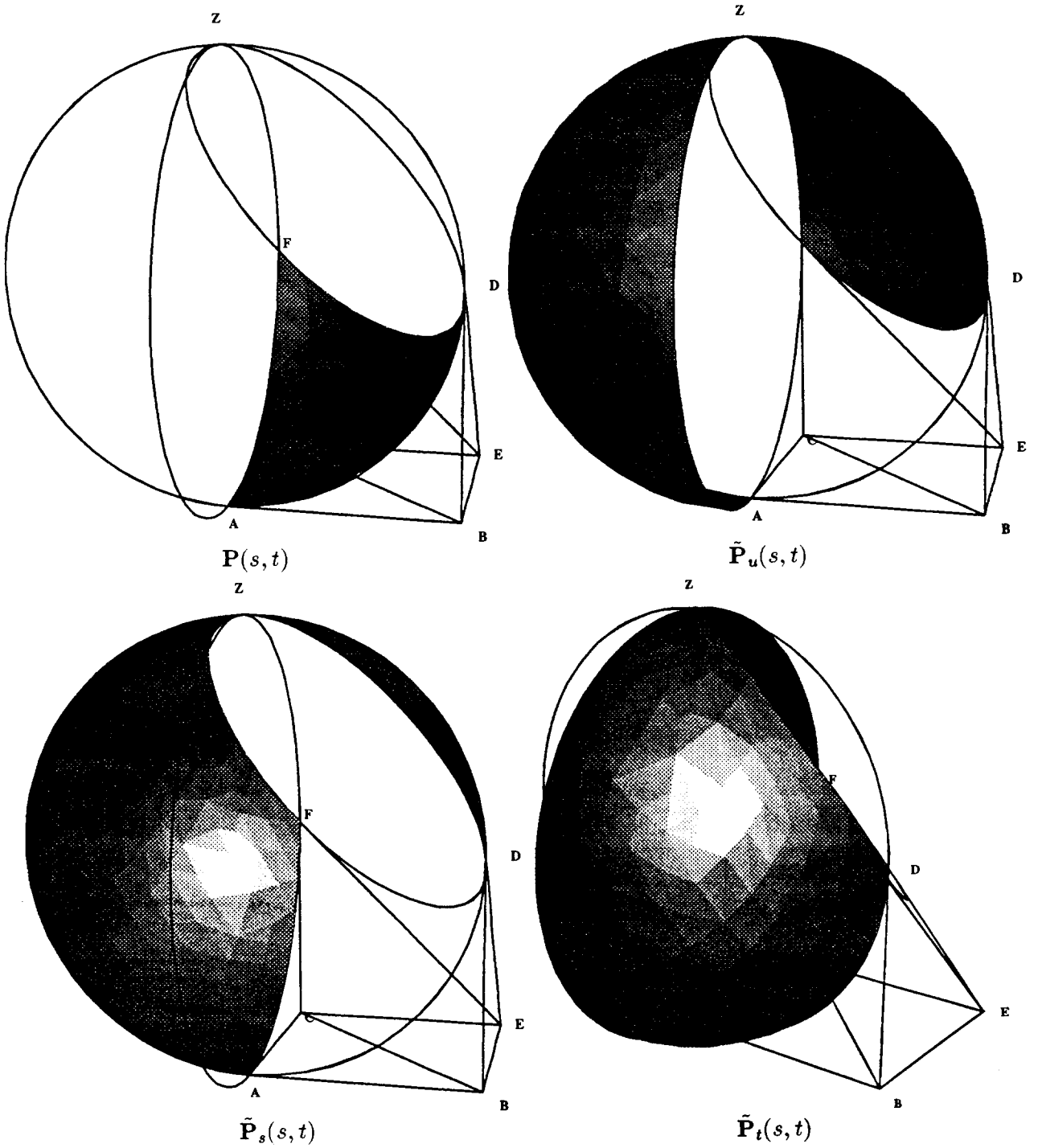

Figure 7.20: A Bézier Patch $\mathbf{P}(s,t)$, and Its Complementary Patches $\tilde{\mathbf{P}}_u(s,t)$, $\tilde{\mathbf{P}}_s(s,t)$, and $\tilde{\mathbf{P}}_t(s,t)$. Each patch has been evaluated over the standard domain, $s,t > 0$, $s+t \leq 1$. Each complemented patch intersects itself at the center of projection $\mathbf{Z}$.

isocurves that is prohibited from occupying the interiors of the halfspaces **ZAD** and **ZAF** (but not **ZDF**). The only patch point contained in all three patch boundary planes is **Z**, the center of projection.

In two dimensions, *complementary segments* and *extended segments* cover the same point locus, although for different parameter values (cf. Equation 4.24). In three dimensions, each complementary patch is created by complementing a family of standard-patch isocurves (i.e., planar segments) anchored at a corner of the standard domain. Thus we may interpret each complementary patch as a reparametrized family of extended isocurves, each family anchored in the same manner to a corner of the standard domain. Figure 7.21 depicts the domain space preimages (i.e., isolines) corresponding to the generator isocurves for each complementary patch.

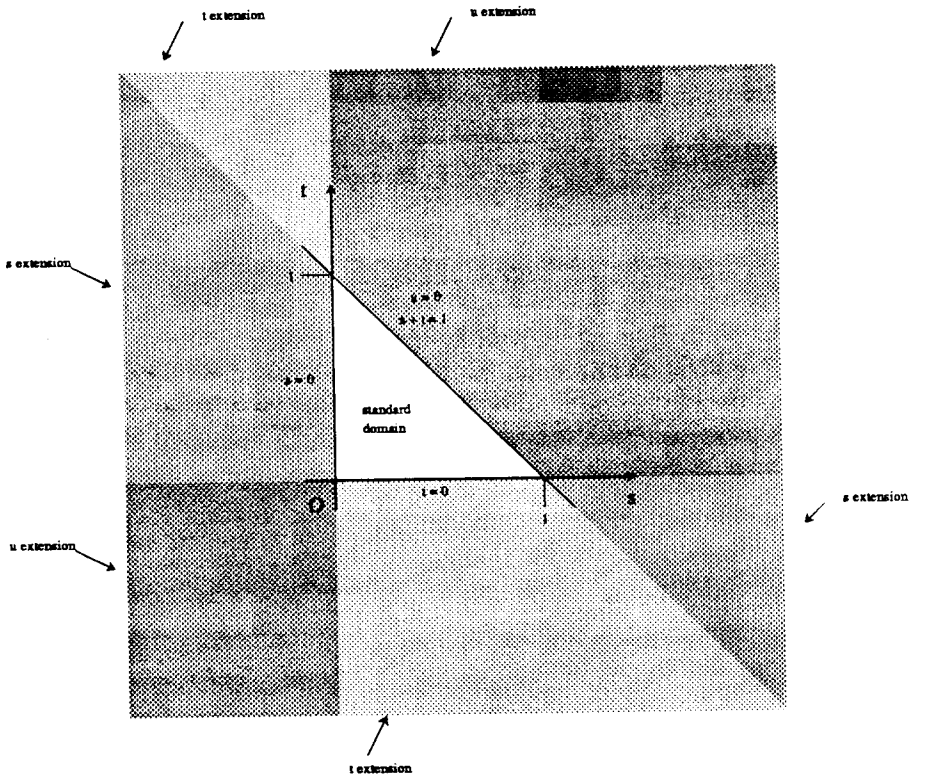

Figure 7.21: An Alternative View of the Mechanism by which Complementary Patches are Swept. Rather than considering the generator isocurves as *complements* of isocurve families embedded in the standard patch, we can interpret them as *extensions* of these families by reparametrizing each isocurve. The figure depicts the isoline preimages of the generator isocurves for the standard patch and each complementary patch.

The second useful property of the complement patches is that they can, in general, cover *unbounded* areas over *bounded* domains. For instance, consider the boundary curves of a standard patch that interpolates a paraboloid. The complements of these boundaries will in general reach ideal points. Thus the complement patches must also contain ideal points, and in this sense cover infinite areas. Thus we are no longer restricted, literally, to modeling "patches" of quadrics; instead, four bounded-domain sections are easily constructible that cover an entire quadric.

One drawback of complement patches is their somewhat odd shape, even over such a symmetric

object as a sphere. This is mitigated by their predictable behavior with respect to the bounding halfspaces of the standard patch, and their representational power in covering complete quadrics.

The odd shape of the complementary patches is also mitigated by the existence of straightforward collinearity and algebraic relations between points $\mathbf{P}(s,t)$ on the standard patch and points on the complementary patches, in analogy to the lower-dimensional case (§4.5.3). We derive these relationships here, for *unrestricted* rational quadratic triangular Bézier patches. That is, our derivations do not require the Bézier patch to interpolate an implicit quadric surface.

We seek an expression relating $\mathbf{P}(s,t)$ and, say, $\tilde{\mathbf{P}}_u(s,t)$. Since each patch can be considered separately as a standard patch, it must be true that each patch, when *extended*, covers the same surface. That is, every point reached by the expression $\mathbf{P}(s,t)$ will also be reached by each of the complementary patches, although perhaps for different (s,t). The common point's preimage under $\mathbf{P}$ will not (in general) be its preimage under $\tilde{\mathbf{P}}_u$. Formally, we claim that for every (s,t), there is some (s',t') such that

$$\mathbf{P}(s,t) = \tilde{\mathbf{P}}_u(s',t') \qquad \text{for } (s,t) \text{ not necessarily equal to } (s',t'). \tag{7.24}$$

As in §4.5.3, we write the standard patch $\mathbf{P}(s,t)$ and complement patch $\tilde{\mathbf{P}}_u(s,t)$ explicitly (negating the weights B_w and C_w in the latter):

$$\mathbf{P}(s,t) = \frac{A_w\mathbf{A}(1-s-t)^2 + B_w\mathbf{B}2s(1-s-t) + C_w\mathbf{C}2t(1-s-t) + D_w\mathbf{D}s^2 + E_w\mathbf{E}2st + F_w\mathbf{F}t^2}{w(t)}$$

$$\tilde{\mathbf{P}}_u(s,t) = \frac{A_w\mathbf{A}(1-s-t)^2 - B_w\mathbf{B}2s(1-s-t) - C_w\mathbf{C}2t(1-s-t) + D_w\mathbf{D}s^2 + E_w\mathbf{E}2st + F_w\mathbf{F}t^2}{\tilde{w}_u(t)}.$$

Here we have defined the weight functions $w(s,t)$ and $\tilde{w}_u(s,t)$ as

$$\begin{aligned} w(s,t) &= A_w(1-s-t)^2 + B_w2s(1-s-t) + C_w2t(1-s-t) + D_ws^2 + E_w2st + F_wt^2 \\ \tilde{w}_u(s,t) &= A_w(1-s-t)^2 - B_w2s(1-s-t) - C_w2t(1-s-t) + D_ws^2 + E_w2st + F_wt^2. \end{aligned}$$

Define the variables

$$\begin{aligned} s' &= \frac{s}{2s+2t-1}, \text{ and} \\ t' &= \frac{t}{2s+2t-1}. \end{aligned}$$

Direct substitution into either the standard or u-complemented equation shows that

$$\mathbf{P}(s,t) = \tilde{\mathbf{P}}_u(s',t') \qquad \text{for all } (s,t).$$

Thus the relation we seek is

$$\mathbf{P}(s,t) = \tilde{\mathbf{P}}_u\left(\frac{s}{2s+2t-1}, \frac{t}{2s+2t-1}\right). \tag{7.25}$$

This equation is symmetric in $\mathbf{P}$ and $\tilde{\mathbf{P}}_u$. For any s and t, Equation 7.25 can be used to compute the preimage of the point $\mathbf{P}(s,t)$ in the domain of the patch $\tilde{\mathbf{P}}_u(s,t)$, and vice-versa. Analogous expressions may be derived relating the complementary patches $\tilde{\mathbf{P}}_s(s,t)$ and $\tilde{\mathbf{P}}_t(s,t)$ to the standard patch $\mathbf{P}(s,t)$.

Recall from §4.5.3 that, for Bézier curves $\mathbf{P}(t)$, the control point $\mathbf{p}_1$, the complement segment point $\tilde{\mathbf{P}}(t)$, and the standard segment point $\mathbf{P}(t)$ are collinear for all t. A similar relation holds for complementary patches, although it involves a *line*, rather than a point, induced by the control hull.

Refer again to Equation 7.25. We seek some point (say, $\mathbf{Q}$), that can be expressed as an affine combination of $\mathbf{P}(s,t)$ and $\tilde{\mathbf{P}}_u(s,t)$. That is, we seek $\mathbf{Q}$ (possibly a function of s and t) such that:

$$\mathbf{Q} = \mathbf{Q}(s,t) = \alpha\mathbf{P}(t) + (1-\alpha)\tilde{\mathbf{P}}_u(s,t) \qquad \alpha \text{ some scalar.}$$

One solution to the above system of equations is

$$\mathbf{Q} = \mathbf{Q}(s,t) = \frac{sB_w}{sB_w + tC_w}\mathbf{B} + \frac{tC_w}{sB_w + tC_w}\mathbf{C} = \frac{w}{w-\tilde{w}_u}\mathbf{P} - \frac{\tilde{w}_u}{w-\tilde{w}_u}\tilde{\mathbf{P}}_u, \tag{7.26}$$

where we have omitted the (s,t) from $w, \tilde{w}_u, \mathbf{P}$, and $\tilde{\mathbf{P}}_u$ for clarity. Since the coefficients of $\mathbf{B}$ and $\mathbf{C}$, and the coefficients of $\mathbf{P}$ and $\tilde{\mathbf{P}}_u$, respectively, sum to unity, we may rewrite Equation 7.26 as:

$$\mathbf{Q} = \alpha\mathbf{P} + (1-\alpha)\tilde{\mathbf{P}}_u = \gamma\mathbf{B} + (1-\gamma)\mathbf{C} \qquad \alpha, \gamma \text{ some scalars.}$$

Thus, under u complementation, points evaluated at like values of s and t on the standard and complementary patches are collinear with a point $\mathbf{Q}$ on the control hull line $\mathbf{BC}$. The point $\mathbf{Q}$ may be expressed solely in terms of s, t, and the control points $\mathbf{B}$ and $\mathbf{C}$ (Equation 7.26).

Figure 7.22 illustrates the collinearity relation 7.26. The patch $\mathbf{P}(s,t)$ has deliberately been parametrized in an asymmetric manner to emphasize the nature of the relation.

Collinearity relations similar to (7.26) are easily found for the case of s and t complementation. These relations involve the control hull lines $\mathbf{CE}$ and $\mathbf{BE}$, respectively.

7.6.4 Projective Domains

DeRose has recently proposed another procedure for covering the complete implicit surface implied by the standard Bézier patch [9]. He observes that the quadratic Bézier basis functions, expressed in barycentric domain coordinates (Equations 7.4) have the property that:

$$B_{i,j,k}(as, at, au) \quad = \quad a^2 B_{i,j,k}(s,t,u). \tag{7.27}$$

Reexpressing the patch definition (Equation 7.5) in (s,t,u) coordinates produces

$$\mathbf{P}(s,t,u) = \frac{\sum w_{ijk}\mathbf{p}_{ijk}B_{ijk}(s,t,u)}{\sum w_{ijk}B_{ijk}(s,t,u)}, \qquad \text{i+j+k} = 2. \tag{7.28}$$

But Equation 7.27 implies that

$$\mathbf{P}(as, at, au) = \mathbf{P}(s,t,u), \tag{7.29}$$

since the factor a^2 appears both in the numerator and denominator of the patch expression. Thus the parameters (s,t,u) may be interpreted as a homogeneous point, and the restriction $s+t+u = 1$ removed.

The problem of covering the entire (s,t) domain of the patch therefore reduces to finding a set of homogeneous (s,t,u) triplets that represent all of the (s,t) domain. Derose shows that this can

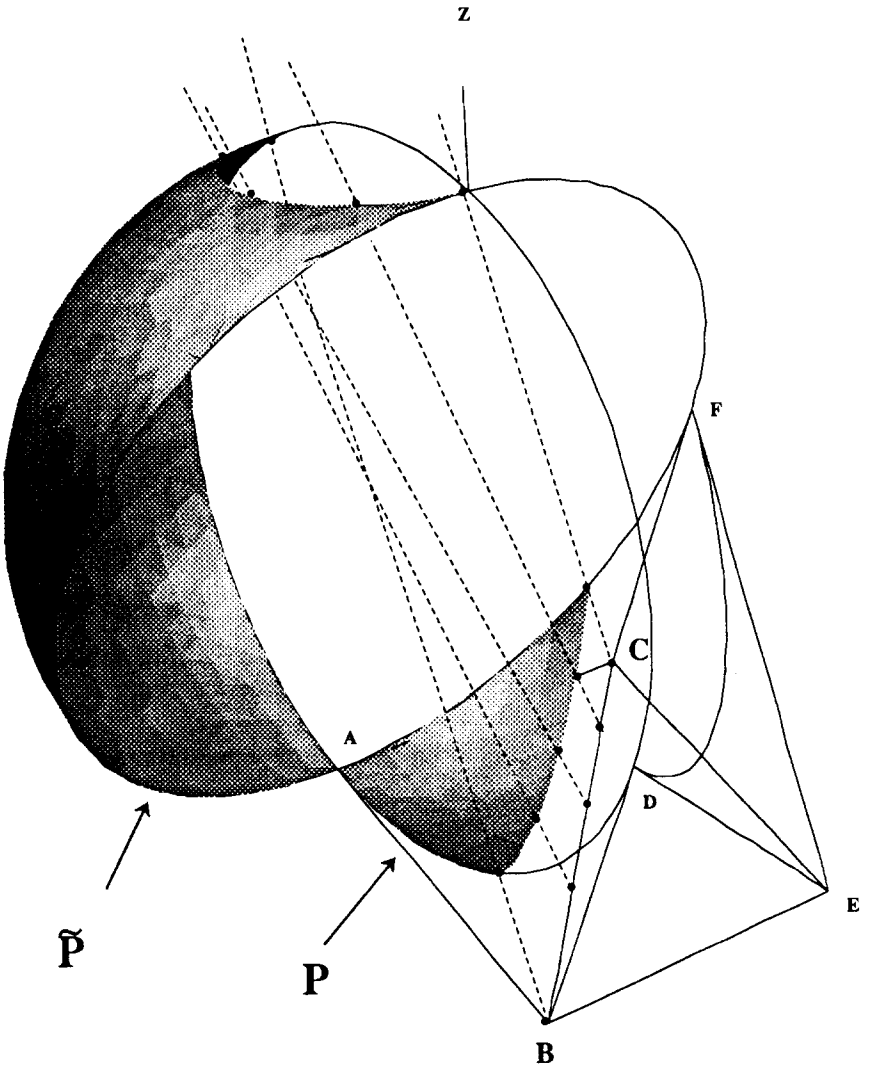

Figure 7.22: An Illustration of the Collinearity Relation (7.26).
The patch $\mathbf{P}(s,t)$ and $\tilde{\mathbf{P}}_u(s,t)$ are shown, evaluated over the same portion of the standard domain. Every pair of points $\mathbf{P}(s,t)$ and $\tilde{\mathbf{P}}_u(s,t)$ are collinear with a point that is a function only of s, t, and the control points $\mathbf{B}$ and $\mathbf{C}$. Several such pairs are shown along a (u = constant) isocurve.

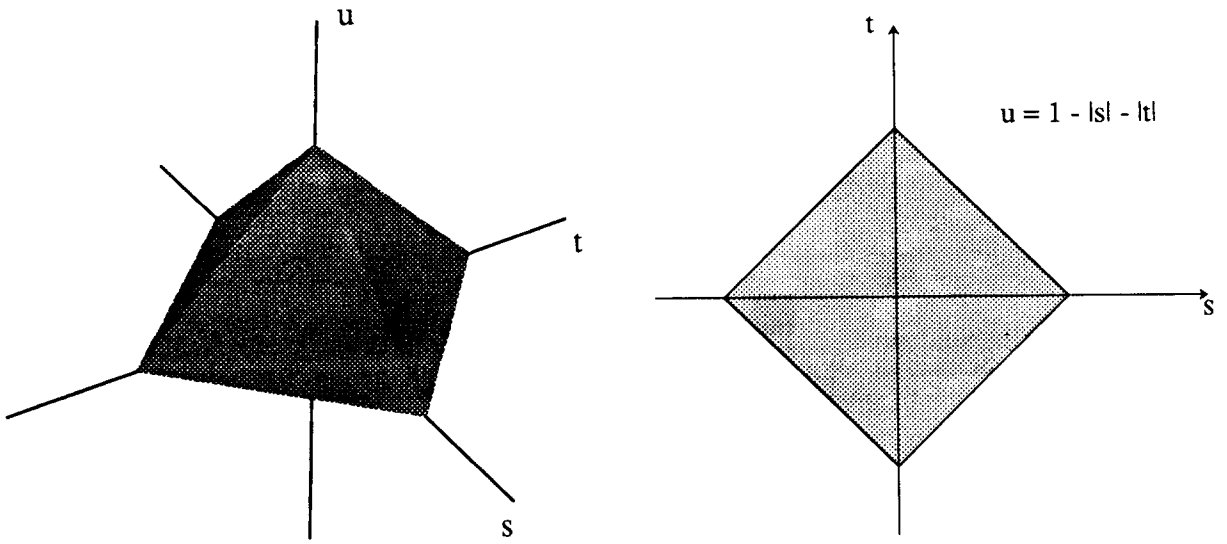

Figure 7.23: DeRose's treatment of the (s,t) domain as the projection of a pyramid in homogeneous (s,t,u) coordinates. Sampling (s,t,u) inside the pyramid yields a representation for every line in the homogenous coordinates of $\Re^2$. The shaded region on the right represents the resulting (s,t) values, with the added constraint that $u = 1 - |s| - |t|$. Both figures after [9].

be done if the (s,t,u) coordinates are restricted to a four-sided pyramid (with u as the apical axis); the resulting (s,t) coordinates tile the base of the pyramid in the (s,t) plane (Figure 7.23) with the constraint $u = 1 - |s| - |t|$.

The method of projective domains is conceptually quite distinct from the patch complementation techniques presented earlier in this work. Somewhat surprisingly, the methods are functionally equivalent. That is, each modified projective patch over one of the domain quadrants on the right side of Figure 7.23 corresponds to a complemented patch evaluated over the standard domain. This is easily seen by expanding the projective patch definition for each of the quadrants. For example, in the $(-1,-1)$ quadrant the projective patch equation is simply Equation 7.28 under the mapping

$$\begin{aligned} s &\rightarrow -s \\ t &\rightarrow -t \\ u &\rightarrow u, \text{ since } u = 1 - |s| - |t|. \end{aligned}$$

Expanding the projective patch equation (7.28) over the $(-1,-1)$ quadrant yields

$$\mathbf{P}(s,t,u) = \frac{A_w\mathbf{A}u^2 - B_w\mathbf{B}2su - C_w\mathbf{C}2tu + D_w\mathbf{D}2s^2 + E_w\mathbf{E}2st + F_w\mathbf{F}2t^2}{A_w u^2 - B_w 2su - C_w 2tu + D_w 2s^2 + E_w 2st + F_w 2t^2}, \tag{7.30}$$

where the terms in u^2, s^2, t^2, and $2st$ are unaffected by the sign changes in s and t, but the terms in $2su$ and $2tu$ are negated (here we have used the alphabetic control hull labeling). By inspection, this expression is identical to Equation 7.25, the definition of the u-complemented patch $\tilde{\mathbf{P}}_u(s,t)$. Similarly, the projective patches evaluated over the $(1,1)$, $(-1,1)$, and (1,-1) domain quadrants are equivalent, respectively, to the standard patch $\mathbf{P}(s,t)$; the s-complemented patch $\tilde{\mathbf{P}}_s(s,t)$; and the t-complemented patch $\tilde{\mathbf{P}}_t(s,t)$ of §7.6.3.

The methods of patch complementation and projective domains both allow the patch equation to cover the extended implicit surface covered only partially by a standard patch. Patch com-

plementation has the drawback that it generates four patches from the single standard patch; its advantage is that each of these patches is in standard form and may be evaluated over the canonical triangular s,t domain. Evaluating the patch requires only two linear and quadratic functions of the domain variables s and t.

In contrast, the method of projective domains has the advantage that it manipulates only one patch equation. However, the projective patch equation is at least as hard to evaluate as the complementary patch equations. The projective patch must be evaluated over a domain that is essentially the standard domain replicated four times. Evaluation involves the same quadratic functions of s and t as does complementary patch evaluation, as well as quadratic functions of u and additional absolute value operations on u.

7.6.5 The Fundamental Curve of a Complemented Bézier Patch That Interpolates a Quadric

The collinearity relation (7.26) implies that every restricted complemented patch must have a *fundamental curve*; that is, a curve in domain space each point of which maps to a single point on the patch (Figure 7.24). To see this, imagine the line segment **BC** projected through the center of projection **Z** onto some curve **M** embedded in the standard patch $\mathbf{P}(s,t)$. This curve is planar, and so must be the image of some conic curve $\mathbf{M}'$ in the domain of $\mathbf{P}(s,t)$. Project the planar curve **M** through **Z** onto the complemented patch $\tilde{\mathbf{P}}_u(s,t)$, producing the degenerate planar curve $\tilde{\mathbf{M}}$ consisting of the single point **Z**. This "curve," by Equation 7.26, must have preimage $\tilde{\mathbf{M}}'$ in the domain of the complemented patch $\tilde{\mathbf{P}}_u(s,t)$. Thus $\tilde{\mathbf{M}}'$ is a fundamental curve of the complemented patch.

In fact, all restricted Bézier patches have fundamental curves. This was shown formally in [32]; in Chapter 8 we arrive at this conclusion using only geometric reasoning.

7.6.6 The Usefulness of Complementary Bézier Patches

Complementary patches are a useful generalization of standard Bézier patches in that they provide a simple method for covering complete implicit quadrics. If the standard patch is not restricted to interpolate an implicit quadric, then the complementary patches are unrestricted as well. They continue, however, to "tile" the extended (superquadratic) surface implied by evaluating the standard patch equation $\mathbf{P}(s,t)$ outside the usual domain. For an unrestricted patch equation, the union of the standard patch and the three complement patches will generally be a self-intersecting quartic surface.

The standard and complement patches are well-behaved in that they are contained within easily-derived halfspaces, and mutually disjoint (except along shared control points and boundary curves). Complemented patches are less useful to modelers wishing to bound *portions* of quadrics, primarily due to the fact that four patches (i.e., **P** and its three complements) must be manipulated, rather than one.

It seems that none of the formulations presented– standard Bézier patches, extended patches, or complement patches– are completely adequate for representation of arbitrarily bounded quadrics. Standard patches are the most obviously inadequate in their inflexibility; their boundary curves are strictly defined by the three corner points and center of projection. These are rigid constraints

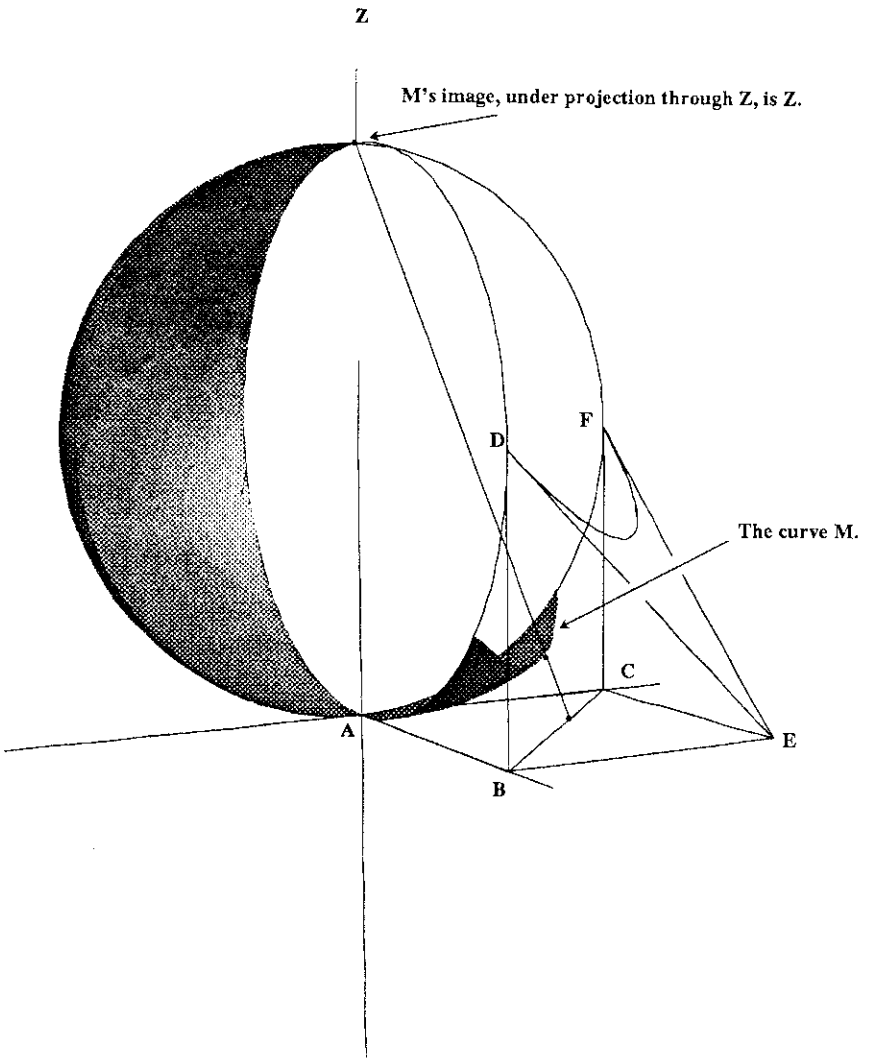

Figure 7.24: Every Restricted Complemented Patch Has a Fundamental Curve. Its image under the complemented patch equation is the center of projection **Z**.

indeed, for a modeling environment in which objects must be adjoined across arbitrary planar (and perhaps nonplanar) boundaries. Extended patches are inadequate without effective control over boundary curve specification. Existing methods provide this control only at the expense of a cumbersome inversion operation. In general, the extended patch formulation does not present to the modeling practitioner a geometric relationship between the shape of the swept patch and the shape of its domain-space preimage. Finally, complementary patches, although attractive in their bounded-domain property, present the difficulties of multiple patches and multiple inversions.

We have developed a novel, constructive method of producing quadratic Bézier patches that interpolate quadric surfaces. The method, presented in the following chapter, generates a single quadratic patch over a specified portion of a given quadric, as does the method presented in this chapter. Our method also yields, for a negligible extra amount of computation, a *trivial inversion* procedure for the patch. We shall show that this property has two immediate benefits. First, the availability of a simple inversion procedure provides simple, robust control over the boundaries and parametrization of the swept patch. Second, patches constructed in this manner have easily identifiable fundamental curves; these may be handled or avoided as modelers or renderers deem appropriate. The adoption of the patch constructions that we propose makes feasible modelers that can, for example, cover arbitrarily bounded portions of quadrics (even for non-planar boundaries). Our method might also facilitate better implementations of parametric surface-intersection algorithms, at least those involving parametrized quadric surfaces.

Chapter 8

Bézier Patches That Interpolate Quadrics, and Their Equivalence to Stereographic Maps of the Plane

This chapter unifies the notions of restricted rational quadratic triangular Bézier patches, and stereographic maps from the plane onto implicit quadrics. We demonstrate a novel correspondence between the two formulations and introduce simple constructions for converting between them. As in the case of conics and Bézier curves, the transformations are purely constructive and geometrically intuitive; they can be implemented with simple geometric and algebraic operations.

We show that this correspondence yields a simple method of constructing Bézier surfaces that interpolate desired quadrics, are bounded by arbitrary collections of planes, and are trivially invertible.

8.1 Stereographic Maps Onto Quadrics

We define stereographic maps in $\Re^3$ in direct analogy to those in two dimensions (cf. Chapter 5). For any quadric ξ, choose a center of projection $\mathbf{Z}$ on ξ and baseplane $\mathbf{L}$ not containing $\mathbf{Z}$. Identify each point $\mathbf{p}$ on $\mathbf{L}$ with its image $\mathbf{M}(\mathbf{p})$ on ξ, such that $\mathbf{M}(\mathbf{p})$ is the intersection (apart from $\mathbf{Z}$) of ξ with the line through $\mathbf{Z}$ and $\mathbf{p}$ (Figure 8.1). We call this identification the stereographic map of $\mathbf{L}$ through $\mathbf{Z}$ and onto ξ.

In two dimensions, a stereographic map baseline $\mathbf{L}$ is coordinatized with an origin $\mathbf{O}$ and unit vector $\hat{\mathbf{L}}$ (cf. Figure 5.1). $\mathbf{L}$ contains a single point at infinity, the *pole* of $\mathbf{M}$, whose image under $\mathbf{M}$ is a single point on the mapped conic. All two-dimensional stereographic maps of conics, with $\mathbf{Z}$ on the conic, are representable as rational quadratic polynomials, and vice-versa.

In three dimensions, coordinatizing the baseplane $\mathbf{L}$ requires an origin $\mathbf{O}$ and *two* basis vectors $\hat{\mathbf{s}}$ and $\hat{\mathbf{t}}$ (Figure 8.1). These vectors need not constitute an *orthonormal* basis[1]. Indeed, we show that $\hat{\mathbf{s}}$ and $\hat{\mathbf{t}}$ generally comprise an *oblique*, *non-normalized* basis set. We require of $\hat{\mathbf{s}}$ and $\hat{\mathbf{t}}$ only that they span the baseplane $\mathbf{L}$.

[1] An orthonormal basis is one in which all vectors have unit length and are mutually perpendicular.

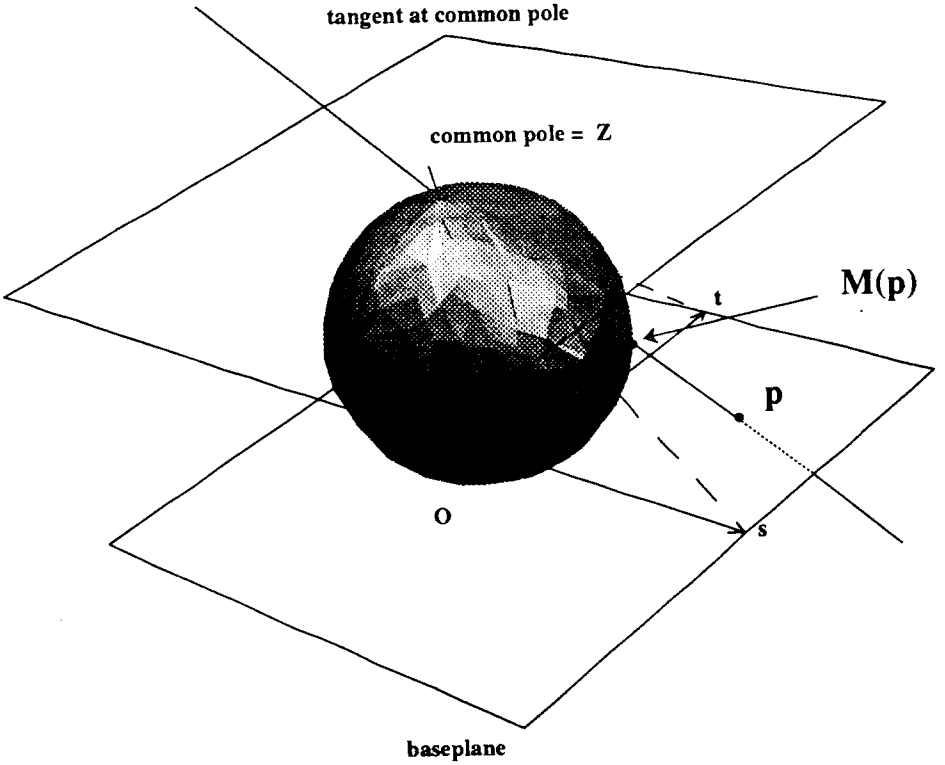

Figure 8.1: A Stereographic Map of a Plane **L** onto a Quadric ξ, in Standard Form.

Rather than a single point at infinity, there is a *line at infinity* on the baseplane **L**. Consider the image of this line under **M**. If the baseplane **L** is parallel to the quadric tangent plane at **Z**, all points at infinity on **L** will be mapped to **Z** under **M** (Figure 8.1). As in two dimensions, we say that a map with this property is in *standard form*. In contrast, if **L** is not parallel to the tangent plane at **Z**, the image of **L**'s line at infinity under **M** will be a planar curve on ξ; namely, the planar curve formed by intersecting the quadric ξ with the unique plane through **Z** and parallel to **L** (Figure 8.2). We call this curve the *image of the line at infinity under* **M**.

Stereographic maps of quadrics are easily *invertible*. That is, given a map **M** of a quadric ξ and any point **p** on ξ, it is easy to find scalars (s,t) such that $\mathbf{M}(s,t) = \mathbf{p}$. Intersect the line through **Z** and **p** with the map baseplane **L**. The resulting baseplane point, expressed in the oblique basis of **O**, $\hat{\mathbf{s}}$, and $\hat{\mathbf{t}}$, has coordinates (s,t).

Lastly, we note that the one-to-one correspondence between conics and rational polynomial expressions in two dimensions does not persist to three-dimensional stereographic maps and quadrics. That is, although (as we have shown) every implicit quadric may be represented as a rational quadratic polynomial, not every rational quadratic polynomial represents a quadric, under stereographic projection or otherwise. This follows immediately from two facts. First, general rational quadratic polynomials are symbolic expansions of general rational quadratic triangular Bézier patches. Second, such patches may have quartic degree when implicitized [32].

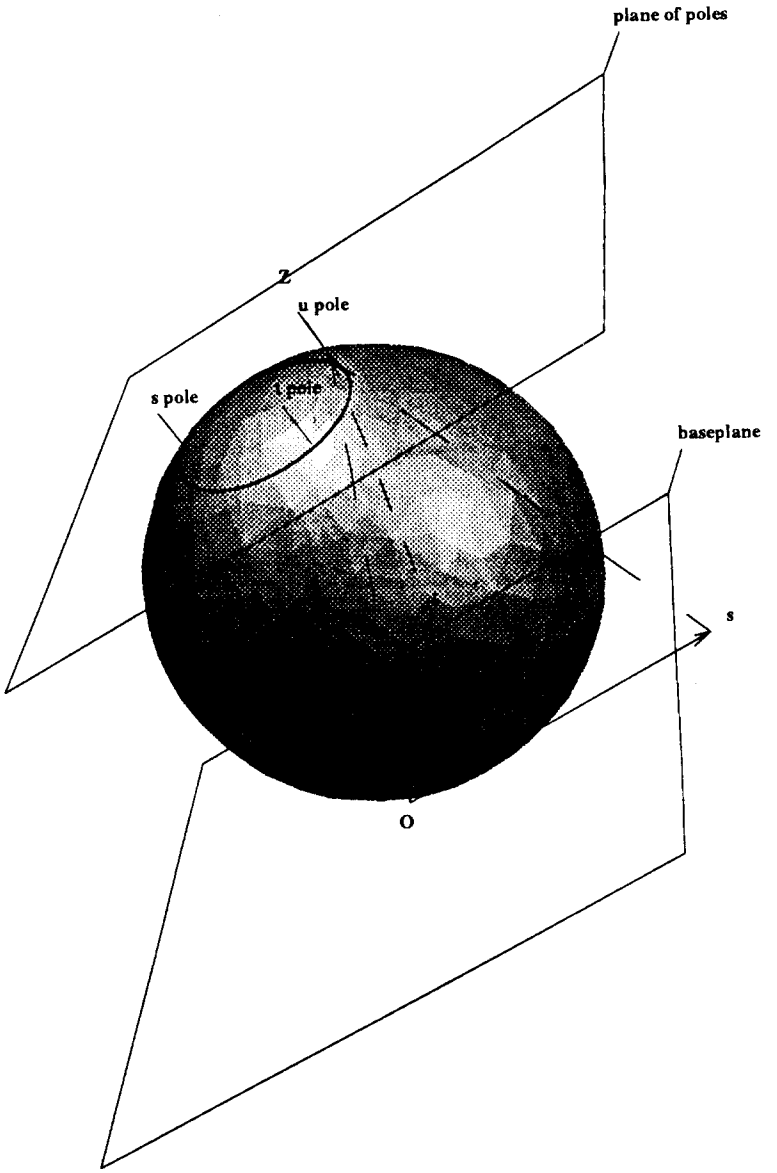

Figure 8.2: A Stereographic Map of a Plane **L** onto a Quadric ξ, In Non-Standard Form. Here ξ is rendered translucently, and the image of the line at infinity under **M** is shown.

8.2 Constructing a Coordinatized Stereographic Map From a Bézier Patch

We generalize the treatment of Chapter 5 to three dimensions. We exhibit a transformation that, given a rational quadratic triangular Bézier patch $\mathbf{P}(s,t)$ interpolating a quadric ξ, produces an equivalent coordinatized stereographic map $\mathbf{M}(s,t)$. This map consists of a center $\mathbf{Z}$; origin $\mathbf{O}$; spanning basis $\hat{\mathbf{s}}$ and $\hat{\mathbf{t}}$; and rational quadratic expression $\mathbf{M}(s,t)$. Figures 8.3 and 8.4 illustrate the construction.

Recall that a necessary and sufficient condition for the patch $\mathbf{P}(s,t)$ to interpolate ξ is that the three patch boundary curves, when extended, intersect in a single point. This point must be the intersection of the planes embedding the three boundary curves. Thus we can compute $\mathbf{Z}$, independently of parametrization, as $\mathbf{ABD} \wedge \mathbf{ACF} \wedge \mathbf{DEF}$.

Next, find the poles $\mathbf{S}$, $\mathbf{T}$, and $\mathbf{U}$ of the s, t, and u boundary curves. There are two cases. If $\mathbf{S}$, $\mathbf{T}$, and $\mathbf{U}$ are coincident, they must coincide at $\mathbf{Z}$, and we choose the baseplane $\mathbf{L}$ parallel to ξ's tangent plane there. If $\mathbf{S}$, $\mathbf{T}$, and $\mathbf{U}$ are distinct, they span some plane (labeled the *plane of poles* in Figure 8.3), and we choose the baseplane $\mathbf{L}$ parallel to this plane. The third case, exactly two of $\mathbf{S}$, $\mathbf{T}$, and $\mathbf{U}$ coincident, cannot occur. Suppose that (say) $\mathbf{S}$ and $\mathbf{T}$ were coincident. Then they coincide at $\mathbf{Z}$, and the tangents to the s and t boundary curves span a plane parallel to ξ's tangent plane at $\mathbf{Z}$. This plane's intersection with ξ (namely, $\mathbf{Z}$) must be the image under $\mathbf{P}$ of the line at infinity. Thus $\mathbf{U}$ must be coincident with $\mathbf{Z}$ (and thus coincident with $\mathbf{S}$ and $\mathbf{T}$). This contradicts our original assumption that exactly two points were coincident.

So far, the construction has produced a center of projection $\mathbf{Z}$ and an orientation, but not placement, of the baseplane $\mathbf{L}$. The baseplane position is restricted only in that it must be disjoint from $\mathbf{Z}$. Without loss of generality, arrange that $\mathbf{L}$ contain the control point $\mathbf{E}$.

The origin $\mathbf{O}$ and basis vectors $\hat{\mathbf{s}}$ and $\hat{\mathbf{t}}$ follow immediately from the two-dimensional treatment. We find $\mathbf{O}$ simply as the projection of control point $\mathbf{A}$ through $\mathbf{Z}$ onto $\mathbf{L}$. Similarly, $\hat{\mathbf{s}}$ and $\hat{\mathbf{t}}$ are found by projecting control points $\mathbf{D}$ and $\mathbf{F}$, respectively[2] (Figure 8.4).

We claim that the resulting coordinatized stereographic map $\mathbf{M}(s,t)$ is equivalent to the given patch $\mathbf{P}(s,t)$ in the following sense. For any scalars (s,t), compute the baseplane point $\mathbf{p} = \mathbf{O} + s\hat{\mathbf{s}} + t\hat{\mathbf{t}}$. Form the line containing $\mathbf{Z}$ and $\mathbf{p}$. Find $\mathbf{p}'$, the intersection (apart from $\mathbf{Z}$) of this line with the quadric ξ (if there is no such intersection, choose $\mathbf{p}' = \mathbf{Z}$). Then $\mathbf{M}(s,t) = \mathbf{p}' = \mathbf{P}(s,t)$.

Imagine the quadric surface as a collection of planar slices (i.e., conics). We show that the correspondence between $\mathbf{P}$ and $\mathbf{M}$ holds everywhere along each slice (Figures 8.5 and 8.6). Choose any *slicing plane* $\mathbf{R}$ that contains $\mathbf{Z}$ and the control point $\mathbf{A}$ of the given patch. $\mathbf{R}$ is free to pivot about the line $\mathbf{AZ}$. The image of the line $s + t = 1$ under $\mathbf{P}$ is some conic. Label as $\mathbf{q}$ the unique intersection of this conic with $\mathbf{R}$. Slicing $\mathbf{M}$ with $\mathbf{R}$ generates a two-dimensional map $\mathbf{M}_2(r)$, where r parametrizes the isocurve $\mathbf{P}_2(r)$ induced by the slicing plane and the given patch. $\mathbf{P}_2(r)$ must be the image, under $\mathbf{P}$, of the patch domain line through the origin and $\mathbf{q}$'s preimage.

By construction, the origin $\mathbf{O}_2$ and center of projection $\mathbf{Z}_2$ of the planar stereographic map $\mathbf{M}_2$ are respectively coincident with $\mathbf{O}$ and $\mathbf{Z}$. The baseline $\mathbf{L}_2$ is just the intersection of the slicing plane $\mathbf{R}$ with the baseplane $\mathbf{L}$. Finally, the single basis vector $\hat{\mathbf{L}}_2$ of the sliced map is just the

[2]More precisely, these projections produce the *points* $\mathbf{O} + \hat{\mathbf{s}}$ and $\mathbf{O} + \hat{\mathbf{t}}$; the basis vectors are then found by subtracting the origin $\mathbf{O}$.

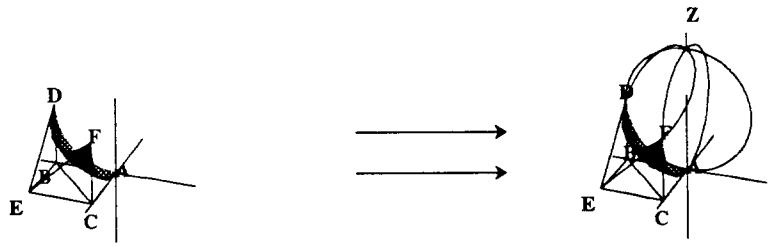

Given: Bezier patch P(s,t).

Find Center of Projection

Z = ABD ^ ACF ^ DEF.

Extend Boundary Curves; Find Poles.

Two Cases:

A) Boundary Curve Poles Coincident.

B) Boundary Curve Poles Distinct.

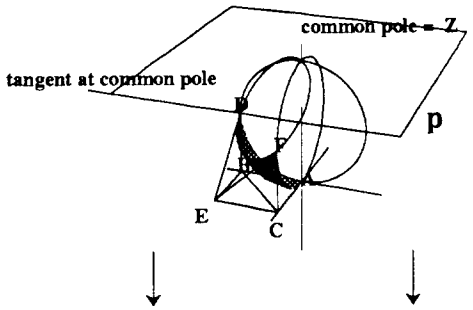

Find Plane p Tangent at Z .

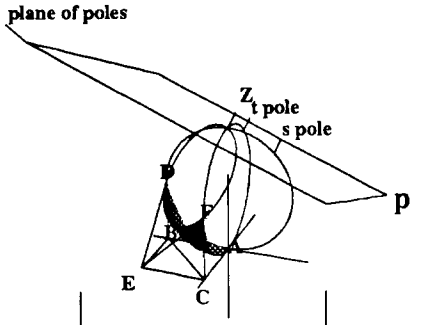

Find Plane p Spanning Three Poles.

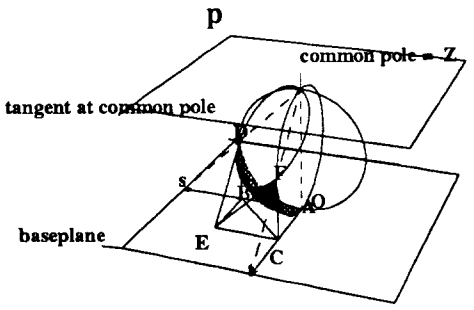

Compute Baseplane Parallel to p,

Through Control Point E.

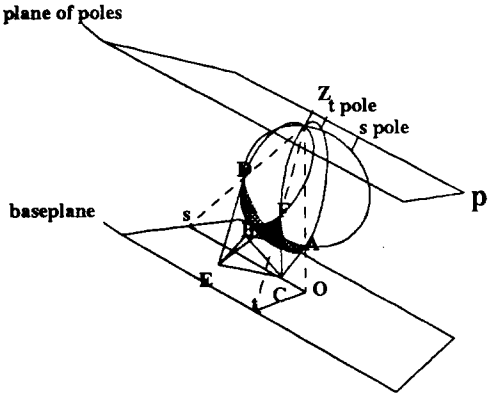

Compute Baseplane Parallel to p,

Through Control Point E.

Figure 8.3: Transforming a Quadratic Bézier Patch to an Equivalent Stereographic Map, Part I.

Case A: Coincident Poles.

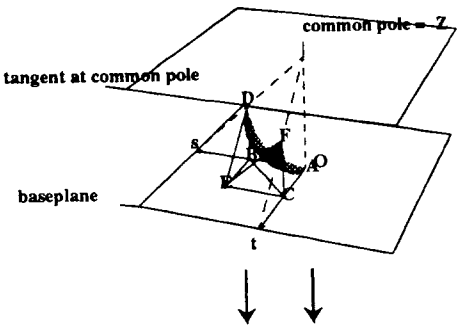

Compute Baseplane Origin, Basis Vectors.

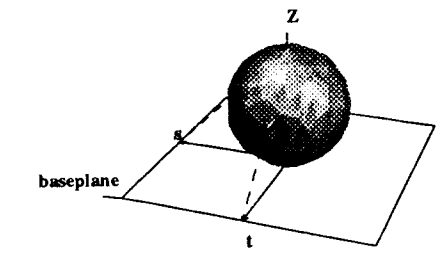

Resulting Coordinatized Stereographic Map M(s,t) is in Standard Form, and is Equivalent to Given Patch P(s,t).

Case B: Distinct Poles.

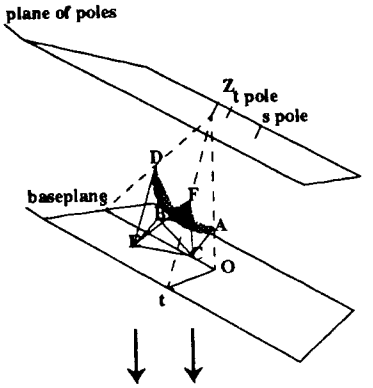

Compute Baseplane Origin, Basis Vectors.

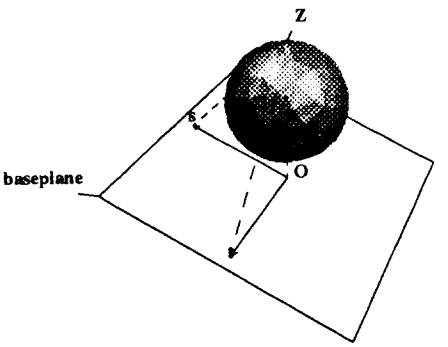

Resulting Coordinatized Stereographic Map M(s,t) is in Non-Standard Form, and is Equivalent to Given Patch P(s,t).

Figure 8.4: Transforming a Quadratic Bézier Patch to an Equivalent Stereographic Map, Part II.

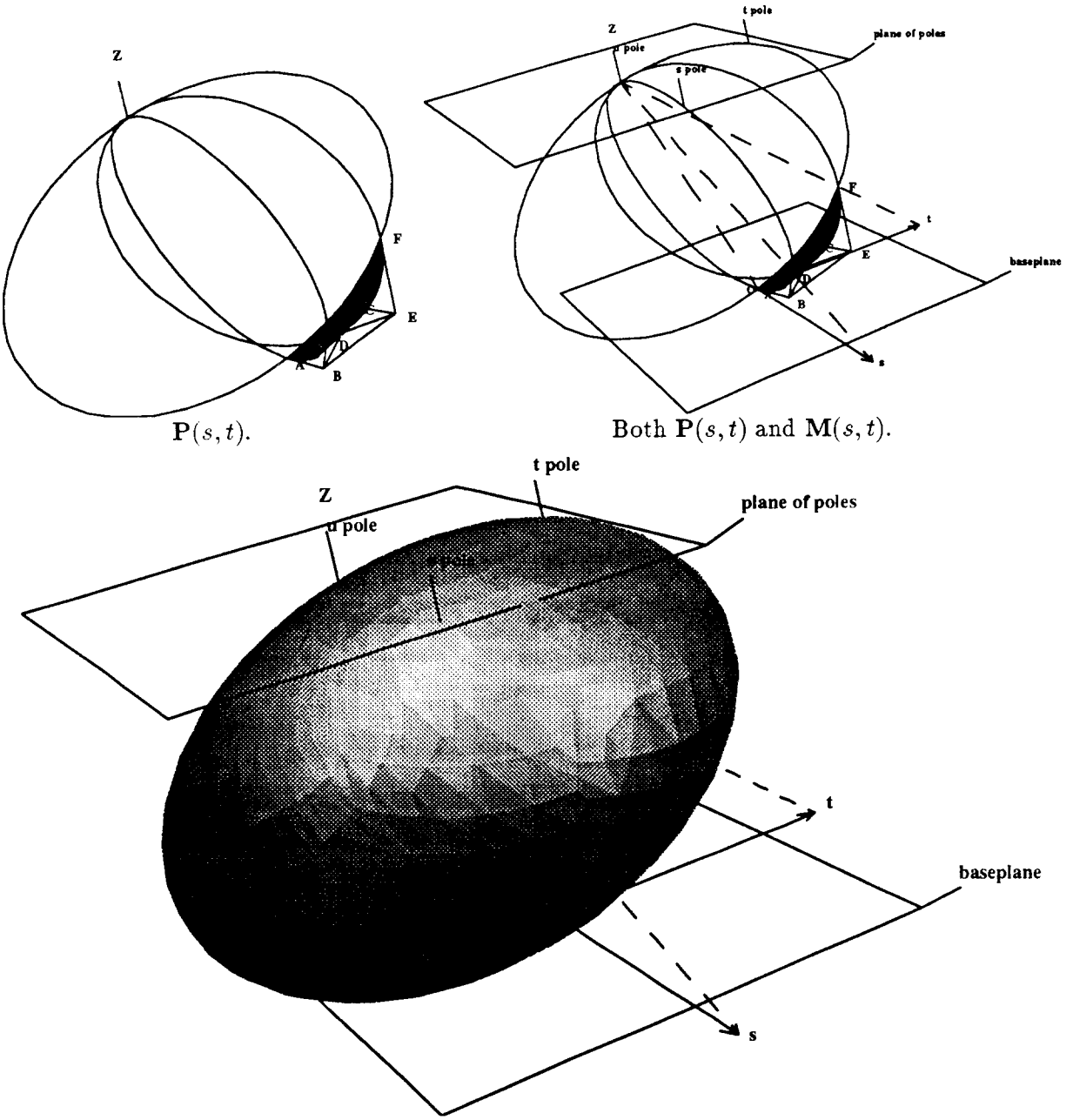

Figure 8.5: A Triangular Bézier Patch $\mathbf{P}(s,t)$ and its Equivalent Stereographic Map $\mathbf{M}(s,t)$.
Above left: $\mathbf{P}(s,t)$ has center of projection $\mathbf{Z}$ and interpolates an ellipsoid.
Above right: $\mathbf{M}$'s plane of poles, baseplane, and spanning basis are shown.
Bottom: the image of the baseplane under $\mathbf{M}$ is the complete quadric.

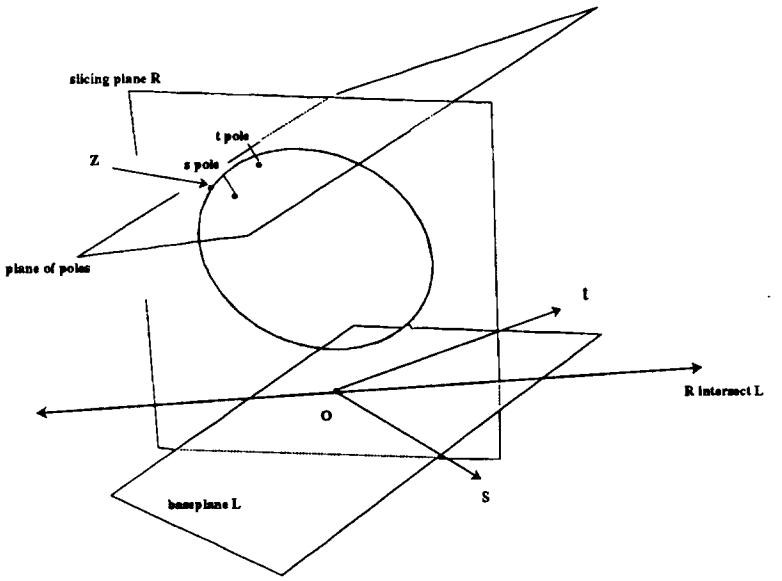

The Slicing Plane **R** induces a line on the map baseplane **L**.

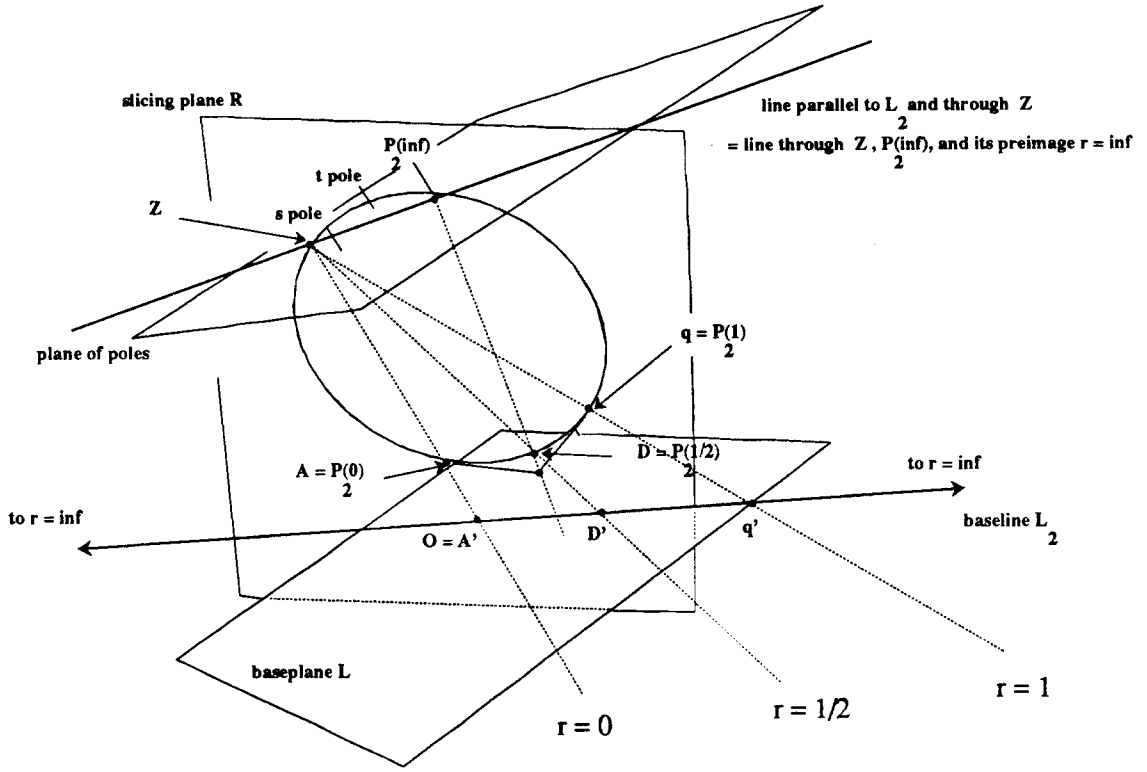

The Slicing Plane **R** induces a line on the plane of poles.

Figure 8.6: Proving the Equivalence of a Bézier Patch and its Constructed Stereographic Map. The quadric and stereographic map of Figure 8.5 have been cut with **R**, a *slicing plane*. **R** contains the center of projection **Z** and the patch point $\mathbf{P}(0,0) = \mathbf{A}$ of the patch, but can pivot freely. **R** has a unique intersection with the image, under **P**, of the domain line $s + t = 1$. This intersection is labeled point **q** in the Figure.

projection, through $\mathbf{Z}$, of the vector $\overline{\mathbf{Aq}}$ onto the baseline $\mathbf{L}_2$.

Clearly $r = 0$ at $(s,t) = (0,0)$, and $r = 1$ everywhere along $s + t = 1$ (and, in particular, at point $\mathbf{q}$ in Figure 8.6). Demonstrating the equivalence of the given Bézier patch and the constructed three-dimensional map requires only that we show that the general slices $\mathbf{P}_2$ and $\mathbf{M}_2$ induced by $\mathbf{R}$ agree at two further values of r: say, $r = \frac{1}{2}$ and $r = \infty$.

We show first that the sliced patch and sliced map agree at $r = \infty$. The pole $\mathbf{P}_2(\infty)$ of the sliced *patch* must be the intersection of the plane $\mathbf{R}$ with the image of the line at infinity under $\mathbf{P}$ (if this image is $\mathbf{Z}$, $\mathbf{P}_2(\infty) = \mathbf{Z}$). But the pole $\mathbf{M}_2(\infty)$ of the sliced *map* must be the intersection of two planar curves: the conic induced by $\mathbf{R}$ slicing ξ, and the line through $\mathbf{Z}$ parallel to $\mathbf{L}_2$. By construction this point lies on the image of the line at infinity under $\mathbf{P}$. Thus $\mathbf{P}_2(\infty) = \mathbf{M}_2(\infty)$.

Finally, we show that $\mathbf{P}_2(\frac{1}{2}) = \mathbf{M}_2(\frac{1}{2})$. The curve $\mathbf{P}_2(r)$ is a rational quadratic Bézier curve. By inspection, its endpoints are $\mathbf{A}$ and $\mathbf{q}$, and its middle control point is the intersection $\mathbf{B}$ of the conic tangents at $\mathbf{A}$ and $\mathbf{q}$ in Figure 8.5. The collinearity relation for Bézier curves (Equation 4.26) yields that $\mathbf{B}$, $\mathbf{P}_2(\frac{1}{2})$, and $\mathbf{P}_2(\infty)$ are collinear. Project $\mathbf{A}$, $\mathbf{D}$, and $\mathbf{q}$ onto $\mathbf{L}_2$ from $\mathbf{Z}$, labeling the resulting points $\mathbf{A}'$, $\mathbf{D}'$, and $\mathbf{q}'$ respectively. By Proposition 2, $\mathbf{D}'$ is the midpoint of $\mathbf{A}'$ and $\mathbf{q}'$ [take $\mathbf{E} = \mathbf{Z}$, $\mathbf{F} = \mathbf{P}_2(\infty)$, $\mathbf{A} = \mathbf{P}_2(0)$, and $\mathbf{C} = \mathbf{P}_2(1)$]. But $\mathbf{A}'$ and $\mathbf{q}'$, by construction, demarcate the points $r = 0$ and $r = 1$ on $\mathbf{L}_2$ respectively. Thus $\mathbf{D}'$ is the preimage of $\mathbf{D}$ under $\mathbf{M}_2$; i.e., $\mathbf{M}_2(\frac{1}{2}) = \mathbf{D}$. But $\mathbf{D} = \mathbf{P}_2(\frac{1}{2})$, yielding immediately that $\mathbf{P}_2(\frac{1}{2}) = \mathbf{M}_2(\frac{1}{2})$.

We have demonstrated the agreement of the sliced patch $\mathbf{P}_2(r)$ and sliced map $\mathbf{M}_2(r)$ for the four r values $r = 0$, $r = \frac{1}{2}$, $r = 1$, and $r = \infty$. Thus the sliced patch and sliced map are identical rational polynomials, and cover identical conics for identical values of r (cf. the degree of freedom argument in §5.3). Since the slicing plane $\mathbf{R}$ has arbitrary orientation, we conclude that the given patch $\mathbf{P}(s,t)$ and the constructed map $\mathbf{M}(s,t)$ are equivalent for all s and t.

8.3 The Fundamental Curve of a Stereographic Map and its Equivalent Rational Quadratic Bézier Patch

Section 7.6.5 described the fundamental curve of a complemented Bézier patch, and demonstrated the existence of this curve for every such patch restricted to interpolate a quadric. Existing methods for determining the existence of, and computing the domain-space equation of, this curve for a general quadratic triangular Bézier patch are somewhat cumbersome [32].

Stereographic maps of quadrics always have a fundamental curve. It is a line in domain space, and can be computed easily as the intersection of two planes: the map's baseplane, and the plane tangent to the quadric at the map's center of projection (Figure 8.7). In the previous section, we showed that restricted Bézier patches are equivalent to stereographic maps of quadrics. Thus, the fundamental curve of any Bézier patches is easily obtained as the fundamental curve of its equivalent stereographic map. By construction, the image of this curve, under either map, is the single point $\mathbf{Z}$. Accordingly, we denote as $\mathbf{Z}'$ the fundamental curve of a patch (or stereographic map) with center of projection $\mathbf{Z}$.

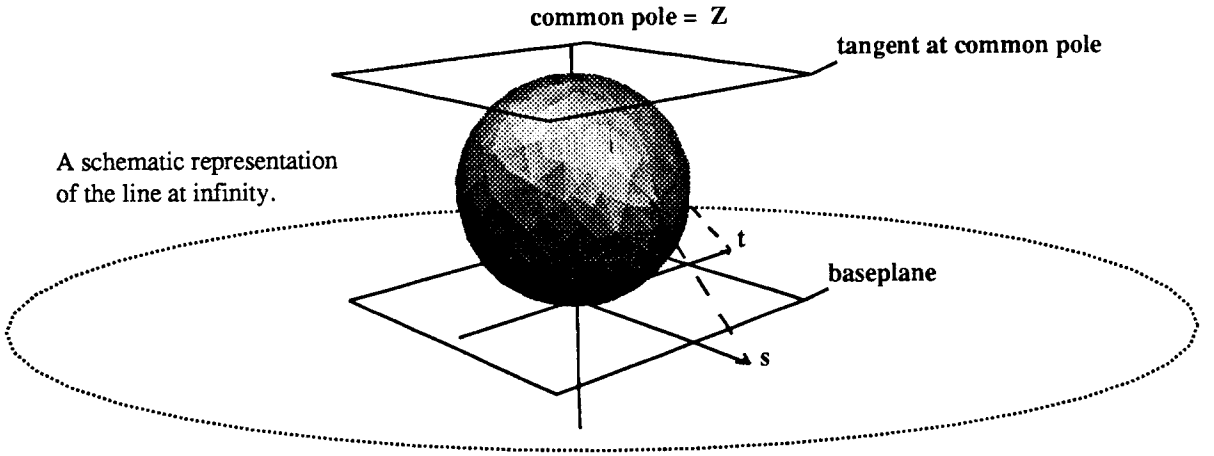

The Fundamental Curve is the Line at Infinity.

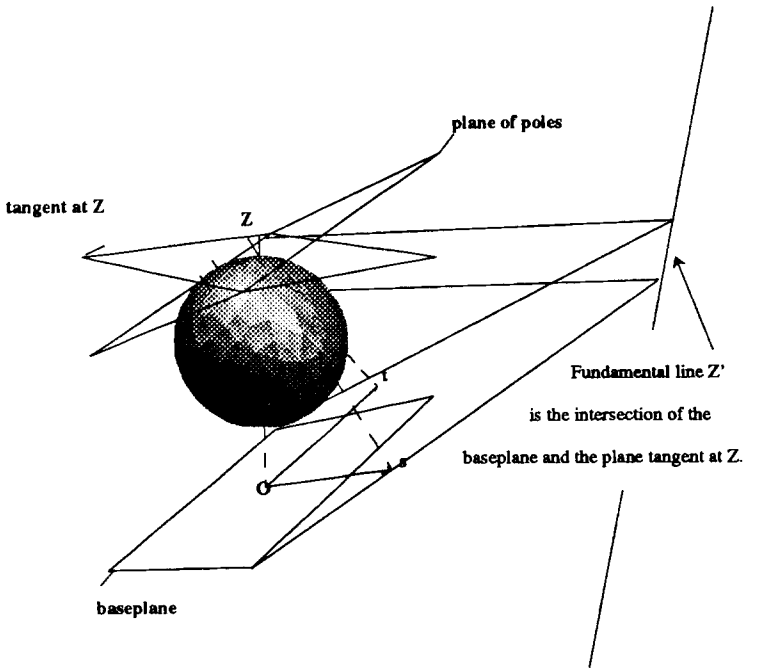

The Fundamental Curve is the Line $\mathbf{Z}'$.

Figure 8.7: The Fundamental Curve $\mathbf{Z}'$ of a Stereographic Map $\mathbf{M}$ is Easily Found.
Top: $\mathbf{M}$ is in standard form. Its baseplane is parallel to the plane tangent to the quadric at $\mathbf{Z}$, and the fundamental curve $\mathbf{Z}'$ is the line at infinity.
Bottom: $\mathbf{M}$ is not in standard form. Its baseplane and the plane tangent to the quadric at $\mathbf{Z}$ intersect in some line $\mathbf{Z}'$ other than the line at infinity. By inspection, all points on $\mathbf{Z}'$ are sent to $\mathbf{Z}$ under $\mathbf{M}$. Thus $\mathbf{Z}'$ is a fundamental curve of $\mathbf{M}$.

8.4 Constructing Portions of Quadrics With Arbitrary Planar Boundaries

The equivalence of stereographic maps of quadrics and restricted quadratic Bézier patches greatly simplifies the task of constructing an interpolating patch with arbitrary boundaries. Moreover, the equivalence obviates complicated analytic evaluation and inversion algorithms; the patch inversion and fundamental curve can be obtained directly, and geometrically, from the stereographic map corresponding to the patch. Thus, for any desired quadric and set of bounding planes, we can easily compute a Bézier patch interpolating the quadric, and a *trimmed domain* for the patch that corresponds exactly to the desired bounded portion of the quadric. Since each bounding plane cuts the quadric in a conic, and conics have conic preimages, we conclude that the trimmed domain must be the intersection of halfspaces bounded by conics, one corresponding to each plane that bounds the patch. These domain-space conics are simply the projections, through $\mathbf{Z}$ and onto the baseplane $\mathbf{L}$, of the conic patch boundaries. Perhaps the simplest example is the plane-bounded standard patch, a triangular area bounded by three conics (whose preimages are straight lines). We call interpolating Bézier patches trimmed in this manner *mapped Bézier patches.*

The presence of the fundamental curve $\mathbf{Z}'$ in the unbounded domain of any restricted patch presents complications to those algorithms that are unable to tolerate singular behavior. We can address this issue in either the image or preimage space of the patch. Since the image of the fundamental curve is just the center of projection $\mathbf{Z}$, excluding $\mathbf{Z}$ from the desired portion of the quadric ensures that $\mathbf{Z}'$ is disjoint from the portions preimage. Similarly, $\mathbf{Z}'$ contains all domain space points sent to $\mathbf{Z}$. Thus, arranging that the trimmed domain is disjoint from $\mathbf{Z}'$ ensures that the domain image (i.e., the swept patch) cannot contain $\mathbf{Z}$.

If the entire quadric is desired (i.e., the set of boundary constraints is empty), the center of projection must be covered and the techniques above are not appropriate. Instead, we can employ the complementary patches of Chapter 7, or partition the quadric along some symmetry plane and use two mapped patches, neither of which covers its center of projection.

The remainder of this section demonstrates the construction of quadric patches with general planar boundaries. The patch *control points* are derived using the construction of §7.6, so that the patch equation $\mathbf{P}(s,t)$ interpolates the desired quadric everywhere. Various parametrization conventions are applied to the boundary curves, producing interpolating patches that have equivalent stereographic maps in either standard or non-standard form. The patch *domain* is derived as the intersection of conic halfspaces, projected (as described above) through $\mathbf{Z}$ and onto the baseplane $\mathbf{L}$ of the stereographic map $\mathbf{M}(s,t)$ corresponding to $\mathbf{P}(s,t)$.

8.4.1 A Hemisphere as a Mapped Quadratic Bézier Patch

We revisit the sphere constructed in §7.6.1, (cf. Figure 7.17). Rather than the standard patch, we now wish to cover the lower half of the sphere, or its Southern hemisphere. Accordingly, we slice the sphere horizontally, and project its equator through $\mathbf{Z}$ (the North pole) onto the baseplane of the equivalent stereographic map. Figure 8.8 illustrates the result, for pole-conic and rho-conic parametrized spheres. The baseplane of the map equivalent to the pole-conic sphere is coincident with the $z = 0$ plane; thus the equator projects through $\mathbf{Z}$ onto a unit circle in baseplane coordinates. The baseplane of the rho-conic sphere is oblique; accordingly, the equator projects onto a baseplane ellipse.

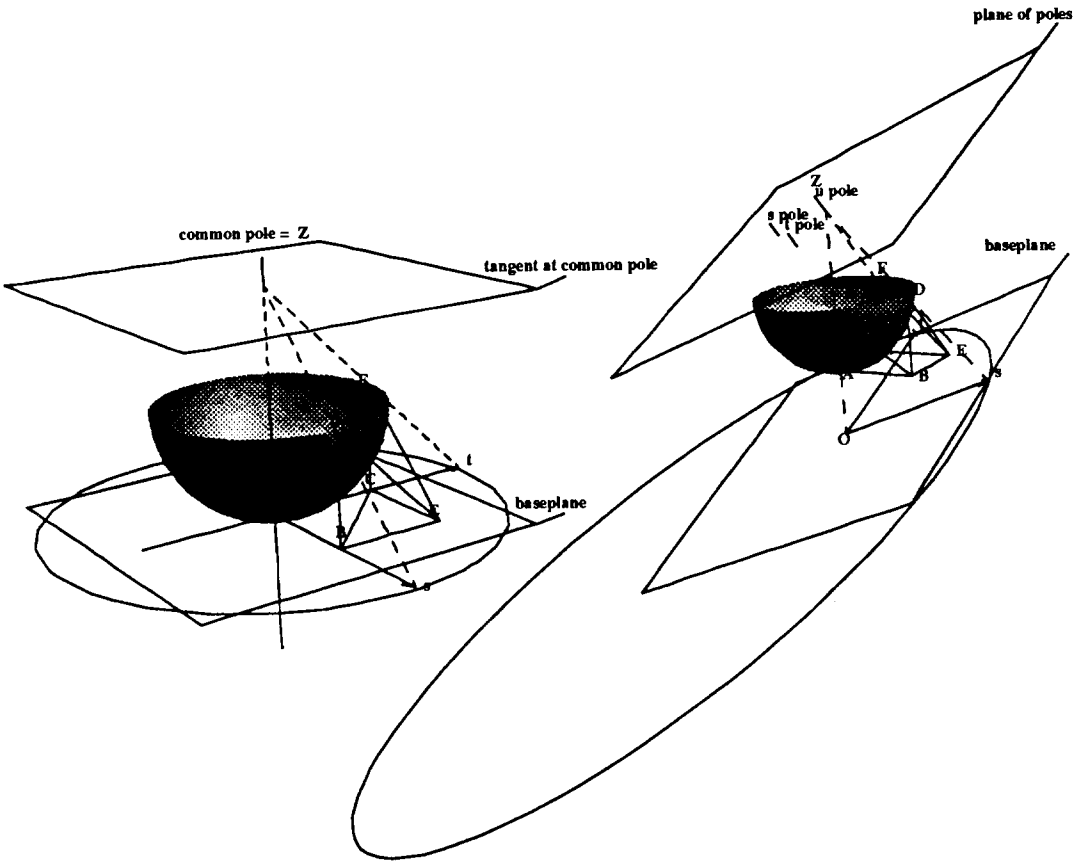

Figure 8.8: Two Instances of a Hemisphere as a Mapped Triangular Bézier Patch.
On the left, the pole-conic parametrization convention was used in constructing the standard patch. The resulting baseplane is $z = 0$, parallel to the plane tangent to the sphere at the North pole. The equator projects through **Z** onto a unit circle in baseplane coordinates. On the right, the rho-conic convention parametrization yields three distinct poles: one each for the s, t, and u boundary curves. Projecting the equator onto the resulting oblique baseplane produces an ellipse.

8.4.2 A Half-Cylinder as a Mapped Quadratic Bézier Patch

We construct a half-cylinder by first constructing a standard patch that interpolates a portion of a cylinder. Here we have chosen a unit-radius cylinder aligned with the z-axis, and the center

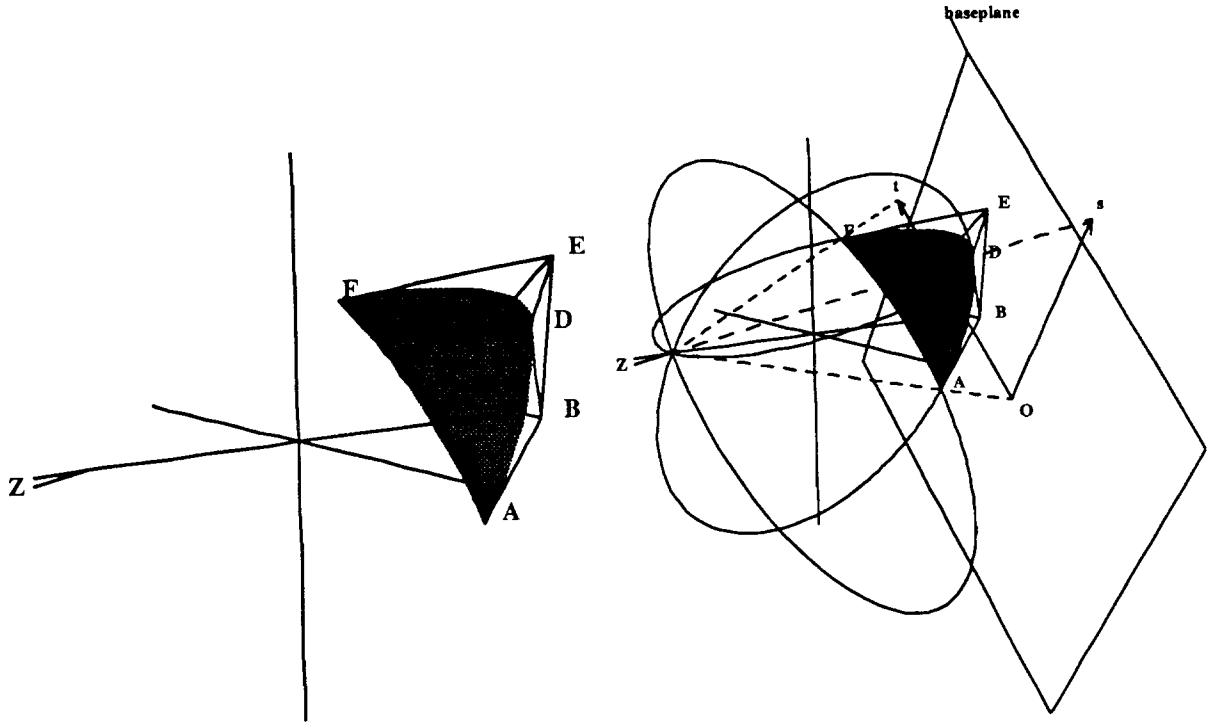

Figure 8.9: A Quadratic Rational Bézier Patch Interpolating a Cylinder. The standard patch is shown on the left. On the right, the boundary curves are extended; they intersect at the center of projection **Z**. The baseplane and basis vectors $\hat{\mathbf{s}}$ and $\hat{\mathbf{t}}$ of the equivalent stereographic map are also shown.

of projection at $(-1, 0, 0)$. This produces a patch with equivalent stereographic baseplane $x = 1$. Figure 8.9 shows the standard patch so created, its extended boundary curves meeting in the center of projection, and the baseplane and basis of the equivalent coordinatized stereographic map. Next, we bound the cylinder with the halfspaces $z \geq -1$, $z \leq 1$, and $x \geq 0$ (Figure 8.10). The first two halfspaces cut the cylinder in circles that project to parabolae on the baseplane. The third halfspace cuts the cylinder in a double line. This conic projects through **Z** onto a baseplane double line.

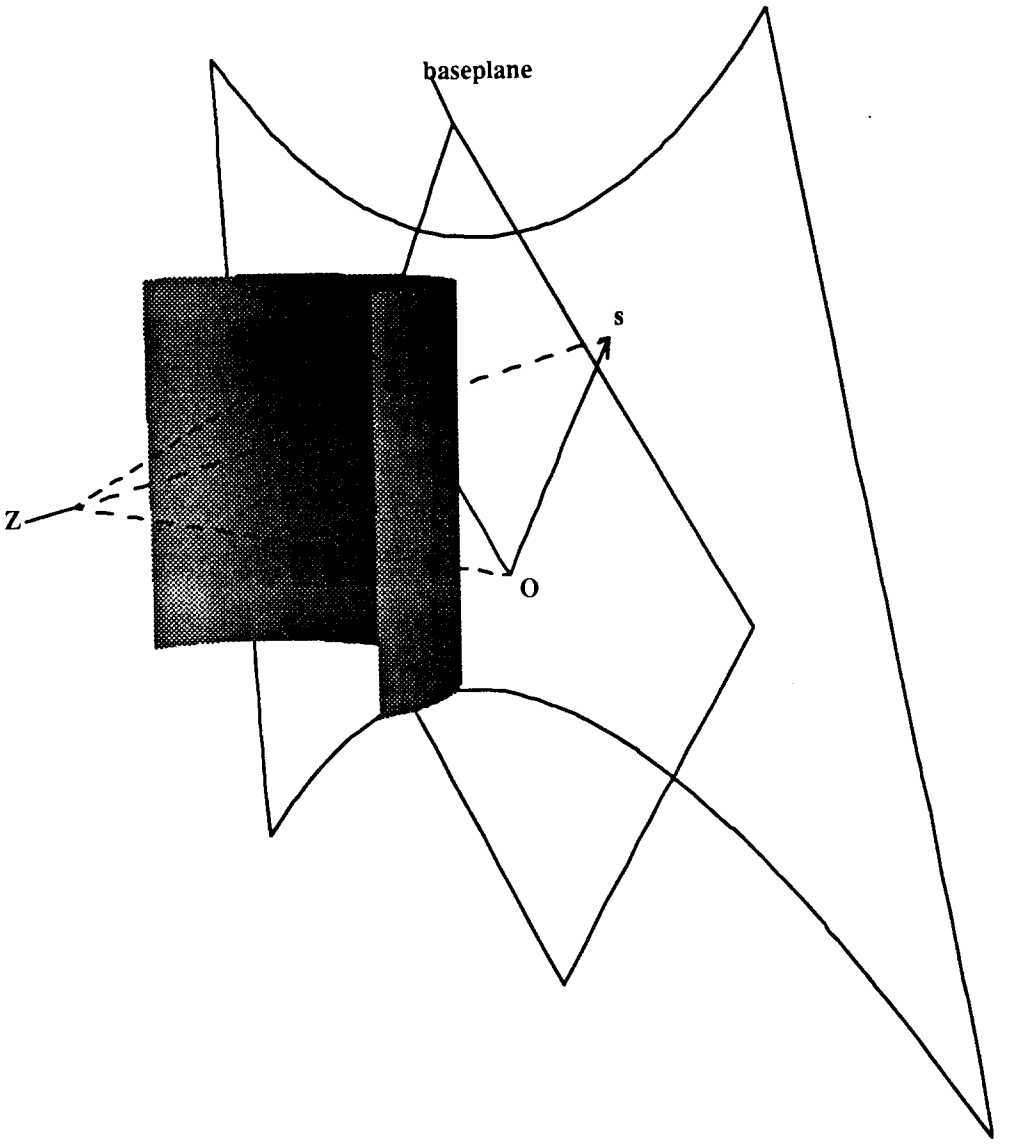

Figure 8.10: A Half Cylinder Swept by a Mapped Bézier Patch.
The circular patch edges are images of domain parabolae;
the linear patch edges are images of domain lines.

8.4.3 A Hyperbolic Fillet as a Mapped Quadratic Bézier Patch

We construct a hyperbolic patch suitable for use as a fillet. Again, an interpolating triangular patch is constructed first. Figure 8.11 shows the standard patch, and the standard domain Δ in the baseplane coordinates of the equivalent stereographic map.

Next we bound the hyperboloid with four halfspaces: above and below by $z \leq \sqrt{2}$ and $z \geq \frac{1}{2}$, respectively; and to the left and right by $x \geq 0$ and $y \geq 0$. The resulting domain has two elliptical and two hyperbolic boundaries (Figure 8.12).

8.5 Constructing a Bézier Patch From a Coordinatized Stereographic Map

Given any coordinatized stereographic map $\mathbf{M}(s,t)$, a simple construction yields an equivalent Bézier patch $\mathbf{P}(s,t)$. The construction is analogous to that of §5.5, which took stereographic maps of the line to Bézier curves. In the three-dimensional case, we simply construct a Bézier patch whose extended boundary curves are images of the baseplane lines $s = 0$, $t = 0$, and $s+t = 1$ under $\mathbf{M}$. The patch control points $\mathbf{A}$, $\mathbf{D}$, and $\mathbf{F}$ are found as $\mathbf{M}(0,0)$, $\mathbf{M}(1,0)$, and $\mathbf{M}(0,1)$ respectively. Differentiating the stereographic map directly yields tangent plane equations and the edge control points $\mathbf{B}$, $\mathbf{C}$, and $\mathbf{E}$. Finally, the pole-conic parametrization convention yields the appropriate control weights.

The argument of §8.2 can easily be applied to the resulting patch to show that $\mathbf{M}(s,t)$ and $\mathbf{P}(s,t)$ are equivalent.

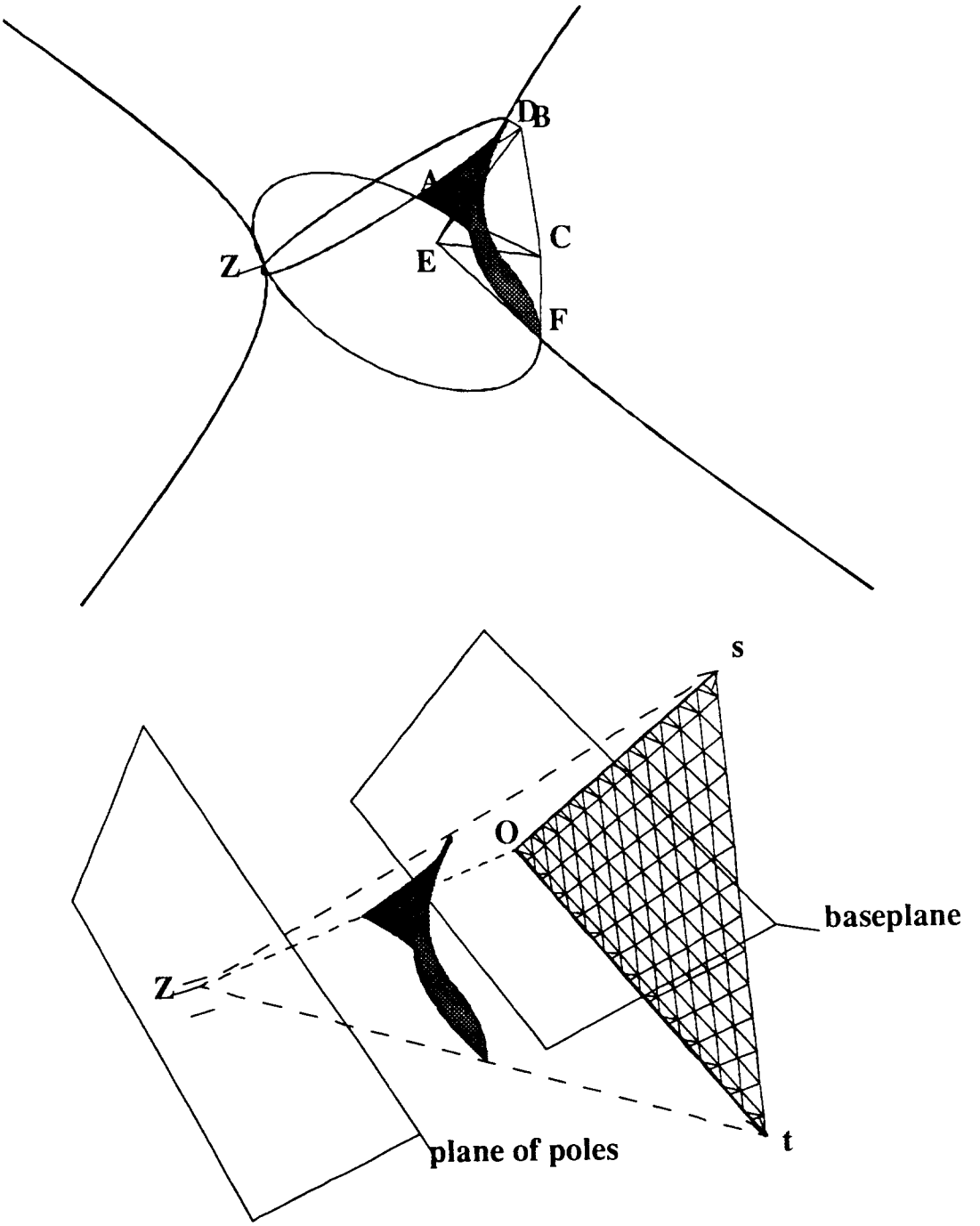

Figure 8.11: A Single-Sheet Hyperboloid Interpolated by a Quadratic Rational Bézier Patch. The equivalent coordinatized stereographic map is displayed; the vectors $\hat{\mathbf{s}}$ and $\hat{\mathbf{t}}$ form an oblique basis. The standard domain Δ is a triangle in the baseplane of the map.

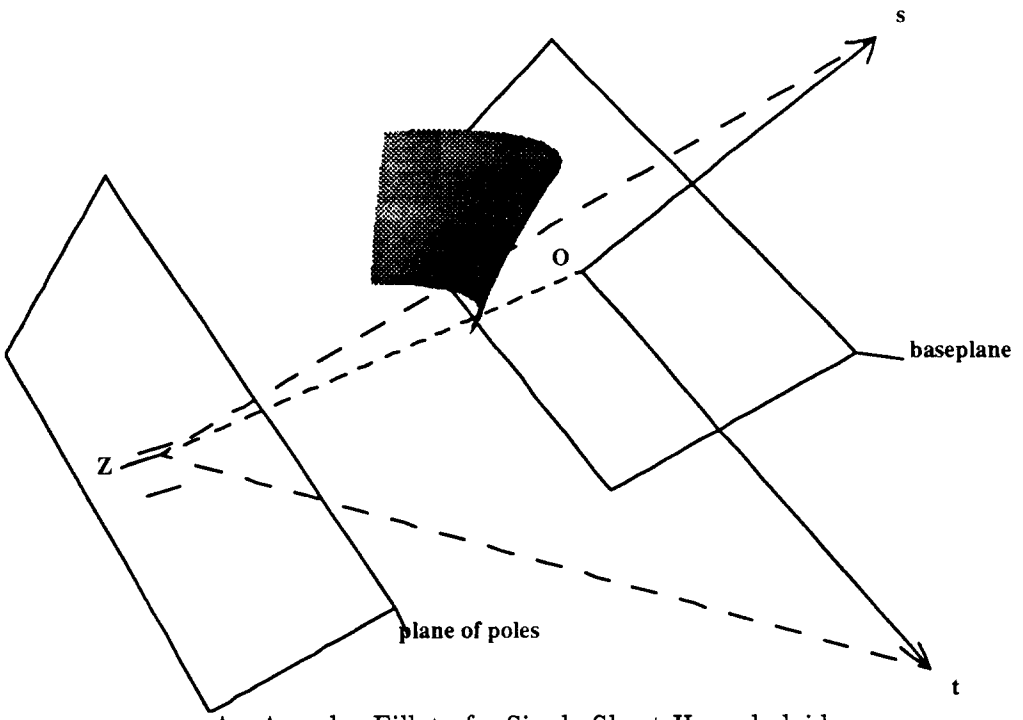

An Annular Fillet of a Single-Sheet Hyperboloid.

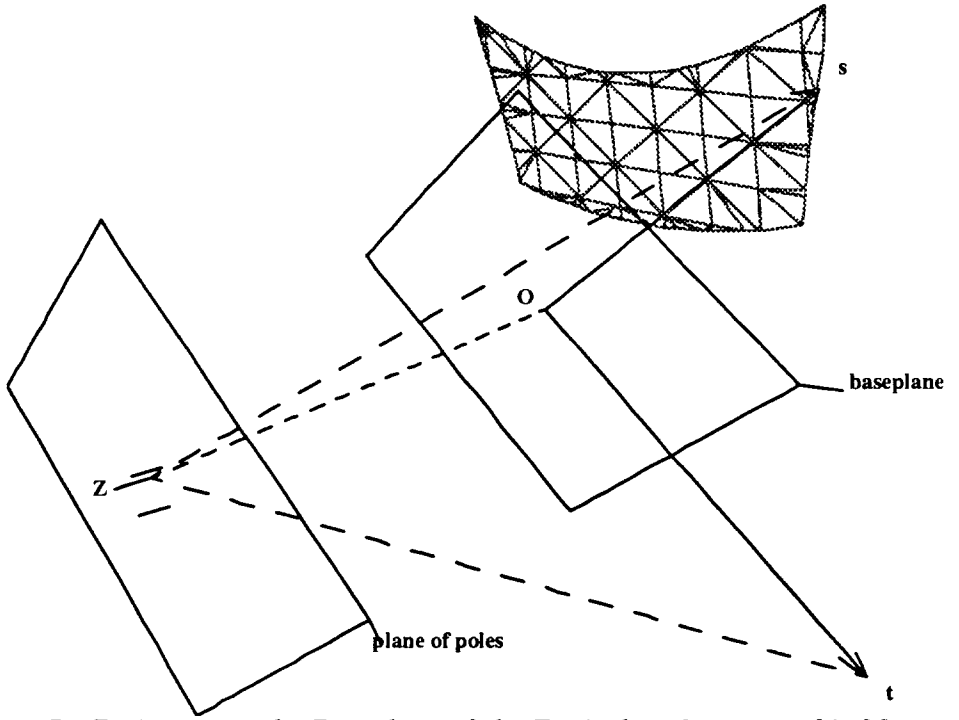

Its Preimage on the Baseplane of the Equivalent Stereographic Map.

Figure 8.12: An Annular Portion of a Single-Sheet Hyperboloid as a Mapped Bézier Patch.
Top: the swept patch. Bottom: its preimage in baseplane coordinates.
The domain is bounded by the conic preimages of the four boundaries of the trimmed patch: two ellipses (top and bottom) and two hyperbolae (left and right). The vectors $\hat{\mathbf{s}}$ and $\hat{\mathbf{t}}$ comprise an oblique basis.

Chapter 9

A Unified Representation For Bézier Patches That Cover Quadrics

Quadric surfaces play an important role in both traditional modeling systems and more recent free-form environments. The operations of constructing, modifying, rendering, and intersecting parametrized quadric surfaces are of primary importance. Existing implementations tend to represent quadrics as a hybridized surface class, intermingling implicit representations (for operations such as surface intersection) with parametric formulations (for efficient rendering). Also, because the representational power of rational quadratic patches has not been fully realized, many implementations have needlessly resorted to higher-order primitives, such as cubic or quartic parametric formulations ([6],[25]), for representing quadrics.

We have demonstrated a correspondence between parameterized quadrics and stereographic maps of the plane. Relating the two representations yields the considerable benefit of a simple inversion procedure, while combining the appealing analytic properties of the Bézier patch with the intuitive geometric nature of the stereographic map.

Implementers may profitably employ the correspondences introduced here by *unifying* current representations of parametric conics and quadrics with their equivalent stereographic representations. For example, for every parametric conic or quadric, implementers might maintain an equivalent *shadow* object in the form of a stereographic map. We demonstrated that these objects are easily constructible from their associated parametric forms. The computation cost is small, and need only be incurred by operations modifying the object. Since the equivalence between the Bézier and stereographic formulation is coordinate independent, the equivalent stereographic map behaves exactly like its corresponding Bézier form under affine transformations.

Maintaining a shadow object allows complete, numerically robust control over the parametric behavior and preimage of a modeled conic or quadric object. This unified representation should have its greatest utility in systems demanding that quadric patches meet along complex, heterogeneous boundaries. We improve on existing inversion methods by substituting a geometric projection operation for the usual numerical inversion techniques. For patches bounded by planar curves, the inversion is even simpler; planar curves invert to conic curves in domain space. Efficient algorithms exist for rendering such "trimmed" patches, even when the domain-space trim curves are themselves quadratic (or higher order) curves [31].

Chapter 10

Tensor-Product Patches

This chapter discusses the rational biquadratic Bézier patch, which we refer to as the "tensor-product patch." This patch can exactly interpolate circular and elliptical tori, as well as more general toroidal shapes. We extend the notion of patch complementation to tensor-product surfaces.

10.1 The Unit Square: A Canonical Patch Domain

In analogy to triangular patches, tensor-product patches are defined over a standard or *canonical* domain, namely $s, t \in [0..1]$. This is simply a unit square in the first octant of a cartesian st coordinate system (Figure 10.1). Explicitly, the tensor-product patch can be written[1]:

$$\mathbf{P}_{\square}(s,t) = (P_x(s,t), P_y(s,t), P_z(s,t)) = \frac{\sum\sum B_i(s)B_j(t)w_{ij}\mathbf{p}_{ij}}{\sum\sum B_i(s)B_j(t)w_{ij}}. \tag{10.1}$$

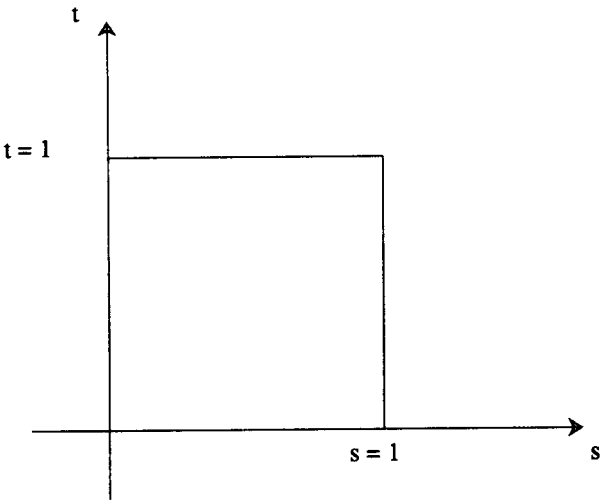

Figure 10.1: The Unit Square Domain of a Standard Tensor-Product Patch $\mathbf{P}_{\square}$.

[1] We will write $\mathbf{P}_{\square}$ to distinguish the tensor-product patch from the triangular patch $\mathbf{P}_{\Delta}$, when the distinction is not clear from context.

The tensor-product patch has four boundary curves; each is the image of one domain edge. Holding s or t fixed yields families of *isocurves* that are simply Bézier sums of linear combinations of the $\mathbf{p}_{ij}$ (cf. §7.6.3). Figure 10.2 depicts a typical standard tensor-product patch, its boundary curves, and some s and t isocurves.

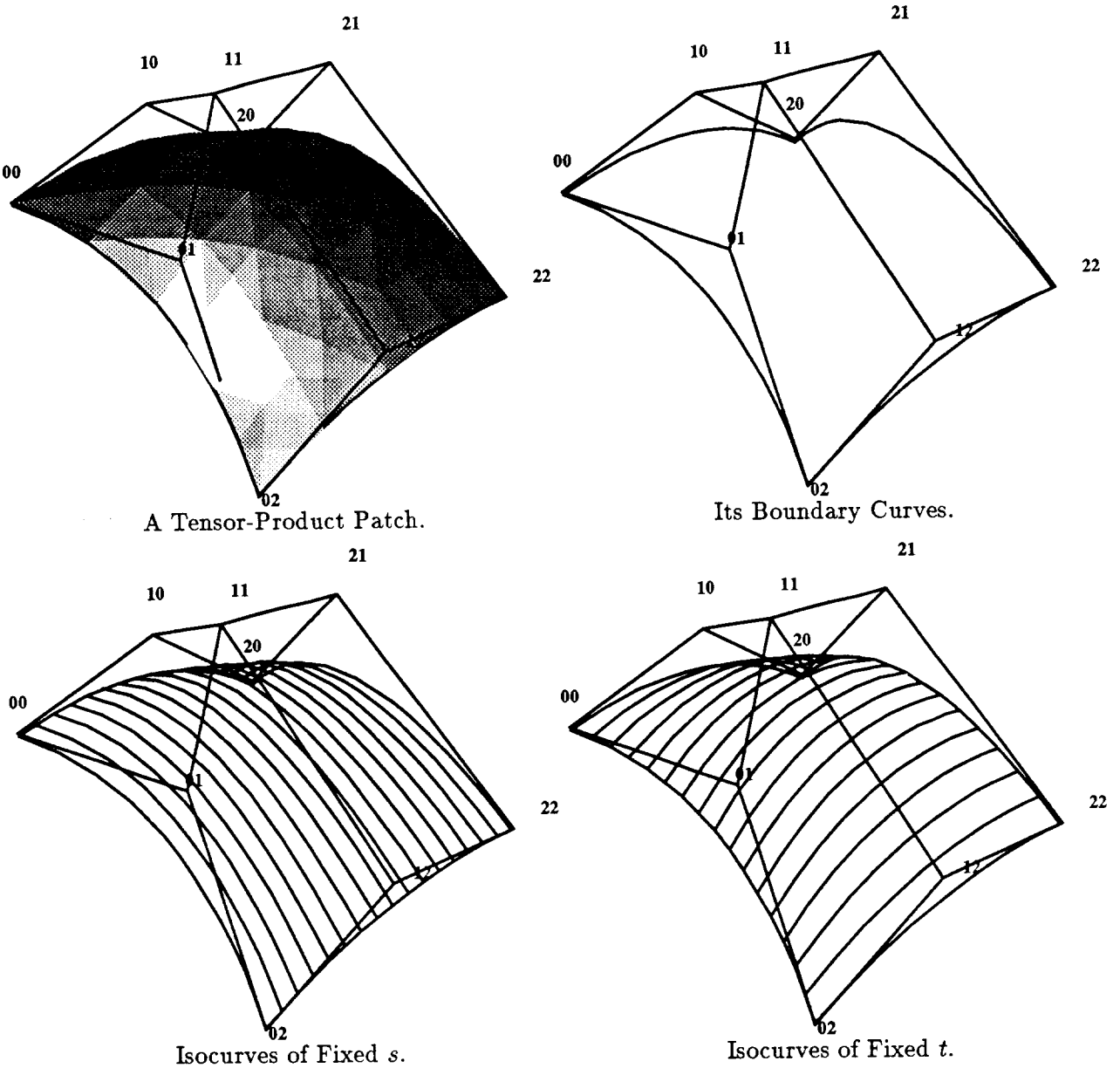

A Tensor-Product Patch. Its Boundary Curves.

Isocurves of Fixed s. Isocurves of Fixed t.

Figure 10.2: A Rational Biquadratic Tensor-Product Bézier Patch $\mathbf{P}(s,t)$.

We can easily derive an expression for any isocurve image of an isoline parallel to the s- or t-axis. Suppose we fix s at some value $s_0, 0 \leq s_0 \leq 1$. Direct substitution into Equation 10.1 produces

$$\mathbf{P}(s_0,t) = (P_x(s_0,t), P_y(s_0,t), P_z(s_0,t)) = \frac{\sum\sum B_i(s_0)B_j(t)w_{ij}\mathbf{p}_{ij}}{\sum\sum B_i(s_0)B_j(t)w_{ij}}. \tag{10.2}$$

Rearranging,

$$\mathbf{P}(s_0, t) = \frac{\sum B_j(t) w_j^* \mathbf{p}_j^*}{\sum B_j(t) w_j^*} \tag{10.3}$$

Each starred "control point" is a point on a Bézier curve formed by a row of the original control hull, parametrized by s, and evaluated at $s = s_0$:

$$\mathbf{p}_i^* = \sum_j B_j(s_0) \mathbf{p}_{ij}. \tag{10.4}$$

Thus evaluation of a point $\mathbf{P}(s_0, t_0)$ on a tensor product patch may be thought of as a "two-stage" operation. The control hull is decomposed into three rows of three points each. Each row is evaluated at $s = s_0$, yielding three weighted "control points." These are then combined in normal Bézier fashion to sweep a curve parametrized by $t \in [0..1]$. This curve, evaluated at $t = t_0$, is the desired tensor-product surface point $\mathbf{P}(s_0, t_0)$.

Isolines (domain lines) parallel to the s- or t-axis have planar isocurves as their images (since they may be expressed as Bézier combinations of three control points). Isolines not parallel to the s- or t-axes have, in general, *quartic* isocurves as images. The surface swept by the patch can, in general, have implicit degree as high as eight [10].

If only quadric surfaces are to be modeled, we propose that the triangular methods exhibited in Chapters 7 and 8 are sufficient for designers' needs. We have shown that, for suitable choice of center of projection and cut planes, a trivially invertible triangular patch interpolating a given quadric may be simply constructed. However, there may be modeling systems that do not accept

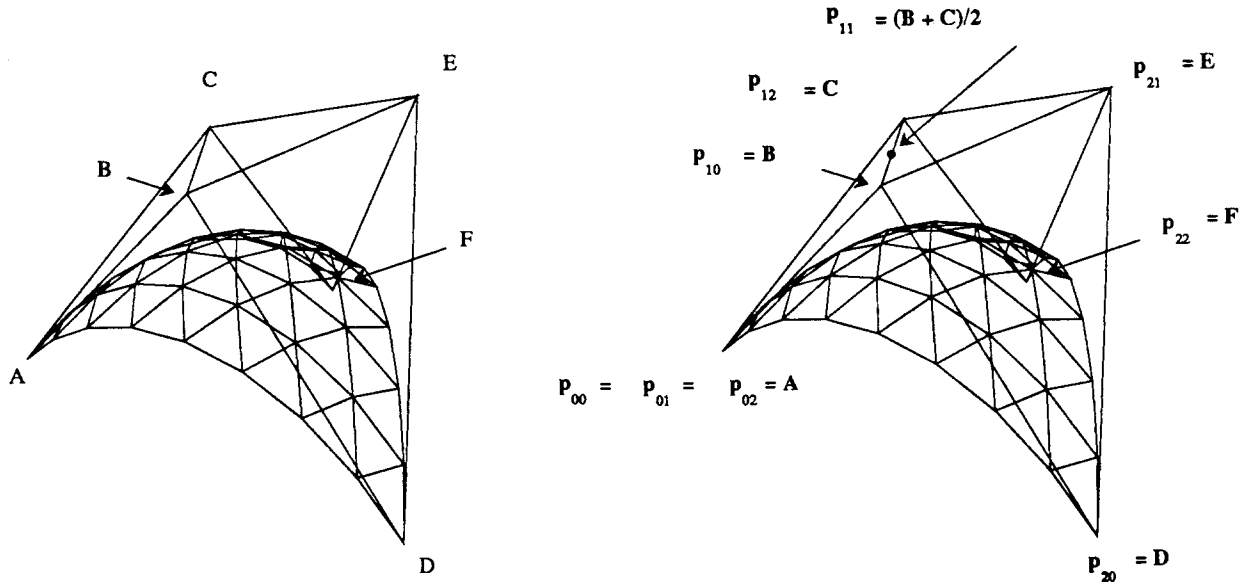

Figure 10.3: A Triangular Patch and its Degenerate Tensor-Product Equivalent.

triangular patches as surface formulations, but do accept tensor-product patches. In this case we must present triangular patches to the modeler as tensor-product patches.

There are at least two ways of achieving a tensor-product patch equivalent to a triangular patch. First, we may construct a *degenerate* tensor-product patch whose *shape*, but not parametrization,

is equivalent to that of the triangular patch (Figure 10.3). We do so by collapsing and combining the control points of the triangular patch:

$$\begin{aligned}
\mathbf{p}_{00} &= \mathbf{p}_{01} = \mathbf{p}_{02} = \mathbf{A} \\
\mathbf{p}_{10} &= \mathbf{B} \\
\mathbf{p}_{11} &= \frac{\mathbf{B}+\mathbf{C}}{2} \\
\mathbf{p}_{12} &= \mathbf{C} \\
\mathbf{p}_{20} &= \mathbf{D} \\
\mathbf{p}_{21} &= \mathbf{E} \\
\mathbf{p}_{22} &= \mathbf{F}.
\end{aligned} \tag{10.5}$$

This procedure is useful in that the patch (10.5) can be evaluated over the canonical unit-square domain. However, the patch is objectionable in at least three ways: coincidence of three control points; a boundary curve that degenerates to a point; and the lack of a well-defined normal at the degenerate boundary (although a reasonable normal may be constructed *ad hoc*).

Another method of accommodating modelers that accept only tensor-product patches is to create a tensor-product patch that, over the canonical *triangular* domain, is parametrically equivalent to a given triangular patch. Suppose we have such a triangular patch $\mathbf{P}_\Delta(s,t)$, with arbitrary control points and weights (it need not interpolate a quadric). An equivalent tensor product patch $\mathbf{P}_\square(s,t)$ is defined by (Figure 10.4):

$$\begin{aligned}
\mathbf{p}_{00} &= \mathbf{A} \\
\mathbf{p}_{10} &= \mathbf{B} \\
\mathbf{p}_{20} &= \mathbf{D} \\
\mathbf{p}_{01} &= \mathbf{C} \\
\mathbf{p}_{11} &= \mathbf{A} + \frac{(\mathbf{C}-\mathbf{A})+(\mathbf{E}-\mathbf{A})+(\mathbf{B}-\mathbf{A})}{2} \\
\mathbf{p}_{21} &= \mathbf{E}+(\mathbf{D}-\mathbf{B}) \\
\mathbf{p}_{02} &= \mathbf{F} \\
\mathbf{p}_{12} &= \mathbf{E}+(\mathbf{F}-\mathbf{C}) \\
\mathbf{p}_{22} &= \mathbf{A}+(\mathbf{F}-\mathbf{C})+(\mathbf{E}-\mathbf{C})+(\mathbf{E}-\mathbf{B})+(\mathbf{D}-\mathbf{B}).
\end{aligned} \tag{10.6}$$

Some arithmetic shows that $P_\square(s,t) = P_\Delta(s,t)$; that is, the tensor product patch $P_\square(s,t)$ so created is identical to the triangular patch $P_\Delta(s,t)$ for all values of s and t. Thus, the tensor-product patch need only be evaluated over Δ to produce a surface that is point-for-point equivalent to the triangular patch over this domain. Moreover, if $P_\Delta(s,t)$ covers a quadric, then so must $P_\square(s,t)$.

10.2 The Complements of a Tensor-Product Bézier Patch

We can define *complemented* tensor-product patches in direct analogy to the complemented triangular patches of §7.6.3. As in the triangular case, we view the tensor-product patch as decomposable into a family of isocurves. However, the isocurves originate along the *edges* of the quadrilateral patch (cf. Figure 10.2), rather than at the corners as in the triangular case. These isocurves are the images, under the quadratic tensor-product map $\mathbf{P}_\square$, of isolines parallel to either the s or t axis.

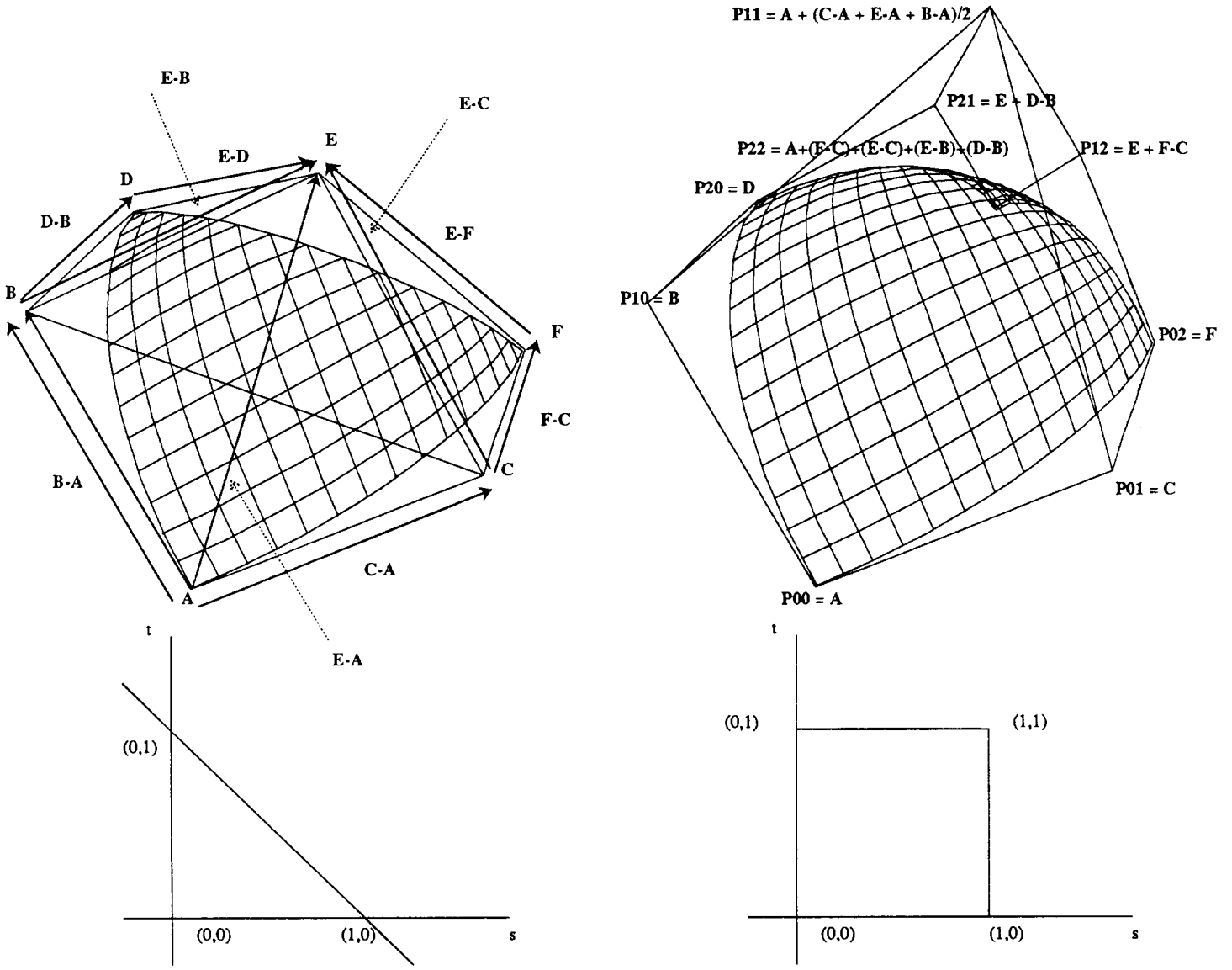

Figure 10.4: A Triangular Patch $\mathbf{P}_{\triangle}(s,t)$, and its Tensor-Product Equivalent $\mathbf{P}_{\square}(s,t)$.

Equation 10.4 expresses the control points for an s isocurve in which s is fixed and t varies from 0 to 1. We can complement all such isocurves simply by negating the control points $\mathbf{p}_1^*$; that is, the "middle" control point of each isocurve. Since each $\mathbf{p}_1^*$ is simply a linear combination of the three $\mathbf{p}_{1j}$, negating these points must cause the negation of $\mathbf{p}_1^*$, and thus the complementation of all s isocurves. Similarly, negating the three $\mathbf{p}_{j1}$ complements all t isocurves; and *composing* the operations complements both all s and all t isocurves. Note that the latter operation leaves the control point $\mathbf{p}_{11}$ unchanged, since it is negated twice. We call the quadratic tensor-product Bézier patches resulting from these operations $\tilde{\mathbf{P}}_s$, $\tilde{\mathbf{P}}_t$, and $\tilde{\mathbf{P}}_{st}$, respectively (Figure 10.5).

The complement patches tile the implicit surface (in this case, a torus). In the triangular case, each complemented patch shared one boundary and one point with the standard patch (cf. §7.6.3). In contrast, each complemented tensor-product patch shares two boundary curves with either the standard patch or a different complement of the standard patch.

Recall Figure 7.21, which reparametrized the curves comprising a complemented Bézier patch, reinterpreting them as *extended* curves. A topology emerged in which the standard patch, considered in turn with each triangular complement patch, could be interpreted as the image of a family of lines through one corner of the triangular patch domain. An analogous reinterpretation can be made for tensor-product patches (Figure 10.6). Here the isolines are not incident on the domain corners, but are parallel to the domain *edges*.

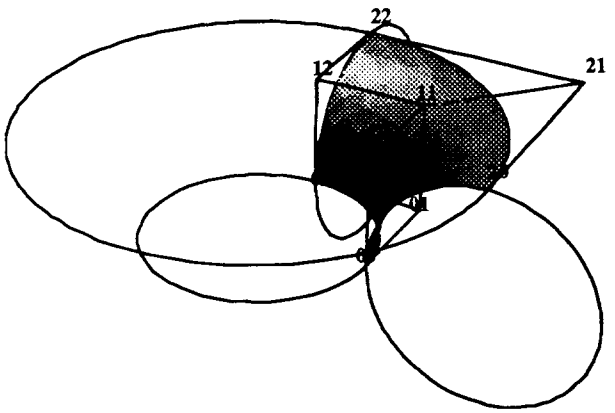

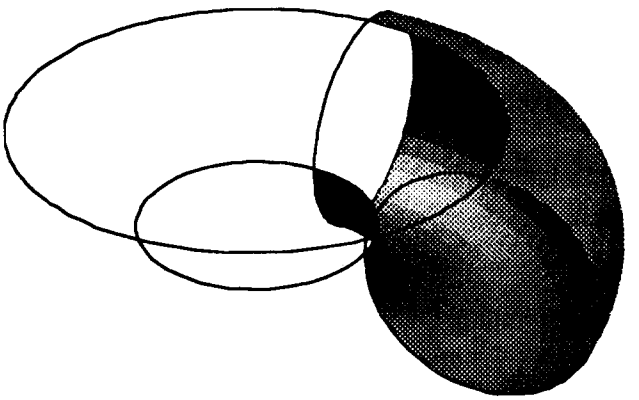

$\mathbf{P}_{\square}(s,t)$

$\tilde{\mathbf{P}}_{s}(s,t)$

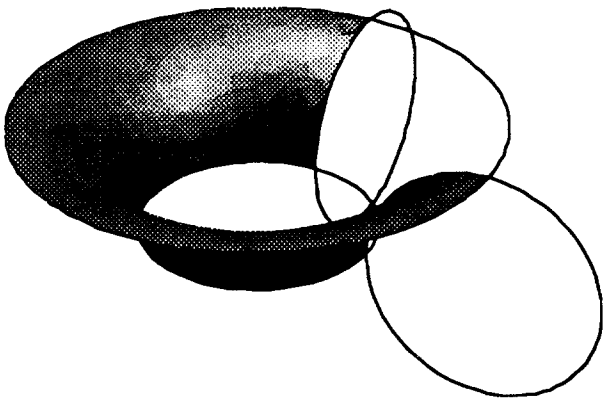

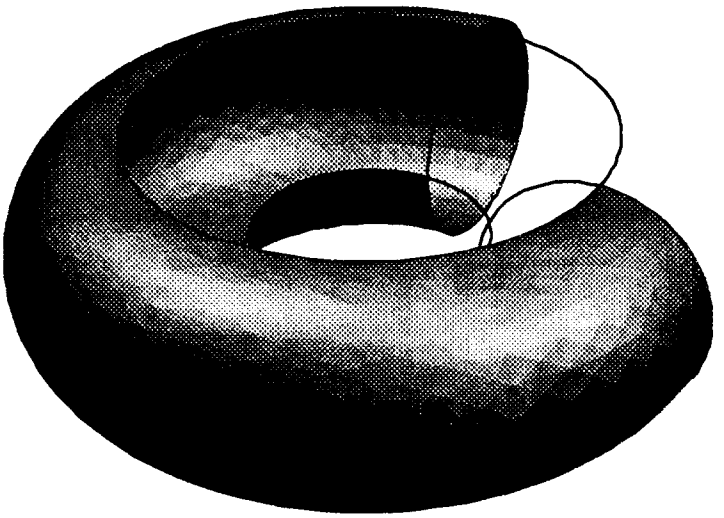

$\tilde{\mathbf{P}}_{t}(s,t)$

$\tilde{\mathbf{P}}_{st}(s,t)$

Figure 10.5: A Tensor-Product Bézier Patch $\mathbf{P}_{\square}(s,t)$, and Its Complementary Patches $\tilde{\mathbf{P}}_{s}(s,t)$, $\tilde{\mathbf{P}}_{t}(s,t)$, and $\tilde{\mathbf{P}}_{st}(s,t)$. Each patch has been evaluated over the standard domain $s,t > 0$, $s,t \leq 1$.

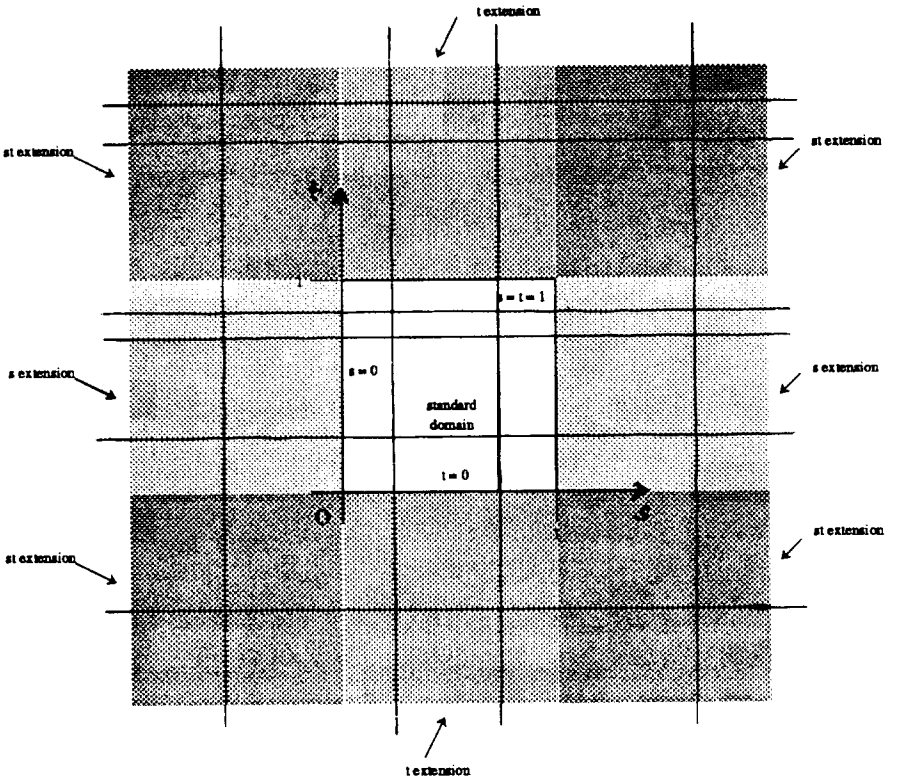

Figure 10.6: An Alternative View of Complementary Tensor-Product Patches.
Rather than considering the generator isocurves as *complements* of isocurve families embedded in the standard patch, we can interpret them as *extensions* of these families by reparametrizing each isocurve. The figure depicts the isoline preimages of the generator isocurves for the standard patch and each complementary patch.

Chapter 11

Some Applications of Quadratic Rational Triangular and Tensor-Product Bézier Patches

This chapter demonstrates the application of triangular and quadrilateral Bézier patches to real modeling situations. We consider patches of increasing implicit degree, starting with restricted triangular patches, and continuing to unrestricted triangular and tensor-product patches.

11.1 Joins, Fillets, and Blends Using Triangular Patches

11.1.1 Spherical/Elliptical Caps

We cap a cone with opening half-angle of 45° using a portion of a sphere. The construction uses three mapped restricted Bézier patches: one for the spherical cap, and two for the cone. The patches are depicted in Figure 11.1.

Since both surfaces are quadrics, only restricted triangular patches are necessary. First we construct patches defining the required implicit quadrics. A 90° cone opening along the z-axis has equation

$$x^2 + y^2 - z^2 = 0.$$

In homogeneous matrix form, this may be written

$$\begin{pmatrix} x & y & z & w \end{pmatrix} \begin{pmatrix} 1 & 0 & 0 & 0 \\ 0 & 1 & 0 & 0 \\ 0 & 0 & -1 & 0 \\ 0 & 0 & 0 & 0 \end{pmatrix} \begin{pmatrix} x \\ y \\ z \\ w \end{pmatrix} = 0. \tag{11.1}$$

Similarly, a unit sphere centered at the origin has equation

$$x^2 + y^2 + z^2 - 1 = 0.$$

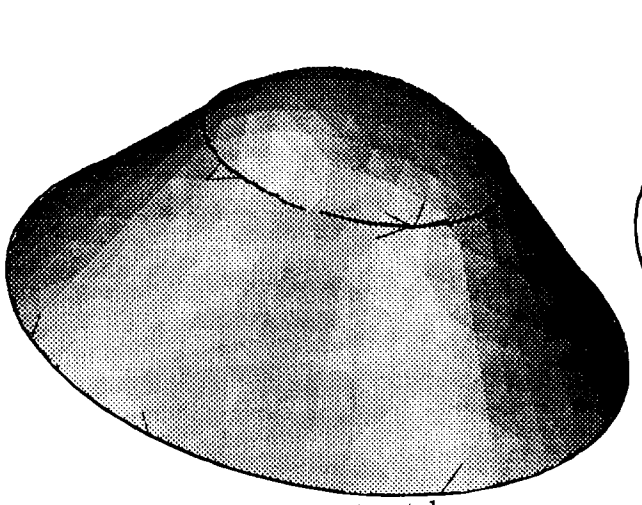

The component patches.

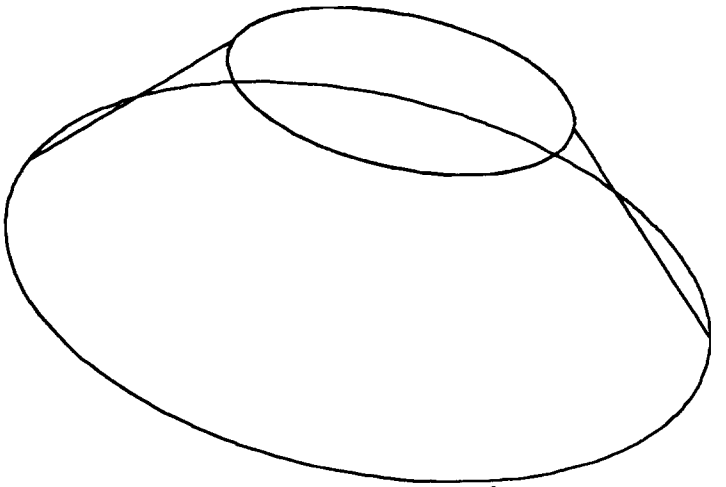

The boundary network.

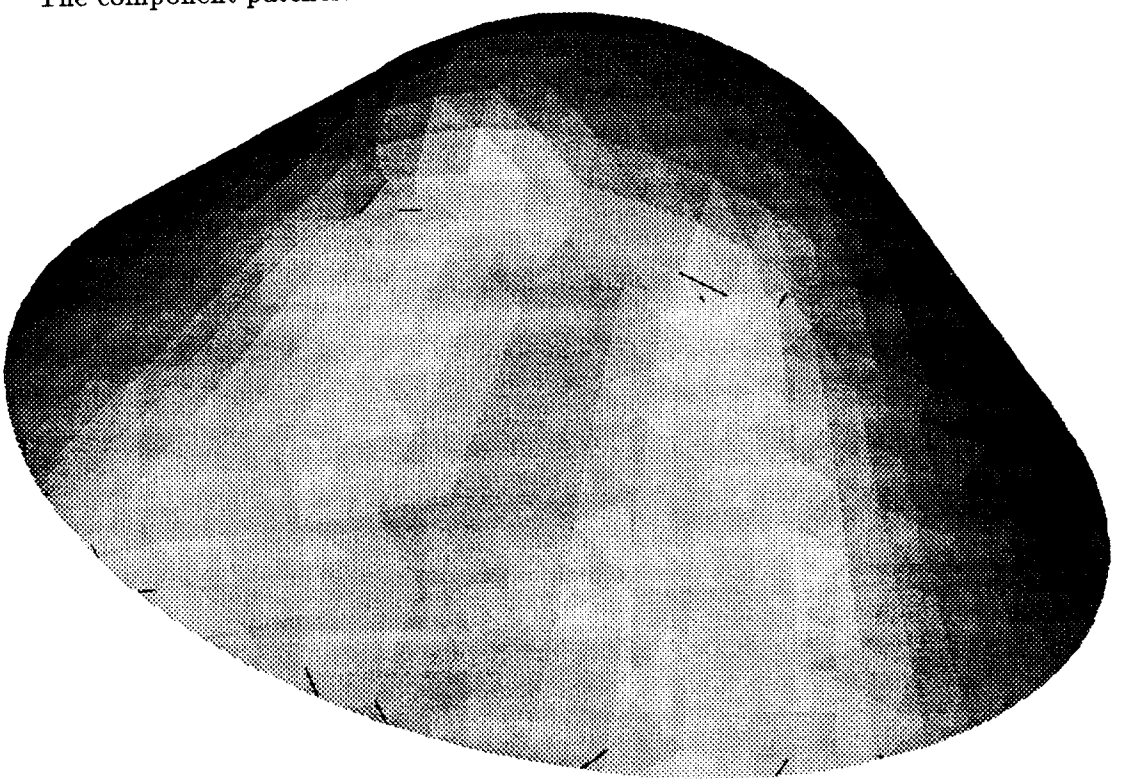

Figure 11.1: A Spherical Cap on a 90° Cone. The cap is a single mapped Bézier patch. The conical portion is represented as two symmetric mapped patches.

In homogeneous matrix form,

$$\begin{pmatrix} x & y & z & w \end{pmatrix} \begin{pmatrix} 1 & 0 & 0 & 0 \\ 0 & 1 & 0 & 0 \\ 0 & 0 & 1 & 0 \\ 0 & 0 & 0 & -1 \end{pmatrix} \begin{pmatrix} x \\ y \\ z \\ w \end{pmatrix} = 0.$$

Using the methods of §7.6, we construct triangular patches that cover the sphere and cone, respectively. The centers of projection need only be chosen off of the surface portions we wish to cover; here, we choose the sphere center of projection at its South pole, and each cone portion's center of projection in the geometric center of its counterpart (Figures 11.2 and 11.3).

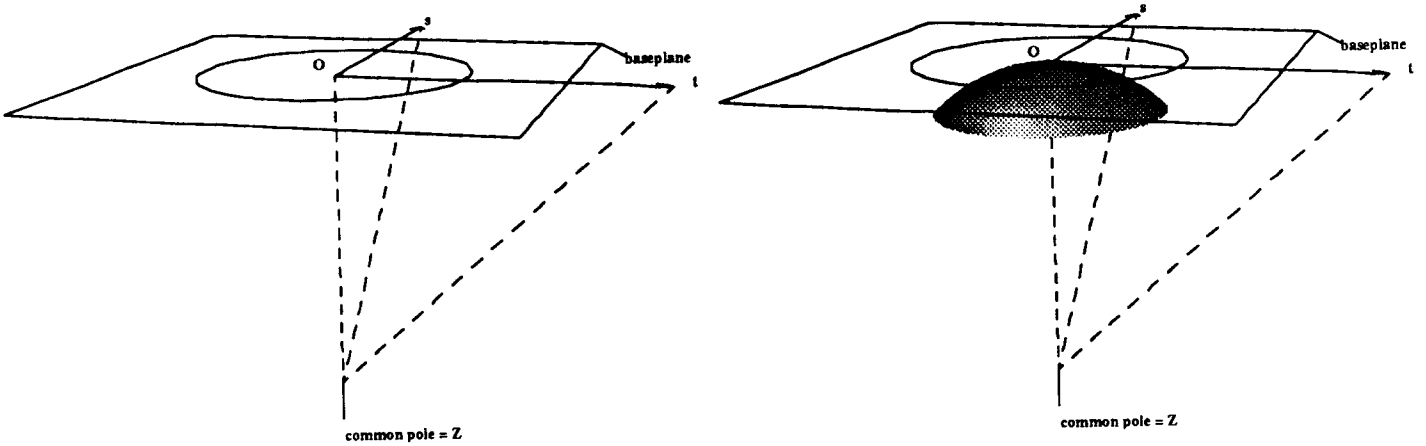

Figure 11.2: A mapped patch covering the unit sphere is constructed by choosing the center of projection at the sphere's South pole. The sphere has been cut by a plane parallel to the xy-plane.

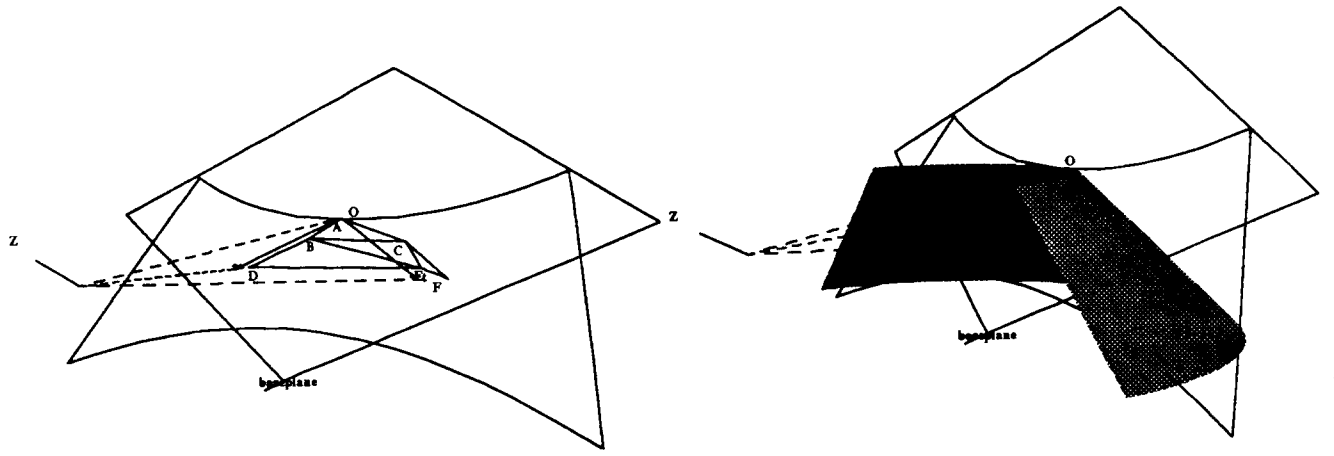

Figure 11.3: A mapped patch covering half of the desired portion of the right cone is constructed by choosing the center of projection off the part of the cone to be covered.

Next we cut the sphere with **C**, the plane $z = \frac{\sqrt{2}}{2}$. The polar point of this cut plane with respect to the sphere is $(0, 0, \sqrt{2})$. Thus we need only translate the apex of the cone from the origin to this point. This is easily done by enclosing the cone matrix (Equation 11.1) in the adjoint coordinate transformation of Equation 7.12. Then we cut the cone with **C**, since it is to share this cutplane

with the sphere. The resulting conic-bounded domains are shown for the sphere and cone patches in Figures 11.2 and 11.3, respectively. The stereographic map baseplanes, centers of projection, and domains for each patch are shown in Figure 11.4.

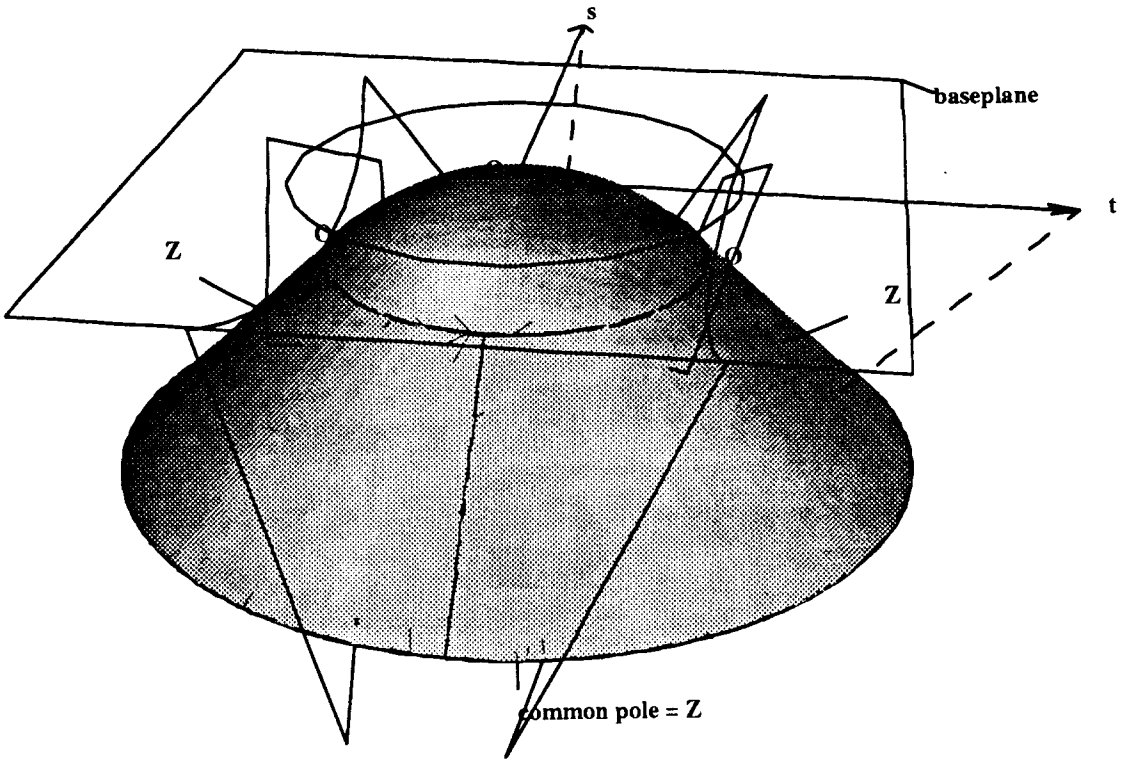

Figure 11.4: The stereographic map baseplanes and domains for all three patches.

11.1.2 Rounding Corners

We can model a parallelepiped with rounded corners using only planes, cylinders, and spheres (Figure 11.5). The sphere is produced as in §8.4.1; the cylinders as in §8.4.2. The components are placed using adjoint modeling transforms.

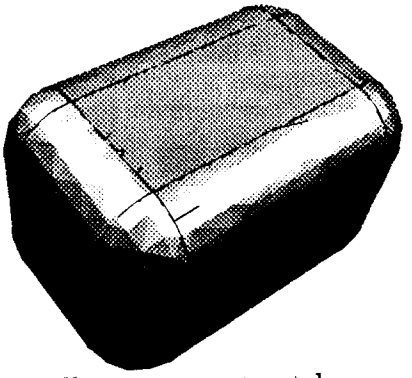

The component patches.

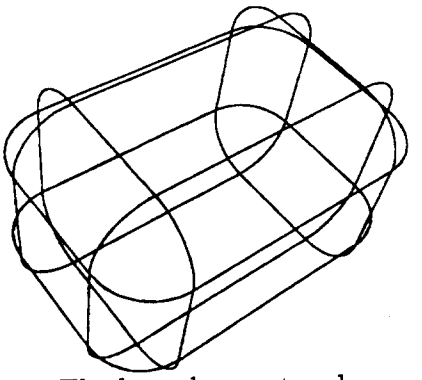

The boundary network.

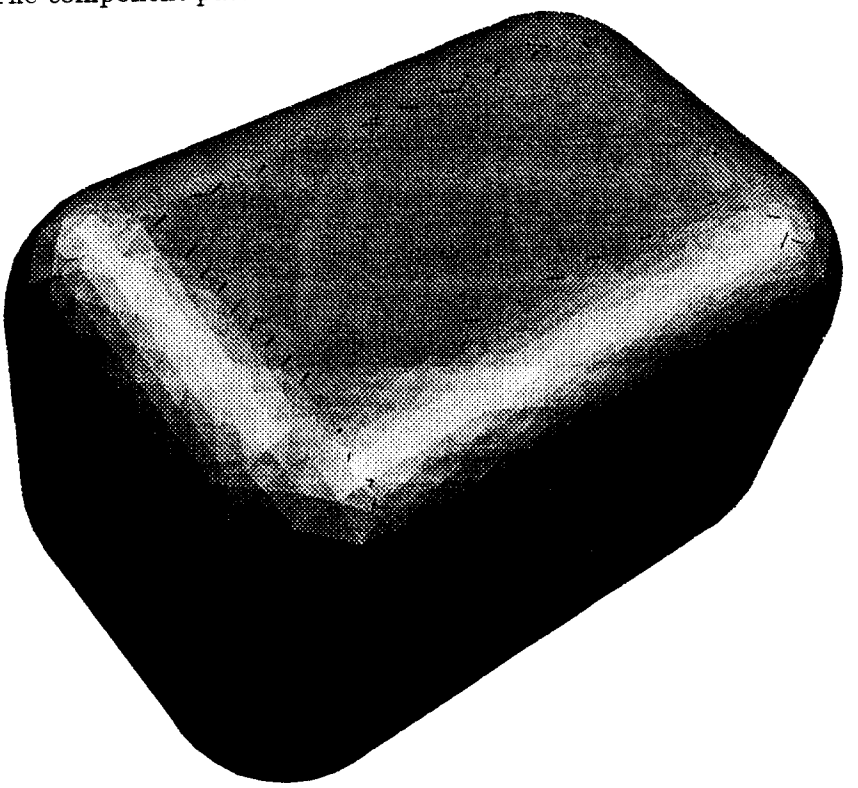

Figure 11.5: A Parallelepiped with Rounded Corners.

11.1.3 Blending Cubes with Three-Fold Symmetry

Chiyokura, in [5], demonstrates a G^1 blending operation on three cubes incident on a saddle vertex of degree six (Figure 11.6). The cube edges should be filleted with circular cylinders. Chiyokura uses bicubic Gregory patches, and achieves a solution with $\frac{2\pi}{3}$ (i.e., three-fold) rotational symmetry. We demonstrate a G^1 solution with the same symmetry using only rational quadratic triangular patches (Figure 11.6).

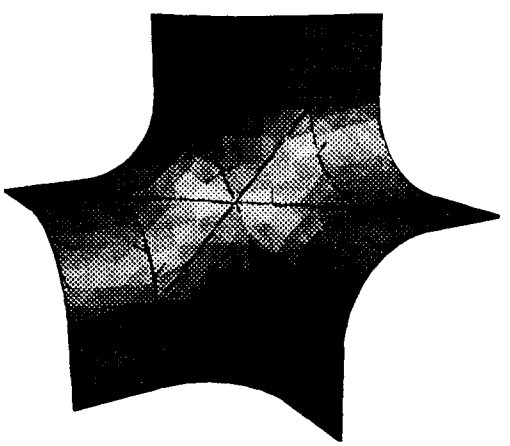

The component patches.

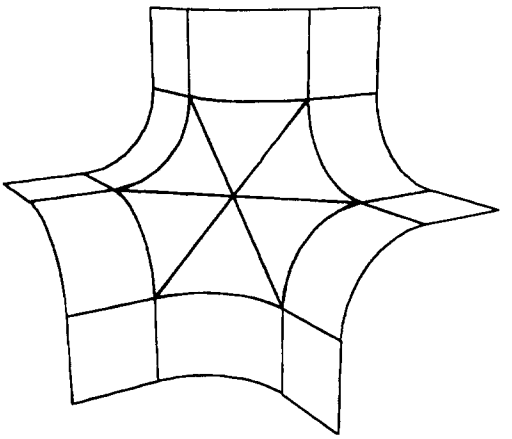

The boundary network.

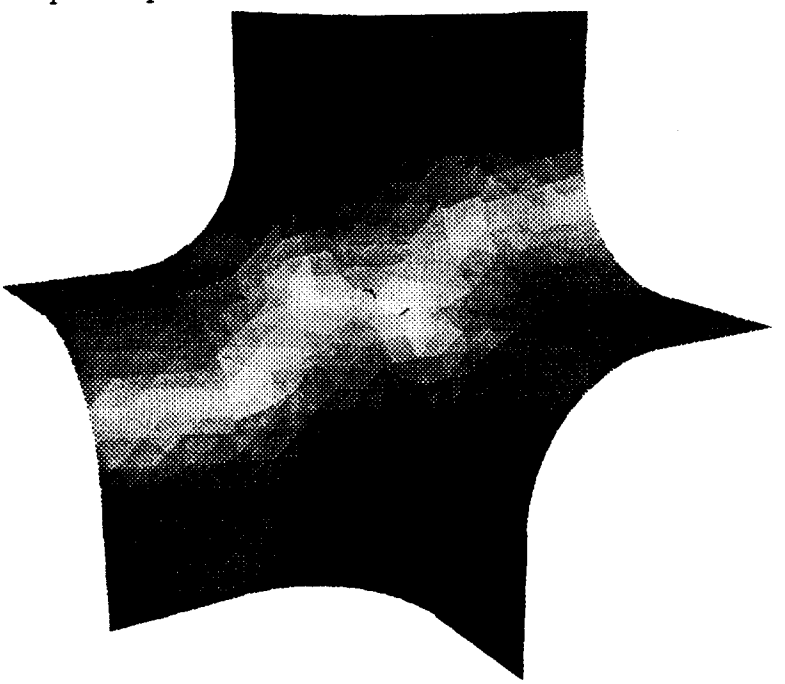

Figure 11.6: A Blend of Three Cubes at a Degree-Six Saddle Vertex with $\frac{2\pi}{3}$ Symmetry.
The construction uses eighteen rational quadratic triangular Bézier patches, and produces a G^1 (visually continuous) surface with $\frac{2\pi}{3}$ (i.e., three-fold) rotational symmetry.

Our solution requires eighteen mapped rational quadratic patches. Six of these are domain-extended to squares. Six are portions of cylinders as demonstrated in §8.4.2. Finally, the six patches in the center of the figure are standard triangular patches, but do not cover any implicit

quadric. Each of these patches has three edges, two of which are lines and one of which is a circular arc. The control point at the junction of the two lines arises from the rotation symmetry of the figure, as do the two control points on the linear edges. The circular edge control points are completely determined by the cylinders abutting the central region.

If three-fold rotational symmetry is not required we can replace the six triangular patches at the shared vertex of Figure 11.6 with two tensor-product patches (Figure 11.7). The resulting object contains twelve mapped rational quadratic triangular patches (the cylinder and square portions) and two rational biquadratic patches (the center portions).

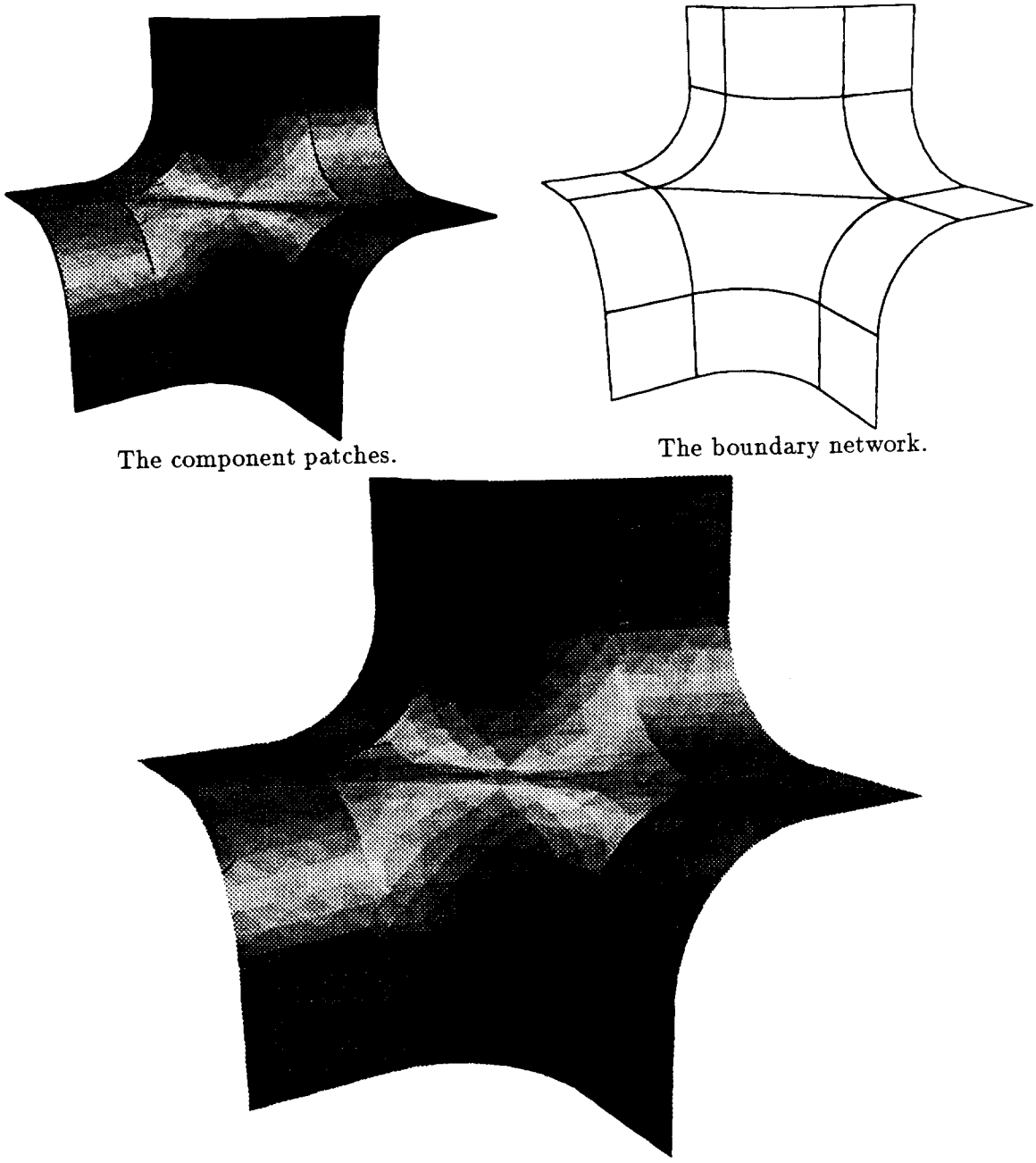

Figure 11.7: A Blend of Three Cubes at a Degree-Six Saddle Vertex.
The construction uses twelve rational quadratic triangular Bézier patches and two rational quadratic tensor-product Bézier patches, and produces a G^1 (visually continuous) surface with no rotational symmetry.

11.2 Toroidal Fillets Using Tensor-Product Patches

11.2.1 Filleting a Plane and Cylinder

The ability to model tori with biquadratic rational Bézier patches allows some convenient blends of linear and quadratic surfaces. For example, a torus symmetric about the z axis has normal $\pm\hat{\mathbf{z}}$ at its z extrema. Similarly, at its r extrema, the torus has purely normal radials (Figure 11.8).

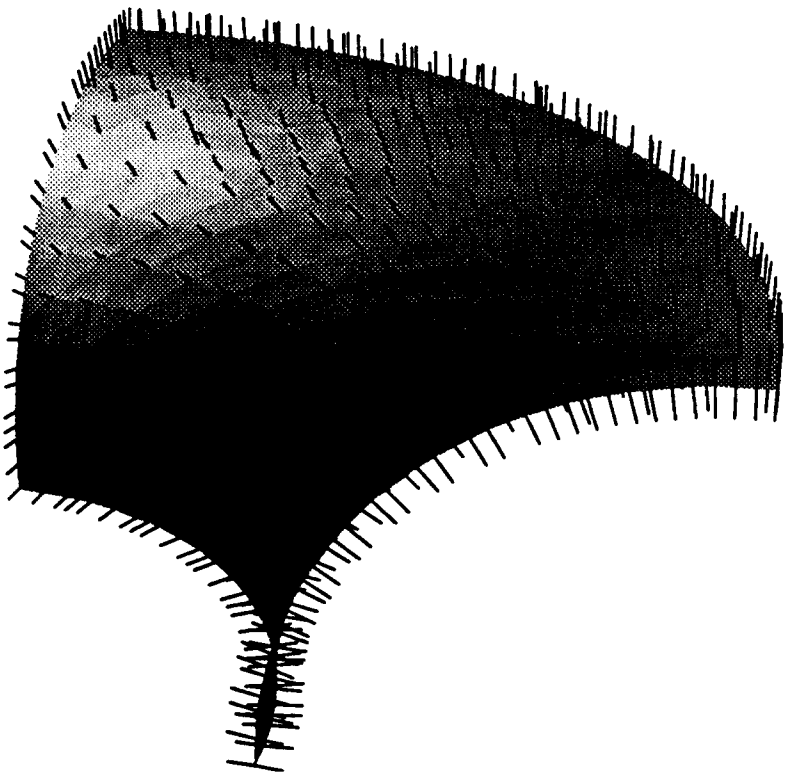

Figure 11.8: The Normal Field of a Circular Torus. The normals are parallel or antiparallel to the torus symmetry axis at the torus axial extrema. At the torus r extrema (where r is perpendicular distance from the symmetry axis), the normals are purely radial or antiradial.

We adjoin a plane to the torus at its z maximum, and a cylinder at its r minimum, employing the torus as a plane-cylinder fillet. The cylinder is constructed in the manner of §8.4.2; the plane is one limb of a stereographically mapped double plane; the center of projection is chosen on the cylinder's symmetry axis. Thus removing a circular "hole" from the plane is equivalent to constraining the domain of this patch to lie outside a circle centered at the origin. Figure 11.9 depicts the resulting object.

11.2.2 Filleting a Cylinder with a Rectangular Shaft

We can fillet a cylinder to more complex surfaces than a plane. Consider the problem of smoothly joining a cylinder and a rectangular prismatic shaft (Figure 11.10). We can treat the plane of the last section as an intermediate surface; then the problem of this section decomposes into two

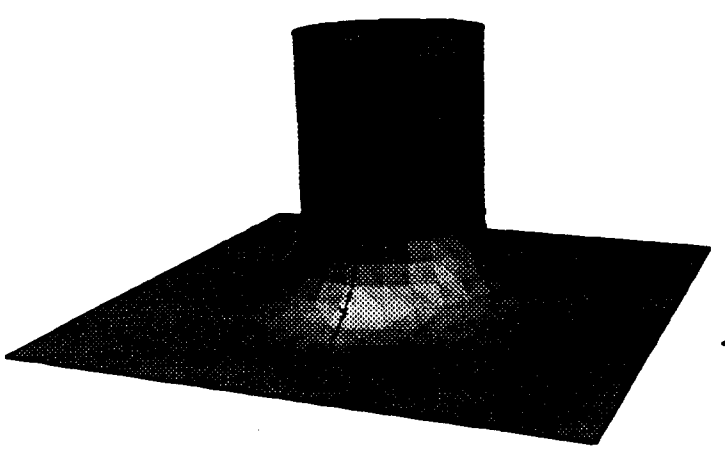

The component patches.

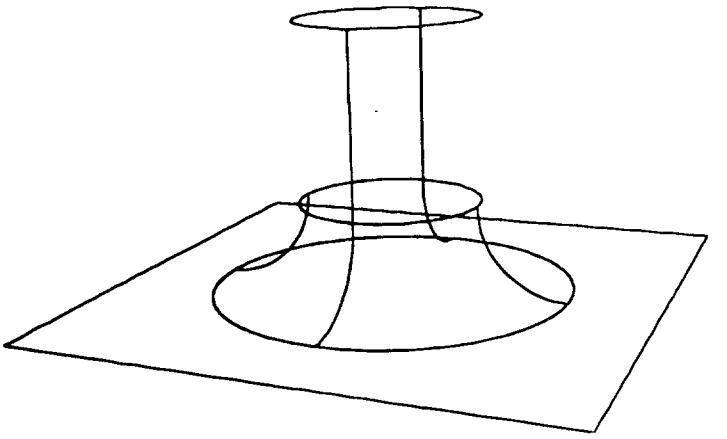

The boundary network.

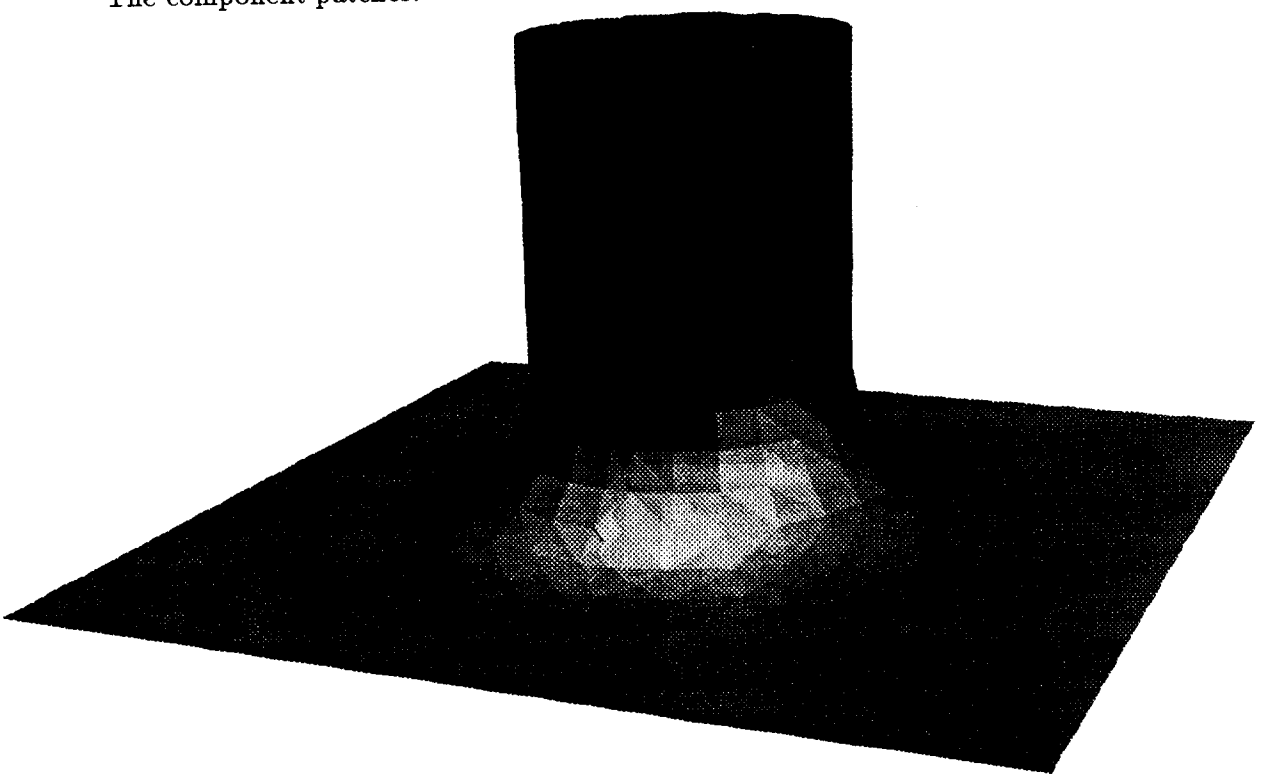

Figure 11.9: A Cylinder-Plane Fillet Using Quadratic and Quartic Patches.

subproblems. First, we fillet the cylinder and the plane using a toroid, as in the last section. Next, we blend the plane and shaft as in the example of the rounded parallelepiped (§11.1.2), using four sphere octants and four cylindrical pieces.

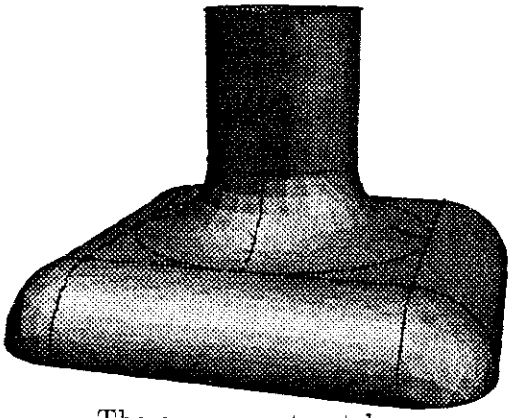

The component patches.

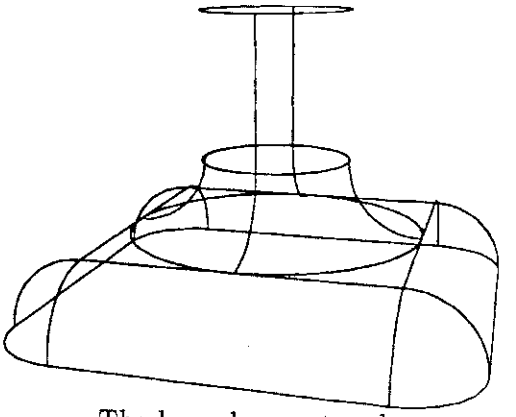

The boundary network.

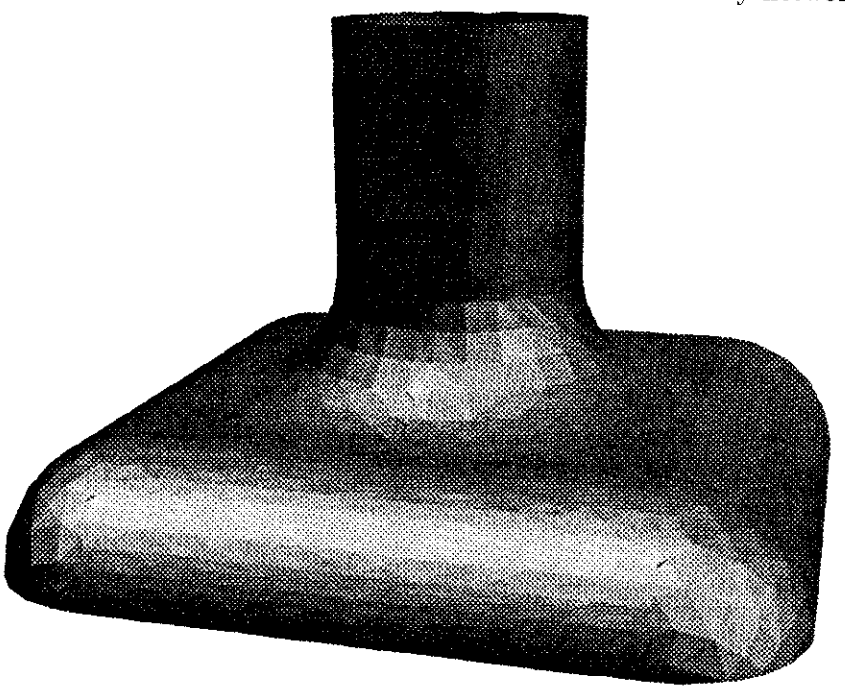

Figure 11.10: A Generalized Cylinder and Plane Filleted Using Quadratic and Quartic Patches.

11.2.3 Filleting Cylinders of Different Radii

Finally, we consider the problem of filleting two cylinders of unequal radii (Figure 11.11). Here, we employ a toroidal patch for each cylinder. The smaller cylinder (top) meets the torus at its r minima. The larger cylinder (bottom) meets the torus at its r maxima. The tori meet eachother in a plane perpendicular to the cylinders' shared symmetry axis. In the figure, elliptical (i.e., axially flattened) tori have been employed; circular tori would serve equally well.

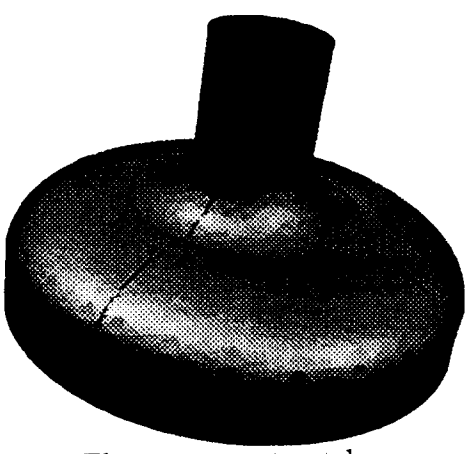

The component patches.

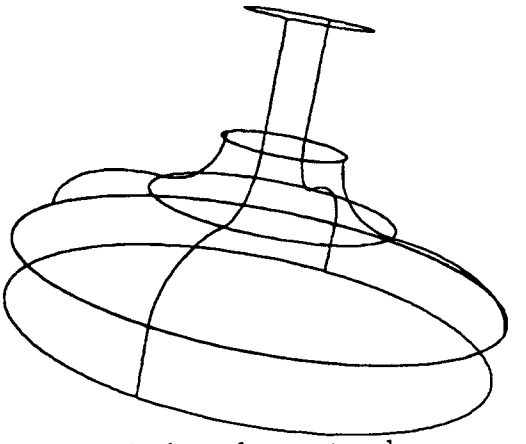

The boundary network.

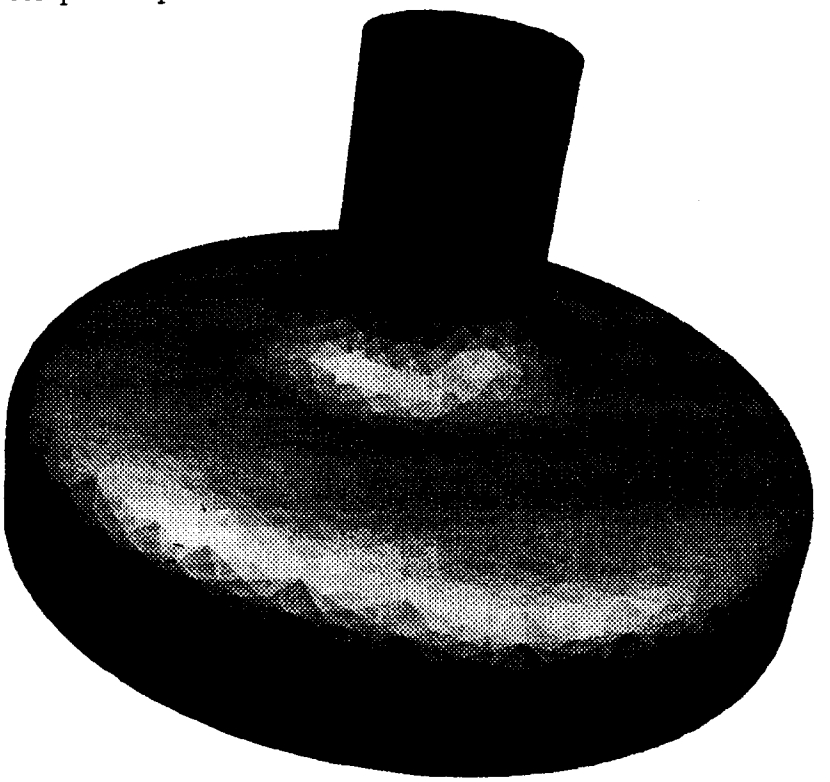

Figure 11.11: Circular and Elliptical Tori Blending Cylinders of Different Radii.

11.2.4 Filleting a Sphere-Cylinder Union

Tori are useful when we must blend surfaces that, if extended, would meet at right angles (such as the cylinder and plane in the example of the previous section). If this joining angle is less than $\frac{\pi}{2}$, however, we may be able to dispense with the torus and achieve the blend using only quadrics. For example, suppose we wish to abut a piece of a cylinder with two spheres, one at each end (Figure 11.12).

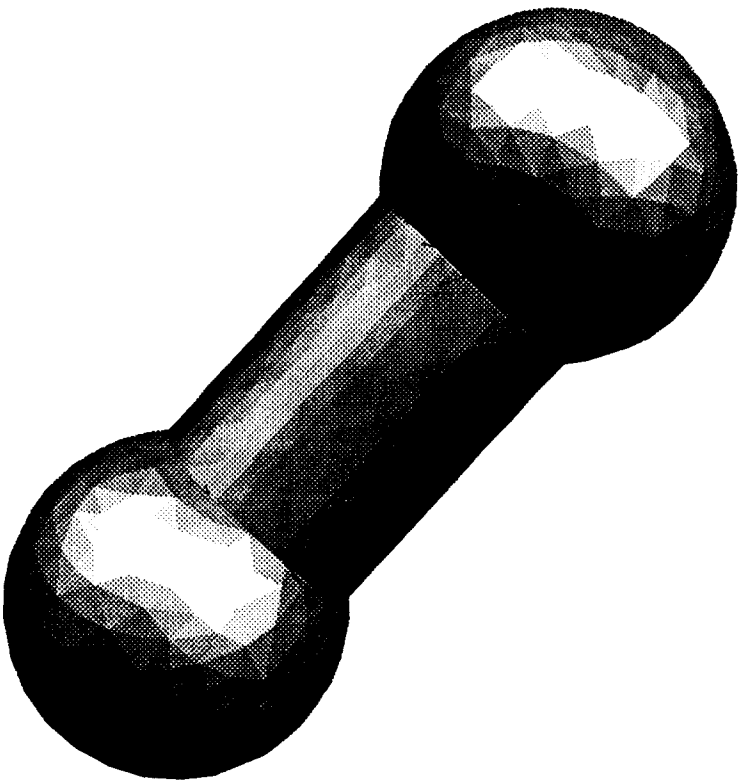

Figure 11.12: A Portion of a Cylinder, Abutted with Spheres at Each End.
No blending or filleting has been done; the object is G^0 continuous across seams.

There are many ways to fillet the G^0 join of the sphere and cylinder. We might use a torus, as in the last section. However, a single-sheet hyperboloid can also serve as a fillet, and has a lower implicit degree (two) than the quartic torus. The hyperbolic fillet is constructed in the manner of §8.4.3. The canonical matrix for a single-sheet hyperboloid is introduced, then anisotropically scaled using the adjoint transformations of §7.4, Equation 7.12. Both the sphere and hyperboloid have been cut such that the cone exscribing the cut has a 90° opening angle; however, any cut plane perpendicular to the cylinder axis may be used. Figure 11.13 depicts the resulting G^1 surface and boundary curve network.

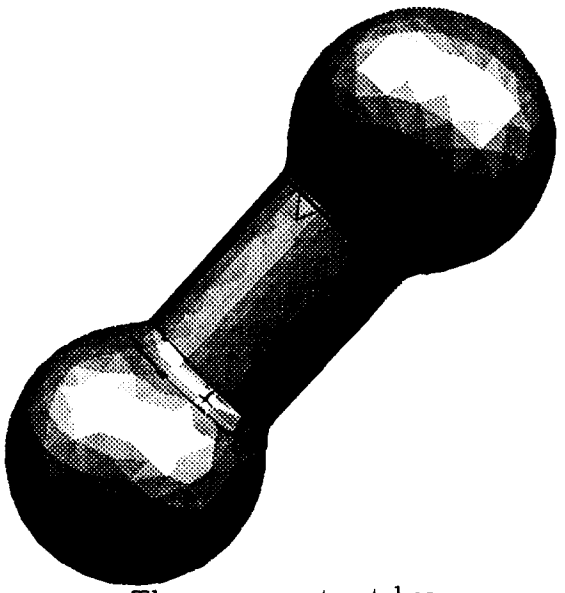

The component patches.

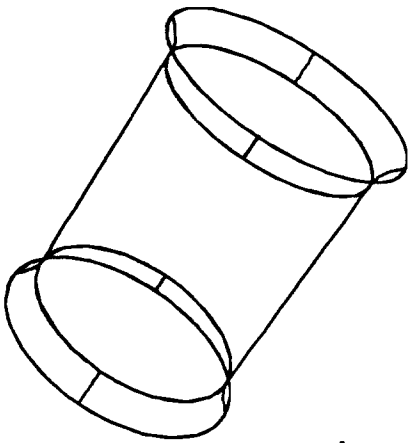

The boundary network.

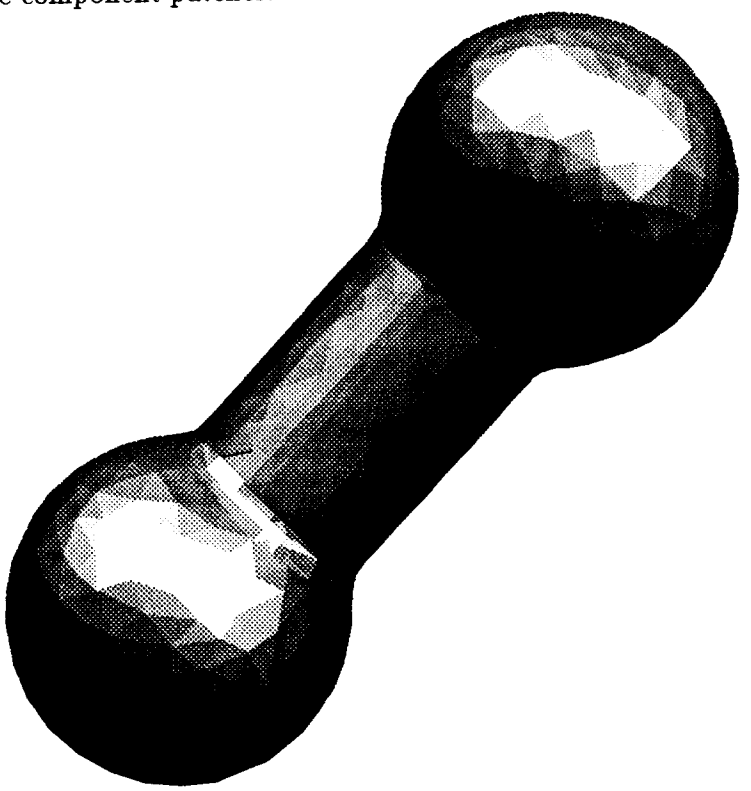

Figure 11.13: A Cylinder-Sphere Union, Blended with a Single-Sheet Hyperboloid.

11.2.5 Filleting a Sphere-Cylinder Difference

In the last section, we constructed the *union* of a cylinder and two spheres, and filleted the resulting G^0 seams with single-sheet hyperboloids. In this section, we construct the *difference* of the two surfaces, and fillet the seams of the difference object with tori (Figure 11.14). Cutaway views of this rather complex object are shown in Figures 11.15.

For simplicity, we have again cut the unit-radius sphere at $z = \frac{\sqrt{2}}{2}$, so that that the cone exscribing the cut has a 90° opening angle. The torus matching the "core" cylinder and external sphere is easily constructed. Its inner radius is the radius of the cylinder; its outer radius is $\frac{\sqrt{2}}{2}$.

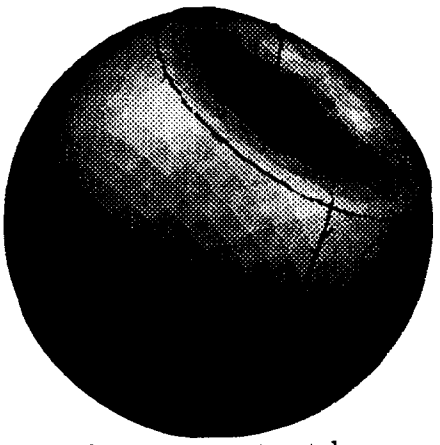

The component patches.

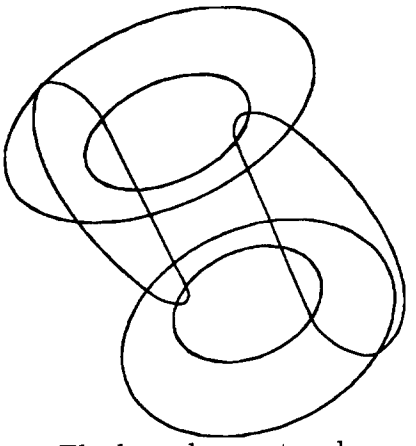

The boundary network.

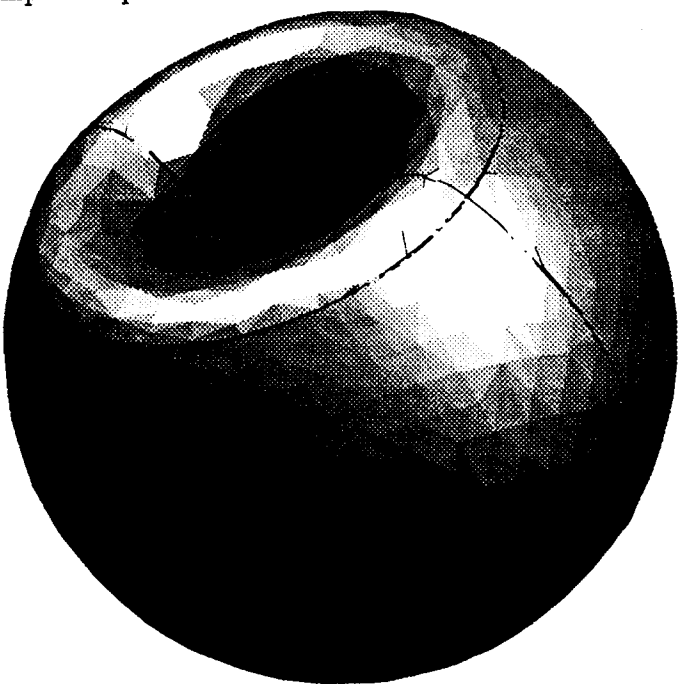

Figure 11.14: A Sphere-Cylinder Difference Blended with a Portion of a Torus.

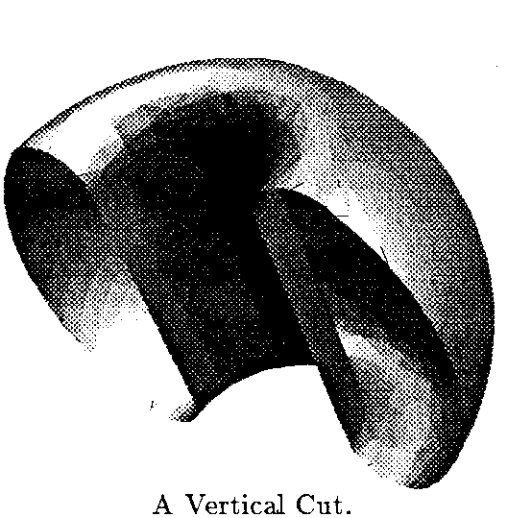

A Vertical Cut.

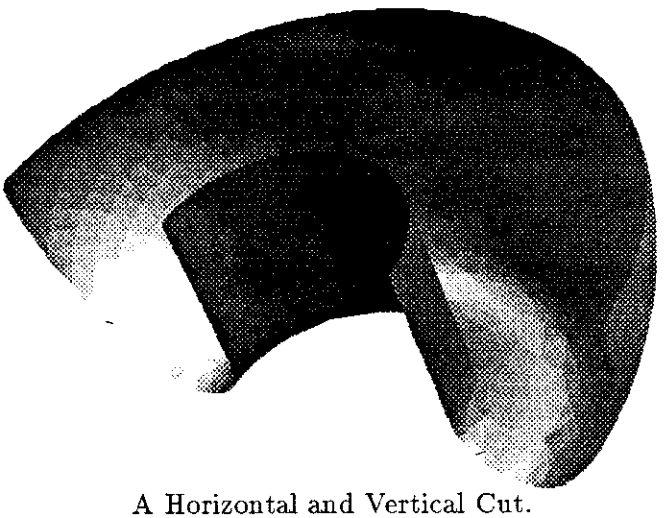

A Horizontal and Vertical Cut.

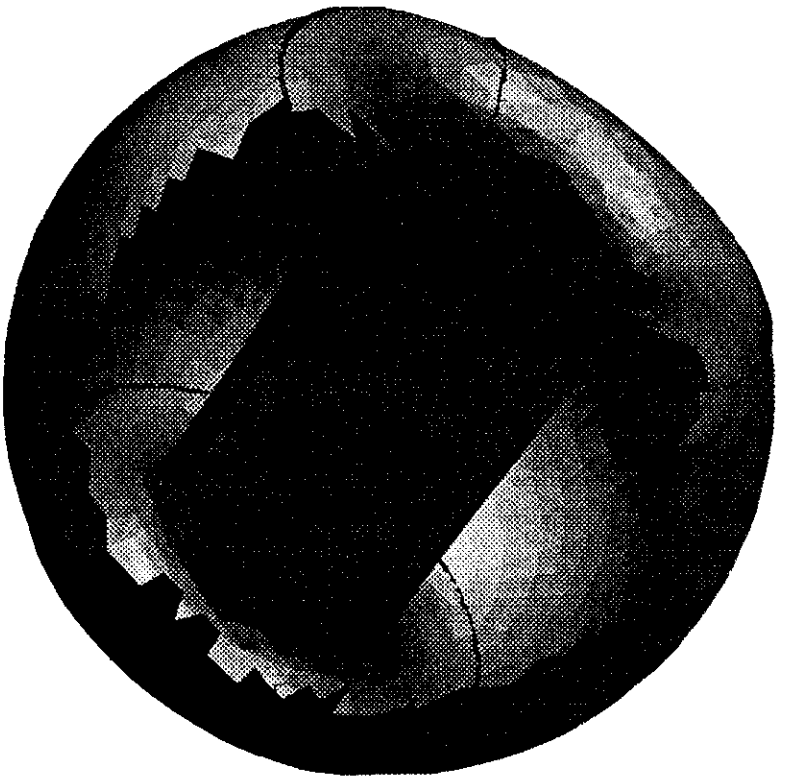

Figure 11.15: Some Cutaway Views of the Filleted Sphere-Cylinder Difference.

11.3 Joins of Quadratic and Higher-Order Patches

11.3.1 Filleting a Plane and Oblique Cylinder

We fillet a cylindrical shaft with a plane, in the case where the cylinder axis meets the plane at an oblique angle. Quadratic patches are not sufficient to form a G^1 seam; however, a rational bicubic (tensor-product) Bézier patch can be molded into an appropriate fillet (Figures 11.16 and 11.17).

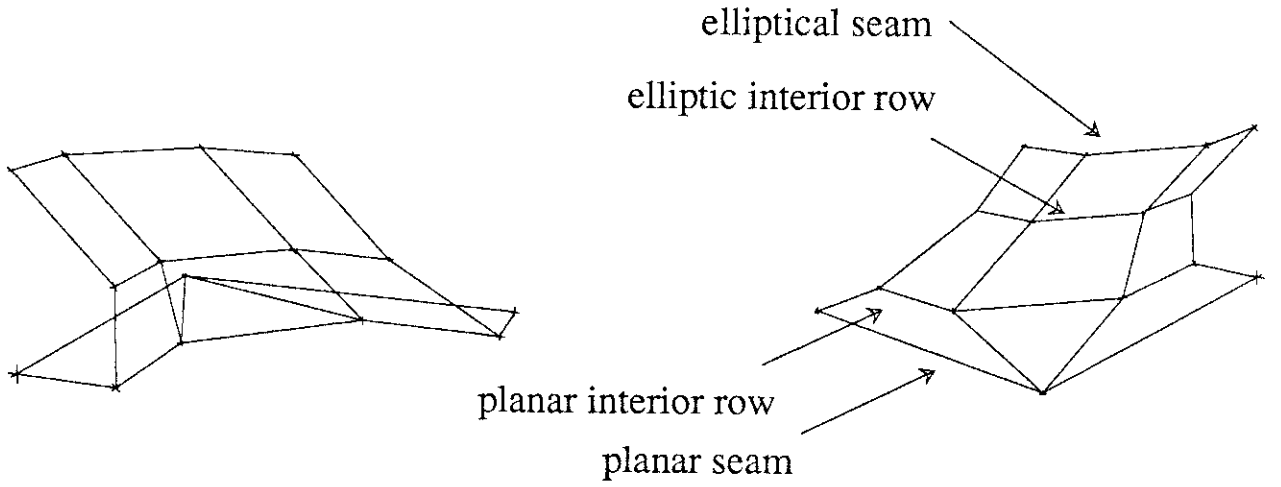

Figure 11.16: A bicubic patch filleting an oblique cylinder with a plane. Two views of the patch are shown; it has three counterparts, differently skewed, that complete the construction.

The construction uses three patch types: a planar portion; an oblique cylindrical piece; and a fillet between them. The planar and cylindrical pieces are mapped triangular patches, as in §11.2.2. The fillet patch is bicubic, and must satisfy four zeroth-order and four first-order constraints in order to meet its neighbors with G^1 continuity (Figure 11.16). It must have an exterior and internal row planar to provide a planar seam and planar first derivatives everywhere on the seam. The other two rows must provide an elliptical, planar seam (since the seam is an oblique cut of a circular cylinder), and first derivatives everywhere parallel to the cylinder axis. The curves corresponding to these control rows must cover implicit conics; thus the fillet patch must be rational.

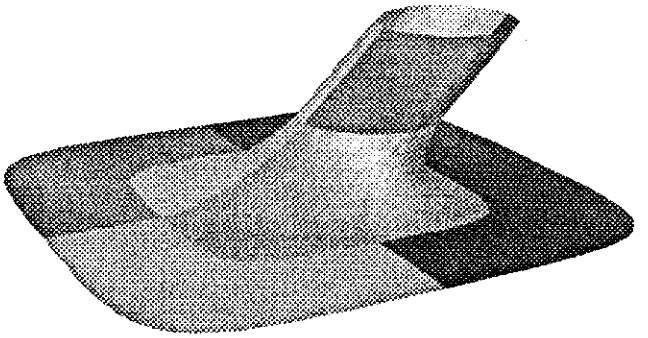

The component patches.

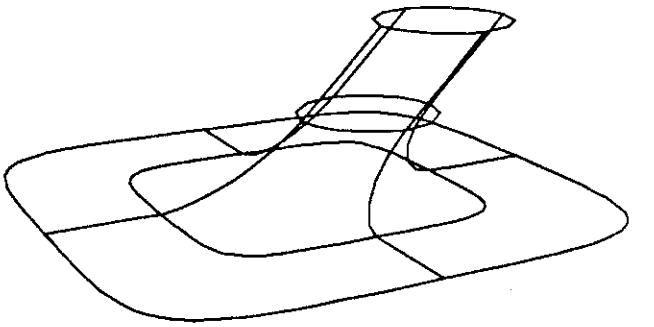

The boundary network.

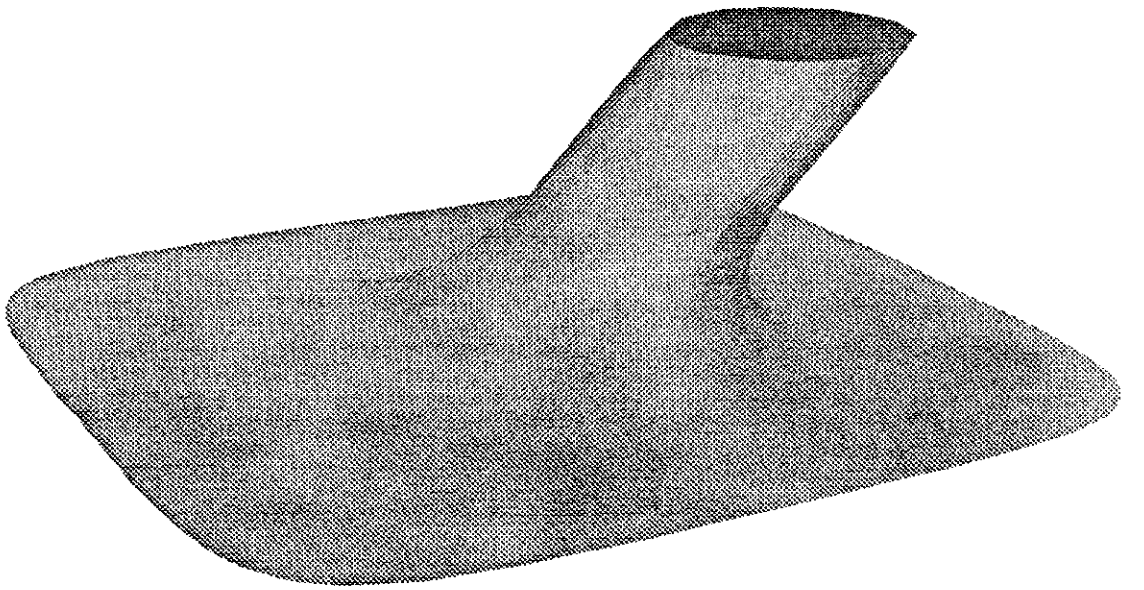

Figure 11.17: A Bicubic Tensor-Product Fillet of a Plane with an Oblique Cylindrical Shaft.

Chapter 12

Incorporating Rational Quadratic Bézier Patches Into Existing Modeling Systems

We briefly consider the issues implicated by modifying existing modeling systems to employ our proposed unified representation for rational quadratic Bézier patches. We assume that, in a modeling system employing heterogeneous parametric primitives, patches of differing types adjoining a common boundary must be C^1 along the shared boundary. We consider several popular parametric patch representations, loosely ordered by complexity, and discuss the constraints on both existing and proposed representations so that the two may be usefully integrated.

12.1 Adjoining Rational Quadratics With Non-Rational Patches

Non-rational patches, regardless of order, can not in general achieve G^0 (positional) continuity with rational patches. Thus for a rational patch and non-rational patch of any order to abut with G^0 continuity, the rational patch must "yield" its rational freedom along the boundary curve, by constraining all weights along the curve to be equal. The conditions for G^1 (i.e., tangent-plane) continuity are less tractable; necessary and sufficient conditions for G^1 continuity of rational quadratic patches have not yet been found. Recent work in [39] gives the tightest existing bounds, under some stringent linearity assumptions. Their scheme allows G^1 joins of triangular and tensor-product patches. Their construction is also applicable to situations in which one or both patches involved are non-rational.

When adjoining rational quadratic patches to higher order (i.e., cubic) non-rational constructs, both participating patches must yield freedoms. The rational patch must present a non-rational boundary curve on the shared seam. The neighboring higher-order patch boundary must degenerate to a quadratic polynomial curve.

The unified representation for quadrics makes feasible some relaxations of these restrictions. For example, the unified representation allows straightforward construction of quadratic patches that interpolate quadrics, but have *non*-planar boundary curves. Thus we might, for example, bound an interpolated patch with cubic curves, and adjoin it to a cubic Bézier patch. In this case, the

cubic patch need not have a degenerate boundary. We have not explored these situations, but note them as possible avenues for future research.

12.2 Adjoining Rational Quadratics With Higher Order Rational Patches

When adjoining quadratic to higher-order patches, the latter must yield freedom to present a degenerate (quadratic) boundary curve to its neighbor. Again, the unified representation allows more generality in the higher-order patch. Bounding the low-order patch with a non-planar curve relaxes some constraints on its neighbor; in this case, the superquadratic boundary curve need not be degenerate (i.e., quadratic).

12.3 Adjoining Rational Quadratics With Gregory Patches

Gregory patches [15] employ "split" internal vertices to avoid the twist constraints inherent in standard tensor-product Bézier surfaces. Evaluated along a boundary, Gregory patches are indistinguishable from Bézier patches to zeroth order. At first order, the split internal control points combine linearly, producing composite points that act as ordinary Bézier control points. Achieving G^1 continuity across the shared seam of a quadratic Bézier and a higher-order Gregory patch in some cases requires that the first interior row of Gregory control points cannot contain split vertices.

We are continuing to study the practical issues involved in integrating rational quadratic Bézier patches, both triangular and tensor-product, into modeling systems that employ Gregory patches, and polynomial and rational B-splines of higher than quadratic order.

Chapter 13

Limitations

Employing rational quadratic patches as a modeling primitive offers advantages in terms of computational efficiency, compactness and intuitiveness of representation. However, the patch construct is not without disadvantages. For example, although a single quadratic patch is everywhere C^∞ continuous, it may not adjoin any other patch with higher than first derivative (C^1) continuity. If it were to do so, the patches would not be piecewise neighbors but would in fact be identical polynomial expressions.

Quadratic patches are not suitable for all situations in free form modeling. Indeed, no finite formulation will ever be appropriate for all situations. We have demonstrated that the quadratic patch is an ideal formulation for parametrized quadrics. The argument in favor of quadratic patches cannot be made so convincingly for more complex modeling situations. For instance, any inflected surface, if it is to be modeled exactly, will require at least two quadratic patches for interpolation. Moreover, quadratic patches may prove inadequate for modeling cubic or higher-order fillets or smoothly abutting patches at saddle corners.

Although implicit quadrics (and thus parametric patches interpolating them) have simple derivative properties, the complexity of the derivative increases considerably for unrestricted quadratic patches, both triangular and tensor-product. As of this writing, no necessary and sufficient conditions for G^1 continuity of rational quadratic patches has been elucidated, although reasonably tight bounds exist. For this reason, the feasibility of "quilting" extended quadratic patches over non-rigid boundary nets (i.e., nets with no global shape constraints) remains an open question.

As we noted in the previous chapter, rational quadratic patches may often have a mismatch of freedoms when coupled with different constructs. On one hand, the quadratic patch must defer to non-rational adjoining patches. But higher-order abutting patches, whether rational or polynomial, must defer through degree-reduction to the quadratic patch. We noted that this difficulty is lessened somewhat by the ease with which a mapped triangular patch may be constructed to have very complex boundaries.

The complementary surface constructions of §7.6.3 have utility in covering entire implicit surfaces: general quadrics, and some types of cubic and quartic surfaces. However, complemented patches are not as simple to manipulate as standard patches, due to the odd shapes and self-intersecting nature of the complementary patches.

We conclude that quadratic patches are most appropriate for renderers and modelers that make heavy use of implicit quadric primitives, in conjunction with CSG-type union, intersection, and difference operations.

Chapter 14

Summary

We have considered the problems of representing implicit conics as rational quadratic Bézier curves, and implicit quadrics as rational quadratic Bézier surfaces. In both cases, we propose methods of representation and construction that are substantial improvements over existing methods.

First, we show that two familiar representations for conics, the stereographic map and rational quadratic Bézier curve formulations, are equivalent under a straightforward geometric construction. This correspondence makes feasible the construction of rational quadratic Bézier curves that cover any chosen conic, and allow trivial geometric inversion procedures.

Using the two-dimensional result, we clarify the degrees of geometric and parametric freedom inherent in the construction of a rational quadratic triangular patch that interpolates some portion of a quadric surface. We exhibit, first, a construction that, for any implicit quadric and choice of bounding planes, produces a triangular Bézier patch on the quadric lying only within the boundary planes.

We extend the two-dimensional result, showing that two familiar surface representations, stereographic maps and an important restricted class of rational quadratic Bézier patches, are actually equivalent under a straightforward, purely constructive, geometric transformation. The value of the correspondence is that it provides a trivial inversion of this class of Bézier patches onto their domain space preimages, obviating any need for cumbersome numerical inversion techniques. This property should prove useful in many contexts, for example rendering, surface-surface intersection, and abutting patches under continuity constraints.

We extend the notion of complementary curves to Bézier surfaces, and show that unbounded surfaces may be swept over finite parameter areas. Rendering and modeling systems that require complete swept quadrics will find complementary curves useful; they do have drawbacks in more general settings.

We briefly consider tensor-product patches, and show that they may be complemented to tile toroids and general quartic surfaces, as well as higher-order implicit surfaces. We demonstrate the combined use of triangular and tensor-product patches in real modeling situations, and show that the stereographic map equivalence and adjoint transformation techniques for implicit quadrics make possible quite straightforward join and fillet operations.

Our constructions are of more than theoretical interest; they provide new geometric interpretations, and unifications, of traditionally disjoint (though separately familiar) Bézier curve and surface formulations, and stereographic map formulations. Hopefully, these geometric insights will increase the comprehension and productive use of the Bézier formulation by students, implementers, and users of modeling systems.

Bibliography

[1] Pierre Bézier. *Mathematical and Practical Possibilities of UNISURF*, pages 127–152. Academic Press, 1965.

[2] Richard Bartels, John C. Beatty, and Brian A. Barsky. *An Introduction to Splines For Use in Computer Graphics & Geometric Modeling.* Morgan Kaufmann, 1987.

[3] James F. Blinn. Geometric representations in computer graphics, part I. In *SIGGRAPH '80 Advanced 3D Raster Graphics Seminar Notes*, July 1980.

[4] James F. Blinn. The algebraic properties of homogeneous second order surfaces. In *SIGGRAPH '84 Course Notes*, pages 1–23, 1984.

[5] Hiroaki Chiyokura. *Solid Modeling with DESIGNBASE, Theory and Implementation.* Addison-Wesley, 1988.

[6] James E. Cobb. Tiling the sphere with rational Bézier patches. Technical Report UUCS-88-009, Department of Computer Science, University of Utah, Salt Lake City, Utah 84112, July 1988.

[7] P. de Casteljau. *Courbes et Surfaces à Pôles.* A.A. Andre Citroen, 1959.

[8] Tony D. DeRose. *Geometric Continuity: A Parametrization Independent Measure of Continuity for Computer Aided Geometric Design.* PhD thesis, University of California, Berkeley, August 1985. Also available as Technical Report No. UCB/CSD 86/255, Computer Science Division, Department of Electrical Engineering and Computer Sciences, University of California at Berkeley.

[9] Tony D. DeRose. Rational Béziers and projective domains. Submitted for publication, 1990.

[10] Gerald Farin. A construction for visual C^1 continuity of polynomial surface patches. *Computer Graphics and Image Processing*, 20:272–282, 1982.

[11] Gerald Farin. Algorithms for rational Bézier curves. *Computer-Aided Design*, 15(2):73–77, 1983.

[12] I.D. Faux and M.J. Pratt. *Computational Geometry for Design and Manufacture.* Ellis Horwood, 1983.

[13] A.R. Forrest. The twisted cubic curve: a computer aided geometric design approach. *Computer Aided Design*, pages 165–172, 1980.

[14] Gordon Fuller. *Analytic Geometry.* Addison-Wesley, 1973.

[15] John A. Gregory. Smooth interpolation without twist constraints. In Richard F. Riesenfeld Robert E. Barnhill, editor, *Computer Aided Geometric Design*, pages 71–87. Academic Press, 1974.

[16] Paul S. Heckbert. The mathematics of quadric surface rendering and SOID. Technical report, New York Institute of Technology, July 1984.

[17] Christoph M. Hoffmann. *Solid and Geometric Modeling.* Morgan Kaufmann, 1989.

[18] Eugene T.Y. Lee. The rational Bézier representation for conics. In Gerald E. Farin, editor, *Geometric Modeling: Algorithms and New Trends*, pages 3–19. SIAM, 1985.

[19] Joshua Levin. A parametric algorithm for drawing pictures of solid objects composed of quadric surfaces. *Communications of the ACM/Graphics and Image Processing*, 19(10):555–563, 1976.

[20] Harry Levy. *Projective and Related Geometries.* Macmillan, 1961.

[21] Lucia Longhi. Interpolating patches between cubic boundaries, Technical Report UCB/CSD 87/313. Master's thesis, University of California at Berkeley, October 1986.

[22] R. Mahl. Visible surface algorithm for quadric patches. *IEEE Transactions on Computers*, C(21):1–4, 1972.

[23] Donald J. Meagher. Interactive solids processing for medical analysis and planning. In *Computer Graphics '84, NCGA Conference Proceedings*, volume 2, pages 96–106. NCGA, 1984.

[24] Laszlo Piegl. Representation of quadric primitives by rational polynomials. *Computer Aided Geometric Design*, 2:151–155, 1985.

[25] Laszlo Piegl. The sphere as a rational Bézier surface. *Computer Aided Geometric Design*, 3:45–52, 1986.

[26] Vaughan Pratt. Techniques for conic splines. *Proceedings of SIGGRAPH '85*, 19(3):151–159, July 1985.

[27] A.A.G. Requicha. Solid modelling: a historical summary and contemporary assessment. *IEEE Computer Graphics and Applications*, 2(2):9–24, March 1982.

[28] A.A.G. Requicha and H.B. Voelcker. *Constructive Solid Geometry, Technical Memo No. 25, Production Automation Project.* University of Rochester.

[29] R.F. Riesenfeld. Homogeneous coordinates and projective planes in computer graphics. *IEEE Computer Graphics and Applications*, pages 50–55, January 1981.

[30] Lawrence G. Roberts. Homogeneous matrix representation and manipulation of n-dimensional constructs. *The Computer Display Review*, July 1966.

[31] Alyn Rockwood, Kurt Heaton, and Tom Davis. Real-time rendering of trimmed surfaces. *Proceedings of SIGGRAPH '89*, 23(3):107–116, July 1989.

[32] T.W. Sederberg and D.C. Anderson. Steiner surface patches. *IEEE Computer Graphics and Applications*, pages 23–36, 1985.

[33] Carlo H. Séquin. Procedural spline interpolation in unicubix. Technical Report UCB/CSD 87/321, University of California at Berkeley, Jan 1987.

[34] M. Shantz and S. Chang. Rendering trimmed NURBS with adaptive forward differencing. *Proceedings of SIGGRAPH '88*, 22(4):189–198, Aug 1988.

[35] Leon Shirman. Symmetric interpolation of triangular and quadrilateral patches between cubic boundaries. Technical Report UCB/CSD 87/319, University of California at Berkeley, December 1987.

[36] D.M.Y. Sommerville. *Analytical Geometry of Three Dimensions.* Cambridge University Press, 1959.

[37] Jorge Stolfi. *Primitives for Computational Geometry.* Dec SRC, 1989.

[38] Seth J. Teller. Bézier surfaces that cover quadrics, and their equivalence to stereographic maps. Master's thesis, University of California at Berkeley, May 1990.

[39] A. Vinacua and P. Brunet. A construction for VC^1 continuity of rational Bézier patches. In Larry L. Schumaker Tom Lyche, editor, *Mathematical Methods in Computer Aided Geometric Design*, pages 601–611. Academic Press, 1989.

[40] Joe Warren and Suresh Lodha. A Bézier representation for quadric surface patches. In *Proceedings of SIAM '90*, 1990.

[41] Robert C. Yates. *Curves and Their Properties.* National Council of Teachers of Mathematics, 1952.